Report No. 164/UILU-ENG 93-4022

Calculation of Notch Strains Under Multiaxial Hominal Loading

by
Mark Edward Barkey

A report of
MATERIALS ENGINEERING - MECHANICAL BEHAVIOR
College of Engineering, University of Illinois at Urbana-Champaign
October 1993

CALCULATION OF NOTCH STRAINS UNDER MULTIAXIAL NOMINAL LOADING

Mark Edward Barkey, Ph.D.
Theoretical and Applied Mechanics
University of Illinois at Urbana-Champaign, 1993
Professor Darrell F. Socie, Advisor

An approximate analytical method is developed to calculate strains at stress concentrators in structures of elastic-plastic, isotropic material subjected to proportional and nonproportional multiaxial nominal loading. The method uses anisotropic plasticity theory to define a structural yield surface in nominal stress space that incorporates both the isotropic material properties and the anisotropic geometry factors of the notch, and accounts for varying degrees of constrained plastic flow at the stress concentrator. Plastic strain increments at the stress concentrator and anisotropic work-hardening effects are then related to this yield surface using standard methods of plasticity.

The method is applied to mildly and sharply notched shafts, and a plate with a central through hole subjected to proportional and nonproportional nominal loading. The results of these calculations are compared with experimental results of a mildly notched shaft subjected to combined tensile and torsional load, and with extensive finite element analyses of all of the structures.

The strain calculations agree well with both qualitatively and quantitatively with the experiments and finite element calculations when using an appropriate uniaxial load-notch plastic strain relationship, and are suitable for strain-life fatigue calculations.

ACKNOWLEDGMENTS

This work was supported by the Fracture Control Program at the University of Illinois at Urbana-Champaign.

Professor Darrell F. Socie, thesis advisor and dissertation director, is gratefully thanked and acknowledged for the initial idea to begin this work, and for discussions regarding this work. Professor K. Jimmy Hsia is thanked for serving as academic advisor, and for many helpful comments regarding the text. Professor James W. Phillips is thanked for serving on the dissertation committee. The author is grateful to Dr. Peter Kurath and Mr. Craig R. Payne for help with setting up the experiments, and to William H. Johnson, David W. Foley, and Kent A. Elam of the machine shop for preparing the specimens.

A special note of thanks is given to Professor Volker B. Köttgen, from the Technical University of Darmstadt, for providing the results of the finite element analysis of the test specimen, and for numerous discussions by electronic communications on the topics of finite element analysis, material behavior, and stress concentrators.

The members of Fatigue Design and Evaluation Committee of the Society of Automotive Engineers, members of the Fracture Control Program, and fellow graduate students are thanked for their interest, and for their comments regarding presentations about this work.

Table of Contents

1 INTRODUCTION AND OBJECTIVE

Engineering components usually have stress concentrators such as notches or holes. An engineering component must typically be designed for specific forces the component is to carry and the useful life the component is to have. Recent advances in the strain-life theory of fatigue have allowed the estimation of the fatigue life of a component from measured strains at critical locations for general states of loading. However, the designer must estimate these strains for the evaluation of a particular geometry, often only knowing the applied loads, which in general may be multiaxial. Although nonlinear finite element analysis can be used to determine strains at critical locations, it can be prohibitively time consuming when considering histories of multiaxial loading.

The objective of this research is to develop an approximate method to calculate elastic-plastic notch root strains for a given multiaxial loading history and to compare these results with nonlinear finite element analysis and experimental results for proportional and nonproportional loading.

The current methods of notch strain estimation and major experimental work on determining elastic-plastic notch strains are reviewed in Chapter 2. The proposed method is developed in Chapter 3, and specialized for a notched shaft and a plate with a hole.

In Chapter 4, the proposed method is compared with the experimental results of Hoffmann and Seeger and the approximate technique developed by them for the analysis of proportionally loaded notched shafts.

Chapters 5, 6, 7, and 8 are analyses of different geometries. In Chapter 5, results using the method are compared with finite element calculations of the Society of Automotive Engineers (SAE) notched shaft in proportional bending and torsion. In Chapter 6,

calculations are compared with finite element analyses and experimental results of a mildly notched steel shaft subjected to proportional and nonproportional tension and torsion. In Chapter 7 a plate with a hole is examined, and in Chapter 8 a more sharply notched shaft is examined. Both of these geometries are compared with results from nonlinear finite element analysis for proportional and nonproportional loading. Concluding remarks are presented in Chapter 9.

2 BACKGROUND

Notches and stress concentrators have been of interest for many years, as these areas often serve as sites for fatigue crack initiation and component failure. The work of the last century and the first half of this century was focused on the elastic analysis of notches. Elastic stress and strain states were often either computed from closed form solutions using elasticity theory, or by careful photoelastic analysis. Peterson's *Stress Concentration Design Factors* (1966)[1] is an invaluable compilation of theoretical stress concentration factors that have been determined using these methods. More recently, the finite element method has been commonly used to determine elastic stress concentration factors for specific geometries.

The examination of elastic-plastic stress and strain states at notches occurred later. Several experimental investigations of strain states at holes in plates were motivated by the need for lightweight, fatigue resistant aircraft components. Griffith (1948) tested aluminum panels with a central circular hole in uniaxial cyclic loading, measuring strains using electromagnetic strain gages. Stresses were determined by comparing the measured strains with the stress-strain curve of uniaxial tension tests of aluminum coupons. Box (1951) also studied plates with holes, using lines inscribed on the surface of the plates to determine the strains.

These experimental investigations encouraged interest in analytical methods that could be used to estimate both the stress and strain states using only the material stress strain curve, notch geometry, and applied loads. Stowell (1950) used Griffith's data to propose a formula to estimate the stress concentration in the plastic range, and Hardrath and Ohman (1951)

[1]References are listed alphabetically at the end of the thesis, beginning on page 198.

modified Stowell's formula for use with other geometries, and compared the results with the experiments of both Griffith and Box, as well as their own experimental work on other notch geometries.

The most well known approximate formula for determining the stress and strain state at a notch was introduced by Neuber (1961) for the special case of a shear-strained prismatical body with a notch, and made of material obeying a nonlinear stress strain law. Neuber's interest in this problem was a natural extension of his work in the theory of elastic stress concentration of notched bodies (1946). For this notch, he showed that the geometrical mean value of the stress and strain-concentration factors at any stress-strain law is equal to the Hookian stress-concentration factor.

Experimental investigations of notch behavior continued with Durelli and Sciammarella (1963) who used the moiré method to determine strains near a circular hole in a plate subjected to uniaxial loading, and the Prandlt-Reuss relations to compute stresses from these strains. And later, Papirno (1971) compared the theories of Hardrath and Ohman with that of Neuber for results obtained from mildly notched thin plates subjected to monotonic uniaxial load, and concluded that the Neuber relation was more accurate.

Interest in determining notch stresses and strains increased as the strain-life theory of fatigue gained continued use. Although Neuber's rule, as it had become known by this time, was derived for a particular geometry and for monotonic loading, it had been modified for use with other notch geometries and for cyclic loading (Wetzel 1968, Topper *et al.* 1969). Although Neuber's rule was restricted to uniaxial loading, investigations of its applicability under various loading conditions were carried out by Lies *et al.* (1973), Wilson (1974), and Conle and Nowack (1977). Further modifications to Neuber's rule were suggested to account for notch constraint of notched round bars by Walker (1977), and to situations

involving net section plasticity by Seeger (1980). Neuber's rule had been incorporated in strain-life fatigue prediction methods, of which several have been described by Brose (1977), Landgraf *et al.* (1977), Dowling *et al.* (1977), and Socie *et al.* (1984). Tipton (1991) has presented a review article describing the modifications made to Neuber's rule for fatigue analysis, and Seeger (1977) has presented a comparison of several notch estimation techniques for notched plates.

An equivalent strain energy approach to calculate notch root stresses and strains from remote stresses and strains was introduced by Molski and Glinka (1981), compared with Neuber's rule for several notch types (Glinka 1985a and Glinka *et al.* 1988) and used to calculate notch stress-strain histories for cyclic loading (Glinka 1985b). This formula was proposed for uniaxial loading, and was shown to predict local strains more accurately than Neuber's rule.

Neuber's rule and Glinka's formula have also been investigated by Sharpe and co-workers for monotonic loading (Sharpe and Wang 1991 and Sharpe *et al.* 1992) and cyclic loading (Wang and Sharpe 1991) using a laser interferometric strain measurement technique (Guillot and Sharpe 1983 and Sharpe 1991) for notched plates subjected to uniaxial load. Sharpe's results indicated that Neuber's rule gave better results than Glinka's formula for plane stress, but that Glinka's formula was better for situations involving large constraint.

Concurrently, the local strain-life approach was extended to multiaxial states of loading using multiaxial fatigue damage models (several of which are reviewed by Garud 1981; see also Socie 1987), and methods were developed for determining the fatigue life of multiaxially stressed components (Bannantine 1989, Chen and Keer 1991). Such methods relied upon measuring strains, and using yield surface plasticity theory to calculate the stress state. As a natural consequence, the uniaxial notch stress and strain approximation techniques were extended to states of multiaxial loading. Experiments on proportionally loaded notched bars

were carried out by Hoffmann *et al.* (1985a) and methods to estimate notch stress and strain under these loading conditions were first considered by Hoffmann and Seeger (1985a-c, 1989a-b) and later by Klann *et al.* (1993). These methods extended stress and strain calculation to multiaxial loading by using Neuber's rule or other suitable approximate uniaxial load-notch formula in conjunction with assumptions about the multiaxial deformation of the material at the notch root. An extension of the energy density method to proportional loading was suggested by Ellyin and Kujawski (1989), and Moftakhar and Glinka (1992), with the analysis of the latter resulting in simultaneous algebraic equations to be solved for the determination of the notch stress and strain state. Use of the finite element method to calculate notch strains was employed by Tipton (1985) and Fash (1985) on the SAE notched shaft subjected to bending and torsion, although it was restricted to simple monotonic loading paths due to the computational complexity of nonlinear finite element analysis.

Nonproportional loading has been the most recent area to be explored. Amstutz *et al.* (1988) and Hoffmann *et al.* (1991) presented a method to estimate notch stresses and strains for nonproportional loading. In the method, the multiaxial loads are first separated, and notch root strain histories are calculated for the loads independently. A compatibility iteration is then used to increase the accuracy of the results. The calculations were compared with finite element analyses. More recently, Barkey *et al.* (1993) have introduced a method for estimating multiaxial notch strains in notched bars subjected to cyclic proportional and nonproportional loading, using the concept of a structural yield surface. With Glinka's rule as the basis of a load-notch plastic strain curve, the calculations agreed favorably for nonproportional tension-torsion tests of a notched steel bar. The work presented in this thesis will be comparison of the method with continued experimental work and with finite element analyses.

3 THE ANALYTICAL METHOD FOR STRAIN CALCULATION

The proposed method of calculating notch strains is based on observed strain behavior of notched bars and the extension of methods of calculating the strain state in a smooth bar subjected to multiaxial loading. Insight into this problem can be gained by examining surface strain states developed in smooth and notched bars of isotropic material subjected to uniaxial tension. The concept of a yield surface is used to calculate strain states in a smooth bar subjected to multiaxial loading, and similarly a concept of a structural yield surface will be used to calculate notch root strain states for a notched bar subjected to multiaxial loading. The discussions of rate independent yield surface plasticity will be taken from books on metal plasticity theory which include those of Hill (1956), Mendelson (1968), and Lubliner (1990), as well as cited literature.

In this chapter, smooth and notched bar behavior will be discussed, a specific yield criterion will be chosen to represent the structural yield surface, and appropriate equations will be presented for cases of a notched round bar subjected to tension (or bending) and torsion, and a plate with a hole subjected to biaxial loading.

3.1 Smooth bar and notched bar behavior

For a smooth bar of isotropic material subjected to uniaxial tension, σ_z, below the yield strength of the material, the elastic strains, ε_z^e, ε_x^e, and ε_y^e, can be determined from generalized Hooke's law

$$\varepsilon_x^e = \frac{1}{E}[-\nu\sigma_z] \qquad \varepsilon_y^e = \frac{1}{E}[-\nu\sigma_z] \qquad (3.1)$$

$$\varepsilon_z^e = \frac{1}{E}[\sigma_z]$$

specialized for a traction free surface of the bar.

For a given state of uniaxial stress, the elastic deformation in the loading direction is related to the stress and the modulus of elasticity, E, and the elastic deformation in the directions transverse to the loading directions are equal, and are related to the axial strain by Poisson's ratio, ν.

However, if the applied loads are large enough such that the yield strength of the material is exceeded, plastic flow occurs, and Hooke's law alone no longer applies. Total strains are then decomposed into elastic and inelastic strains. For metals, plastic deformation is usually assumed to be volume conserving, which can be expressed as zero dilatation of plastic normal strains

$$\varepsilon_x^p + \varepsilon_y^p + \varepsilon_z^p = 0. \tag{3.2}$$

In addition, for a smooth bar subjected to uniaxial tension, the plastic strains transverse to the loading directions are one-half the magnitude and of opposite sign of the strain in the loading direction, expressed as

$$\varepsilon_x^p = \varepsilon_y^p = -\frac{1}{2}\varepsilon_z^p. \tag{3.3}$$

The stress and strain states of the smooth bar subjected to uniaxial stress are shown in Figure 3.1.[1]

The uniaxial yield strength is extended to multiaxial states of stress by the assumption of a yield criterion, which is a function of all the stress components that, when satisfied, defines

[1]Figures are collected at the end of the thesis, beginning on page 56.

the onset of plastic flow. One such yield criterion for isotropic metals is that proposed by Mises (1928), although others are often used. If plotted in stress space, the yield criterion creates a surface, of which all combinations of stress are either inside, or on the surface, as determined by the scalar value from the yield criterion. Those states of stress inside the yield surface are elastic states of stress, in which case the strains are related to stress by Hooke's law, and those that lie on the yield surface are at the onset of plastic flow.

For states of stress on the yield surface, this defined yield criterion is treated as a potential function, and partial differentiation of this function determines the direction of plastic strain increments. A formula often used to relate the stress and plastic strain increments is the normality flow rule, which states that the plastic flow is normal to the yield surface in stress space.

For continuing applied loads, observed material work-hardening characteristics such as the Bauschinger effect are related to the yield surface by deforming or translating the yield surface in stress space, or by a combination of both. The choice of hardening rule depends on the complexity of the loading path, as well as the material hardening characteristics. These models have met with success in calculating strains for metals subjected to a variety of loading paths, and have been the object of much research in the last few decades (Lamba 1978, McDowell 1985a-b, 1987). Within the last several years, yield surface plasticity has been increasingly used in industry to determine stress or strain states for use with fatigue life prediction techniques (Chu 1991).

Analogous to the strain behavior developed during a uniaxial tension test of a smooth bar, the strain behavior developed during a uniaxial tension test of a notched bar will motivate a mathematical description of an assumed *structural* yield surface of the notched bar. During a uniaxial tension test of a notched bar in the elastic range, the notch root elastic strains may be

related to the applied loading through the use of a *nominal* stress, S_z, and elastic stress concentration factors. The nominal stress, as the name implies, is a fictitious quantity, and is obtained by dividing the applied load by an area. Any area may be used, so long as the stress concentration factors are defined accordingly.

Because the entire notch surface strain state must be known, a transverse stress concentration factor (K_z') must be determined for the notch, as well as the usual axial stress concentration factor (K_z). The transverse stress concentration factor is a measure of the elastic notch constraint, and is a function of the geometry of the notch. Both the axial and transverse stress concentration factors can be determined by careful finite element analysis or by experimental methods, or in some cases, from closed form calculations using the theory of elasticity (Neuber 1946).

Substitution of the non-zero components of local notch stress in terms of the nominal stress and stress concentration factors into Hooke's law for a traction free element at the notch root,

$$\varepsilon_x^e = \frac{1}{E}[K_z' - \nu K_z]S_z \qquad \varepsilon_y^e = \frac{1}{E}[-\nu(K_z' + K_z)]S_z \qquad (3.4)$$

$$\varepsilon_z^e = \frac{1}{E}[K_z - \nu K_z']S_z$$

results.

Equation (3.4) states that for a given applied axial nominal stress in which a multiaxial stress field develops in the notch root, elastic deformation will result in the directions transverse and normal to the notch root, as well as in the loading direction. However, because of the local multiaxial stress field, the transverse strains are no longer equal, and are no longer related to the axial strain (ε_z^e) only by Poisson's ratio, as is the case in the smooth bar.

Similar behavior occurs in the plastic range. The geometry of the notch, un-yielded material around the notch, and the local multiaxial notch stress state developed under an applied uniaxial nominal stress constrains the plastic deformation in the notch plane. For an isotropic metal, volume will still be conserved during plastic flow (equation (3.2)), so this will necessitate a larger plastic flow normal to the notch surface than in the notch plane ($\varepsilon_x^p < \varepsilon_y^p$), making the inequality

$$\varepsilon_x^p \neq \varepsilon_y^p \neq -\frac{1}{2}\varepsilon_z^p \tag{3.5}$$

hold in general. The stress and strain states for the notched bar are shown in Figure 3.2.

In terms of nominal stress, the notch root strains exhibit preferred directions of plastic flow, or anisotropy, when subjected to a uniaxial nominal stress. Therefore, the notch structure may be treated as an equivalent element of anisotropic material that has a yield surface that may be described by the developed theory of plasticity of anisotropic materials. In the following section, one particular anisotropic yield criterion will be chosen to represent the yield surface; however, other anisotropic yield criteria may be used as well, depending on preference, or requirements of the analysis.

3.2 Anisotropic metal plasticity

Hill's theory of plasticity of anisotropic materials (1948, 1989) was developed to model metals that exhibited preferred directions of plastic flow, and his main application was to study the forming of these metals. For this application, the material response was assumed to be of interest only for monotonic loading in the plastic range with negligible amounts of elastic strain, which are conditions under which the Lévy-Mises equations were developed for isotropic materials. However, in the previous section, it was demonstrated that notch root

strains also exhibit directional behavior due to geometric constraint. Therefore, if the nature of the notch is treated as an intrinsic material property, Hill's theory of anisotropic metal plasticity can be used for this application as well. This section outlines Hill's theory of anisotropic metal plasticity and presents the theory in a suitable manner for implementation in an incremental cyclic plasticity approach.

3.2.1 A yield criterion

A material exhibiting directionally dependent properties is considered to be anisotropic. In Hill's theory, these directionally dependent properties are yield strengths that vary with direction, and hence induce preferred directions of plastic flow in the material. To determine the onset of plastic flow for a directionally dependent material, Hill introduced a yield criterion which is

$$\begin{aligned} 2f(S_{ij}) \equiv F(S_y - S_z)^2 + G(S_z - S_x)^2 + H(S_x - S_y)^2 \\ +2LS_{yz}^2 + 2MS_{zx}^2 + 2NS_{xy}^2 = 1, \end{aligned} \tag{3.6}$$

where the coefficients F, G, H, L, M and N are determined from the current values of the directional yield strengths X, Y, Z, R, S, and T associated with the directions of the stress components S_x, S_y, S_z, S_{yz}, S_{zx}, and S_{xy}. These relations are:

$$\begin{aligned} 2F &= \frac{1}{Y^2} + \frac{1}{Z^2} - \frac{1}{X^2} & 2L &= \frac{1}{R^2} \\ 2G &= \frac{1}{Z^2} + \frac{1}{X^2} - \frac{1}{Y^2} & 2M &= \frac{1}{S^2} \\ 2H &= \frac{1}{X^2} + \frac{1}{Y^2} - \frac{1}{Z^2} & 2N &= \frac{1}{T^2}. \end{aligned} \tag{3.7}$$

The values of X, Y, Z, R, S, and T are all determined from the initial values of the uniaxial or simple shear yield strengths, X_0, Y_0, Z_0, R_0, S_0, and T_0, and a hardening parameter.

Hill's yield criterion for anisotropic materials is a generalization of the Mises yield criterion for isotropic materials, and there are some restrictions to its use. During the development of the criterion, it was assumed that the material possesses three mutually orthogonal planes of symmetry at every point, and the yield criterion is in the present form only when the Cartesian coordinates are along the intersection of these planes, known as the principal directions of anisotropy. The assumption of the existence of the planes of symmetry means that elastic coupling between the shear and normal terms is not allowed in these directions.

3.2.2 The normality flow rule

As in Hill's derivation of Lévy-Mises type equations for a rigid plastic material (Hill 1956), the yield criterion will be treated as a plastic potential function and the normality flow rule,

$$d\varepsilon_{ij}^{p} = d\lambda \frac{\partial f}{\partial S_{ij}}, \tag{3.8}$$

can be used in the principal directions of anisotropy to develop equations analogous to the Prandtl-Reuss equations of plasticity for isotropic materials. The partial derivatives in the flow rule must be evaluated noting that for purposes of differentiation $S_{ij} \neq S_{ji}$, for $i \neq j$, and are presented as follows:

$$\frac{\partial f}{\partial S_x} = H(S_x - S_y) - G(S_z - S_x) \qquad \frac{\partial f}{\partial S_{yz}} = LS_{yz} \qquad \frac{\partial f}{\partial S_{zy}} = LS_{zy}$$

$$\frac{\partial f}{\partial S_y} = F(S_y - S_z) - H(S_x - S_y) \qquad \frac{\partial f}{\partial S_{xz}} = MS_{xz} \qquad \frac{\partial f}{\partial S_{zx}} = MS_{zx} \qquad (3.9)$$

$$\frac{\partial f}{\partial S_z} = G(S_z - S_x) - F(S_y - S_z) \qquad \frac{\partial f}{\partial S_{xy}} = NS_{xy} \qquad \frac{\partial f}{\partial S_{yx}} = NS_{yx}.$$

These partial derivatives, when substituted into the normality flow rule, give the six unique components of plastic strain increment tensor:

$$d\varepsilon_x^p = d\lambda[H(S_x - S_y) - G(S_z - S_x)] \qquad d\varepsilon_{yz}^p = d\lambda[LS_{yz}]$$

$$d\varepsilon_y^p = d\lambda[F(S_y - S_z) - H(S_x - S_y)] \qquad d\varepsilon_{xz}^p = d\lambda[MS_{xz}]$$

$$d\varepsilon_z^p = d\lambda[G(S_z - S_x) - F(S_y - S_z)] \qquad d\varepsilon_{xy}^p = d\lambda[NS_{xy}]. \qquad (3.10)$$

Built into this theory is the assumption that volume is conserved during plastic flow, or that equation (3.2) holds identically.

3.2.3 A hardening parameter

The plasticity constant $d\lambda$ can be obtained if an assumption about the work-hardening behavior is made. Hill's assumption (Hill 1956) was that if there exists a pronounced preferred orientation in the material, then this orientation will remain in the same directions and in the same relative magnitude. If this assumption holds true, $X = hX_0, Y = hY_0, \ldots$, and from equation (3.7), $F = F_0/h^2, G = G_0/h^2, \ldots$, where the subscript zero denotes the initial value and "h is a parameter increasing monotonically from unity and expressing the amount

of hardening.'' These equations state that as hardening proceeds, the value of h increases, the yield strengths increase from their initial value, and the coefficients decrease from their initial value, thereby maintaining the equality in equation (3.6).

Hill (1956) then assumed an equivalent stress, and derived an expression for an equivalent strain, and proved a relationship between the equivalent quantities. These expressions are summarized as follows:

$$\overline{S} = \left(\frac{3}{2}\right)^{\frac{1}{2}} \frac{h}{(F_0 + G_0 + H_0)^{\frac{1}{2}}} \tag{3.11}$$

$$h = [F_0(S_y - S_z)^2 + G_0(S_z - S_x)^2 + H_0(S_x - S_y)^2 + 2L_0 S_{yz}^2 + 2M_0 S_{zx}^2 + 2N_0 S_{xy}^2]^{\frac{1}{2}} \tag{3.12}$$

$$\begin{aligned} d\overline{\varepsilon}^p = \left(\frac{2}{3}\right)^{\frac{1}{2}} (F_0 + G_0 + H_0)^{\frac{1}{2}} [F_0 & \left(\frac{G_0 d\varepsilon_y^p - H_0 d\varepsilon_z^p}{F_0G_0 + G_0H_0 + H_0F_0}\right)^2 + G_0\left(\frac{H_0 d\varepsilon_z^p - F_0 d\varepsilon_x^p}{F_0G_0 + G_0H_0 + H_0F_0}\right)^2 \\ & + H_0\left(\frac{F_0 d\varepsilon_x^p - G_0 d\varepsilon_y^p}{F_0G_0 + G_0H_0 + H_0F_0}\right)^2 + \frac{2d\varepsilon_{yz}^{p\,2}}{L_0} + \frac{2d\varepsilon_{zx}^{p\,2}}{M_0} + \frac{2d\varepsilon_{xy}^{p\,2}}{N_0}]^{\frac{1}{2}} \end{aligned} \tag{3.13}$$

$$d\lambda = \overline{S}\, d\overline{\varepsilon}^p. \tag{3.14}$$

The equivalent quantities can be related to the uniaxial stress-plastic strain relationship as follows:

$$\overline{S} = \left(\frac{3}{2}\right)^{\frac{1}{2}} \left(\frac{F_0 + G_0}{F_0 + G_0 + H_0}\right)^{\frac{1}{2}} S_z \tag{3.15}$$

$$d\overline{\varepsilon}^p = \left(\frac{2}{3}\right)^{\frac{1}{2}} \left(\frac{F_0 + G_0 + H_0}{F_0 + G_0}\right)^{\frac{1}{2}} d\varepsilon_z^p. \tag{3.16}$$

The term $d\lambda$ is determined for a state of applied load, S_{ij}, from equation (3.14) using $\overline{S}$ from equation (3.11) and $d\overline{\varepsilon}^p$ from the equivalent stress-plastic strain curve as indicated in Figure 3.3. The equivalent behavior is determined, in turn, from equations (3.15) and (3.16) and the uniaxial behavior of the anisotropic material.

3.2.4 Proportional loading

A set of closed form equations relating proportionally applied loads to plastic strains can now be determined without further assumptions. These equations can be developed in the same manner as presented in Mendelson (1983) for the determination of the Hencky equations from the flow equations of Prandtl-Reuss. If $S_{ij} = KS_{ij}^0$, where S_{ij}^0 is an arbitrary reference state of nonzero stress, and K is a monotonically increasing function of time, then $h = Kh_0$, and $F, \ldots = F_0/K^2h_0^2, \ldots$, and it can be seen that the explicit dependence on the stress state drops out of the stress-plastic strain increment relations. The equations can be integrated, and from it can be concluded that the plastic strains are a function of only the current state of stress and not of the loading path for proportional loading. These equations are stated in terms of the hardening parameter h, and the initial coefficients of anisotropy:

$$\begin{aligned}
\varepsilon_x^p &= \frac{\lambda}{h^2}[H_0(S_x - S_y) + G_0(S_x - S_z)] & \varepsilon_{yz}^p &= \frac{\lambda}{h^2} L_0 S_{yz} \\
\varepsilon_y^p &= \frac{\lambda}{h^2}[F_0(S_y - S_z) + H_0(S_y - S_x)] & \varepsilon_{zx}^p &= \frac{\lambda}{h^2} M_0 S_{zx} \\
\varepsilon_z^p &= \frac{\lambda}{h^2}[G_0(S_z - S_x) + F_0(S_z - S_y)] & \varepsilon_{xy}^p &= \frac{\lambda}{h^2} N_0 S_{xy},
\end{aligned} \tag{3.17}$$

where $\lambda = \overline{S}\,\overline{\varepsilon}^p$.

3.2.5 Nonproportional loading

The analysis of nonproportional loading requires the use of an incremental approach to determine the plastic strains, as they will generally be path dependent. The Bauschinger effect and effects of work-hardening under nonproportional loading must also be taken into account by the choice of a suitable hardening rule. Derivations of the incremental stress-incremental strain relations will be presented in this section, and a specific kinematic work-hardening model will be chosen to complete the description of the incremental plasticity model.

Plastic strain increment relations

For a given uniaxial material response of stress versus plastic strain, an instantaneous plastic modulus, E_p, can be found (Figure 3.4). It is necessary to relate the plastic modulus to the slope of the equivalent stress-equivalent plastic strain curve, $\overline{E}_p$, shown in Figure 3.3.

For the equivalent stress-strain curve,

$$\overline{E}_p = \frac{d\overline{S}}{d\overline{\varepsilon}^p}. \tag{3.18}$$

From Hill's equations (3.15-3.16) reduced for uniaxial stress, S_z, the equivalent plastic modulus becomes:

$$\overline{E}_p = \frac{3}{2}\left(\frac{F_0+G_0}{F_0+G_0+H_0}\right)\frac{dS_z}{d\varepsilon_z^p}. \tag{3.19}$$

The ratio $dS_z/d\varepsilon_z^p$ is the plastic modulus of the uniaxial curve, E_p, which when substituted into equation (3.19) yields:

$$\overline{E}_p = \frac{3}{2}\left(\frac{F_0+G_0}{F_0+G_0+H_0}\right)E_p. \tag{3.20}$$

The equivalent plastic modulus will be used to determine the plasticity constant $d\lambda$.

Re-arranging equation (3.18) and substituting into equation (3.14), yields

$$d\lambda = \frac{\overline{S}\,d\overline{S}}{\overline{E}_p}. \tag{3.21}$$

The expression for the numerator of equation (3.21) can be obtained from

$$\overline{S}\,d\overline{S} = d\left(\frac{1}{2}\overline{S}^2\right) = \frac{1}{2}\frac{\partial}{\partial S_{kl}}\left[\frac{3}{2}\frac{1}{(F_0+G_0+H_0)}h^2\right]dS_{kl}. \tag{3.22}$$

One-half the derivative of the square of the hardening parameter with respect to the stresses is

$$\begin{aligned}\frac{1}{2}\frac{\partial}{\partial S_{kl}}(h^2)dS_{kl} &= F_0(S_y-S_z)dS_y - F_0(S_y-S_z)dS_z + G_0(S_z-S_x)dS_z \\ &-G_0(S_z-S_x)dS_x + H_0(S_x-S_y)dS_x - H_0(S_x-S_y)dS_y \\ &+L_0S_{yz}dS_{yz} + L_0S_{zy}dS_{zy} + M_0S_{zx}dS_{zx} + N_0S_{xy}dS_{xy} + N_0S_{yx}dS_{yx},\end{aligned} \tag{3.23}$$

thereby making the expression for the proportionality constant,

$$d\lambda = \frac{3}{2}\frac{1}{F_0+G_0+H_0}\left[\frac{1}{2}\frac{\partial}{\partial S_{kl}}(h^2)dS_{kl}\right]\frac{1}{\bar{\bar{E}}_p} \tag{3.24}$$

for a given state of stress, S_{ij}, where the term in brackets is given by equation (3.23).

Finally, stating the plastic strain increments in terms of the initial coefficients of anisotropy and the hardening parameter, the following results:

$$\begin{aligned}
d\varepsilon_x^p &= \frac{d\lambda}{h^2}[H_0(S_x-S_y)+G_0(S_x-S_z)] & d\varepsilon_{yz}^p &= \frac{d\lambda}{h^2}L_0S_{yz} \\
d\varepsilon_y^p &= \frac{d\lambda}{h^2}[F_0(S_y-S_z)+H_0(S_y-S_x)] & d\varepsilon_{zx}^p &= \frac{d\lambda}{h^2}M_0S_{zx} \\
d\varepsilon_z^p &= \frac{d\lambda}{h^2}[G_0(S_z-S_x)+F_0(S_z-S_y)] & d\varepsilon_{xy}^p &= \frac{d\lambda}{h^2}N_0S_{xy}.
\end{aligned} \tag{3.25}$$

The kinematic work-hardening model of Mróz

The work-hardening model of Mróz (1967) was developed to describe deformation induced anisotropy for complex nonproportional loading paths. Several variations now exist (Krieg 1975 and Chu 1987, 1992), but the basic concept of all the models is that there exists a "field of work-hardening moduli" that influence the work-hardening of the material. The model that will be described here is the simplest of the models, and assumes that the field of moduli can be described by the same functional relationship as the yield criterion. The surfaces will be allowed to translate in stress space, but will not be allowed to rotate, expand, or contract.

The hardening rule as first implemented by Mróz used a number of discrete yield surfaces representing the field of constant work-hardening moduli in stress space. Following that model, the model used here will model the anisotropy of deformation by the movement of geometrically similar and initially concentric surfaces in stress space. The initial surface in the stress space is the initial yield surface, and further surfaces are activated at higher values of equivalent stress. The surfaces move in such a manner that the currently active surface (f_l) translates in stress space along a path parallel to a line joining the active surface normal (n_l) at the stress point and a point located on the next surface (f_{l+1}) with the same normal (n_{l+1}), as illustrated in Figure 3.5.

The point on the next surface may be found by using the homogeneity of the yield function. Denoting the currently active surface by l and the next active surface by l+1, the expression for the point on the next surface is

$$S_{ij}^{(l+1)} - \alpha_{ij}^{(l+1)} = \frac{\overline{S}_0^{(l+1)}}{\overline{S}_0^{(l)}} (S_{ij}^{(l)} - \alpha_{ij}^{(l)}), \tag{3.26}$$

where α_{ij} represents the center of each yield surface, and is often called the back stress tensor.

The increment of translation of the currently active surface is given by

$$d\alpha_{ij}^{(l)} = \frac{d\mu}{\overline{S}_0^{(l)}} \left[\left(\overline{S}_0^{(l+1)} - \overline{S}_0^{(l)} \right) S_{ij}^{(l)} - \left(\alpha_{ij}^{(l)} \overline{S}_0^{(l+1)} - \alpha_{ij}^{(l+1)} \overline{S}_0^{(l)} \right) \right], \tag{3.27}$$

where the quantity $d\mu$ is given by:

$$d\mu = \frac{\frac{\partial f}{\partial S_{ij}} dS_{ij}}{\frac{\partial f}{\partial S_{kl}} (S_{kl}^{(l+1)} - S_{kl}^{(l)})}. \tag{3.28}$$

and is found by invoking the consistency condition, or the need for the current state of stress (at the onset of plastic flow) to be located on the active yield surface.

Because the yield surfaces are allowed to translate in stress space, the expressions for the yield criterion and strain increment will now be expressed in terms of the difference of the stress state, S_{ij}, and the center of the active yield surface, α_{ij}^{l}, and will be denoted by ξ_{ij}^{l}, where $\xi_{ij}^{l} = S_{ij} - \alpha_{ij}^{l}$. This expression can be directly substituted into the yield criterion and stress-strain increment relations as the back stress tensor is not a function of stress and so does not affect the differentiation involved in determining the stress-strain increment relations.

3.3 Specialization for a notched round bar

This section outlines the application of Hill's plasticity theory to a notched bar. The notched bar will be treated as an anisotropic material subjected to the nominal stresses of the bar, calculated elastically based on the net section. The yield criterion and equations for strain increments will be expressed in terms of the variable ξ_{ij}^{l}, where $\xi_{ij}^{l} = S_{ij} - \alpha_{ij}^{l}$ and the superscript l denotes the active yield surface. In the remainder of this chapter the equations will be stated in terms of the active yield surface, and so the superscript l will be omitted.

3.3.1 Elastic notch behavior

For states of notch stress for which the notch material is still in the elastic range, the strains can be determined by using generalized Hooke's law and by considering the multiaxial stress

state at the notch root. As mentioned in Section 3.1, these strains can be expressed in terms of the axial nominal stress and axial and transverse stress concentration factors (K_z and K_z', respectively) and also the torsional nominal stress and shear stress concentration factor (K_{xz}). The equations stated in terms of stress and strain increments are

$$d\varepsilon_x^e = \frac{1}{E}[K_z' - \nu K_z]dS_z \qquad d\varepsilon_y^e = \frac{1}{E}[-\nu(K_z' + K_z)]dS_z$$
$$d\varepsilon_z^e = \frac{1}{E}[K_z - \nu K_z']dS_z \qquad d\varepsilon_{xz}^e = \frac{1+\nu}{E}K_{xz}dS_{xz} \tag{3.29}$$

and in terms of total stresses and strains are

$$\varepsilon_x^e = \frac{1}{E}[K_z' - \nu K_z]\xi_{\sigma z} \qquad \varepsilon_y^e = \frac{1}{E}[-\nu(K_z' + K_z)]\xi_{\sigma z}$$
$$\varepsilon_z^e = \frac{1}{E}[K_z - \nu K_z']\xi_{\sigma z} \qquad \varepsilon_{xz}^e = \frac{1+\nu}{E}K_{xz}\xi_{\sigma xz}. \tag{3.30}$$

3.3.2 The yield criterion

Simplification of Hill's yield criterion is possible if a traction free notch root element on the surface of the shaft is considered. Further reduction is possible if the shaft is restricted to only torsion and tension (or bending) nominal loading. In these instances, the yield criterion becomes

$$2f(\xi_{\sigma ij}) = (F+G)\xi_{\sigma z}^2 + 2M\xi_{\sigma xz}^2. \tag{3.31}$$

The hardening parameter also reduces, to

$$h = [(F_0+G_0)\xi_{\sigma z}^2 + 2M_0\xi_{\sigma zx}^2]^{\frac{1}{2}}. \tag{3.32}$$

An assumption made about the hardening rule was that yield strengths remained in the same proportion, or equivalently, that the coefficients of anisotropy remain in proportion. The general applicability of this assumption will be discussed after the coefficients of anisotropy have been determined in terms of the stress concentration factors of the notched bar.

3.3.3 Uniaxial notch behavior

The equivalent stress-plastic strain curve required to determine the behavior of the material will be based on a uniaxial nominal stress-notch plastic strain curve. The uniaxial notch curve can be determined from experiment, finite element analysis, or from one of the uniaxial notch strain approximation formulas, such as the theories of Neuber (1961), or Glinka (1985), with suitable corrections for notch constraint as suggested by Dowling (1977), and corrections for net section plasticity, suggested by Seeger (1980).

Care should be taken to separate the plastic part and the recoverable part of the total notch strain, because the plastic coupling term, $d\lambda$, is highly influenced by the compliance of the nominal stress-notch root *plastic* strain response.

3.3.4 Determination of coefficients of anisotropy

The coefficients of anisotropy can be determined from the nominal yield strengths of the shaft, which can in turn be found from the stress concentration factors of the notch and the yield strength of the material, and additional knowledge or assumptions about the plastic constraint of the notch. The initial nominal yield strengths will be taken as the load that causes yield at the notch root. If the Mises yield criterion (1928) is assumed to hold at the notch root, then the axial nominal yield strength, Z_0, and the torsional nominal yield strength, S_0, become

$$Z_0 = \frac{\sigma_0}{\sqrt{K_z^2 - K_z K_z' + K_z'^2}} \tag{3.33}$$

$$S_0 = \frac{\sigma_0}{\sqrt{3}\,K_{xz}}. \tag{3.34}$$

Any definition of nominal yield strength and a consistent definition of the stress concentration factors ensure that the yield criterion and hardening parameter are independent of the definition of the nominal area, as the product $K_i S_i$ appears in these formulas from the product of the coefficient of anisotropy and the stress term.

The nominal yield strengths transverse to the loading direction and normal to the surface of the notch can be adjusted to give the proper amount of plastic constraint in the respective directions as determined by a uniaxial analysis. For example, a smooth bar in tension will have equal amounts of plastic flow in the normal and transverse directions. In this case, the nominal yield strengths in these directions will both be equal to the base yield strength of the material. For bars with mild notches in uniaxial tension, this will be approximately the case. In sharp or deep notches, plastic flow is almost entirely constrained to flow in the normal direction of the surface of the notch, and in axial direction. For this case, the coefficient of anisotropy G_0 can be set equal to zero, and the proper yield strengths can be determined.

The validity of the assumption that the coefficients of anisotropy remain in the same proportion as determined by the scalar hardening, h, may now be discussed. The coefficients of anisotropy F, G, and M in equation (3.31) can be written in terms of the nominal yield

strengths, which can in turn be written in terms of the stress concentration factors of the notch through the use of equations (3.33-34). Doing so, and representing the denominator of equation (3.33) by K_q,

$$2f(\xi_{ij}) = \frac{K_q^2}{\sigma_e}\xi_{zz}^2 + \frac{3K_{xz}^2}{\sigma_e}\xi_{xz}^2 \tag{3.35}$$

becomes the expression for the yield criterion.

If σ_e represents the current value of the local equivalent notch stress, then it is readily apparent that the assumption that the coefficients of anisotropy remain in the same proportion is equivalent to the assumption that the current values of stress concentration remain in the same proportion. This assumption should hold approximately true until the notch is grossly distorted and the bar approaches general net section plasticity.

In addition to this, it is seen that as hardening proceeds the coefficients of anisotropy must decrease. Because the local notch root equivalent stress, σ_e, increases, the result is that the stress concentration factors decrease with increasing applied load, which is a commonly observed phenomenon of notch root deformation.

3.3.5 Nominal stress-notch strain relations

Reduced equations for notched shafts are presented in this section for a traction free notch root surface element for proportional and nonproportional loading. Total strains will be expressed as the sum of the elastic and plastic strains as

$$\varepsilon_x = \frac{1}{E}[K_z' - \nu K_z]\xi_{\sigma z} + \lambda[-G\xi_{\tau z}]$$

$$\varepsilon_y = \frac{1}{E}[-\nu(K_z' + K_z)]\xi_{\sigma z} + \lambda[-F\xi_{\tau z}] \qquad (3.36)$$

$$\varepsilon_z = \frac{1}{E}[K_z - \nu K_z']\xi_{\sigma z} + \lambda[(G+F)\xi_{\tau z}]$$

$$\varepsilon_{xz} = \frac{1+\nu}{E} K_{xz}\xi_{xz} + \lambda M\xi_{xz}$$

for the case of proportional loading, or strain increments as

$$d\varepsilon_x = \frac{1}{E}[K_z' - \nu K_z]dS_z + d\lambda[-G\xi_{\tau z}]$$

$$d\varepsilon_y = \frac{1}{E}[-\nu(K_z' + K_z)]dS_z + d\lambda[-F\xi_{\tau z}] \qquad (3.37)$$

$$d\varepsilon_z = \frac{1}{E}[K_z - \nu K_z']dS_z + d\lambda[(G+F)\xi_{\tau z}]$$

$$d\varepsilon_{xz} = \frac{1+\nu}{E} K_{xz}dS_{xz} + d\lambda M\xi_{xz}$$

for nonproportional loading.

3.3.6 Determination of notch stresses

Once the strain state at the notch has been determined, the notch stresses can be found by using the calculated strains and the theory of plasticity of isotropic materials. Such procedures have been described by Bannantine (1989), for example. Because of the notch constraint, however, the entire strain state must be used to determine the stresses.

3.4 Specialization for a plate with a hole

In this section, the method presented for determining strains at the stress concentrator will be specialized for a plate with a hole. The goal of the simplified analysis is to calculate the strain state at the hole when the plate is subjected to time varying loads, including out-of-phase edge loading, from a minimum amount of input data. The available input data will be restricted to the elastic stress concentration factors and an elastic-plastic analysis to determine the load-notch plastic strain curve. In addition to this data, the boundary conditions at the hole must be explicitly stated and the nature of the local elastic stress state must be determined. Finally, a relationship that relates the applied remote loading to this stress state must be determined.

3.4.1 Hole boundary conditions

The inside edge of the hole and the top and bottom surface of the plate are traction free surfaces. Therefore, the only nonzero stress that is allowed on a small element at the inside edge of the hole is in the hoop direction, meaning that every point on the inside edge of the hole is subjected to uniaxial tension, for any combination of remote plate edge loads. The local stress state is illustrated in Figure 3.6.

This uniaxial stress state at the hole will be expected to produce a simple Poisson contraction in the radial direction when the local stress is still in the elastic range, and volume conserving plastic flow in the plastic range, with the radial and normal plastic strains equal to one-half the value and of opposite sign of the hoop strain. Because there are no preferred directions of plastic flow at the hole for this geometry, an isotropic yield criterion, such as the Mises yield criterion, may be used to form the basis of a constitutive model for the plate with a through hole. As discussed previously, the Hill yield criterion reduces to the Mises yield criterion for

special choices of the coefficients of anisotropy, and will be used here as well. For thick plates with a hole, plastic flow in the radial or through thickness directions may vary appreciably along the thickness of the plate, and an analysis similar to that presented in Section 3.3 using an anisotropic yield criterion may be used to determine the local strains.

3.4.2 Nominal stress-equivalent stress relationship

A relationship must be presented that relates the remote loading to the local stress state. The new equivalent, or nominal stress will be a fictitious stress that is calculated by the remote, elastically calculated edge stresses (S_x and S_y) and the consistently defined stress concentration factors of the hole (K_x and K_y). The form of this stress will be the same as that presented by Hoffmann *et al.* (1991) for an analysis of the same problem, and takes the form of

$$S_{nom} = K_y S_y + K_x S_x \tag{3.38}$$

for the position along the x-axis at the edge of the hole.

The value of K_y is the elastic stress concentration of a load applied in the y-direction, and K_x is the elastic stress concentration at the same point for a load applied in the x-direction. This stress term is then used to construct a uniaxial nominal stress-notch plastic strain curve.

3.4.3 Determination of notch stresses

Because the material at the notch root is not constrained for this notch, the local stress may determined from the previously calculated notch strain in a straight forward manner by comparison with the uniaxial smooth specimen stress-strain curve of the material.

4 RESULTS OF HOFFMANN AND SEEGER

Hoffmann and Seeger (1989) presented a method for estimating the notch root stress and strain state for a notched round bar subjected to proportional nominal loading. The primary assumption in this work was that the ratio of the principal notch strains were constant and equal to the elastic strain ratio. However, they also recognized that this cannot be true for all notches, as can be demonstrated by the results of a uniaxial tension test of a smooth bar, effectively a very mild notch.

Recalling the discussion of the uniaxial tension test in Section 3.1, the ratio of the principal strains of a smooth bar in uniaxial tension in the elastic range is the negative of Poisson's ratio. In the plastic range, this value approaches $-1/2$, when plastic strains dominate. A smooth transition occurs between these limits, the rate of transition depending on the compliance of the material's uniaxial stress-strain curve.

For notched bars in uniaxial tension, the same phenomenon occurs. The elastic ratio is the elastic notch constraint and the plastic limit is the amount of plastic notch constraint. For sharp or highly constrained notches, there may be little difference between the two limiting values. Thus, in these cases the principal strains stay approximately constant.

The method developed in Chapter 3 can capture the behaviors of smooth bars to highly constrained notches quite readily by the proper selection of coefficients of anisotropy. A method of determining the notch behavior for a known variation of principal strains under proportional loading was also presented by Hoffmann and Seeger (1985c). So, the method developed here for proportional loading is equivalent to that of Hoffmann and Seeger, given the same load-notch strain approximation rule and elastic and plastic notch constraint.

Insight into the presented method for notch strain calculation and Hoffmann and Seeger's method can be obtained by examining the calculated principal strain behavior. An expression for the principal strains can be determined from the closed form equations presented for the case proportional nominal tension and torsion, and is

$$\varepsilon_{1,2}=\frac{S_z}{2}\left[\frac{(1-\nu)}{E}(K_z+K_z')+\frac{\lambda}{h^2}F_o\right]\pm\sqrt{\frac{S_z^2}{4}\left[\frac{(1+\nu)}{E}(K_z-K_z')+\frac{\lambda}{h^2}(F_o+2G_o)\right]^2+S_{xz}^2\left[\frac{(1+\nu)}{E}K_{xz}+\frac{\lambda}{h^2}M_o\right]^2}. \quad (4.1)$$

In the elastic range, the terms containing λ do not apply, and the ratio of the strains is constant. In the elastic-plastic range, the ratio will begin to deviate from this value at a rate dependent on the term λ. This term depends on the relative compliance of the of the equivalent nominal stress-notch plastic strain curve.

Experiments were conducted by Hoffmann *et al.* (1985a) on three types of notched steel bars. The bars contained either a mild surface notch, sharp surface notch, or a sharp deep notch, all of which are illustrated in Figure 4.1, taken from the report Kerbbeanspruchungen I (Hoffmann *et al.* 1985a). The elastic stress concentration factors for each notch are listed in Table 4.1. Pure bending and proportional bending and torsion were among the loading cases tested. Figures 4.2-4.4 contain the results of the experiments and calculations for simple bending and proportional bending and torsion for the three notch types. In these figures, solid lines represent finite element calculations, dashed lines represent their approximation method (*Näherungslösung*), and the symbols represent the experimental results (*Versuche*).

The strain ratio plots of the simple bending experiments in Figures 4.2b-4.4b illustrate the effect of notch severity on the constraint of plastic flow. The principal strain ratio on the surface of the shaft ($\varepsilon_2/\varepsilon_1$) begins at the value determined by the elastic stress concentration factors of the notch, and approaches the limiting value of the ratio of the plastic strains. For

the mild notch, this limiting plastic value is around –0.3, while it is almost zero for the sharp notches. Similarly, the strain ratio plots of the experimental results (indicated by symbols) for the combined loading cases in Figures 4.2c-4.4c show that there is variation in the strain ratio for the mild notch, but very little variation in the strain ratio for the sharp notches, up to about 1% principal strain.

The experimental data obtained from the simple bending analyses were used with the newly developed equations for proportional loading to compare with the experimental results of the combined loading cases. The nominal stress-notch plastic strain curve was approximated from the experimental simple bending results (Figures 4.2b-4.4b), the elastic stress concentration factors were used to determine the amount of elastic constraint, and the strain ratio at large values of plastic strain from the simple bending experimental results were used to determine the amount of plastic notch constraint. The elastic and plastic notch constraint determine the coefficients of anisotropy.

The results of the calculations using the newly developed method for the combined loading cases for each notch type are presented in Figure 4.5. The piece wise nature of the calculated results is due to the crude approximation of the nominal stress-notch plastic strain response from the simple bending experiments. The calculations of the strain ratio $\varepsilon_2/\varepsilon_1$ (indicated by the solid line) for the mild notch (Figure 4.5a) bends slightly and the sharp notches (Figure 4.5b-c) shows very little deviation from the elastic constraint ratio. This is because of the amount of plastic notch constraint determined from the simple bending analyses. The essential character of the experimental results are captured well by newly developed equations for these notches, up to at least 1% strain, where the net section is approaching general yield (indicated by S_p in Figures 4.2c-4.4c). The experimental results beyond this strain level indicate that the strain ratio varies even for the sharp notches, but the significance of that variation may be lost in a strain-based fatigue life prediction at such high strain levels.

5 SAE NOTCHED SHAFT

Fash (1985) used an elastic-plastic finite element analysis to determine multiaxial notch strains of the proportionally loaded notched steel bar used in the SAE multiaxial test program (Downing and Galliart 1985). Total strains were reported for the notch root of the shaft subjected to monotonically applied proportional bending and torsion. This chapter describes the implementation of the proposed method of calculating notch strains to this notched shaft, and compares the results with Fash's finite element analysis.

5.1 Determination of notch properties

Elastic stress concentration factors were determined from Fash's elastic simple bending and torsion analyses. The specimen geometry and Fash's finite element mesh are in Figure 5.1 (taken from Fash's thesis). The axial stress concentration factor (K_z), transverse stress concentration factor (K_z'), and shear stress concentration factor (K_{xz}) were found using Fash's results and equation (3.30), and are

$$\begin{aligned} K_z &= 1.63 \\ K_z' &= 0.30 \\ K_{xz} &= 1.39. \end{aligned} \tag{5.1}$$

The initial nominal yield strengths in the axial direction (Z_0) and the torsional nominal yield strength (S_0), were found from equations (3.33) and (3.34) respectively. The initial coefficients of anisotropy were then determined from equation (3.7), and the observation that the ratio of the plastic strains in the transverse and normal directions ($\varepsilon_x^p:\varepsilon_y^p$) from the elastic-plastic simple bending analysis was approximately 0.42:1. The nominal stress-notch plastic strain curve was determined from a curve fit of the axial nominal stress-axial plastic

strain results from the same finite element analysis. The curve fit and the assumption of the plastic constraint are illustrated in Figure 5.2a. These were the only data used to determine the coefficients of anisotropy.

5.2 Comparison of results

Figures 5.2a-h are the results of the calculations. The graphs are of strain components versus Mises equivalent nominal stress

$$S_q = (S_z^2 + 3S_{xz}^2)^{1/2}, \tag{5.2}$$

where S_z and S_{xz} are the nominal axial and nominal shear stresses, respectively.

The strain components for this shaft are defined in Figure 5.1b, and are ε_{xx}, ε_{yy}, ε_{zz}, and γ_{xz} for the transverse, normal, axial, and shear directions, respectively. The solid circles represent the finite element results of Fash, and the lines are calculations made using the equations developed for proportional loading. The dotted line in each figure represents the level of load above which Fash conducted elastic-plastic finite element analyses (E-P FEA).

The close match to the finite element results in Figure 5.2a is expected, since this data was fit to determine the nominal stress-notch plastic strain curve, and the amount of plastic constraint. The results for the multiaxial nominal loading cases are in very good agreement both qualitatively and numerically for all of the cases examined.

The plastic constraint assumption used here is different than that presented previously (Barkey *et al.* 1993), in which the ratio of the plastic strains in the transverse and normal directions were assumed to be 1:1. Because the notch is mild, either assumption yields reasonable results, although the current assumption matches the finite element results more

closely for the strains in the transverse and normal directions.

6 THE FULLY NOTCHED ROUND SHAFT

In this chapter, experimental results of a proportionally and nonproportionally loaded notched shaft are compared with calculations using nonlinear finite element analysis and the proposed simplified method for calculation of notch strains. Calculations using the finite element method and the approximate method are also compared for loading paths that were not examined by experiment, and for material properties less compliant and more compliant than used in the experiments.

6.1 Experimental setup

A solid 1070 steel shaft with a circumferential notch was selected for testing. The net section was 25.4 mm in diameter and the notch radius was 12.7 mm. The specimen geometry and dimensions are shown in Figure 6.1. This is a relatively mild notch that has stress concentration factors that would be typical of notched components such as those found in many ground vehicle applications.

The smooth specimen uniaxial material properties were determined by data provided by Jiang (1992), and are listed in Table 6.1. To determine the uniaxial material properties, Jiang used a multiple step test on a single specimen, loaded in strain control. The hysteresis loops obtained from these tests are plotted in Figure 6.2. The Ramberg-Osgood (1943) power law plasticity parameters for the formulation of the cyclic stress-strain curve were determined by subtracting the elastic strains from the total strains, and the subsequent hysteresis loops of plastic strain range versus stress range were analyzed by the method suggested by Morrow (1965). The fit of the data resulted in a cyclic hardening exponent, n', equal to 0.199, and a cyclic strength coefficient, k', equal to 1736 MPa. The cyclic stress-strain curve is indicated by the solid line connecting the tips of the hysteresis loops in Figure 6.2.

Notched specimens of 1070 steel were machined to the proper geometry, then heat treated to give uniform material properties. The heat treatment was to the specifications of the material used in the uniaxial smooth bar test of Jiang.

Because the complete state of surface strain was to be measured for the tests, a three element strain gage rosette was used. Micro-Measurements gages EA-06-031RB-120 were adhered to the notch root using AE-10 strain gage cement. The meaning of the strain gage designation is explained in Table 6.2. The placement of the rectangular rosette was such that the middle gage of the rosette was aligned approximately in the axial direction, with the other two gages 45 degrees on either side of the axial gage.

The tests were conducted in load control using Instron and MTS tension-torsion biaxial test frames controlled by Instron 8500 test controllers connected to a control and data acquisition computer that digitally stored the loads, gage strains, and actuator travel. After data collection, the rosette strain gage data was corrected for rosette misalignment, and transformed to specimen coordinates aligned in the axial direction of the shaft.

6.2 Finite element analysis

A converged finite element mesh of the notched shaft was constructed by Volker B. Köttgen (Köttgen 1992, Köttgen and Seeger 1993a). A three-dimensional slice of the shaft was modelled with boundary conditions of the faces of the slice being constrained to move the same in the radial and hoop directions. A full view and a detailed view of one of the models used in the analysis is shown in Figure 6.3. An ABAQUS USER MATERIAL implementation of the Mróz work-hardening plasticity model (Köttgen *et al.* 1992a-b) was used for the analyses of the nonproportional loading paths, and unless otherwise noted, all finite element calculations using the 1070 steel material properites and this notched shaft

were done by Volker B. Köttgen *et al.* (1993a) at the Technical University of Darmstadt[1], and finite element calculcations using other material properties were conducted at the University of Illinois using the finite element mesh provided by Köttgen.

6.3 Approximate method

The coefficients of anisotropy were determined using equations 3.33-3.34 from the elastic stress concentration factors obtained from tests of the specimens conducted in the elastic range of the material. Notched specimen uniaxial cyclic tests were conducted to determine the elastic-plastic uniaxial behavior of the specimen. These tests were conducted on one specimen in load control at several increasing values of load. As in the case of the smooth bar, a cyclic stress-strain curve was determined for the notched bar. The hysteresis loops obtained for the notched bar are shown in Figure 6.4, and the cyclic nominal stress-strain curve is indicated by the solid line connecting the tips of the hysteresis loops. The cyclic hardening exponent for the notched bar was found to be 0.201, and the strength coefficient was determined to be 1832 MPa.

6.4 Comparison of results

In this section, experimental results, and finite element and simplified calculations are presented and compared with each other for various tension-torsion loading paths. A convenient graphical means to display the loading paths is to plot axial nominal stress versus shear nominal stress. Similarly, the results of experiments and calculations will be presented as plots of notch root axial strain (ε_z) versus notch root engineering shear strain (γ_{rz}).

[1]A note from Köttgen concerning the disretization of the uniaxial stress-strain curve used in the finite element analysis appears in the Appendix.

Because most of the calculations and experiments were conducted for many cycles, plotting the strain results for all of the methods on one plot would cause a lack of distiction between the methods, and would obscure some overall features of the notch strain behavior. Therefore, the results of the experiments, simplified calculations, and finite element calculations will be presented in separate, but identically scaled plots.

6.4.1 Experimental, FEA, and approximate method

In Figures 6.5-6.28, the loading path, experimental strain response, the results of the simplified model, and finite element results are presented for the various loading paths examined by the experiments. The values of load used in the finite element and simplified calculations were slightly different than actually applied to the specimen; the sharp corners of the intended loading path were not always obtained in the experiments. All calculations, however, were made using the idealized loading path. The slightly rounded corners of the experimental loading path are reflected in the strain response as rounded corners in the plots of axial strain versus shear strain. Although noticeable at low levels of load, the difference in loading paths has little effect at the higher values of load.

For each load level, multiple cycles of the calculated strain response are plotted. However, due to data acquisition problems during the testing of specimen A, only the first two cycles of experimentally measured strains are plotted. For most of the loading cases, the specimen was cycled at the load level before data was collected, but not to one-hundred cycles. However, further testing on different specimens after the problem was corrected has shown there to be little difference in the strain response between that presented for specimen A and the strain response at one-hundred cycles measured on the other specimens for the same loading paths.

Specimen A

Initial testing began with a series of box-shaped loading paths in nominal tension-torsion stress space. For this loading path, the elastic plastic response of the simplified model is expected to predict regions of elastic unloading at each corner point of the loading path, followed by elastic-plastic loading to the next corner. In the elastic unloading portions of the path, the model predicts the axial-shear strain response to be uncoupled, and in the elastic-plastic portions of the path the shear and axial strains will be coupled by the term $d\lambda$ in the plastic strain equations. Therefore, the box shaped loading path provides a critcal test of the proposed method for notch strain calculation. By plotting the axial strain against the shear strain, these regions of coupled and uncoupled strain are easily seen.

Initially, when the loads are low, the notch root material is still in the elastic range. The axial and shear strain are uncoupled, and the strain response to the loading path is simply a box-shaped strain path with the sides parallel to the shear and axial strain axes of the plot. This is observed in Figures 6.5-6.6 in the measured and calculated strain responses. As the loads are increased further, the notch root material enters the plastic range and the axial and shear strains become coupled. The coupling is seen as segments of non-axis parallel portions of the strain response, with both the axial and shear strain increasing as the corners of the loading path are reached. This is most noticeable in Figures 6.9-6.11.

Both the finite element model and the simplified model capture these features of the strain response, and agree well numerically to the measured strains.

Specimen B

This specimen was used to determine the nominal stress-notch strain curves presented in Figure 6.4. In addition to the uniaxial cyclic tests, this specimen was tested for some other

nonproportional and proportional loading paths. Several nonproportional paths during which the ratio of the frequency of the applied loads were unequal were conducted, and these loading paths, experimental results, and results of the simplified calculations are presented in Figures 6.12-6.23. Nonproportional loading due to the application of unequal frequencies of applied load is a common loading of machine components.

For example, Figure 6.12 is from a test in which five cycles of torsional load occurred in the same period of time as one cycle of axial load. Other tests were conducted at unequal frequencies of applied torsional load to tensile load in the ratio of 3:1, 2:1, 1:2, 1:3, and 1:5, and at loading levels corresponding to the two most severe box-shaped loading paths. The data acquisition frequency was sub-optimal for some of the experimental results, and can be noticed as the clipped appearance of peaks in the plots of the experimental data.

The calculations using the simplified method agree well with experimental results in the qualitative shape and numerical values of the strains for the stabalized paths, and in the case of the loading path shown in Figure 6.23, even for some transient material behavior as indicated by the initial loading response of the material and simplified model in Figures 23b and 23c, repsectively.

The last two box-shaped loading paths of specimen A were repeated, and the experimental results of 100 cycles of applied load are presented in Figures 6.24b and 6.25b. The finite element and simplified calculations for several cycles at these loading levels are repeated for convenience.

A proportional tension-torsion test was conducted on this specimen, as well. The experimental strain response is presented in Figure 6.26b. The most noticeable feature of the strain response is that a thin loop is formed in the plot of axial strain versus shear strain. The

loop indicates that the ratio of axial strain to shear strain does not remain exactly constant, and this behavior is modelled well by the results of the finite element analysis for this loading path, Figure 6.26d.

The result of the simplified calculation, however, is a line, and not a loop in the strain plot of Figure 6.26c. The reason for this is the assumptions of the model regarding the relationship of the plastic and elastic ratio of the components of axial and shear strain. For the plastic component of the total strains, the ratio of the axial and shear strains is assumed to be constant by the model (by the plasticity constant, $d\lambda$), and the ratio of the elastic component of the total axial strain to shear strain is also assumed to be constant, as discussed in Section 3.3.4. Thus, the result of the simplfied model for this loading path is not unexpected.

And finally, a box-shaped loading path with the opposite direction of travel as the loading path of Figure 6.25 was conducted on this specimen, and is plotted in Figure 6.27. The strain range and qualitative behavior of the stabalized experimental results of this loading path are identical to that of Figure 6.25, with only difference in appearance being caused by the direction of travel around the loading path. This qualitative behavior is well-captured and expected from the simplified yield surface model.

Specimen C

This specimen was tested at low levels of load to determine another set of elastic stress concentration factors, the results of which are presented in Table 6.3, along with the converged finite element results. In addition, the same elastic-plastic proportional loading test that was presented for specimen B was conducted. The results for this test and the comparison with the finite element and simplified calculation are presented in Figure 6.28. Note that the plot of the initial cycles of the strain response of this previously un-yielded

specimen shows that the axial and shear strains are constant, as there is no loop formed initially in the Figure 6.28b. Only after several cycles does a thin loop form, and the plot becomes similar to that of specimen B in Figure 6.26b.

6.4.2 Approximate method and additional FE analyses

The notch strain response for several loading paths other than those that were used in the experiments were calculated using the finite element method (Köttgen 1992) and the approximate method. These analyses focus on the effect of different starting paths on the strain response for zero mean nominal loading paths, and cycling about a non-zero mean load. The cases involving a non-zero mean load induce ratcheting behavior in the strain response, and point out a limitation of the using the Mróz work-hardening model for the simplified calculation of notch strains. All calculations used the 1070 steel material properties.

Figures 6.29 through 6.40 show the results of the methods for various box-shaped paths with zero mean nominal load. In all of the cases, the shape and numerical values using the two methods agree very well.

Figures 6.41 through 6.54 show the results of the methods for various loading paths with nonzero mean loads. The loading paths cause ratcheting, or increasing, of strains in the two models even though the nominal loading path stays at the same level of mean load. However, the degree of ratcheting is much greater in the simplified model than the finite element model. This is because the strains behavior at the notch root is constrained by the surrounding elastic material.

In the ratcheting cases the strains calculated by the finite element method tend toward a limiting value because of the constraint. This is well illustrated in Figures 6.47-6.54. As the

simplified model does not take the entire component into account, it does not exhibit this behavior and the strains increase by the same amount for each loading cycle. The finite element calculations are expected to be much closer to the behavior of shaft for these types of loading paths. Although the strains calculated by the simplified method are much higher than the finite element calculations, the qualitative shape of the path and general trends agree.

The constant ratchetting rate of the Mróz model is an expected feature of the model for these types of loading paths (Köttgen and Seeger 1993b), and should not be considered a limitation of the concept presented in Chapter 3. As other deformation models are developed to better describe material ratcheting behavior, they may be substituted for the Mróz model in the particular implementation used in this thesis.

6.4.3 Change of material properties

In this section, the strain response of the shaft will be presented for different compliances of the uniaxial stress-strain curve input into the finite element model. For each different material model, the shaft was subjected to a box-shaped nominal loading path (Figure 6.55) of sufficient magnitude as to induce a significant amount of plastic flow at the notch root. The simplified method of determining the notch strains was also used to calculate the notch strain response, using an equivalent nominal stress-notch plastic strain curve obtained from an elastic-plastic tensile finite element analysis of the notched shaft for each different set of material properties.

A total of seven sets of uniaxial stress strain curves were analyzed ranging from elastic-perfectly plastic to nearly completely elastic, shown in Figure 6.56. For each curve, the yield strength was taken to be 250 MPa. The jump in the smooth specimen stress-strain curves at this value is due to the abrupt change from the elastic stress strain curve to the

elastic-plastic stress-strain curve. The elastic properties were taken to be the same as those of the 1070 steel. The elastic-plastic 1070 steel response is represented as material four in the figure, and the material properties used to generate the curves are listed in Table 6.4.

The structural nominal stress-notch strain curve was determined for each material description by a uniaxial finite element analysis with the converged finite element mesh for the notched round shaft provided by Köttgen (1992, 1993a). This information, and the elastic stress concentration factors were used to determine the coeficients of anisotropy. These results are compared with calculations using the finite element method and an implementation of the Mróz kinematic work-hardening model as a USER MATERIAL model in the finite element program ABAQUS (Köttgen *et al.* 1991a-b).

The strain response and the applied loads subjected to each material are given in the caption of Figure 6.57. The calculations for material 4 (the 1070 steel) have been presented in Section 6.4.1, and are not repeated here. Results for material 8 (completely elastic) are not included either.

It is worth noting that for the elastic-perfectly plastic material (material 1), the nominal stress-notch strain curve has stiffness associated with it, until the the shaft is loaded to its plastic limit load. For this reason, a stress-space formulation of the yield surface is possible for all materials and geometries, except for the limiting case of a smooth bar of elastic-perfectly plastic material.

For the geometry, loading paths, and materials chosen, the qualitative shape of the finite element and simplified calculations was very similar for all materials and close in values of calculated strains as well, with the best numerical agreement occurring for the relatively less compliant sets of material properties for this particular shaft.

7 A PLATE WITH A CIRCULAR HOLE

In this chapter, the method of the simplified analysis is compared with finite element results for a thin plate with a circular hole.

7.1 Plate geometry

A thin square plate with a width of six times the hole diameter was modelled for the analysis. The hole-to-width ratio was chosen because experimental elastic stress concentration data were available for the similar geometry used by Griffith (1948). A square plate was chosen to simplify the determination of stress concentration factors. The definition of nominal stress is based on the net section (plate width minus the hole diameter). The plate geometry and nominal loading is shown in Figure 7.1.

7.2 Finite element analysis

A one-quarter symmetric section of the plate was modelled by finite element analysis. The discretization of the plate is shown in Figure 7.2. The mesh was composed of 8-noded reduced integration quadrilateral plane stress elements, and the finite element program ABAQUS with a USER MATERIAL implementation of the Mróz kinematic work-hardening model (Köttgen 1991a-b) was used for the analyses. The mesh was subdivided to check for convergence of the elastic solution with and without reduced integration elements, with no appreciable change in stresses or strains.

The following dimensions were used for the analysis: plate width, $w = 300$ mm, plate thickness, $t = 2$ mm, hole diameter, $d = 50$ mm. Elastic and elastic-plastic material properties were taken as 1070 steel, used in the analysis of the notched shaft in Chapter 6.

A single elastic analysis of the mesh shown in Figure 7.2 was conducted to determine the elastic stress concentration factors of the plate. A unit nominal tensile load was applied in the y-direction. A detailed view of the notch with nodal numbering is shown in Figure 7.3.

The analysis resulted in an elastic stress concentration factor of 2.65 at node 127, and –0.94 at node 193. Griffith's measurements resulted in an elastic stress concentration factor of 2.57 in the position corresponding to node 127 of the finite element mesh. The slight difference in the measured and calculated stress concentration factors is most likely due to the shorter length of the plate in the loading direction than that used by Griffith.

An elastic-plastic uniaxial finite element analysis was conducted to determine a load-notch strain relationship for the plate. The nominal stress-notch strain diagram is in Figure 7.4, with the elastic, plastic, and total strain plotted against the nominal load.

7.3 Comparison of results

In Figure 7.5, the results of the monotonic analyses for different ratios of applied nominal loads are plotted. This ratio, R, is defined as:

$$R = S_x/S_y. \tag{7.1}$$

Finite element results from the loading $R = 0$ for the hoop strain (e_y) indicated in Figure 7.5 determined the nominal load-notch plastic strain curve for the hole. Using information from this curve and the elastic stress concentration factors, the notch strain response was calculated for other ratios of applied nominal load, and compared with finite element analyses. In the figure, the finite element results are indicated by solid lines, and the results

of the simplified calculation are indicated by the dashed lines. The results of the two methods are in very good agreement for loadings ranging from $R = 0.25$ to $R = 1$ for not only the hoop strain, but for the radial strain (e_x) as well.

A proportional cyclic nominal loading path shown in Figure 7.6a was also examined. The loading ratio chosen for this path was $R = 1$, or balanced biaxial nominal cyclic tension. The finite element results and the results of the simplified calculation are presented in Figures 7.6b-e, for increasing levels of nominal load. The plots are of normalized time for the loading path versus notch strain. Both the hoop strain and the radial strain are presented in the same figure for node 127, with the hoop strain having the larger magnitude. Finite element results are again represented by solid lines, and the simplified calculation by dashed lines. The is little difference in the methods until the notch strain approached one percent amplitude. However, even at this level, the character of the strain behavior is captured very well.

To examine the strain response of the hole when subjected to nonproportional nominal loading, the simplified method and finite element method were used to calculate strains for the box-shaped nominal loading path in Figure 7.7a. The calculated response for several increasing levels of load are presented in the strain time history plots of Figures 7.7b-d. Again, the finite element calculations are represented by solid lines, and the simplified method by dashed lines. Similar to the results of the proportional loading, the character of the methods of calculating notch strains agree well for all loading cases, and the numerical values agree also, until strains approach about one percent in amplitude.

8 A MORE SHARPLY NOTCHED SHAFT

In this chapter, the simplified method of calculating the notch strain response is compared with the finite element method for the analysis of a more sharply notched shaft subjected to proportional and nonproportional nominal loading in tension and torsion. The geometry of this notched shaft causes more notch constraint than examined in the mildly notched shafts presented previously.

8.1 Shaft geometry

The geometry of this shaft is very similar to the sharp surface notch used in the analyses and experiments of Hoffmann and Seeger (1985a). For the shaft examined here, the net section diameter is 120 mm, the gross section diameter is 144 mm, and the notch root radius of the hyperbolic notch is 3 mm. A schematic of the shaft is in Figure 8.1.

8.2 Finite element analysis

A converged finite element mesh was constructed for this geometry. A fifteen degree, three-dimensional slice of the shaft was modelled, using boundary conditions that corresponding nodes on either side of the slice must have the same deformations in the radial, hoop, and axial directions. The finite element mesh used for the finite element calculations is shown in Figure 8.2. The coordinate system used is indicated in Figure 8.2; the axial direction the shaft is the z-direction, the transverse direction at the notch root is the x-direction, and the direction normal to the notch surface is the y-direction.

Material properties used for this notched shaft were taken to be the same as 1070 steel shaft, also used in the analysis of the mildly notched round shaft and the plate with a central hole.

As in the previous finite element analyses, the ABAQUS USER MATERIAL implementation of the Mróz work-hardening plasticity model (Köttgen 1991a-b) was used for the analyses of the nonproportional loading paths.

The results of a single, elastic-plastic tensile finite element analysis of the shaft was used to determine the elastic stress concentration factors in tension and the amount of plastic notch constraint. An additional elastic analysis of the shaft in torsion was conducted to determine the elastic shear stress concentration factor of the notched bar. The elastic stress concentration factors for the notch are

$$\begin{aligned} K_z &= 2.98 \\ K_z' &= 0.81 \\ K_{xz} &= 1.72, \end{aligned} \tag{8.1}$$

and agree with those obtained by Hoffmann and Seeger (1985a) and Neuber (1946).

The initial nominal yield strengths in the axial direction (Z_0) and the torsional nominal yield strength (S_0), were found from equations (3.33) and (3.34) respectively. The initial coefficients of anisotropy were then determined from equation (3.7), and the observation from the unaxial finite element analysis that the ratio of the plastic strains in the transverse and normal directions (ε_x^p:ε_y^p) from the elastic-plastic simple tension analysis was approximately 0.18:1. The nominal stress-notch plastic strain curve was determined from the axial nominal stress-axial plastic strain results from the uniaxial finite element analysis. The strain components from the uniaxial finite element analysis are shown in Figure 8.3. These were the only data used to determine the coefficients of anisotropy.

The uniaxial nominal stress-notch root plastic strain curve generated by the finite element model (Figure 8.3) shows the effect of the sharp geometry on the notch constraint. In the

elastic range, the transverse strain, ε_x, is almost zero, meaning that the biaxial stress field at the notch root overcomes the Poisson contraction of the material due to the axial stress. At large values of axial load, the transverse strain, ε_x, varies only slightly from zero. Therefore, the uniaxial finite element analysis to determine the equivalent nominal stress-notch root strain curve could have been foregone if the assumption was made that the notch root was in a state of plane strain, and if Glinka's plane strain approximate notch formula (Glinka 1985a) was used to determine the equivalent nominal stress-notch root strain curve. Such an assumption would change the results of the simplified method very slightly for this notched shaft.

8.3 Comparison of results

The finite element model and the simplified model were used to calculate the notch root strain response of the shaft subjected to proportional and nonproportional loading paths. Three proportional analyses were conducted, and the loading paths are shown in Figure 8.4. The three loading paths were chosen to give Mises equivalent nominal stresses of the loading components S_z:$\sqrt{3}S_{xz}$ in the ratios of 1:2, 1:1, and 2:1 for the loading paths indicated in Figure 8.4 by paths 1, 2, and 3, respectively. These paths will allow the demonstration of the applicability of the model to multiaxial loadings that vary from mostly tensile loading to mostly shear loading.

The results of the calculations of the finite element method and the simplified method are presented in Figure 8.5a-c. Finite element results are indicated by the dashed-dotted lines, and the results of the proportional equations of the simplified model are indicated by the dashed lines. The figures indicate that excellent agreement was obtained between the two

models, with the advantage of the simplified method being that the calculations using the closed-formed equations for proportional loading (equations 3.36) were instantaneous, whereas the finite element calculations obtained were computationally lengthy and involved.

The strain response for three nonproportional box-shaped loading paths were also calculated using the finite element model of the shaft and the simplified method, and are presented in Figures 8.6-8.8. The ratios of applied load for the initial loading segments of the box path were in the same ratio as the proportional loading paths of Figure 8.5. Again, agreement between the two models is very good, in particular with regard to the strain ranges.

9 CONCLUSIONS

1. An approximate technique has been developed to calculate notch strains based a concept of a structural yield surface. The approach applies results of anisotropic metal plasticity theory to define a yield surface in nominal stress space that relates nominal stress directly to notch strain. The required data for the model includes the elastic stress concentration factors of the notch, knowledge or assumptions about the plastic notch constraint under uniaxial loading, and the uniaxial nominal stress-notch plastic strain response for the notch.

2. Results of calculations using this method for proportional and nonproportional nominal cyclic loading histories have compared very well with experimental results conducted on a notched steel shaft, and also with extensive finite element analyses conducted using various material properties and geometries.

3. Using yield surface plasticity theory of anisotropic metals presents the method in a way familiar to those knowledgeable about yield surface plasticity theory of isotropic metals, including limitations of the method for loading paths with non-zero mean load.

TABLES

	K_z	K_{xz}	K'_z
Mild surface notch	1.40	1.22	0.25
Sharp surface notch	3.32	2.19	0.89
Sharp deep notch	2.93	2.03	0.91

Table 4.1. Stress concentration factors for notched shafts subjected to bending and torsion (Hoffmann *et al.* 1985a).

Elastic Modulus, E	210 GPa
Poisson's ratio, ν	0.3
Cyclic strength coefficient, k'	1736 MPa
Cyclic hardening coefficient, n'	0.199

Table 6.1. 1070 steel material properties.

E	Open-faced, polyimide backing
A	Constantan alloy in self-temperature-compenstated form
06	Approximate thermal expansion coefficient in PPM/degrees
	F of the structural material on which the gage is to be used
031	Active gage length in thousandths of an inch
RB	Rectangular rosette
120	Resistance in Ohms

Table 6.2. Code for strain gage designation. Source: Measurements Group Education Division Bulletin 309A, 1983.

	K_z	K_{xz}	K'_z
Specimen A	1.45	1.17	0.30
Specimen B	1.42	1.15	0.30
Specimen C	1.47	1.13	0.32
Converged FEA	1.41	1.15	0.26

Table 6.3. Experimentally determined stress concentration factors and stress concentration factors from converged finite element analysis (Köttgen and Seeger 1993) for fully notched round shaft.

material number	n'	k' (MPA)
1	elastic-perfectly plastic	-
2	0.050	400
3	0.100	700
4	0.199	1736
5	0.250	2900
6	0.300	5000
7	0.400	15000

Table 6.4. Hardening exponents (n') and strength coeficients (k') for materials used in compliance analysis of the fully notched round shaft. Material 4 represents the 1070 steel used in the experiments.

FIGURES

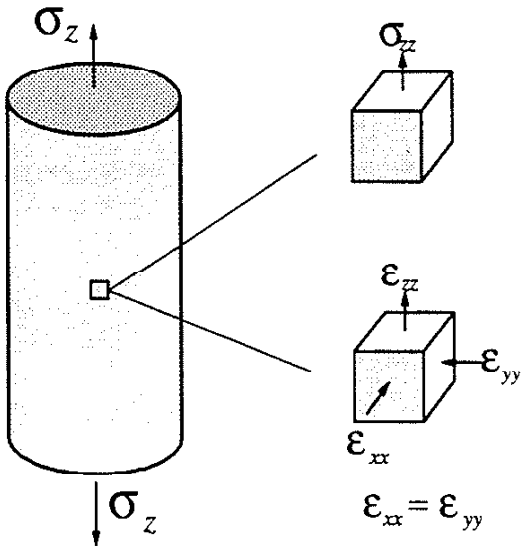

Figure 3.1. Smooth bar stress and strain state due to uniaxial load.

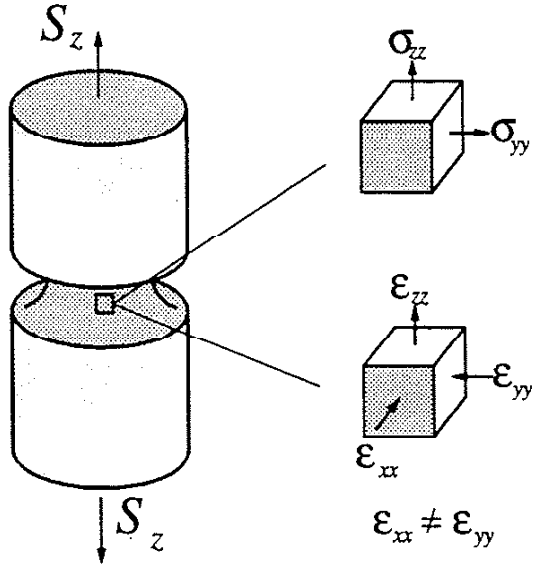

Figure 3.2. Notched bar stress and strain state due to uniaxial load.

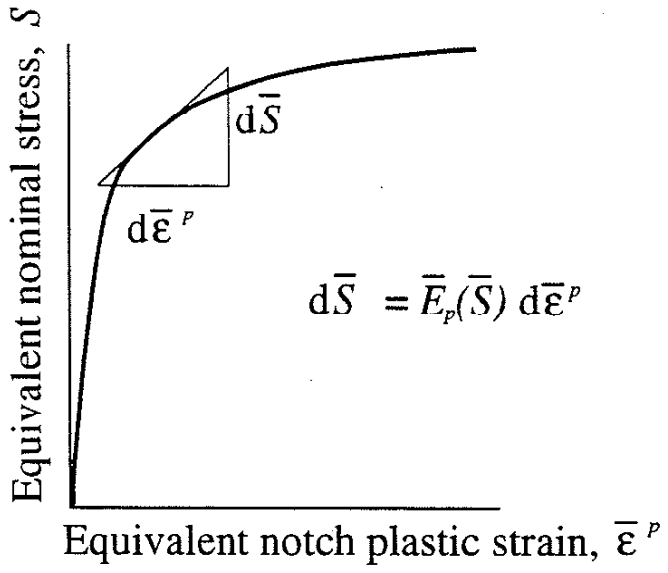

Figure 3.3. Equivalent uniaxial stress-strain response.

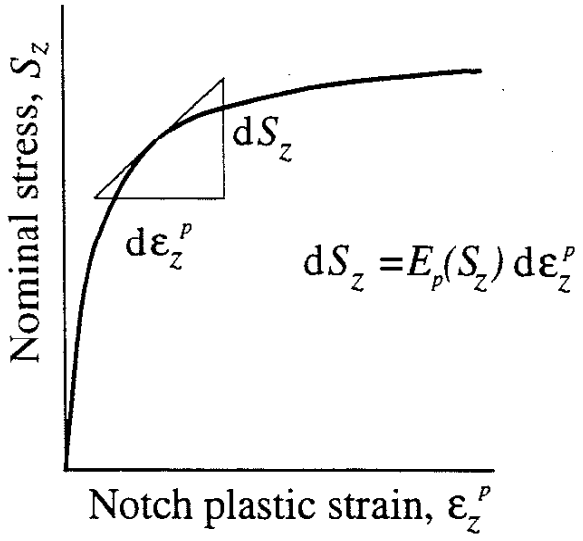

Figure 3.4. Uniaxial stress-strain response.

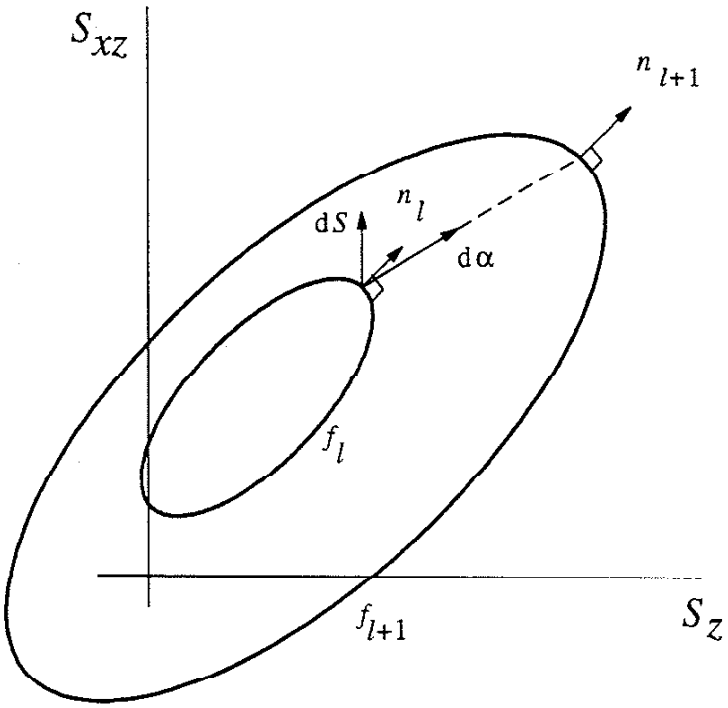

Figure 3.5. Mróz model in stress space.

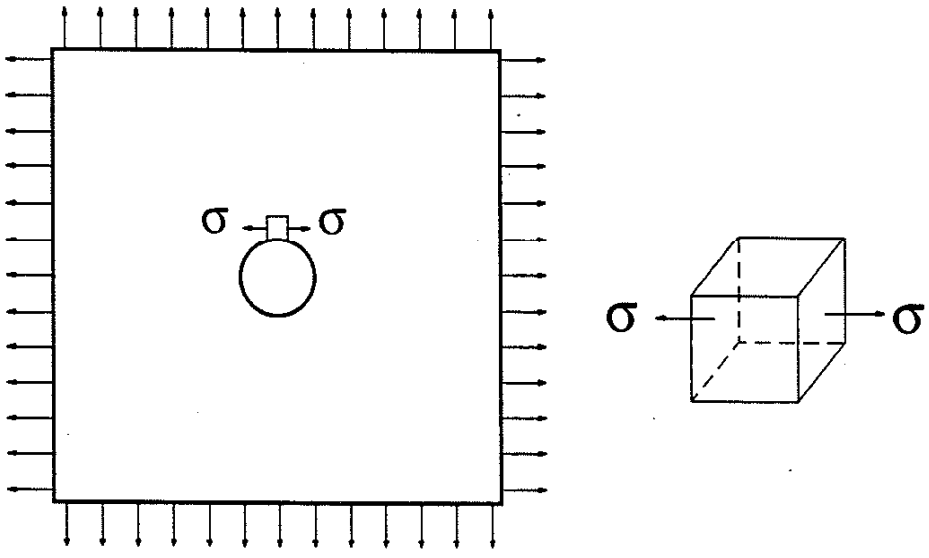

Figure 3.6. Local notch stress state for a plate with a hole.

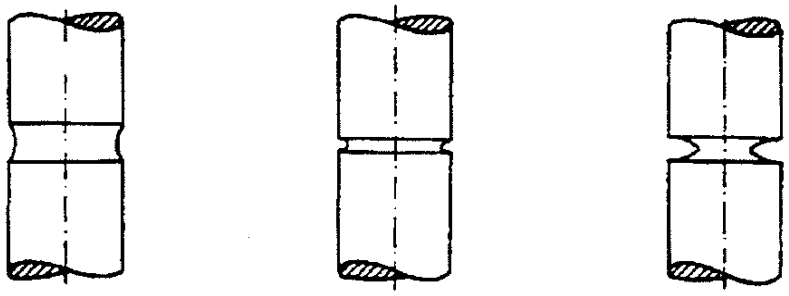

Figure 4.1. Notch types examined by Hoffmann and Seeger in Kerbbeanspruchungen I. From left to right: mild surface notch, sharp surface notch, and sharp deep notch.

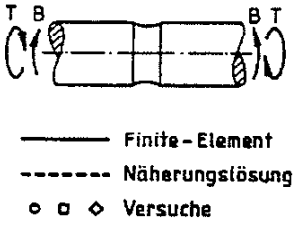

Figure 4.2a. Mild surface notch and loading conditions. Source: Hoffmann *et al.* (1985a).

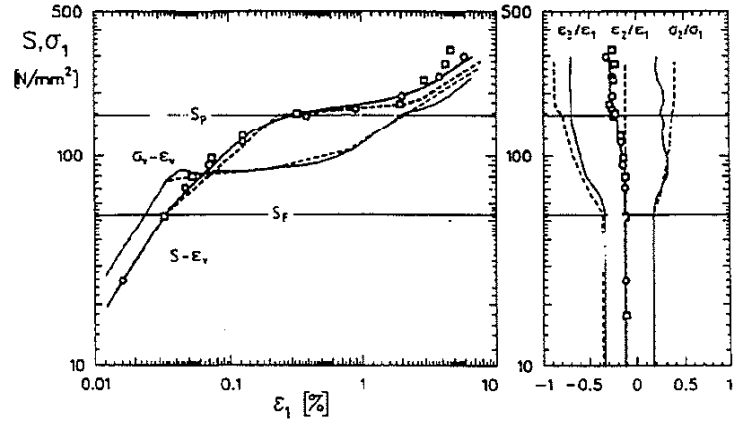

Figure 4.2b. Simple bending results for mild surface notch. Source: Hoffmann *et al.* (1985a).

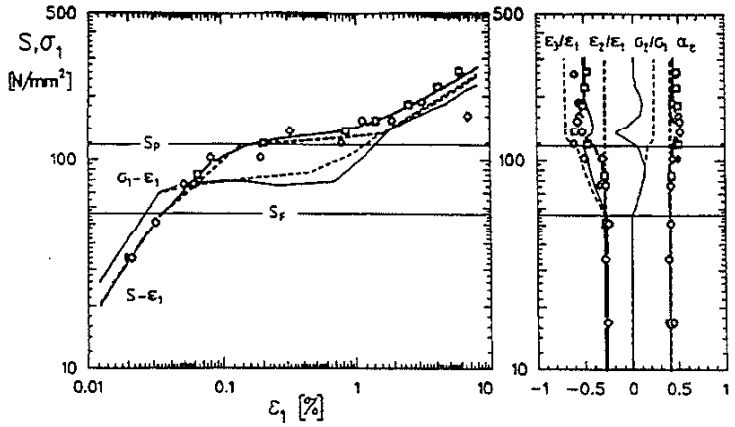

Figure 4.2c. Combined loading results for mild surface notch. Source: Hoffmann *et al.* (1985a).

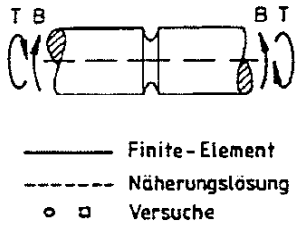

Figure 4.3a. Sharp surface notch and loading conditions. Source: Hoffmann *et al.* (1985a).

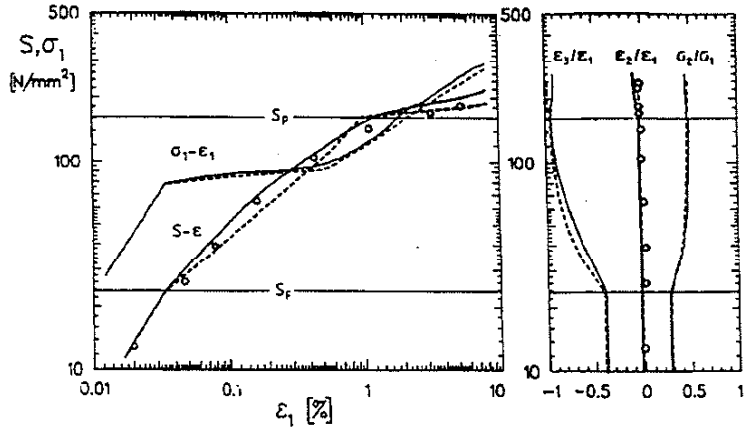

Figure 4.3b. Simple bending results for sharp surface notch. Source: Hoffmann *et al.* (1985a).

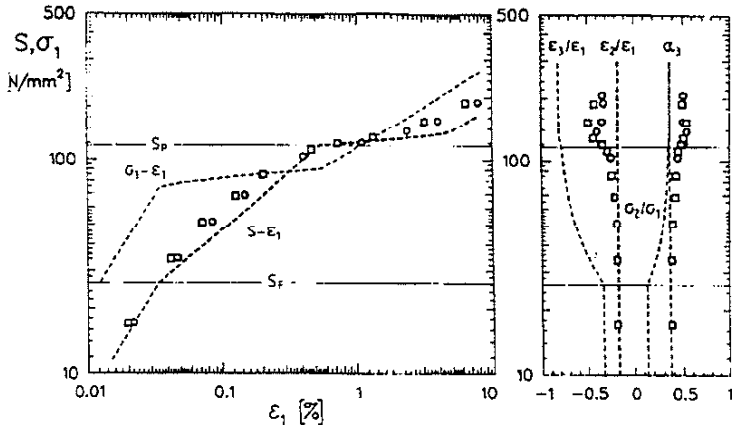

Figure 4.3c. Combined loading results for sharp surface notch. Source: Hoffmann *et al.* (1985a).

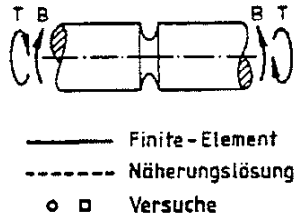

Figure 4.4a. Sharp deep notch and loading conditions. Source: Hoffmann *et al.* (1985a).

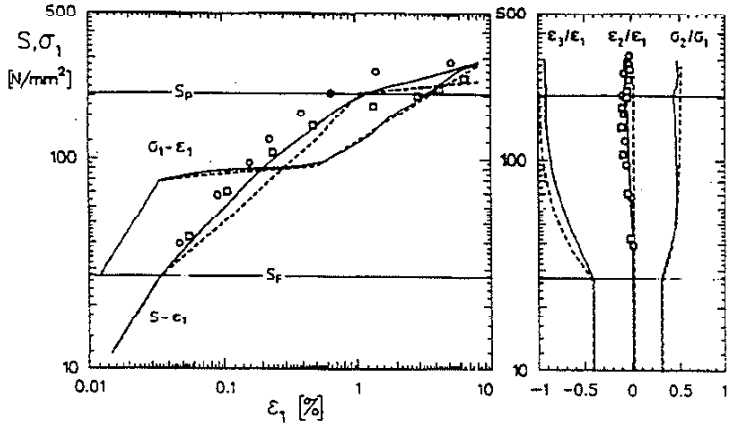

Figure 4.4b. Simple bending results for sharp deep notch. Source: Hoffmann *et al.* (1985a).

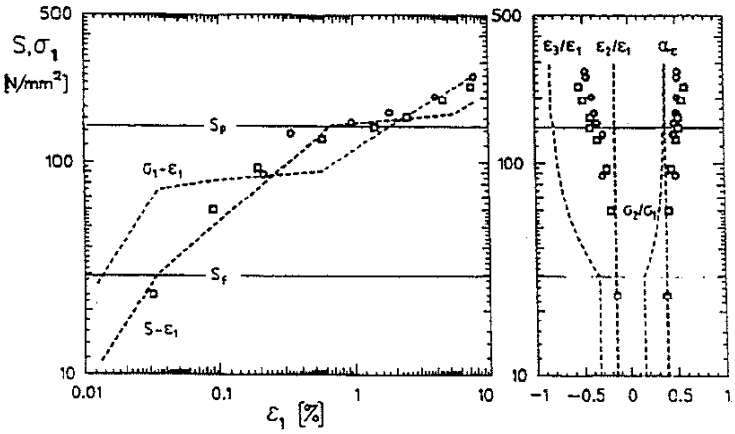

Figure 4.4c. Combined loading results for sharp deep notch. Source: Hoffmann *et al.* (1985a).

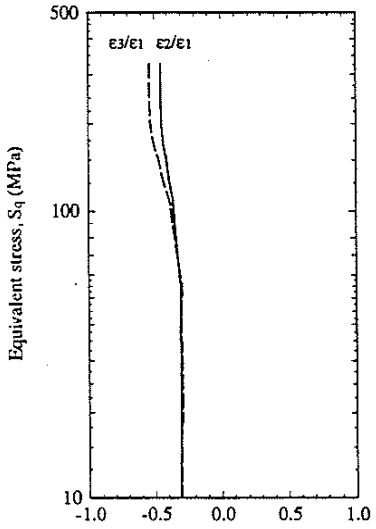

Figure 4.5a. Calculated results for the mild surface notch subjected to combined loading.

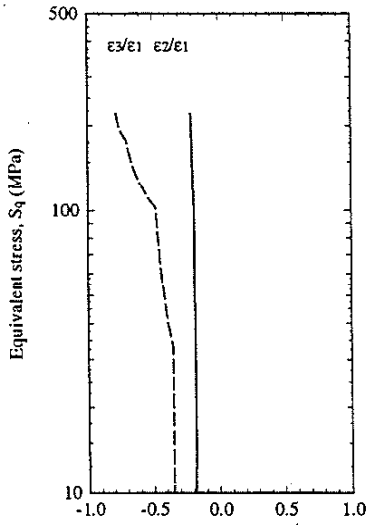

Figure 4.5b. Calculated results for the sharp surface notch subjected to combined loading.

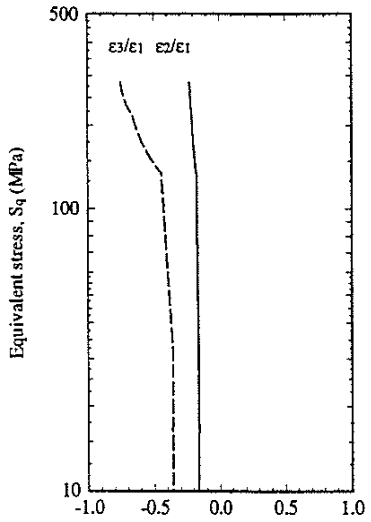

Figure 4.5c. Calculated results for the sharp deep notch subjected to combined loading.

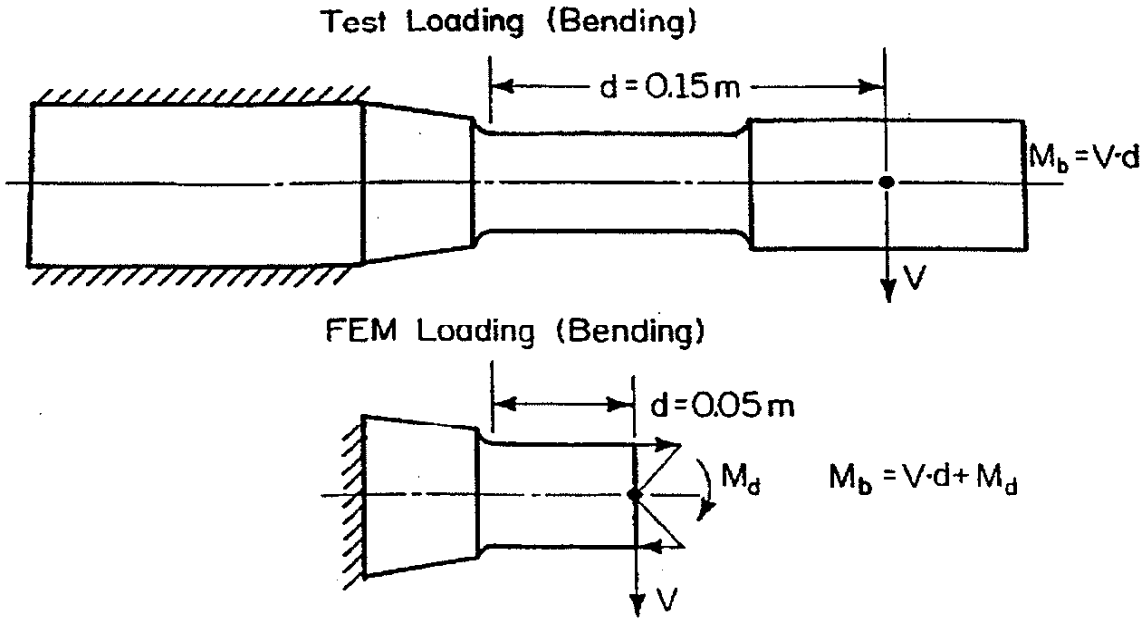

Figure 5.1a. SAE notched shaft geometry and loading conditions.

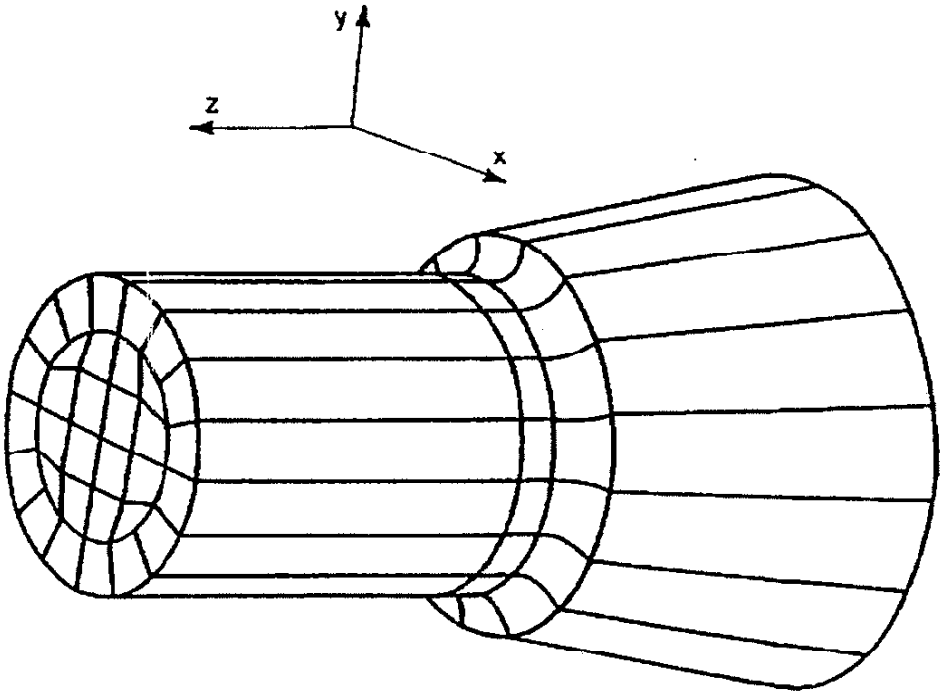

Figure 5.1b. Fash's finite element mesh for the SAE notched shaft.

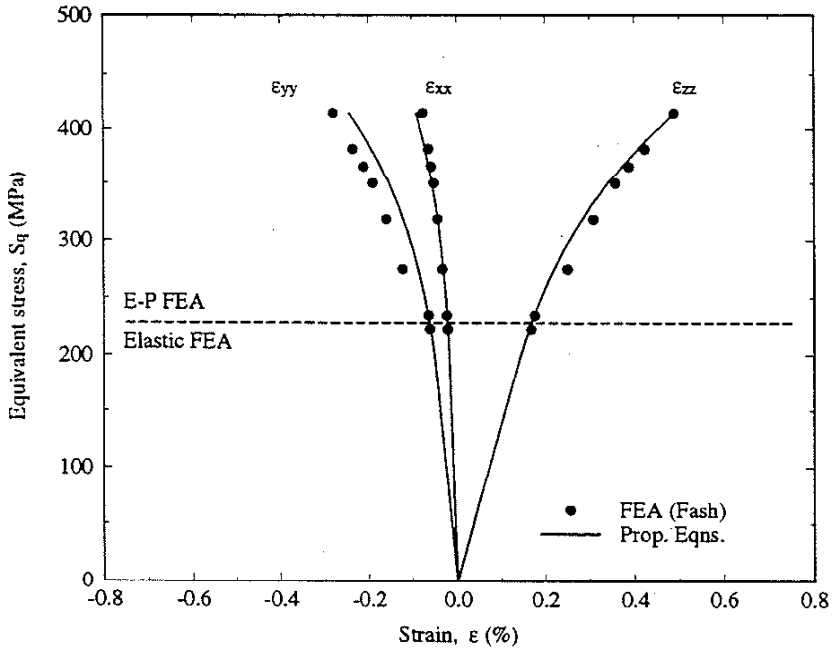

Figure 5.2a. Notch root strains for pure bending calculated by the finite element method and equations developed for proportional loading with curve fit to determine coefficients of anisotropy.

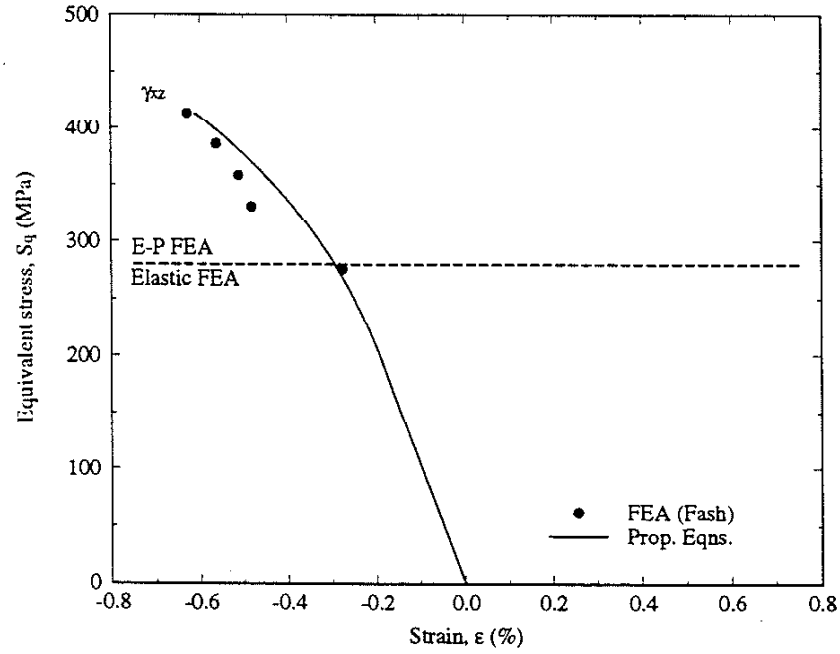

Figure 5.2b. Notch root strain for pure torsion calculated by the finite element method and equations developed for proportional loading.

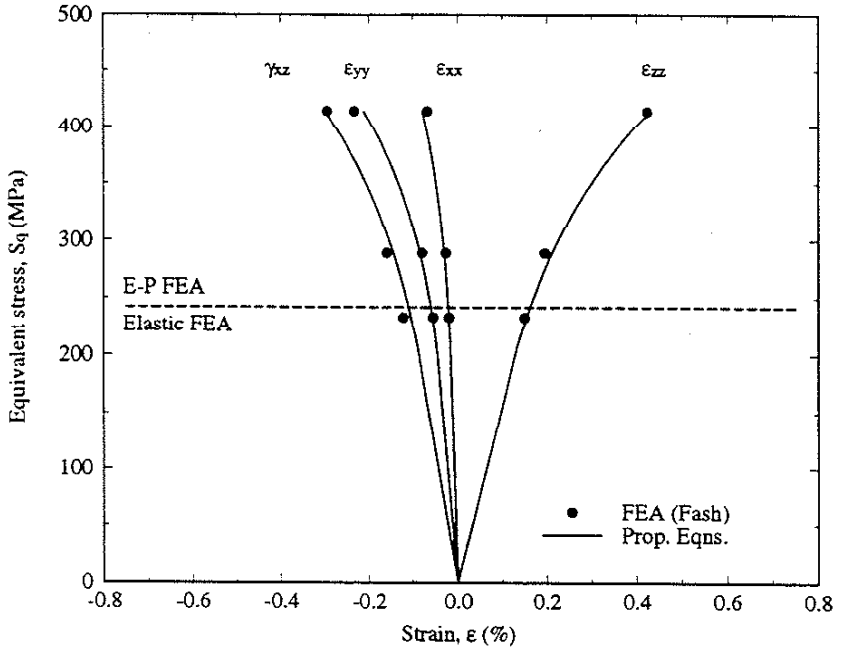

Figure 5.2c. Notch root strains for proportional torsion and bending (T/B = 0.6) calculated by the finite element method and equations developed for proportional loading.

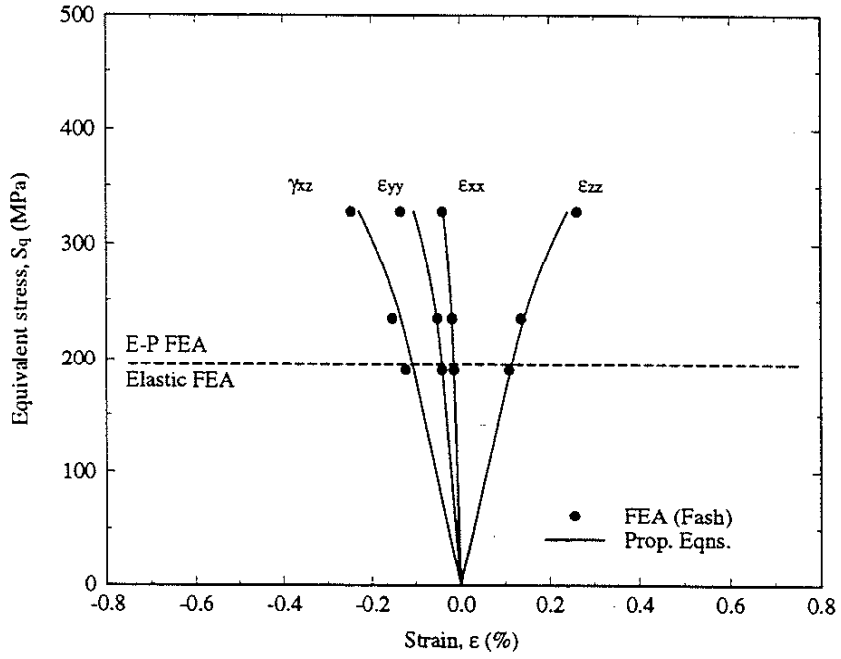

Figure 5.2d. Notch root strains for proportional torsion and bending (T/B = 0.8) calculated by the finite element method and equations developed for proportional loading.

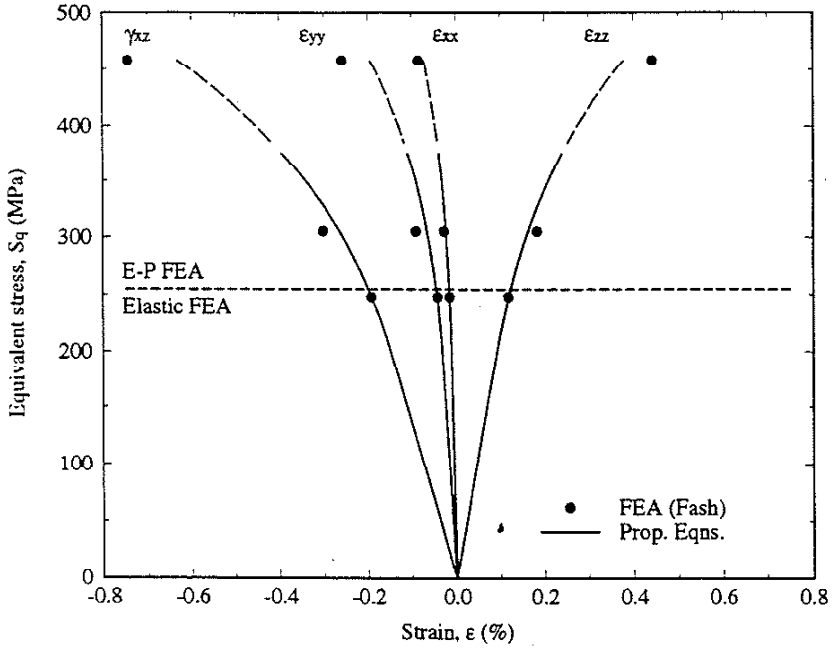

Figure 5.2e. Notch root strains for proportional torsion and bending (T/B = 1.4) calculated by the finite element method and equations developed for proportional loading. The dashed portions of the calculated results indicate results based on an extrapolation of the uniaxial curve of Figure 5.2a.

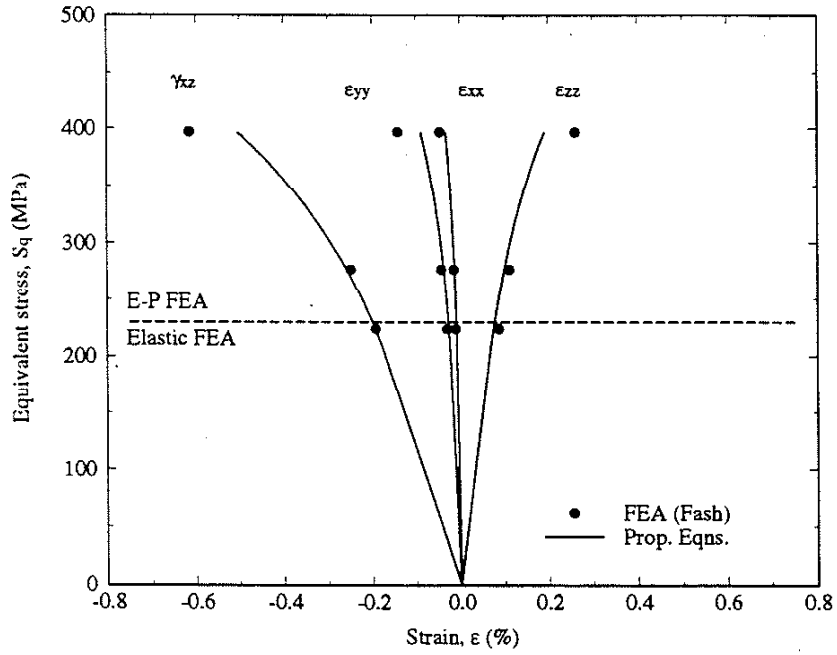

Figure 5.2f. Notch root strains for proportional torsion and bending (T/B = 2.2) calculated by the finite element method and equations developed for proportional loading.

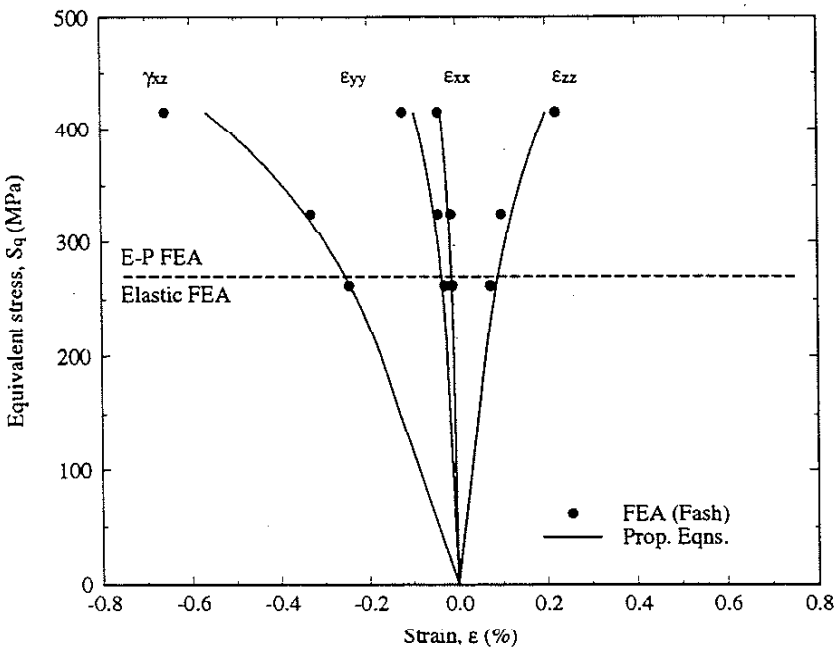

Figure 5.2g. Notch root strains for proportional torsion and bending (T/B = 2.3) calculated by the finite element method and equations developed for proportional loading.

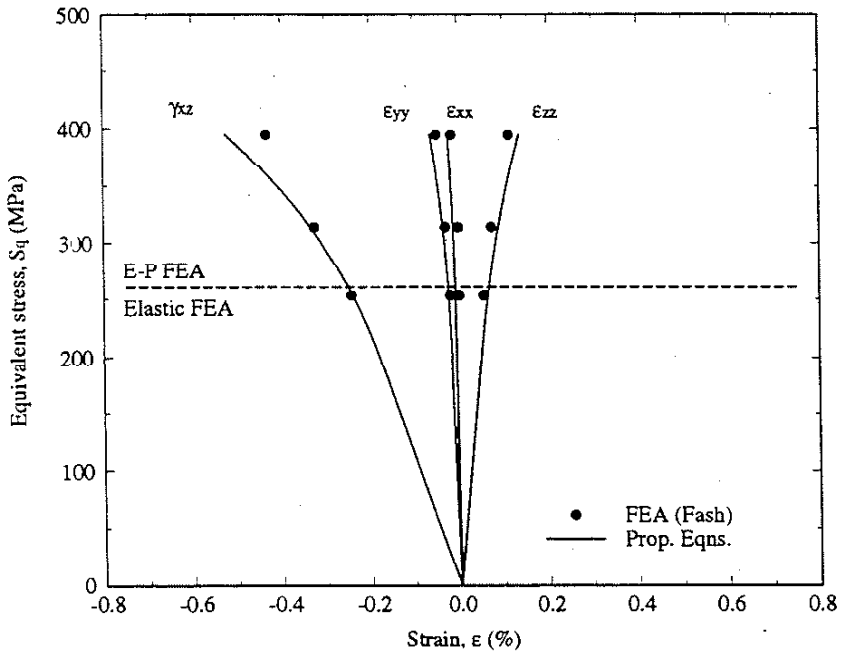

Figure 5.2h. Notch root strains for proportional torsion and bending (T/B = 3.2) calculated by the finite element method and equations developed for proportional loading.

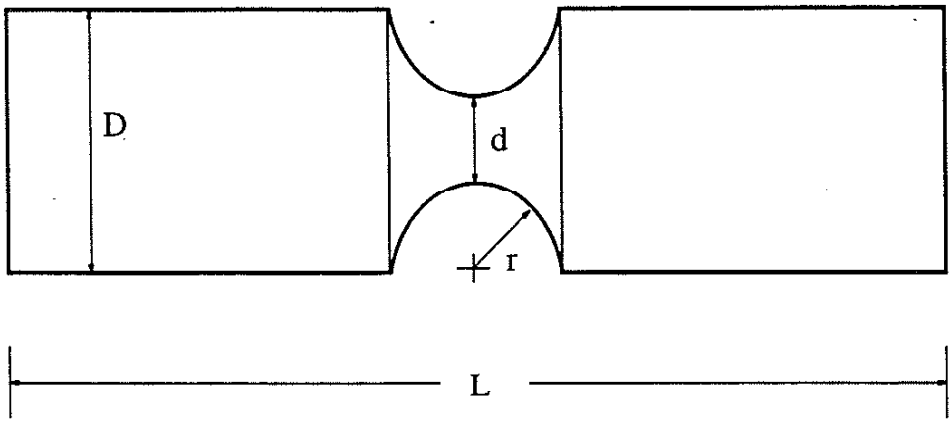

D = 50.8 mm d = 25.4 mm

L = 254 mm r = 12.7 mm

Figure 6.1. Fully notched round shaft geometry and dimensions.

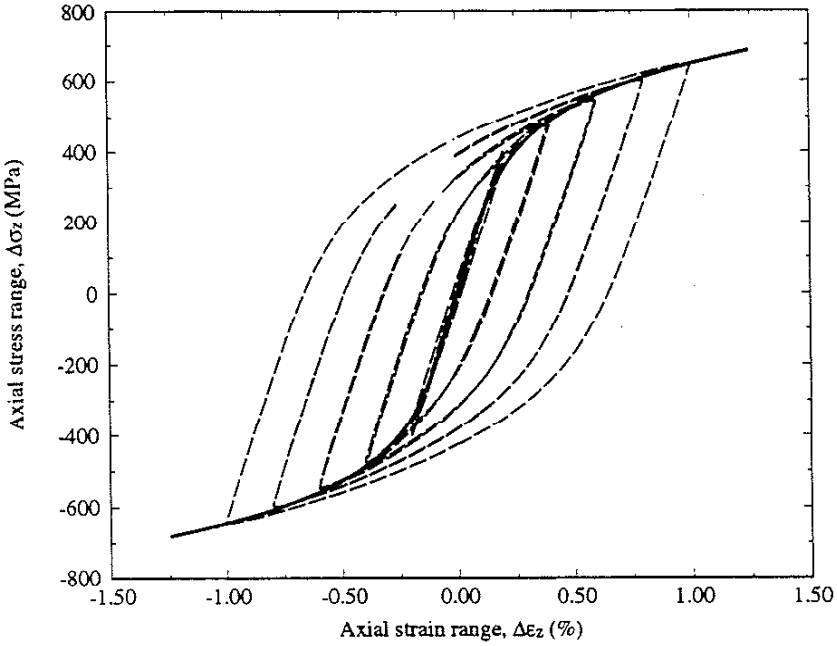

Figure 6.2. Uniaxial Cyclic Stress-Strain Response for 1070 Steel.

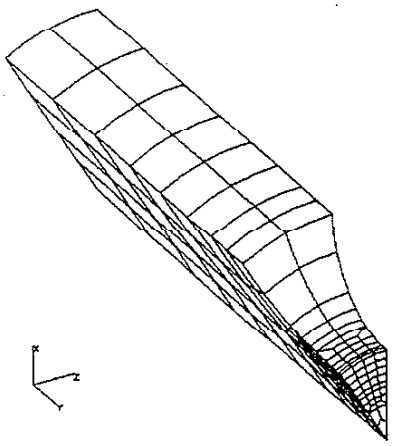

Figure 6.3a. Finite element mesh of notched shaft by Köttgen.

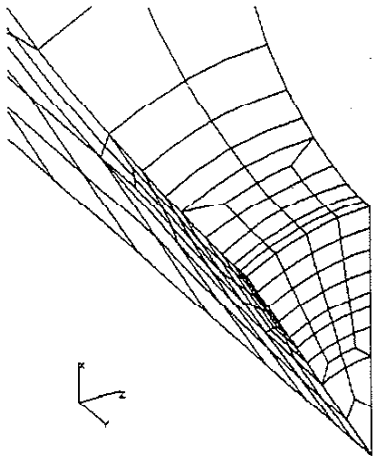

Figure 6.3b. Detailed view of notch root.

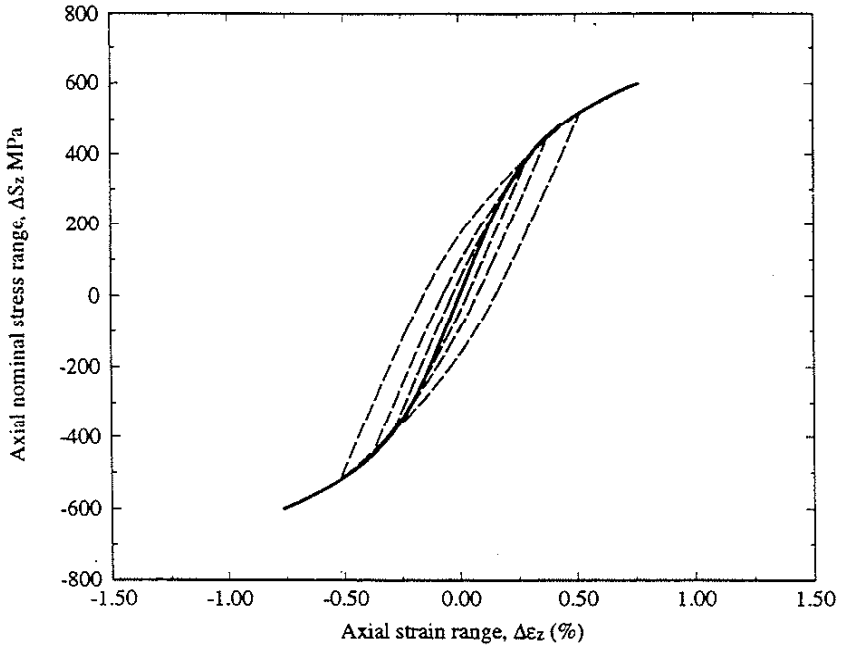

Figure 6.4. Uniaxial Cyclic Stress-Strain Response for Notched Shaft.

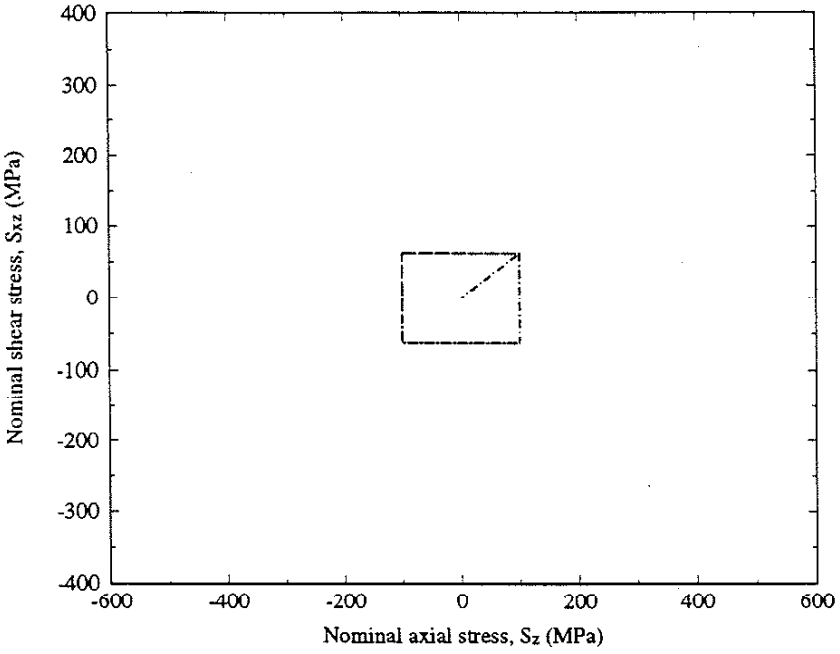

(a)

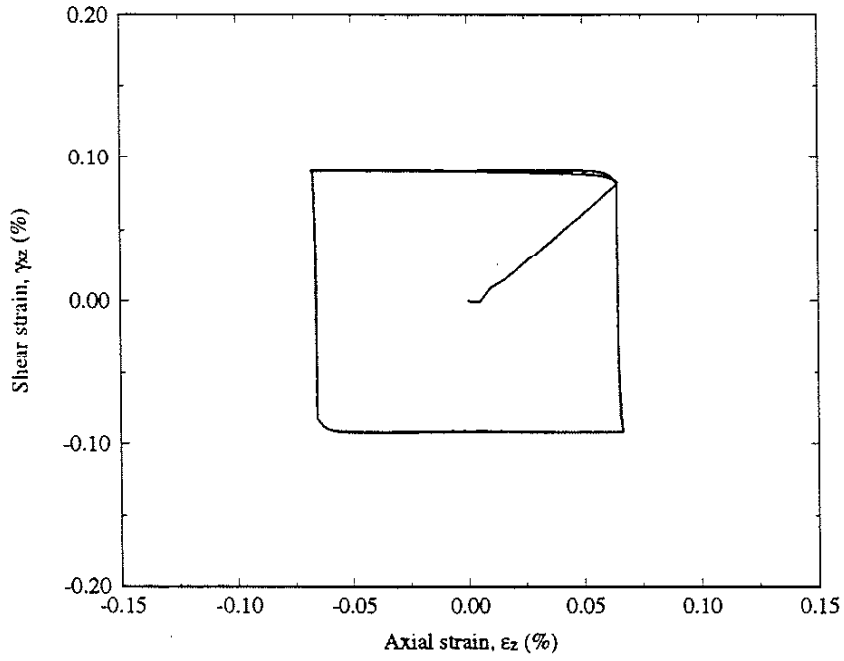

(b)

Figure 6.5. (a) Nominal stress path and (b) measured strain response for maximum nominal stresses of S_z=100 MPa, and S_{xz}=62.5 MPa.

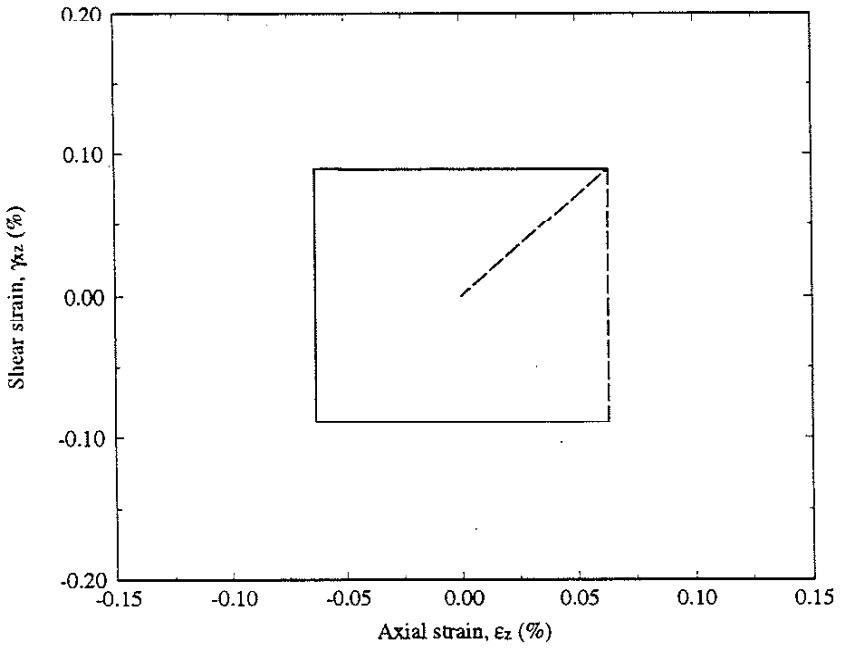

(c)

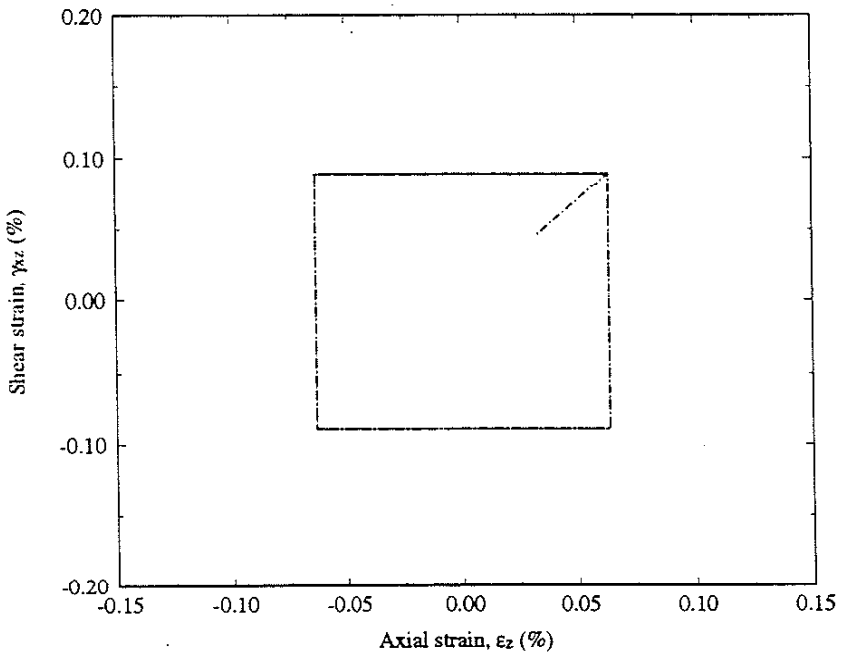

(d)

Figure 6.5 (continued). (c) Calculation using the simplified method and (d) calculation using the finite element method for maximum nominal stresses of S_z=100 MPa, and S_{xz}=62.5 MPa.

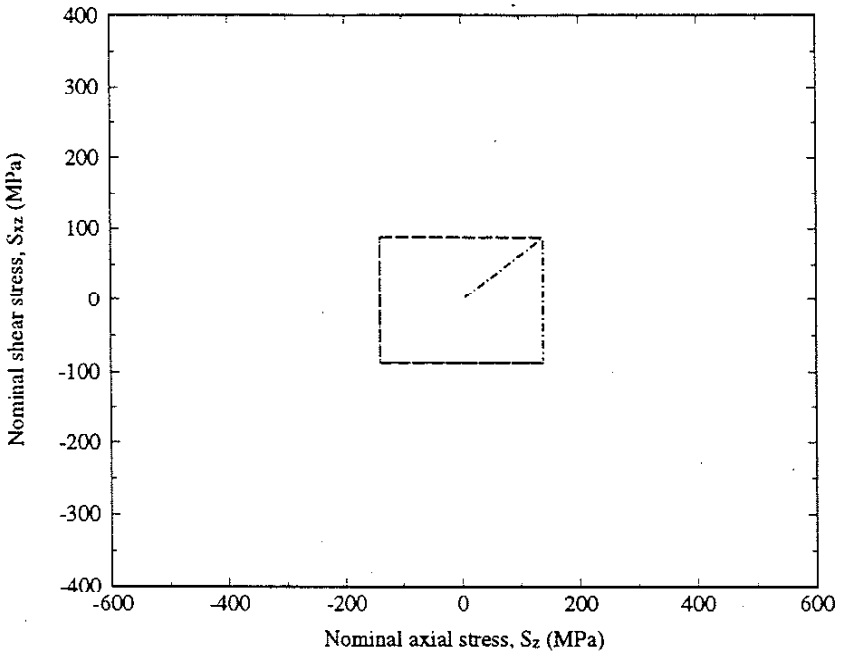

(a)

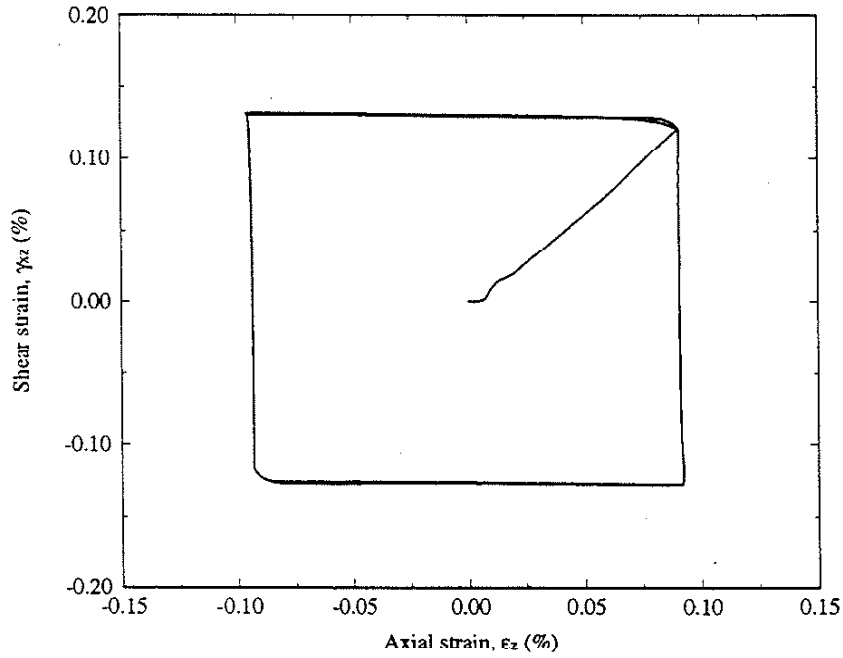

(b)

Figure 6.6. (a) Nominal stress path and (b) measured strain response for maximum nominal stresses of S_z=139 MPa, and S_{xz}=87.5 MPa.

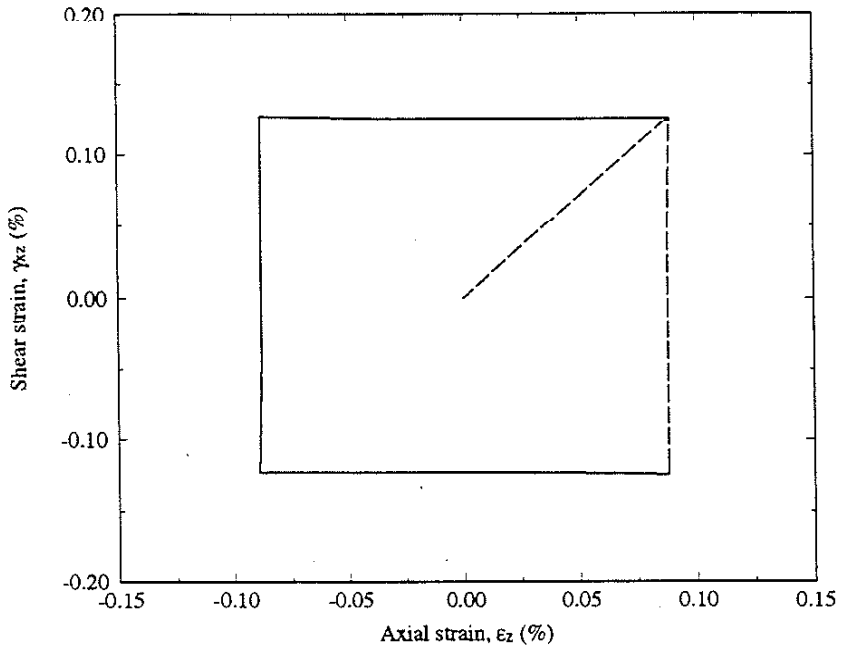

(c)

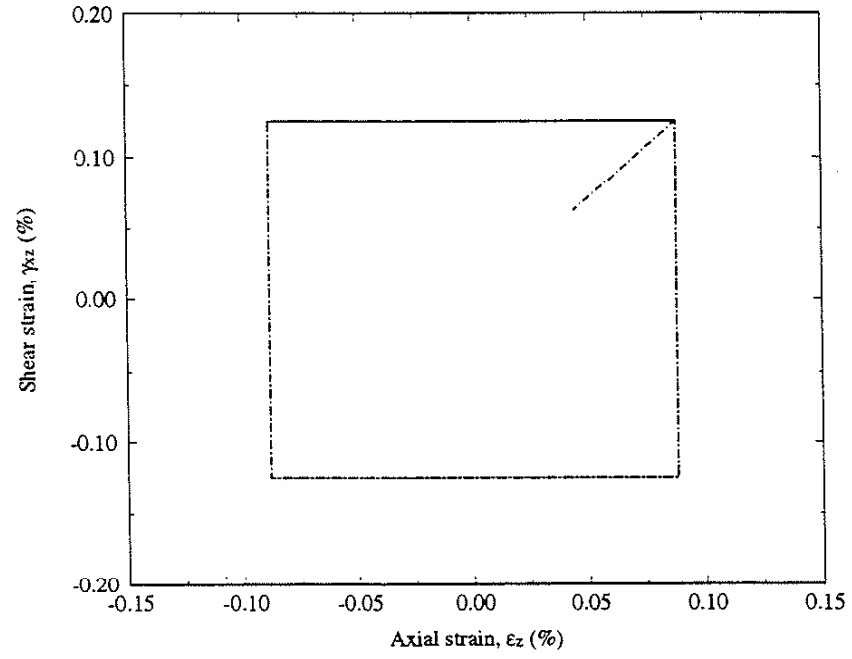

(d)

Figure 6.6 (continued). (c) Calculation using the simplified method and (d) calculation using the finite element method for maximum nominal stresses of S_z=139 MPa, and S_{xz}=87.5 MPa.

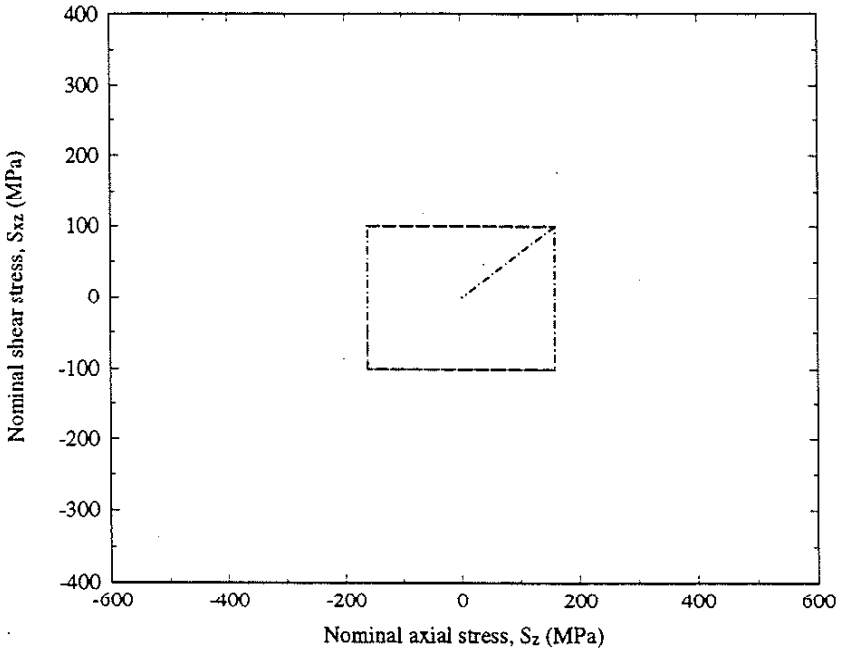

(a)

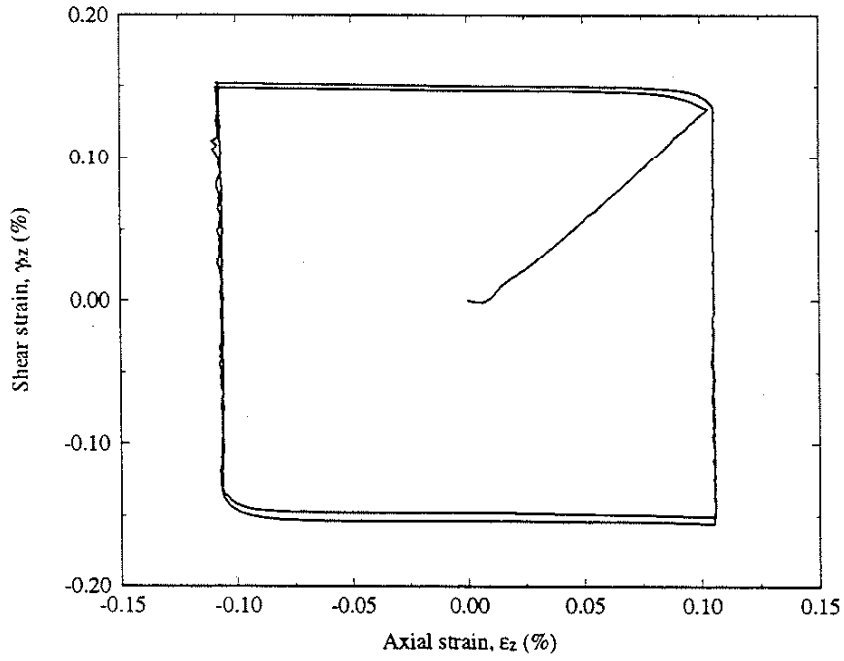

(b)

Figure 6.7. (a) Nominal stress path and (b) measured strain response for maximum nominal stresses of S_z=160 MPa, and S_{xz}=100 MPa.

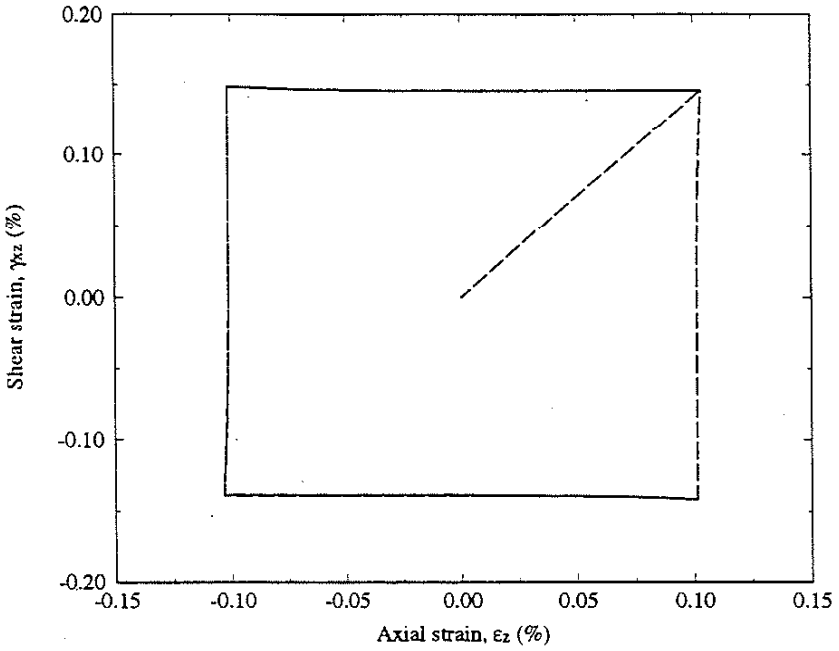

(c)

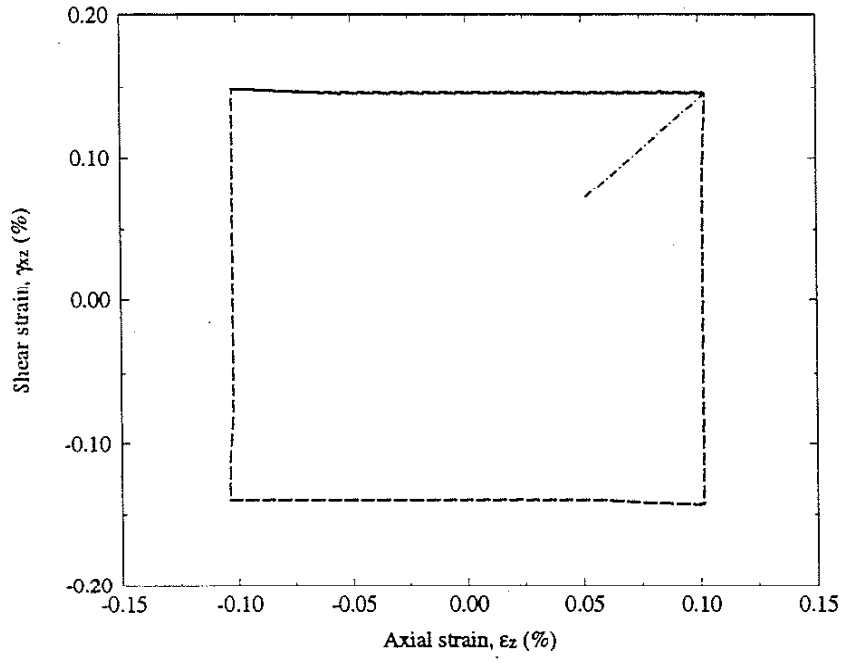

(d)

Figure 6.7 (continued). (c) Calculation using the simplified method and (d) calculation using the finite element method for maximum nominal stresses of S_z=160 MPa, and S_{xz}=100 MPa.

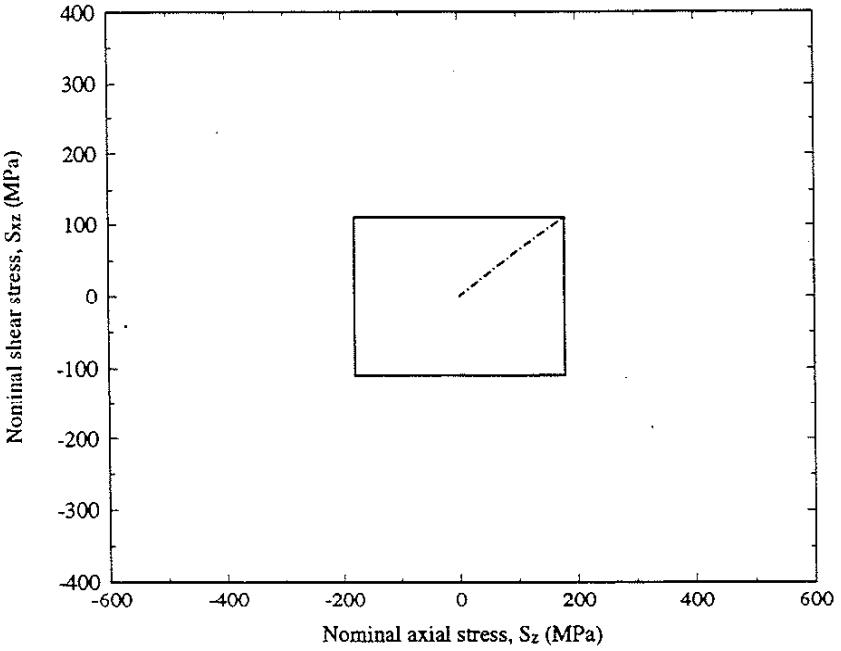

(a)

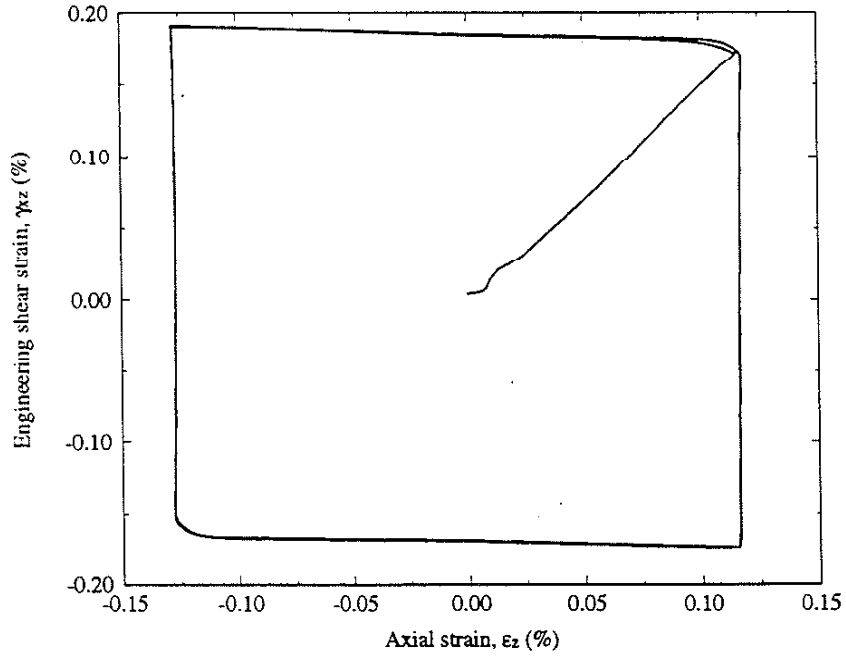

(b)

Figure 6.8. (a) Nominal stress path and (b) measured strain response for maximum nominal stresses of S_z=179 MPa, and S_{xz}=117 MPa.

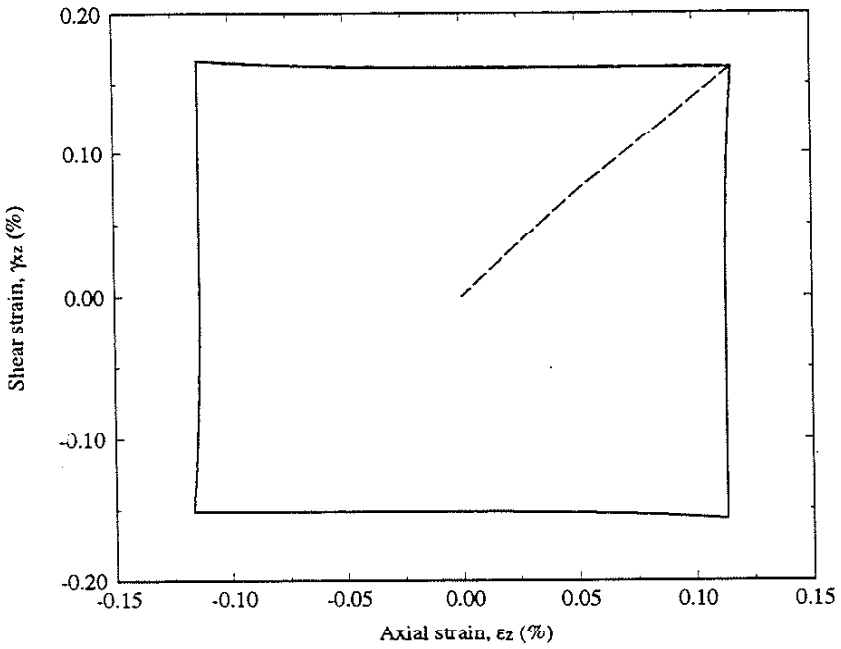

(c)

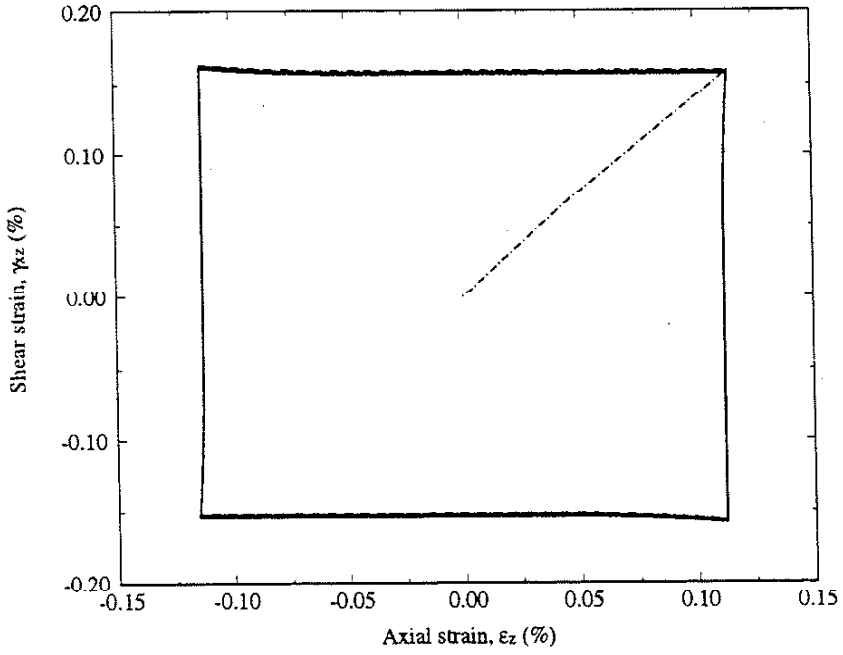

(d)

Figure 6.8 (continued). (c) Calculation using the simplified method and (d) calculation using the finite element method for maximum nominal stresses of S_z=179 MPa, and S_{xz}=117 MPa.

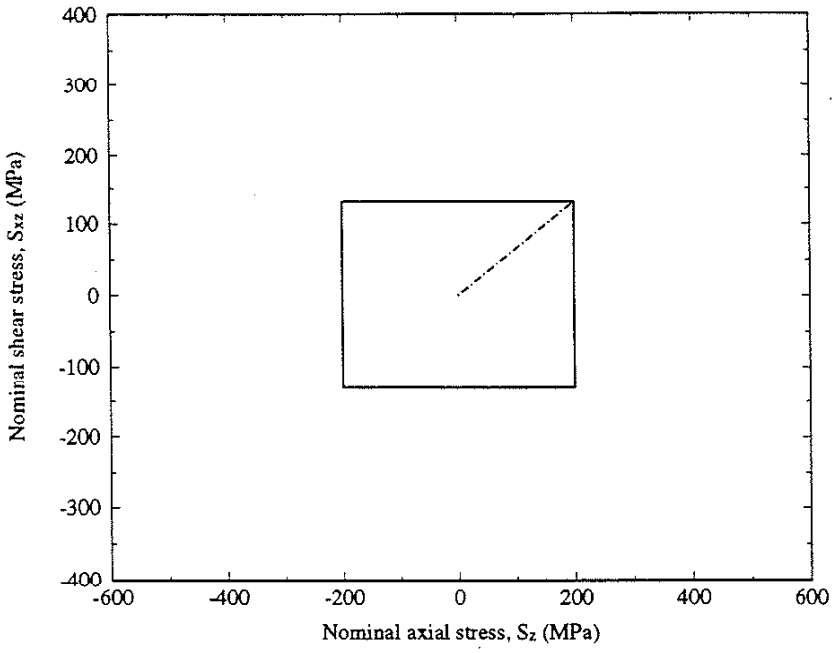

(a)

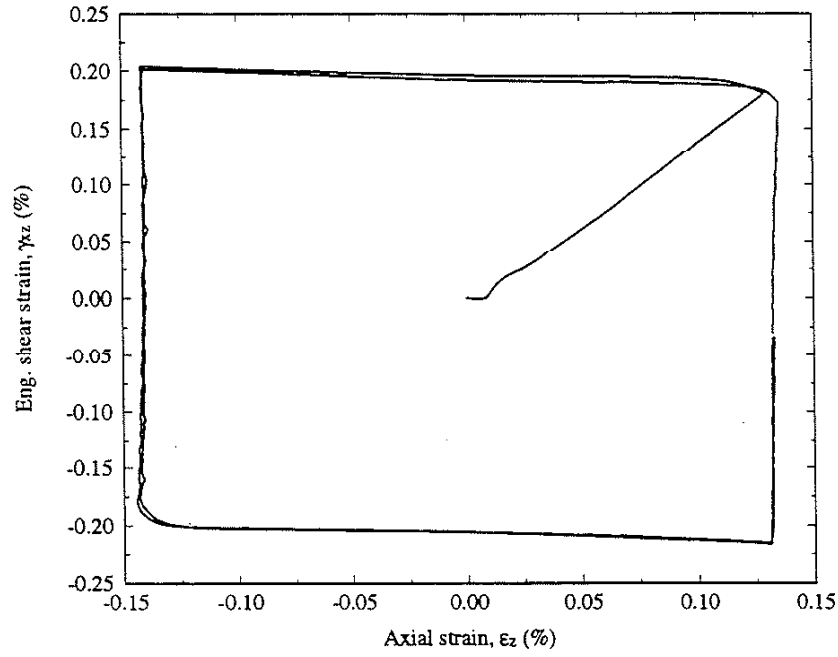

(b)

Figure 6.9. (a) Nominal stress path and (b) measured strain response for maximum nominal stresses of S_z=200 MPa, and S_{xz}=131 MPa.

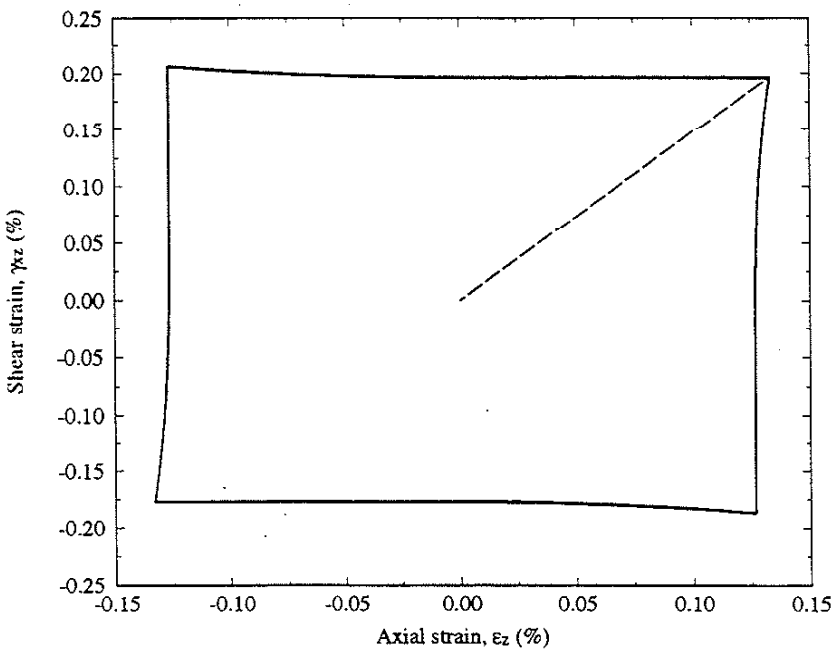

(c)

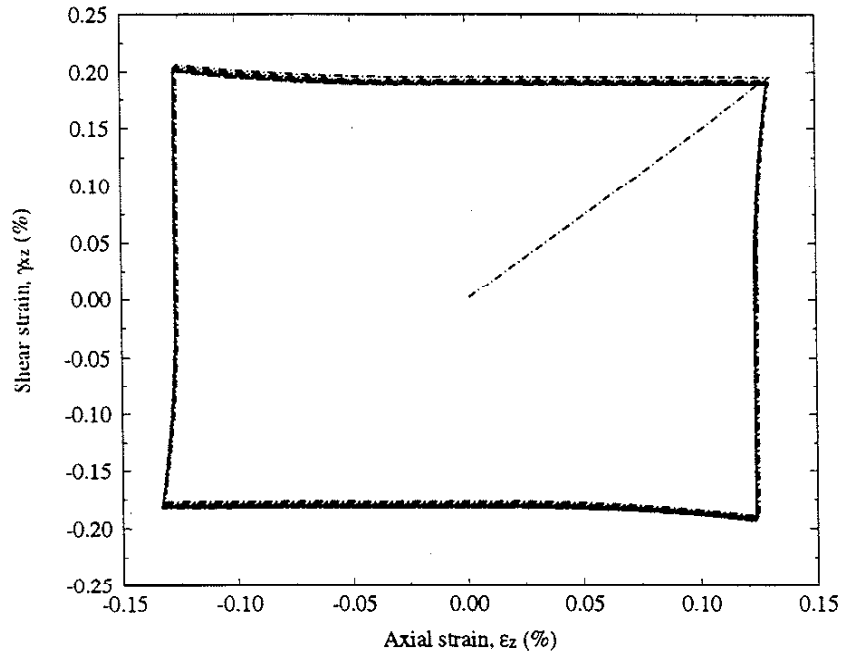

(d)

Figure 6.9 (continued). (c) Calculation using the simplified method and (d) calculation using the finite element method for maximum nominal stresses of S_z=200 MPa, and S_{xz}=131 MPa.

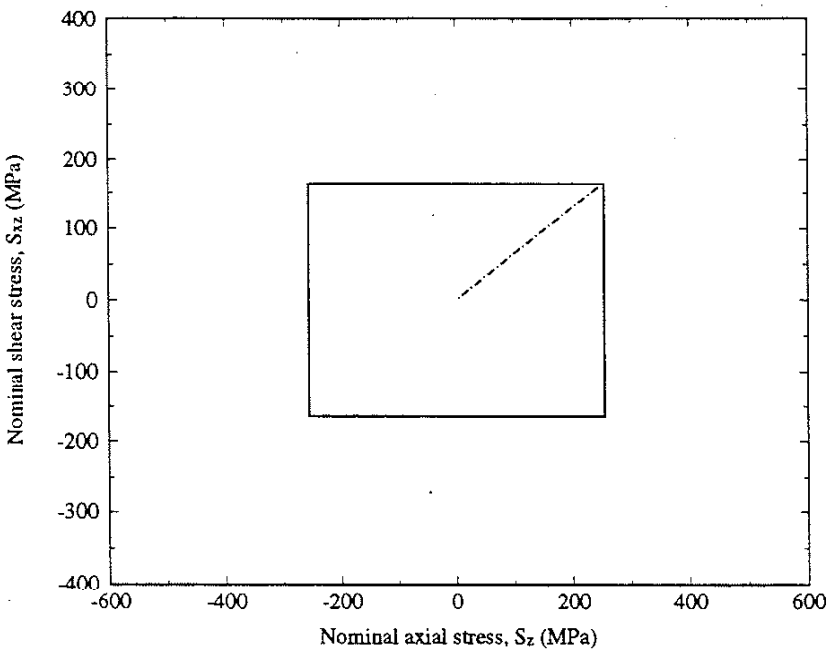

(a)

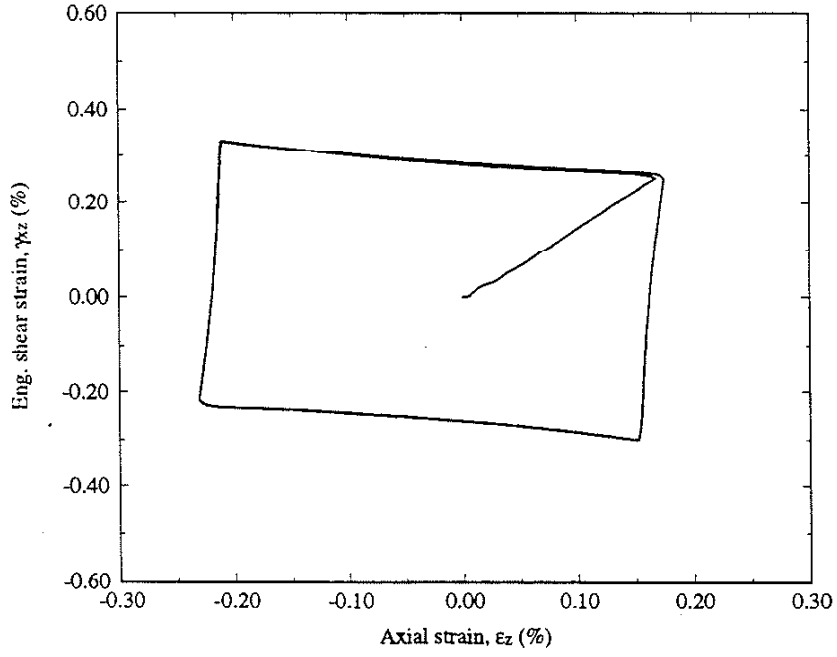

(b)

Figure 6.10. (a) Nominal stress path and (b) measured strain response for maximum nominal stresses of S_z=258 MPa, and S_{xz}=168 MPa.

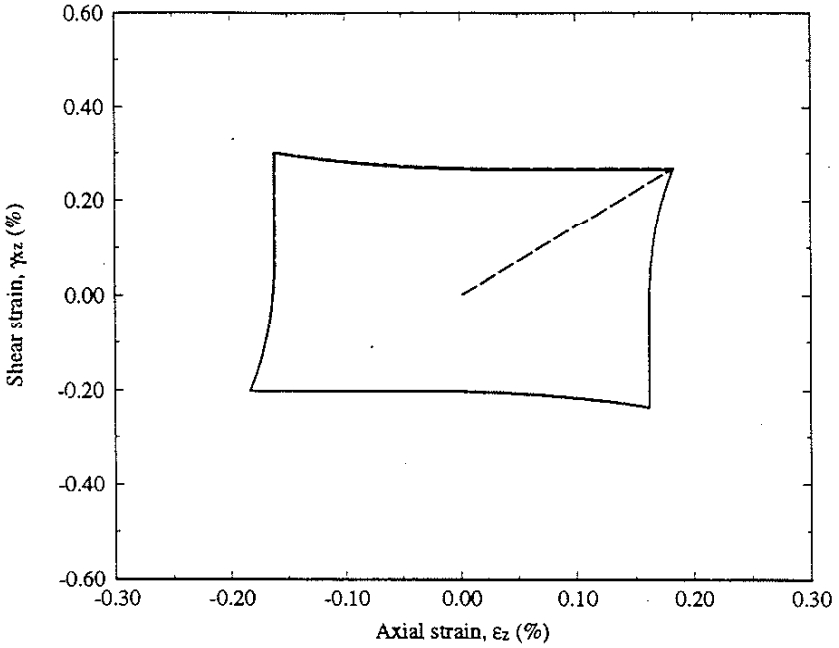

(c)

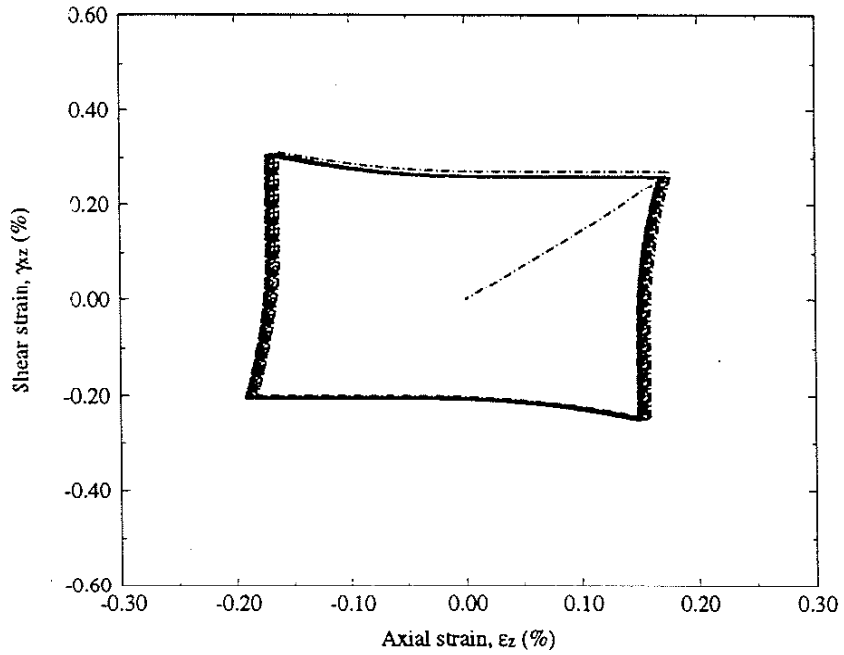

(d)

Figure 6.10 (continued). (c) Calculation using the simplified method and (d) calculation using the finite element method for maximum nominal stresses of S_z=258 MPa, and S_{xz}=168 MPa.

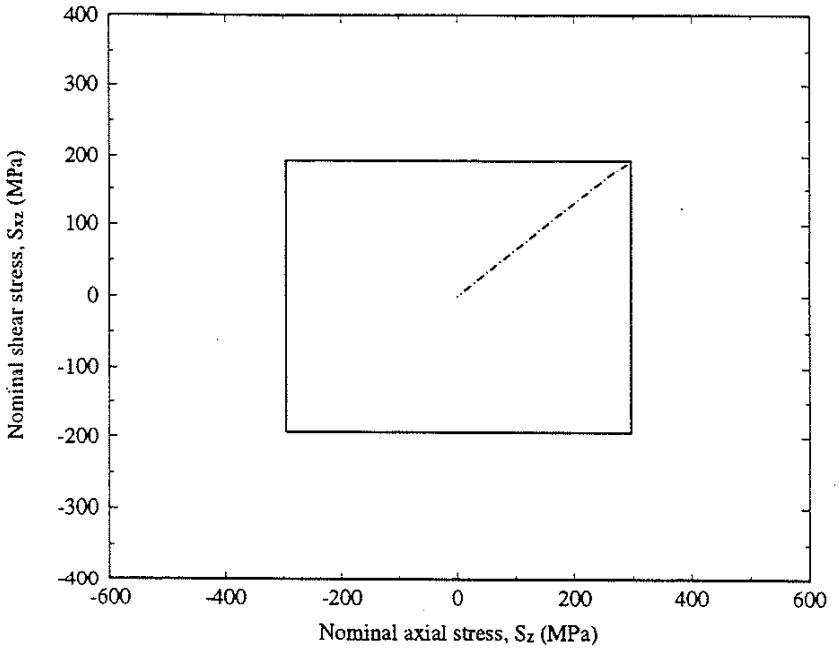

(a)

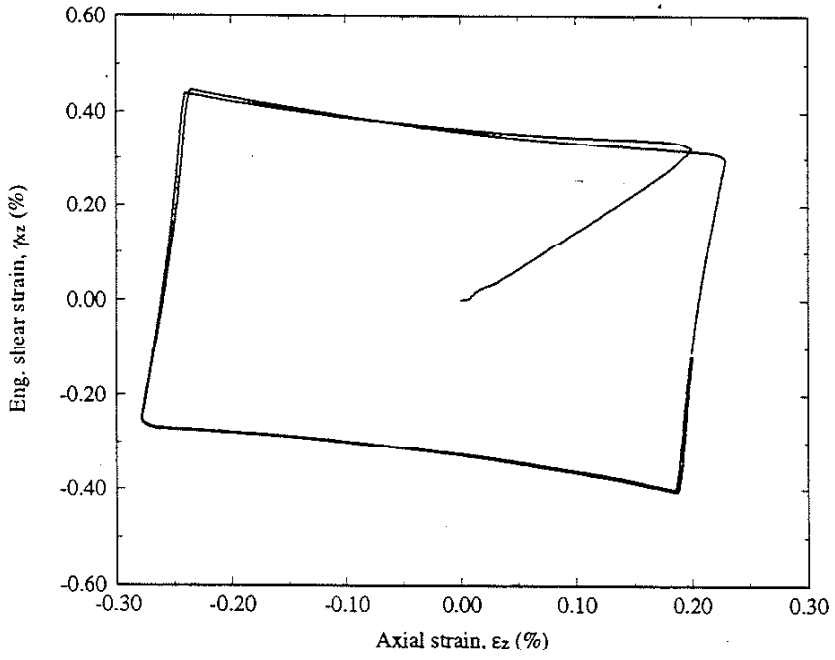

(b)

Figure 6.11. (a) Nominal stress path and (b) measured strain response for maximum nominal stresses of S_z=296 MPa, and S_{xz}=193 MPa.

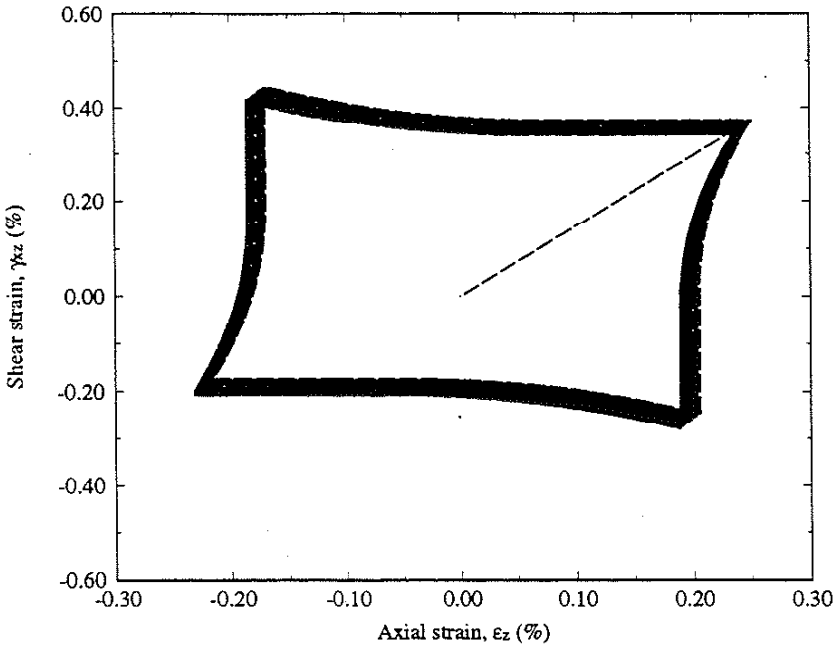

(c)

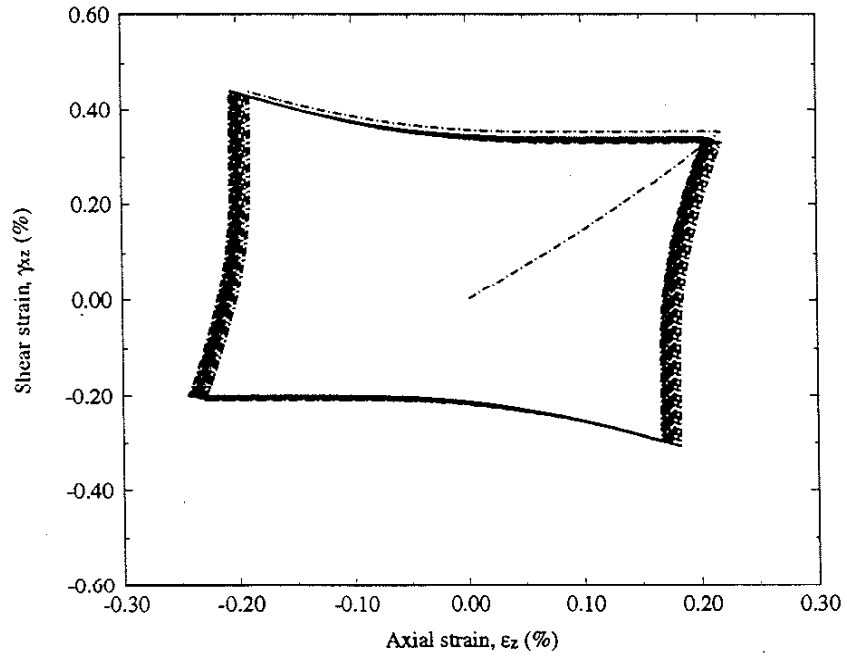

(d)

Figure 6.11 (continued). (c) Calculation using the simplified method and (d) calculation using the finite element method for maximum nominal stresses of S_z=296 MPa, and S_{xz}=193 MPa.

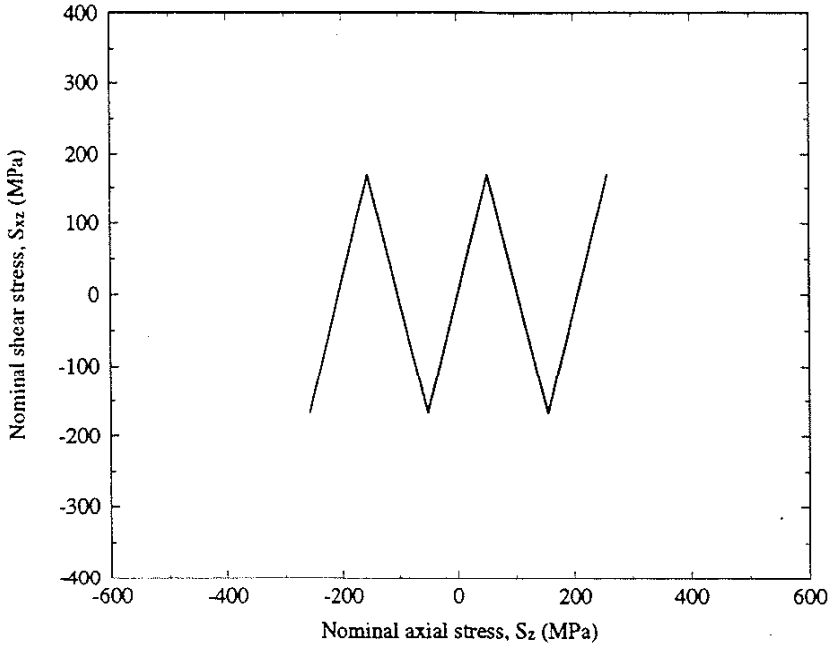

(a)

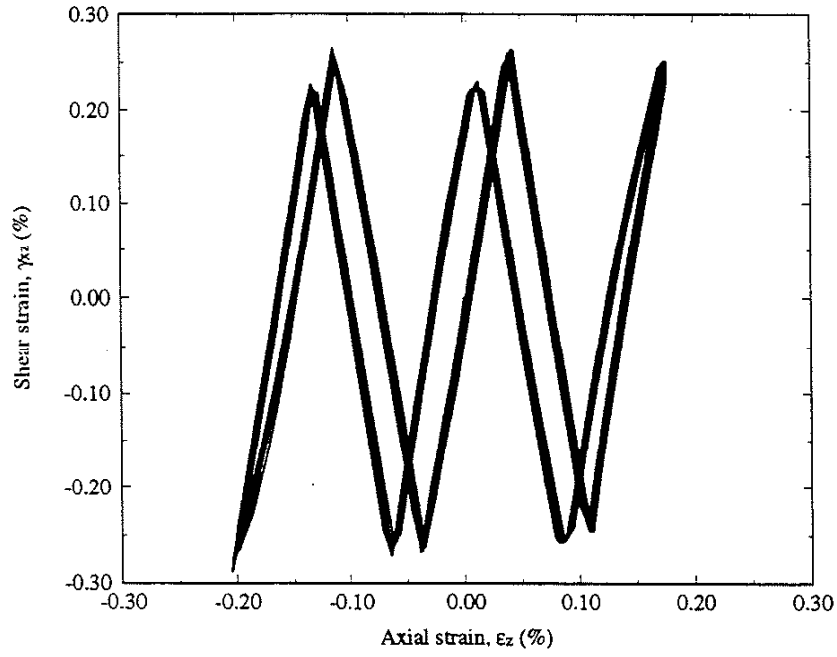

(b)

Figure 6.12. (a) Nominal stress path and (b) measured strain response for maximum nominal stresses of S_z=258 MPa, and S_{xz}=168 MPa.

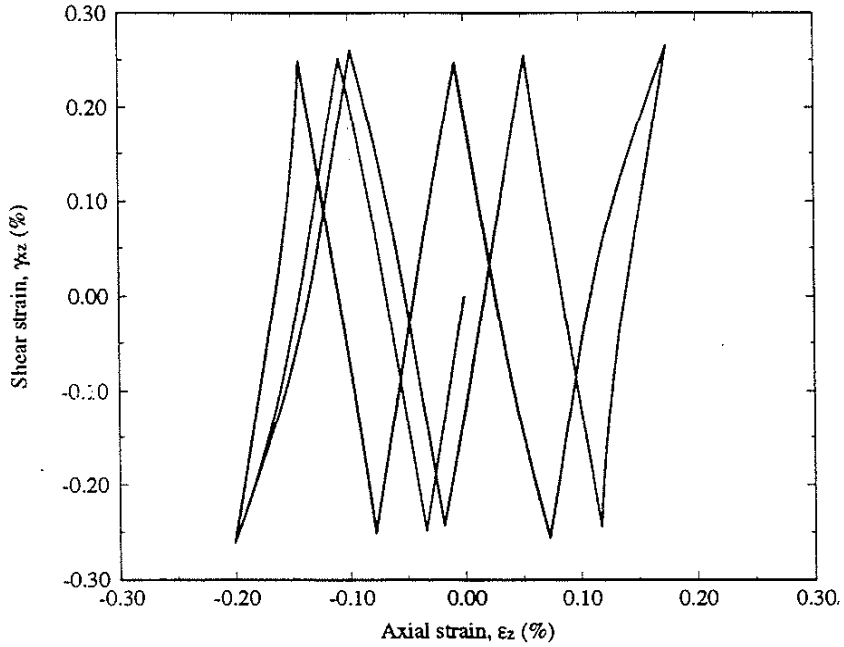

(c)

Figure 6.12 (continued). (c) Calculation using the simplified method for maximum nominal stresses of S_z=258 MPa, and S_{xz}=168 MPa.

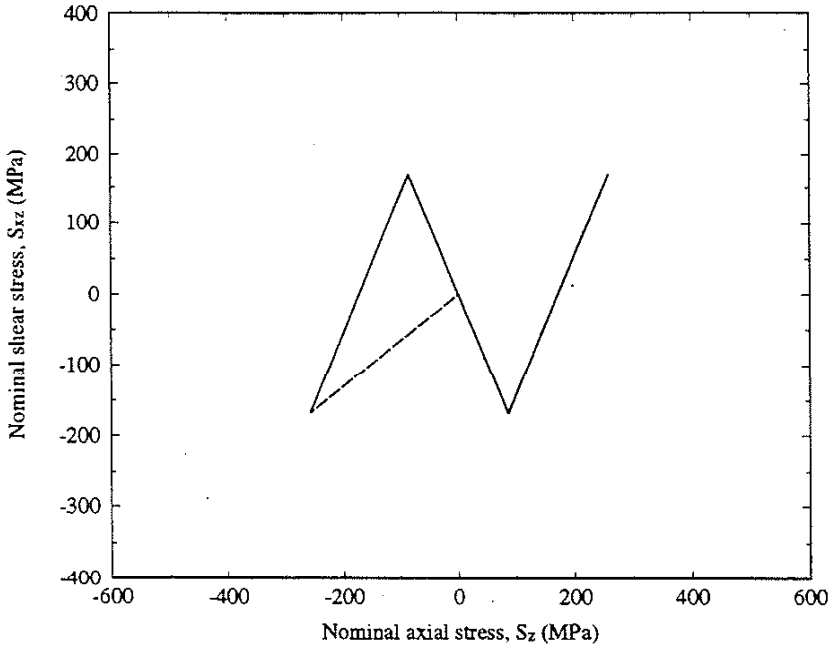

(a)

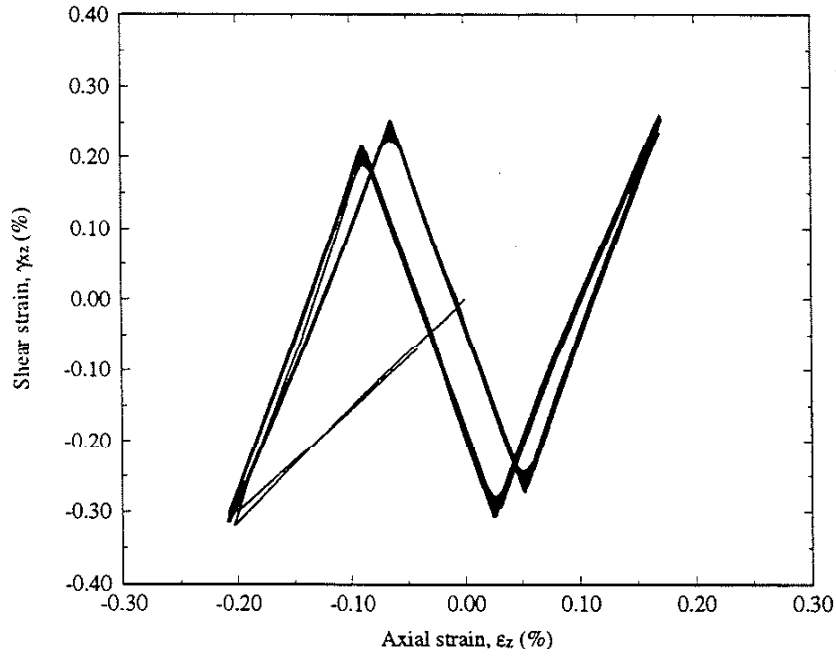

(b)

Figure 6.13. (a) Nominal stress path and (b) measured strain response (b) for maximum nominal stresses of S_z=258 MPa, and S_{xz}=168 MPa.

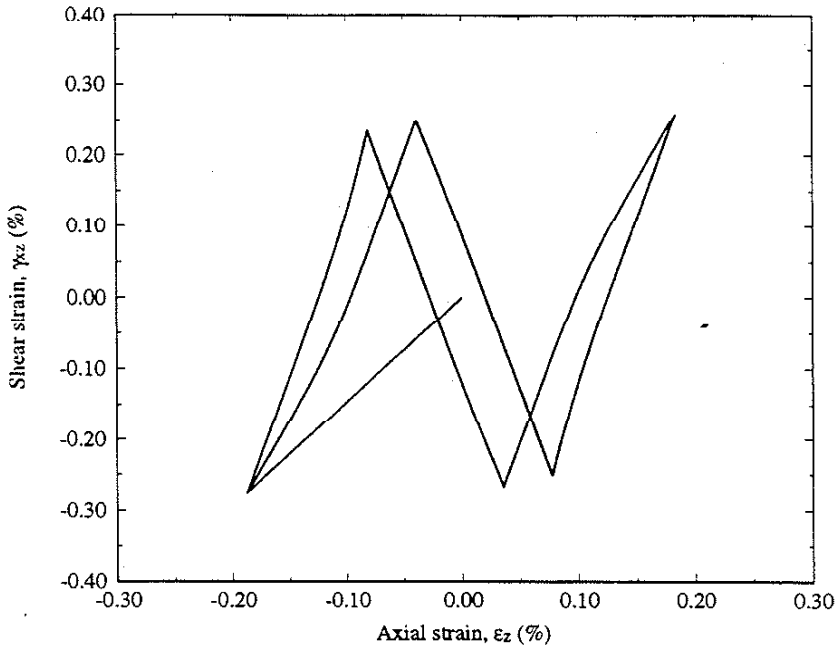

(c)

Figure 6.13 (continued). (c) Calculation using the simplified method for maximum nominal stresses of S_z=258 MPa, and S_{xz}=168 MPa.

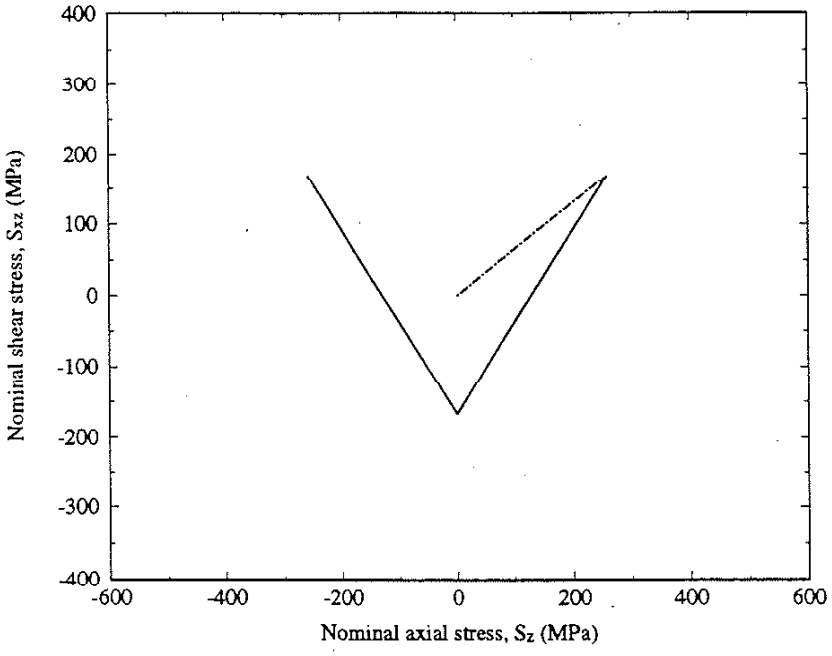

(a)

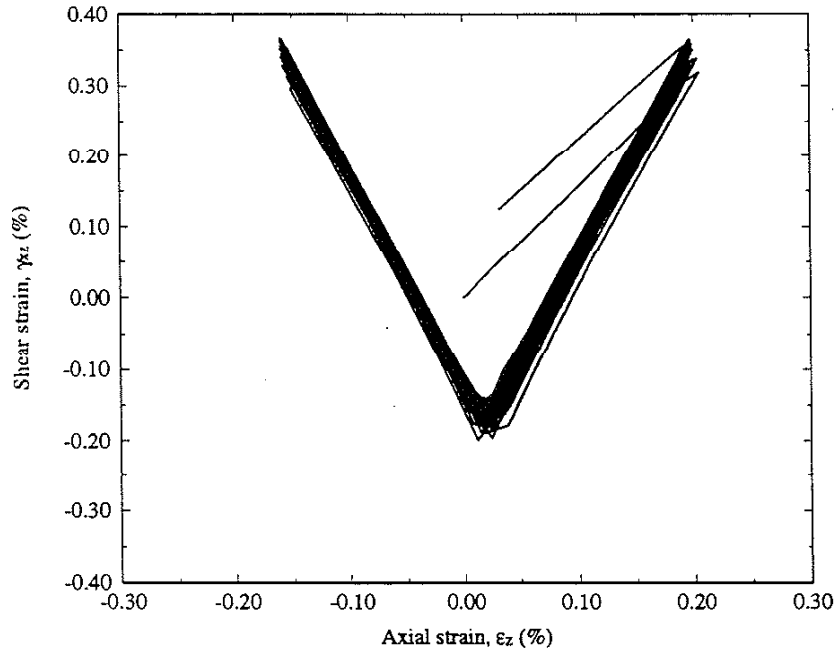

(b)

Figure 6.14. (a) Nominal stress path and (b) measured strain response for maximum nominal stresses of S_z=258 MPa, and S_{xz}=168 MPa.

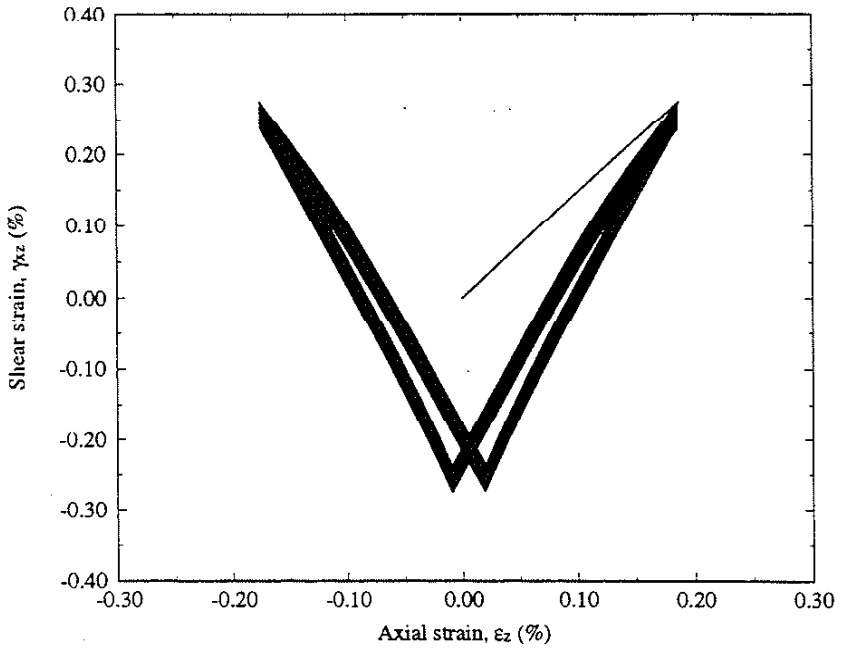

(c)

Figure 6.14 (continued). (c) Calculation using the simplified method for maximum nominal stresses of S_z=258 MPa, and S_{xz}=168 MPa.

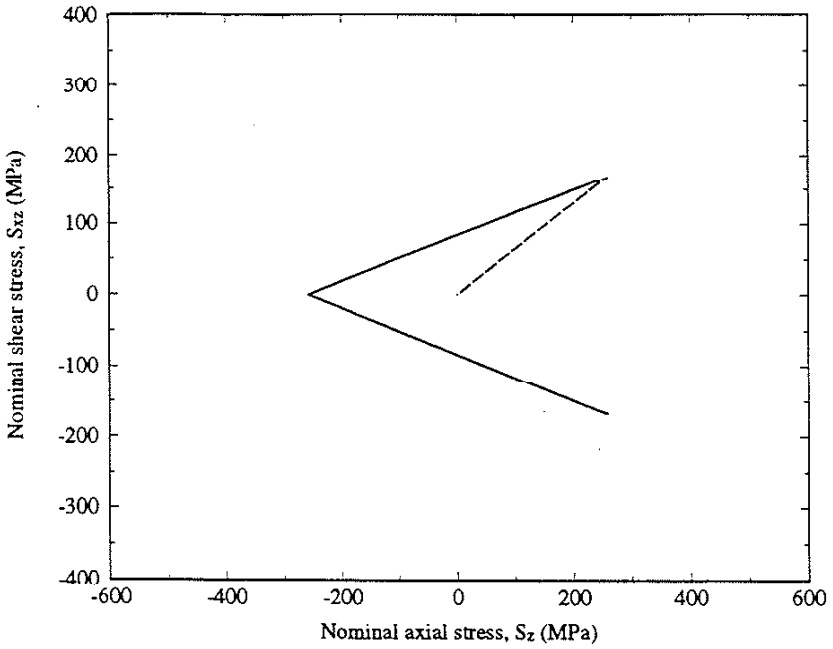

(a)

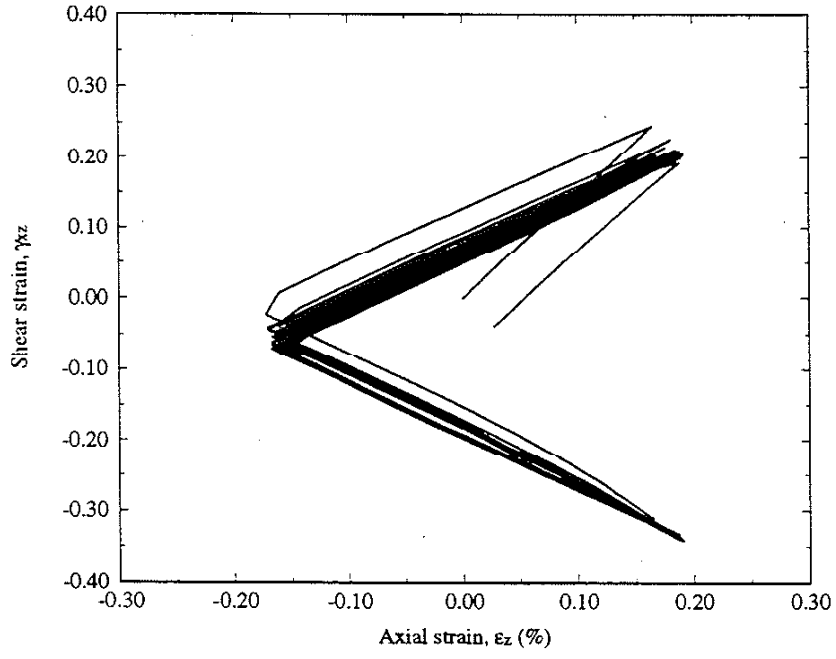

(b)

Figure 6.15. (a) Nominal stress path and (b) measured strain response for maximum nominal stresses of S_z=258 MPa, and S_{xz}=168 MPa.

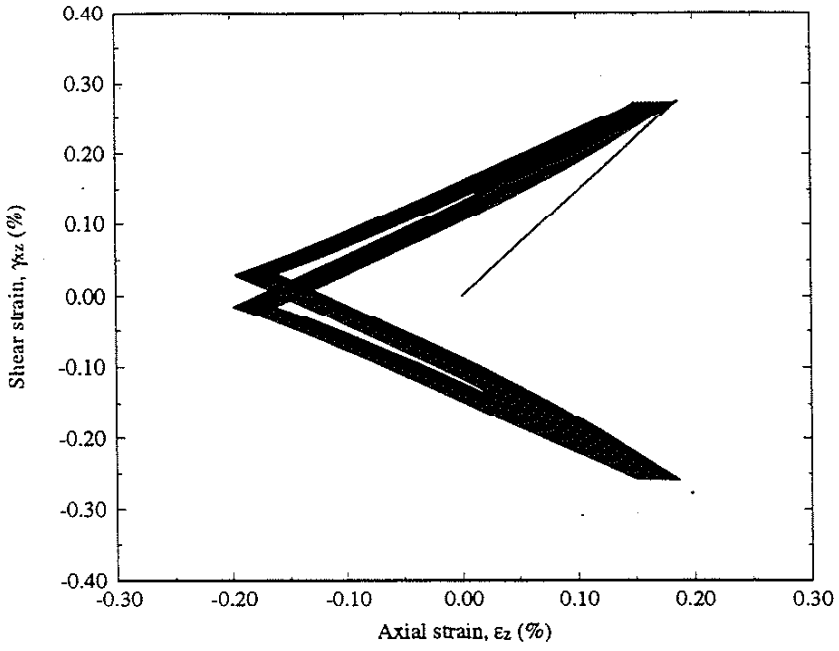

(c)

Figure 6.15 (continued). (c) Calculation using the simplified method for maximum nominal stresses of S_z=258 MPa, and S_{xz}=168 MPa.

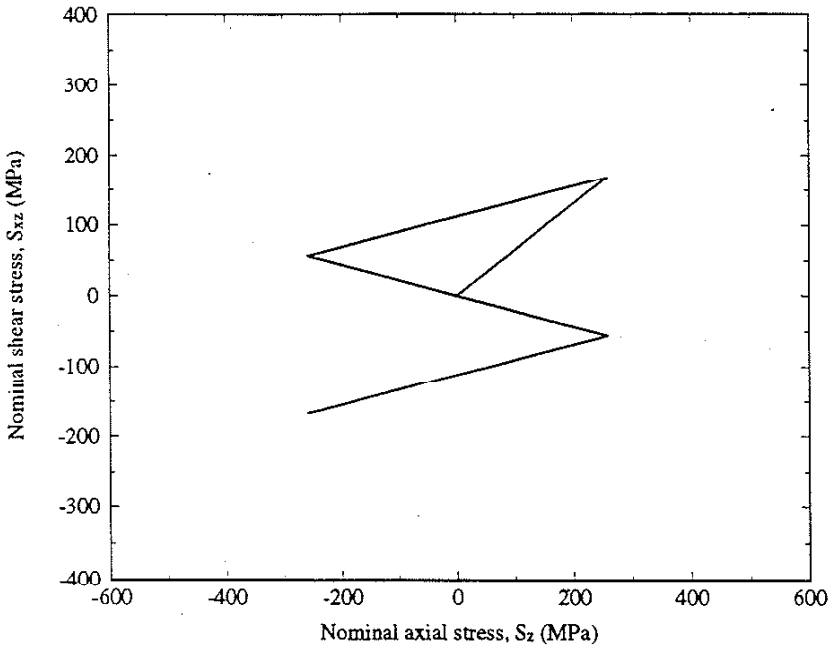

(a)

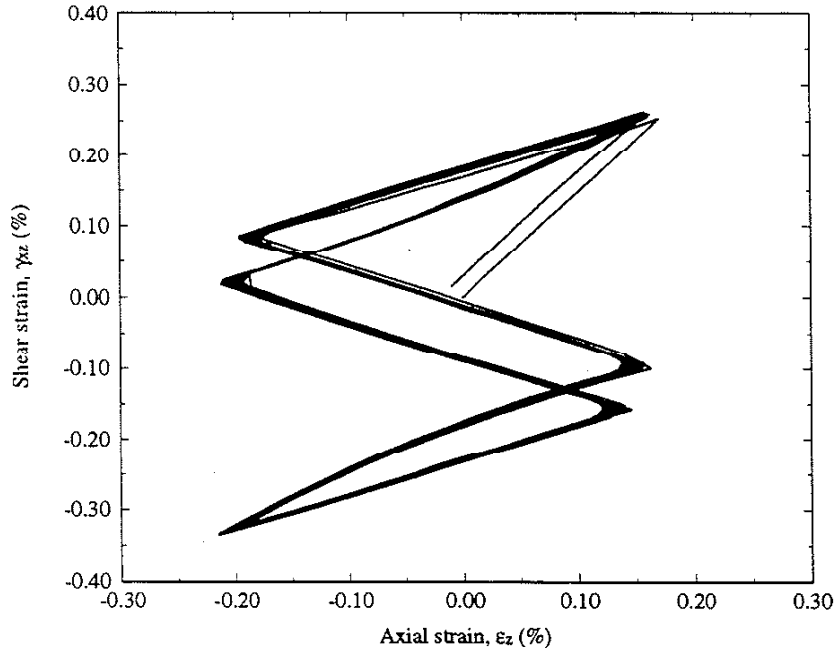

(b)

Figure 6.16. (a) Nominal stress path and (b) measured strain response for maximum nominal stresses of S_z=258 MPa, and S_{xz}=168 MPa.

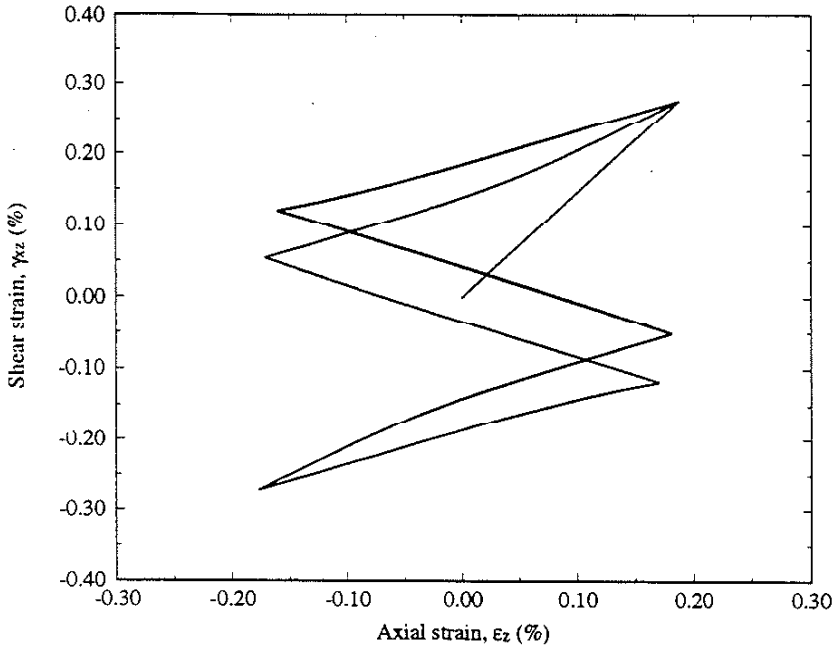

(c)

Figure 6.16 (continued). (c) Calculation using the simplified method for maximum nominal stresses of S_z=258 MPa, and S_{xz}=168 MPa.

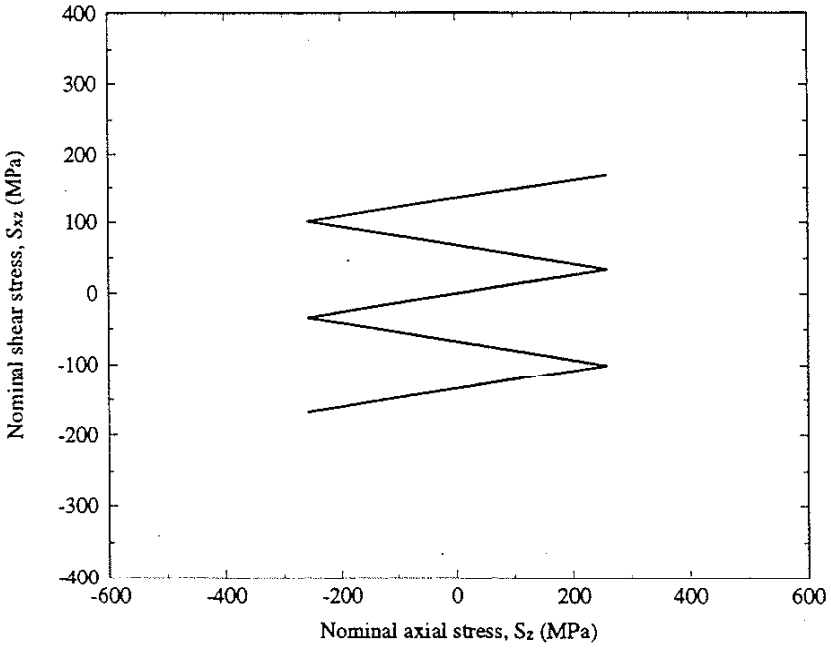

(a)

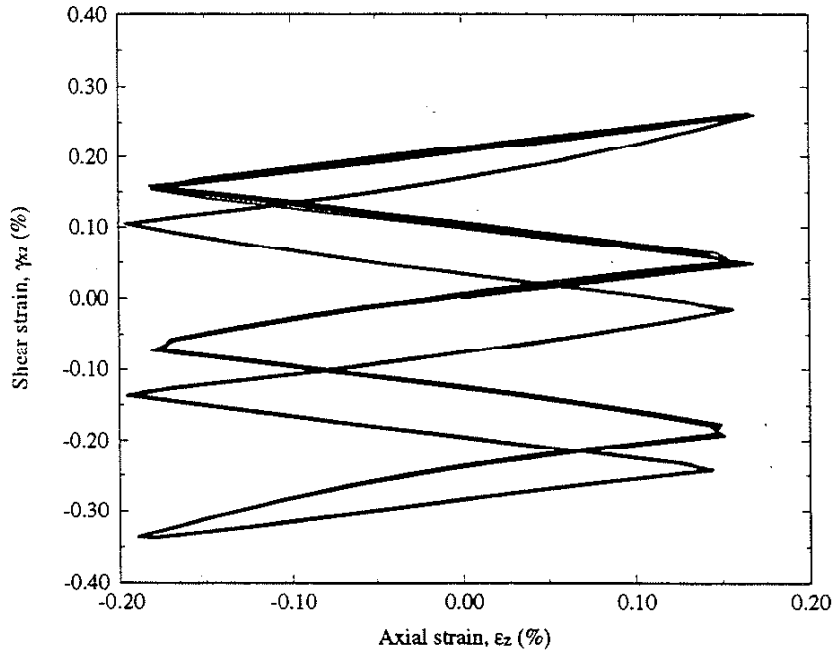

(b)

Figure 6.17. (a) Nominal stress path and (b) measured strain response for maximum nominal stresses of S_z=258 MPa, and S_{xz}=168 MPa.

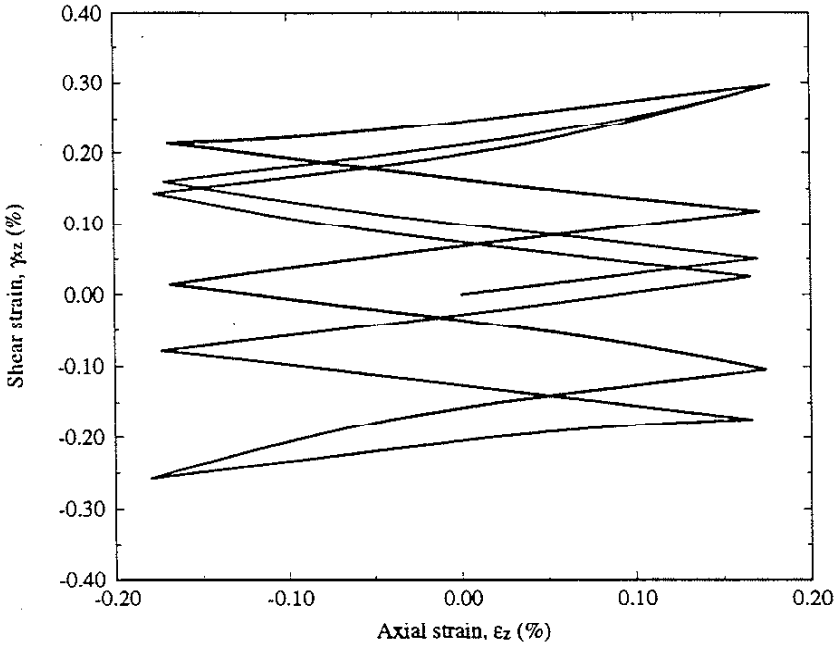

(c)

Figure 6.17 (continued). (c) Calculation using the simplified method for maximum nominal stresses of S_z=258 MPa, and S_{xz}=168 MPa.

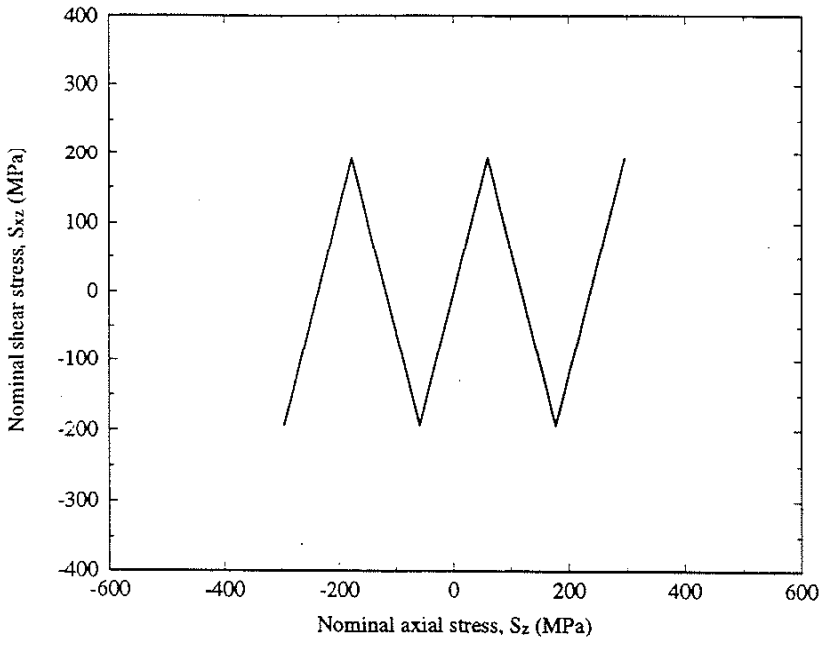

(a)

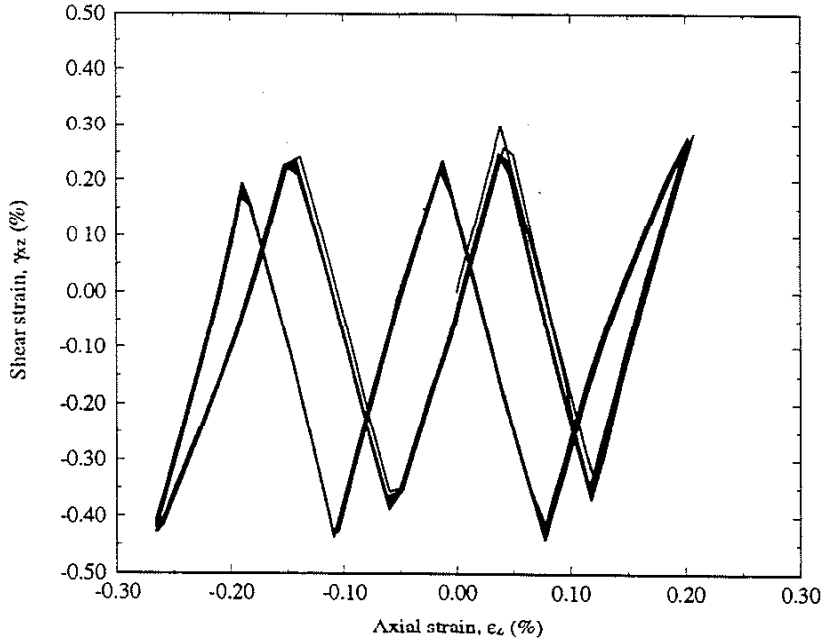

(b)

Figure 6.18. (a) Nominal stress path and (b) measured strain response for maximum nominal stresses of S_z=296 MPa, and S_{xz}=193 MPa.

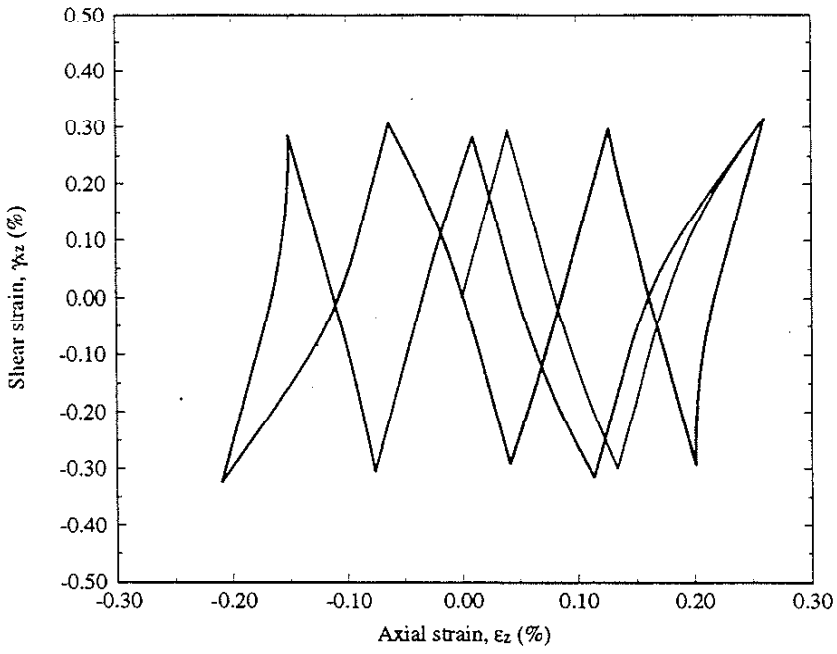

(c)

Figure 6.18 (continued). (c) Calculation using the simplified method for maximum nominal stresses of S_z=296 MPa, and S_{xz}=193 MPa.

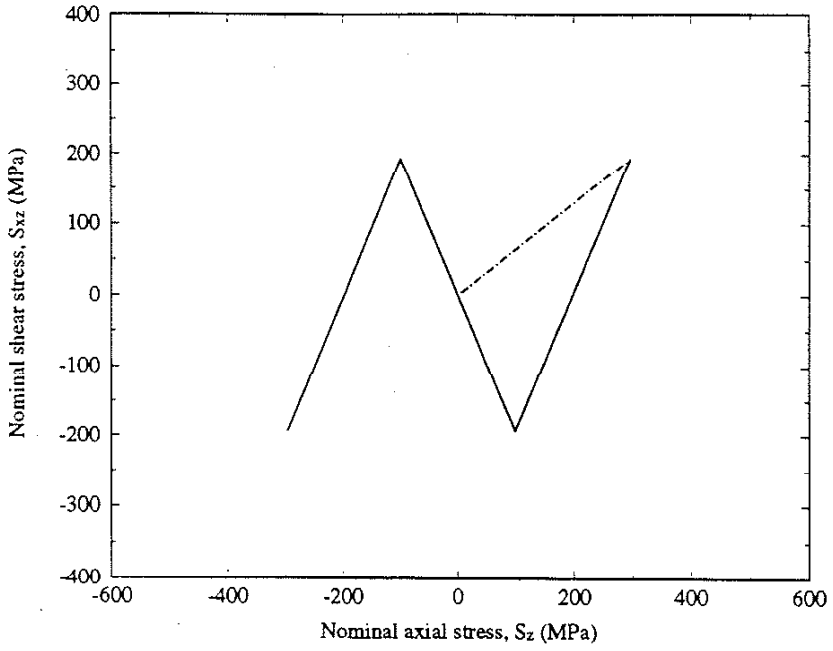

(a)

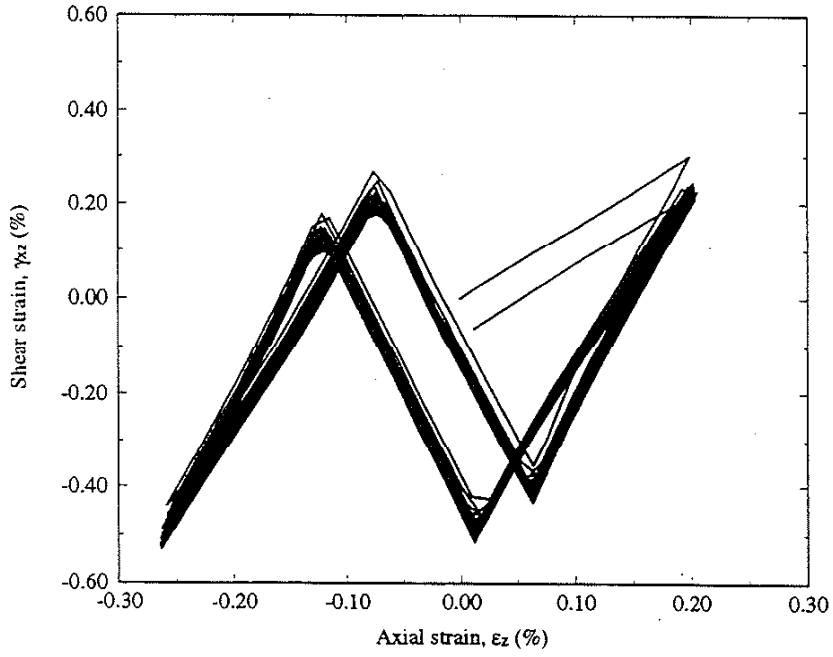

(b)

Figure 6.19. (a) Nominal stress path and (b) measured strain response (b) for maximum nominal stresses of S_z=296 MPa, and S_{xz}=193 MPa.

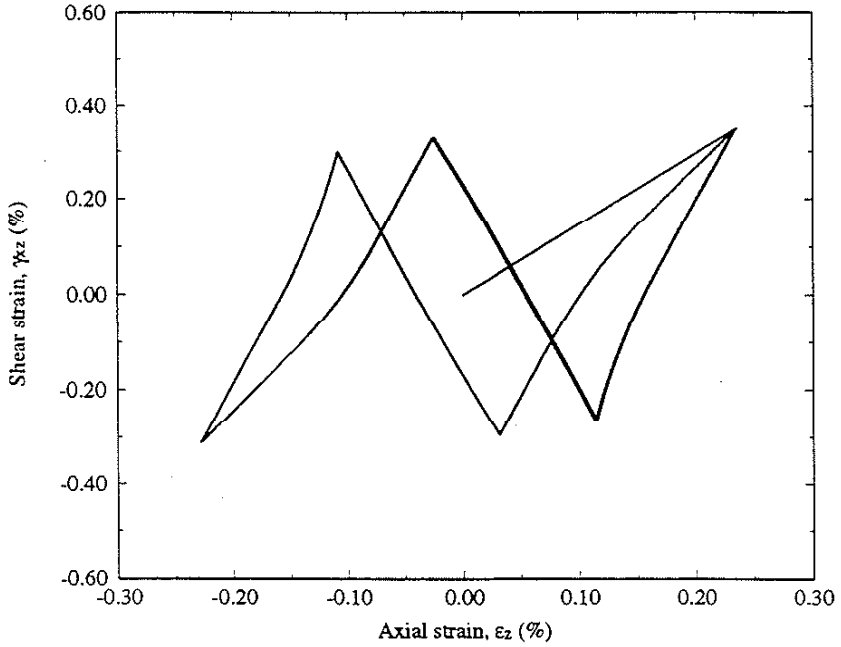

(c)

Figure 6.19 (continued). (c) Calculation using the simplified method for maximum nominal stresses of S_z=296 MPa, and S_{xz}=193 MPa.

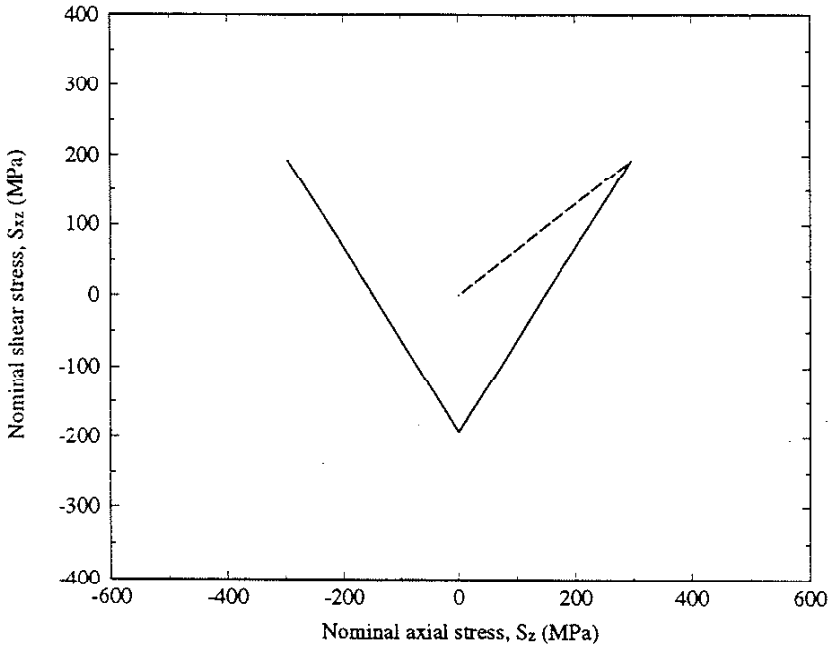

(a)

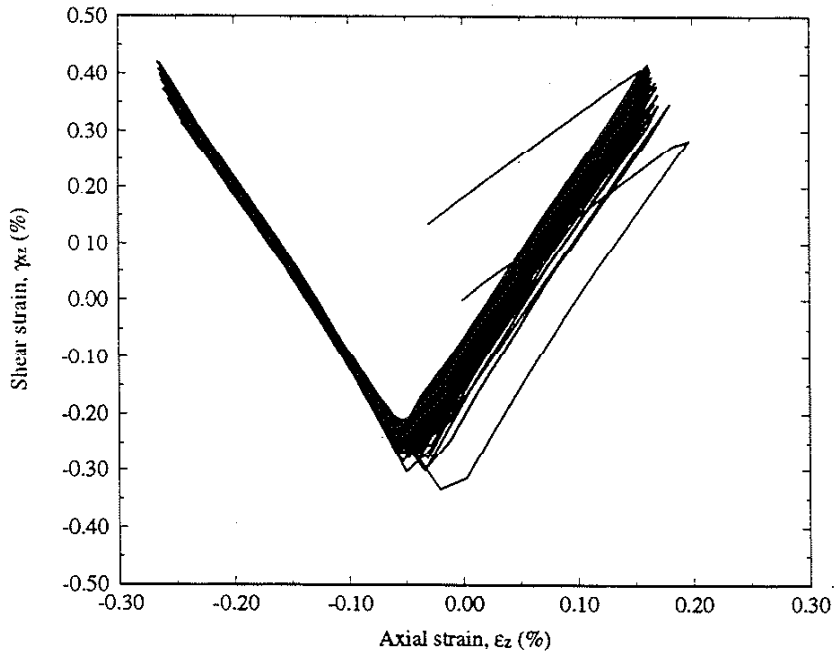

(b)

Figure 6.20. (a) Nominal stress path and (b) measured strain response for maximum nominal stresses of S_z=296 MPa, and S_{xz}=193 MPa.

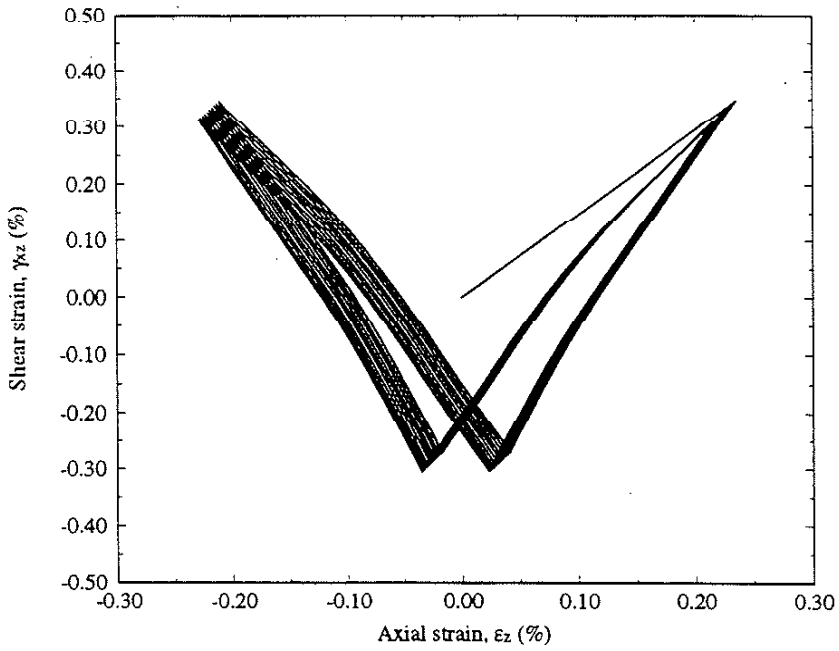

(c)

Figure 6.20 (continued). (c) Calculation using the simplified method for maximum nominal stresses of S_z=296 MPa, and S_{xz}=193 MPa.

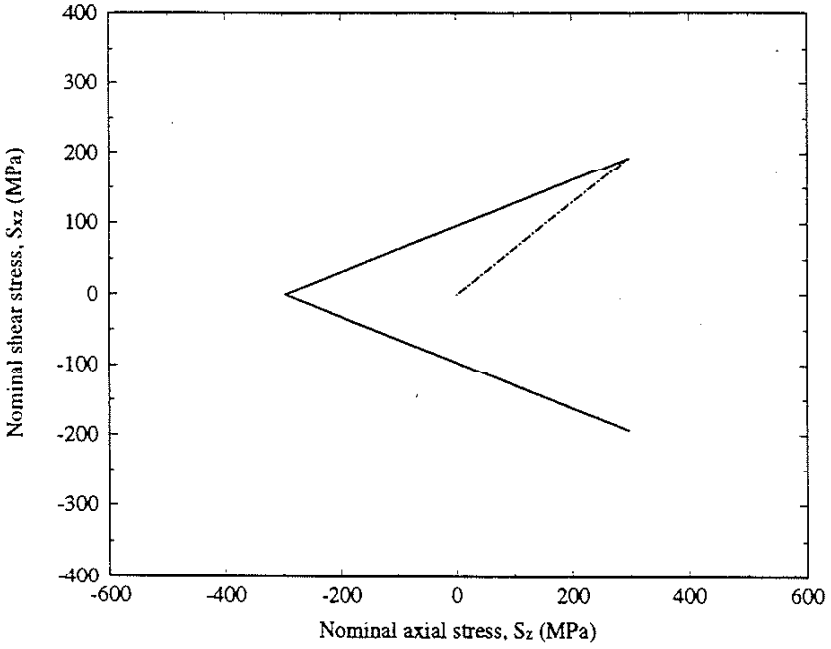

(a)

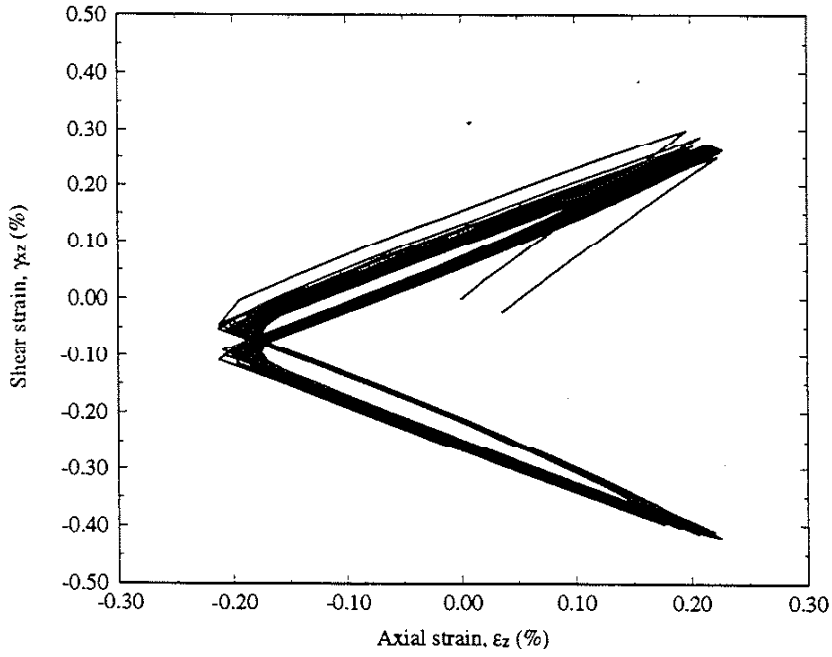

(b)

Figure 6.21. (a) Nominal stress path and (b) measured strain response for maximum nominal stresses of S_z=296 MPa, and S_{xz}=193 MPa.

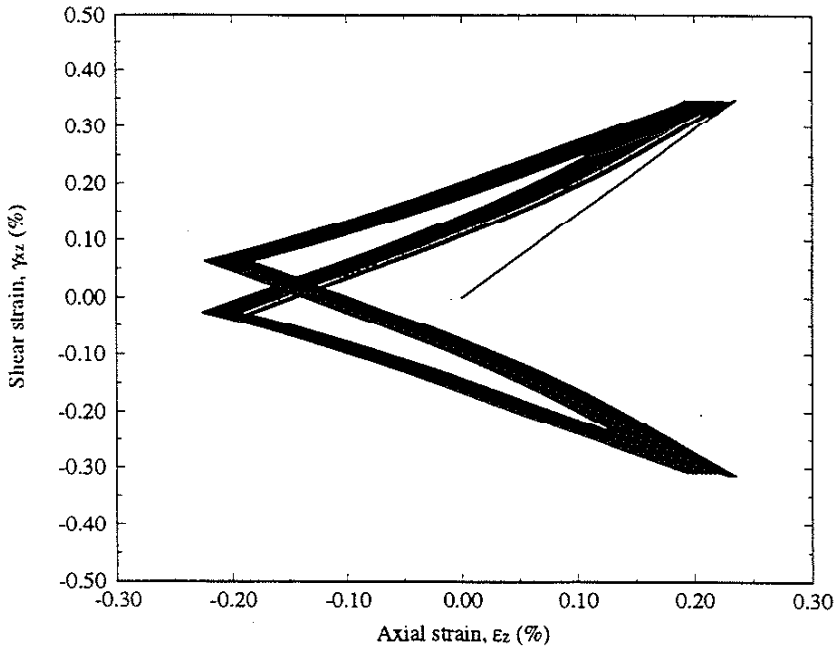

(c)

Figure 6.21 (continued). (c) Calculation using the simplified method for maximum nominal stresses of S_z=296 MPa, and S_{xz}=193 MPa.

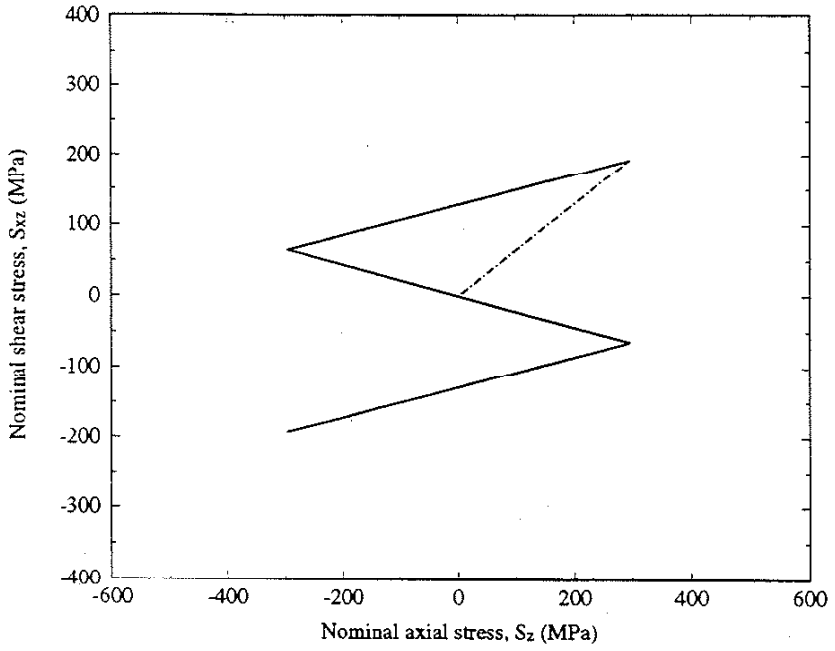

(a)

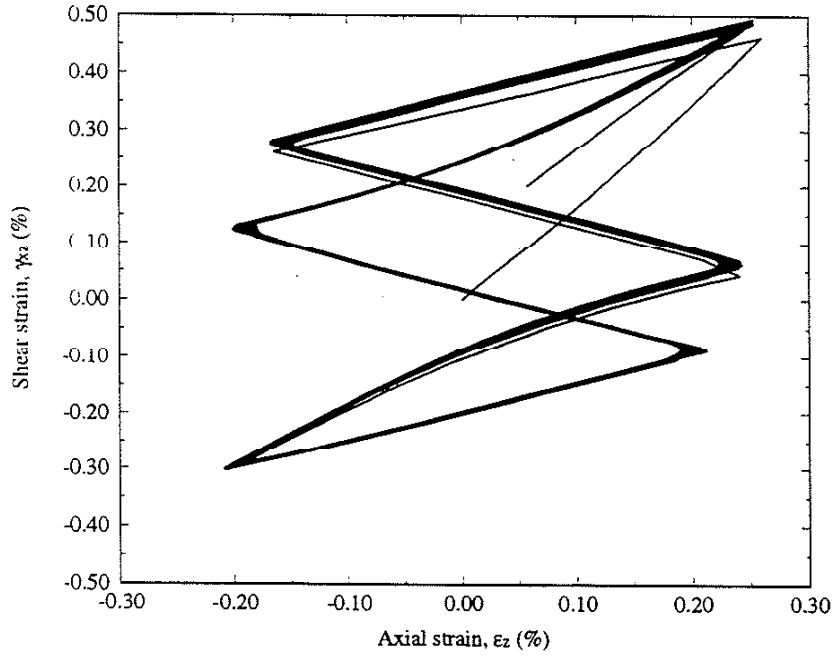

(b)

Figure 6.22. (a) Nominal stress path and (b) measured strain response for maximum nominal stresses of S_z=296 MPa, and S_{xz}=193 MPa.

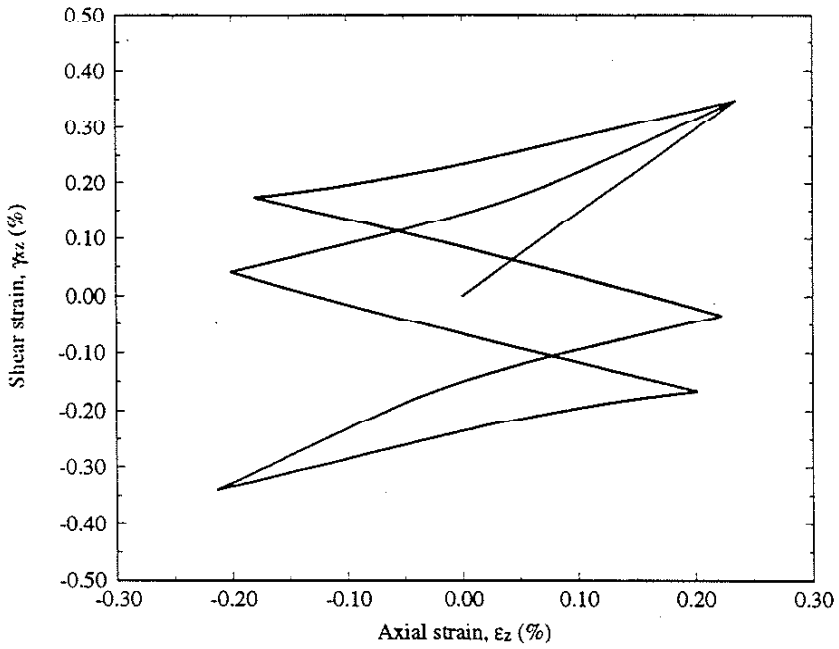

(c)

Figure 6.22 (continued). (c) Calculation using the simplified method for maximum nominal stresses of S_z=296 MPa, and S_{xz}=193 MPa.

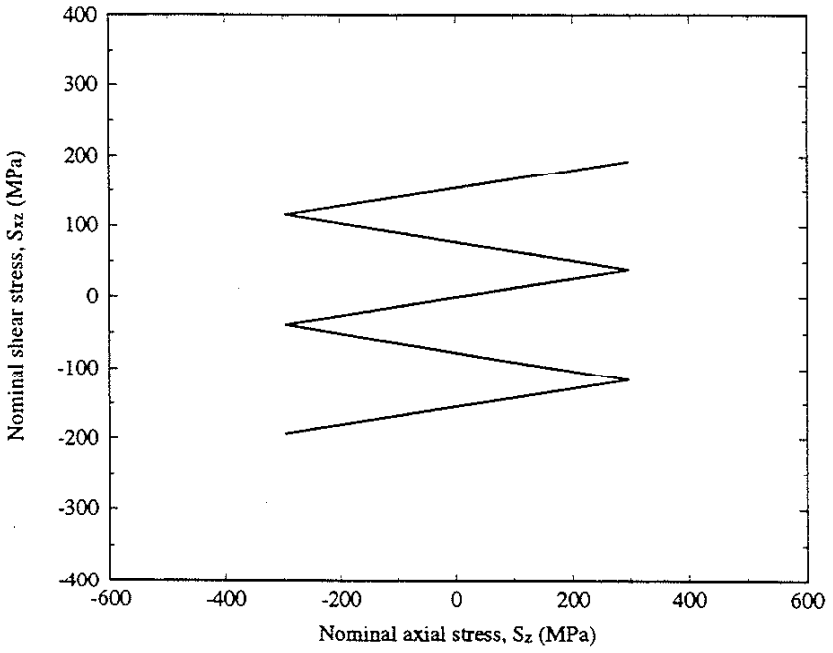

(a)

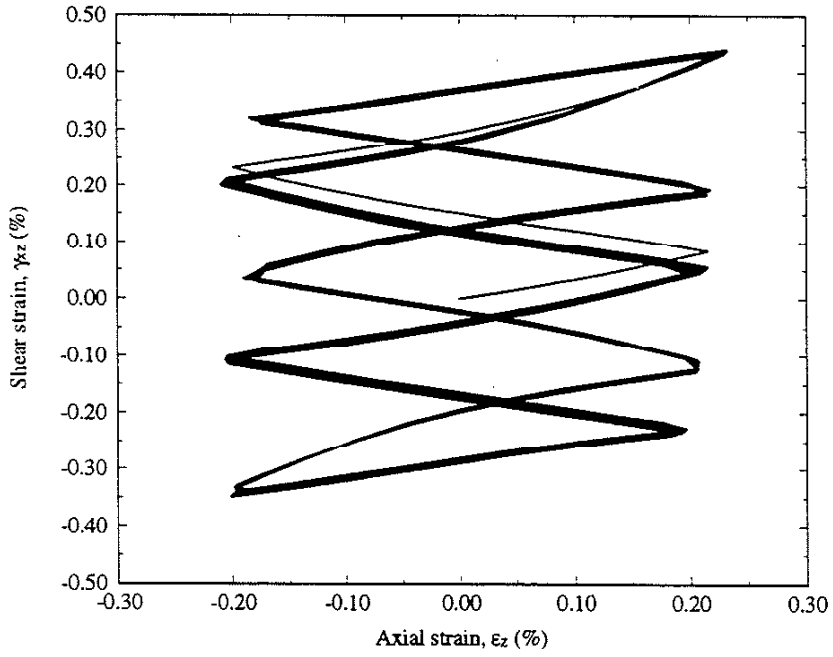

(b)

Figure 6.23. (a) Nominal stress path and (b) measured strain response for maximum nominal stresses of S_z=296 MPa, and S_{xz}=193 MPa.

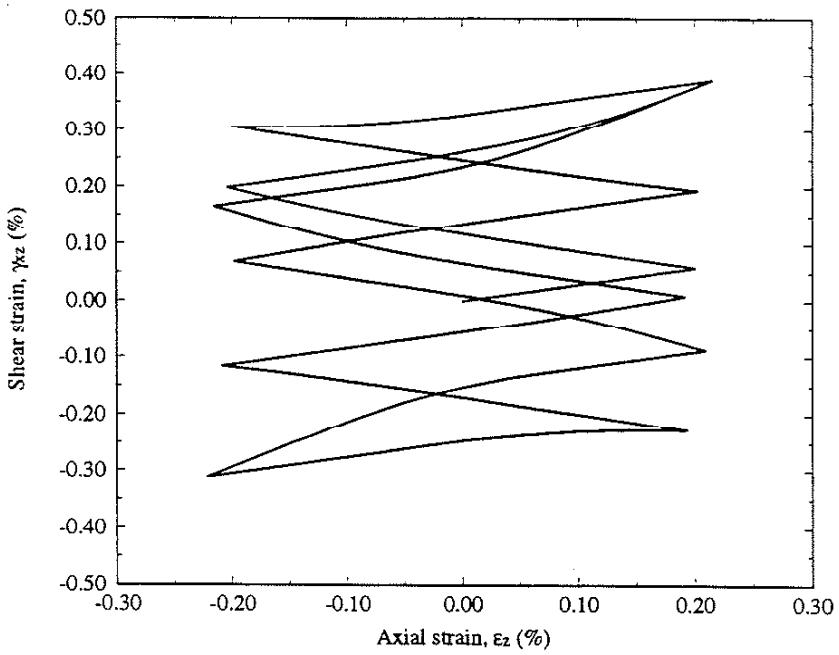

(c)

Figure 6.23 (continued). (c) Calculation using the simplified method for maximum nominal stresses of S_z=296 MPa, and S_{xz}=193 MPa.

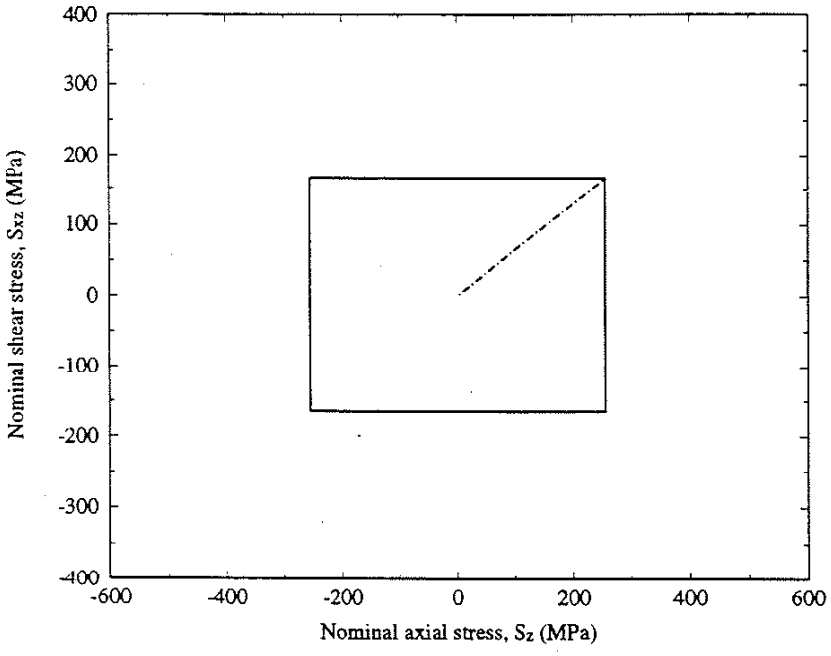

(a)

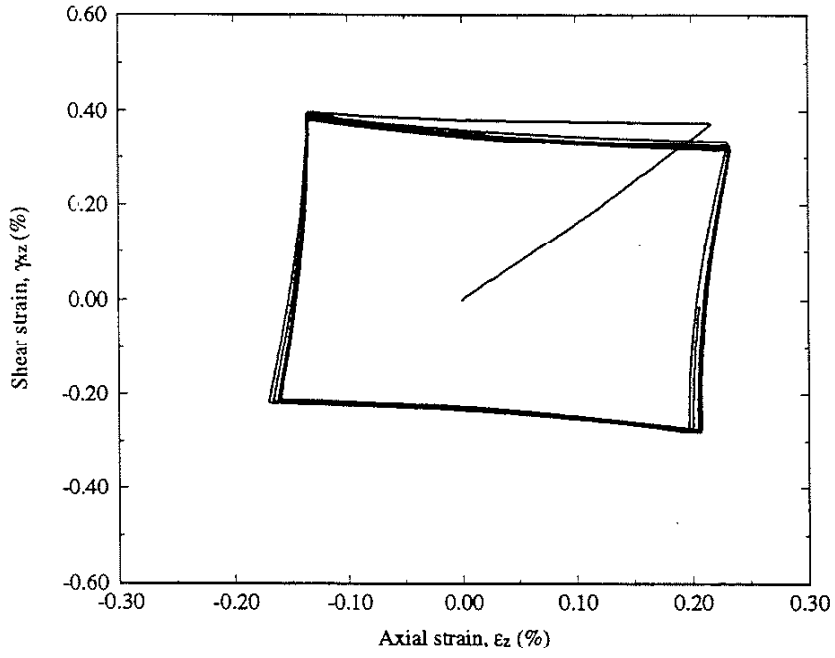

(b)

Figure 6.24. (a) Nominal stress path and (b) measured strain response for maximum nominal stresses of S_z=258 MPa, and S_{xz}=168 MPa.

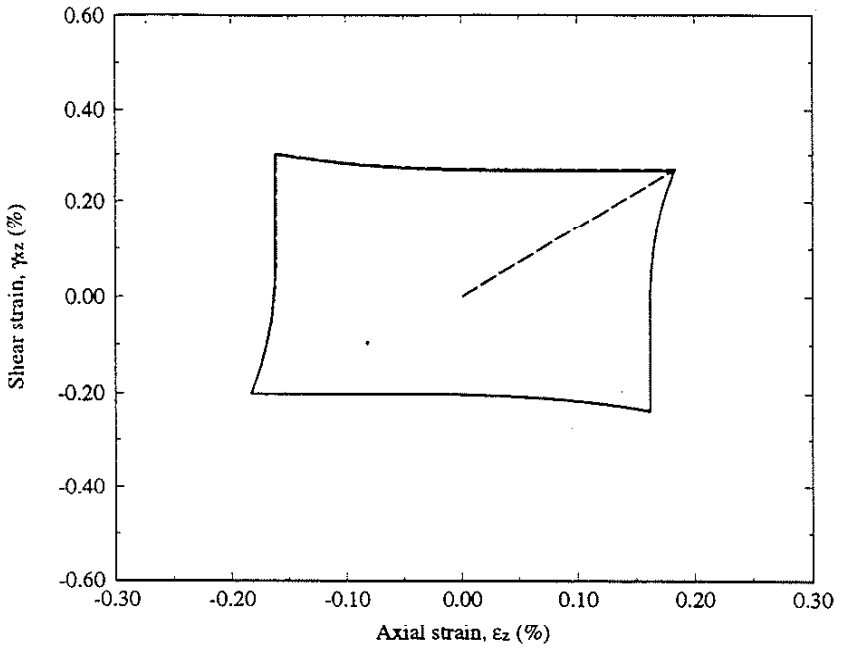

(c)

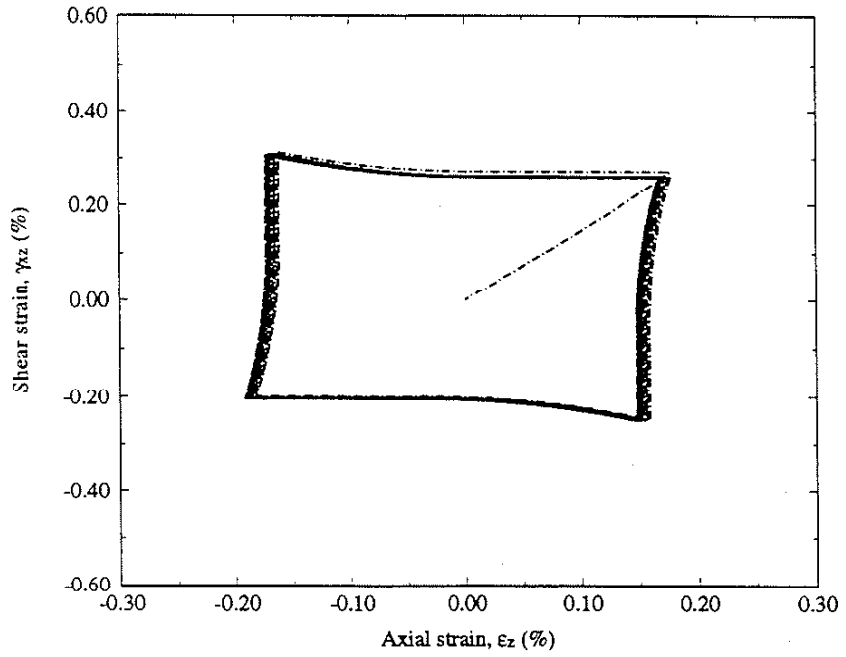

(d)

Figure 6.24 (continued). (c) Calculation using the simplified method and (d) calculation using the finite element method for maximum nominal stresses of S_z=258 MPa, and S_{xz}=168 MPa.

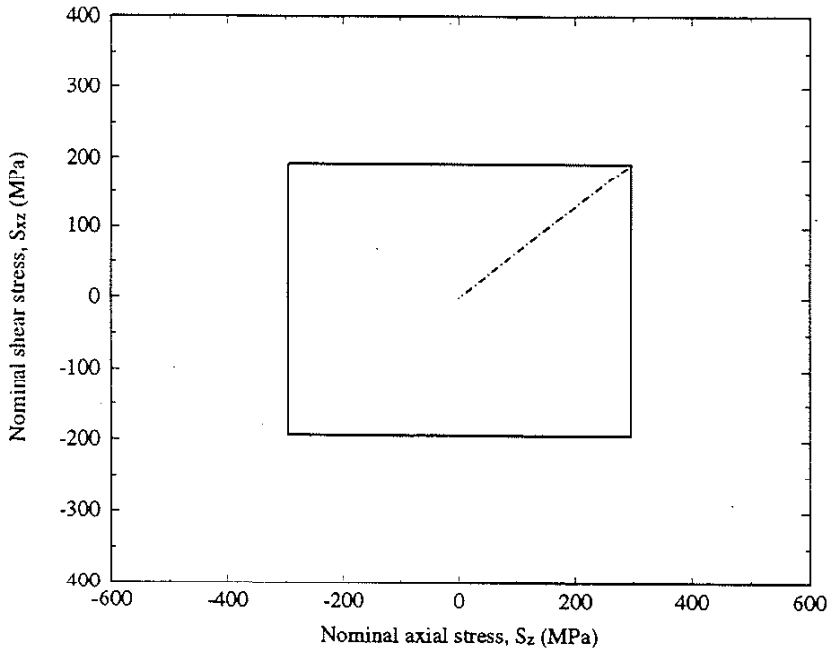

(a)

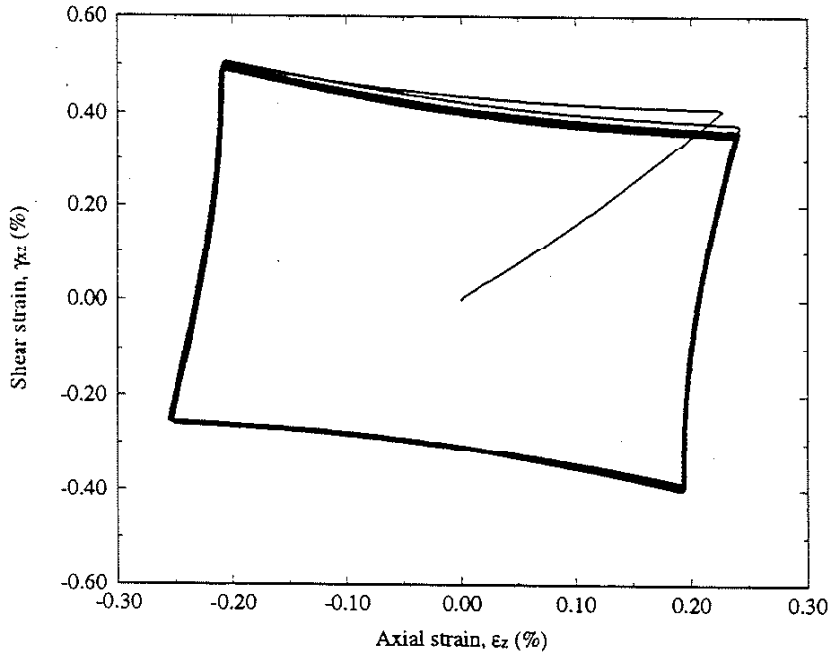

(b)

Figure 6.25. (a) Nominal stress path and (b) measured strain response for maximum nominal stresses of S_z=296 MPa, and S_{xz}=193 MPa.

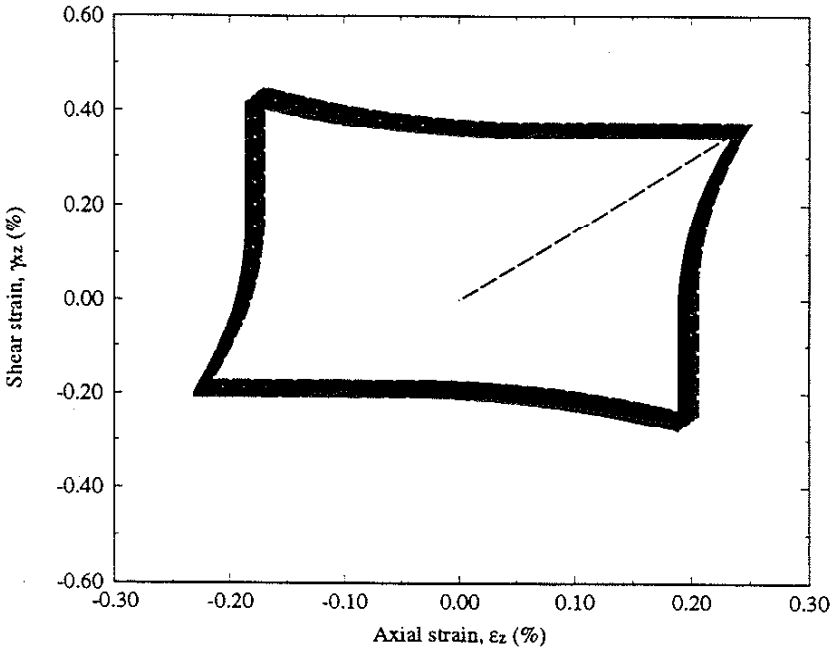

(c)

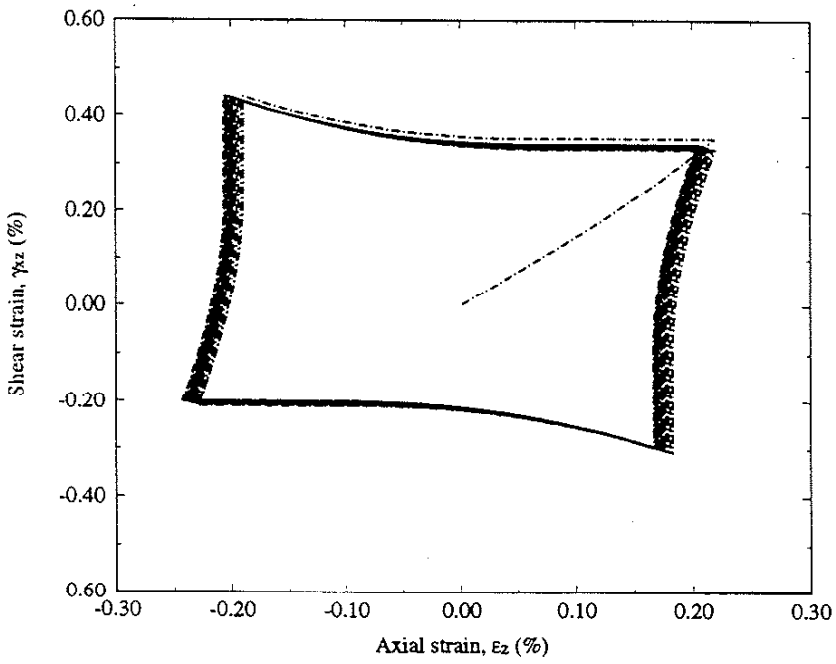

(d)

Figure 6.25 (continued). (c) Calculation using the simplified method and (d) calculation using the finite element method for maximum nominal stresses of S_z=296 MPa, and S_{xz}=193 MPa.

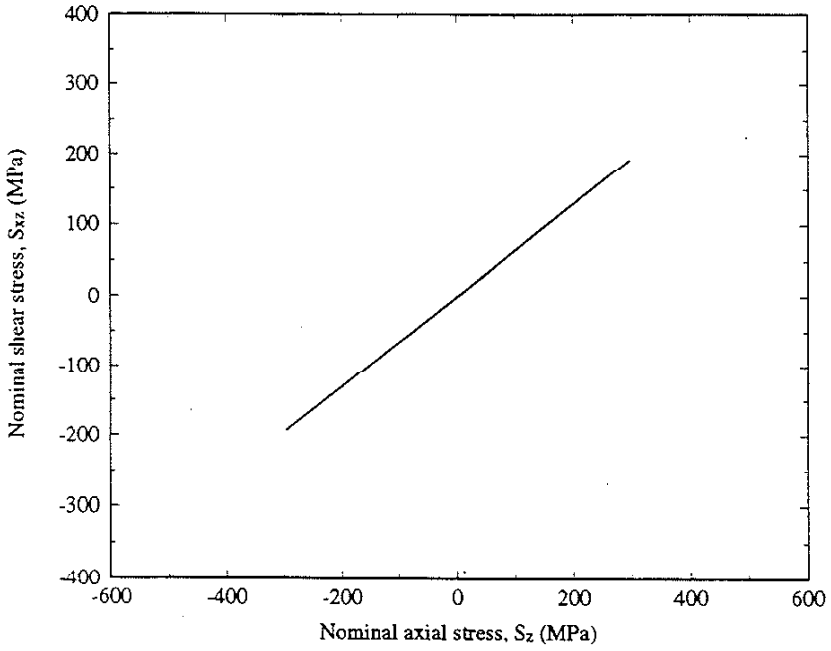

(a)

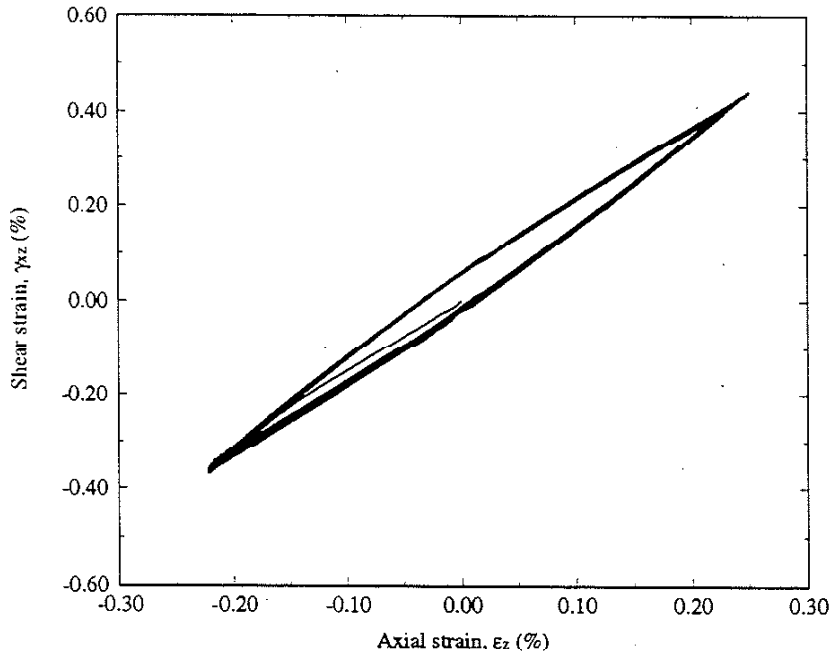

(b)

Figure 6.26. (a) Nominal stress path and (b) measured strain response for maximum nominal stresses of S_z=296 MPa, and S_{xz}=193 MPa.

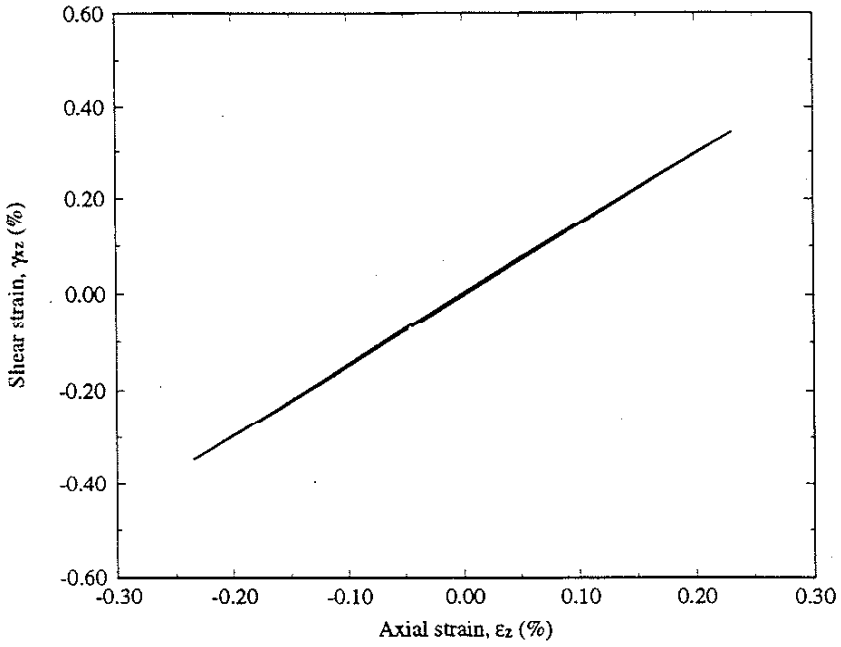

(c)

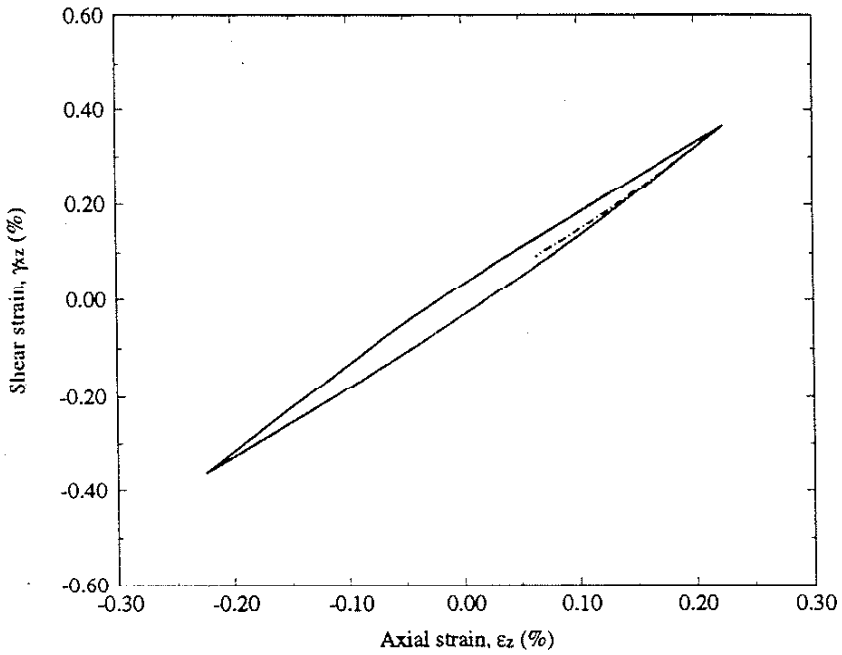

(d)

Figure 6.26 (continued). (c) Calculation using the simplified method and (d) calculation using the finite element method for maximum nominal stresses of S_z=296 MPa, and S_{xz}=193 MPa.

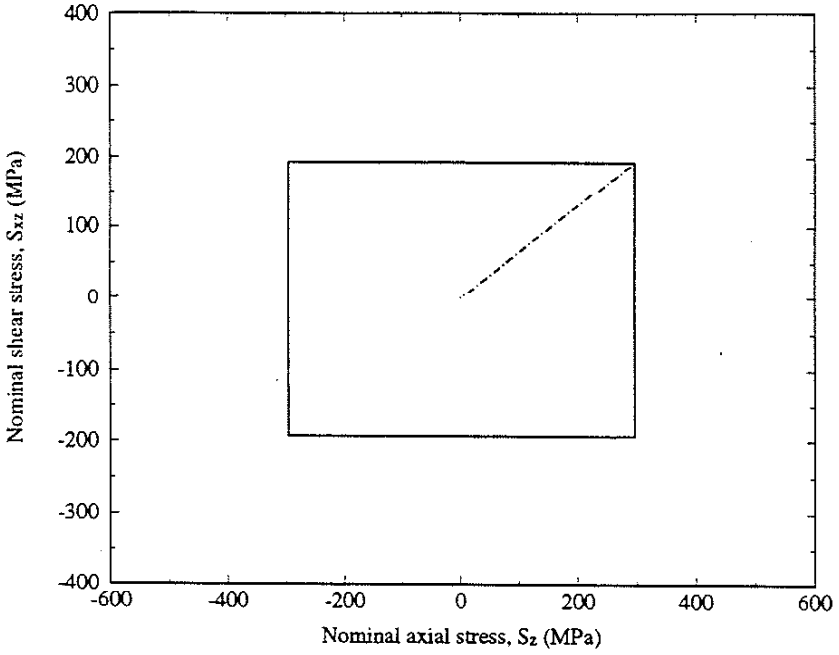

(a)

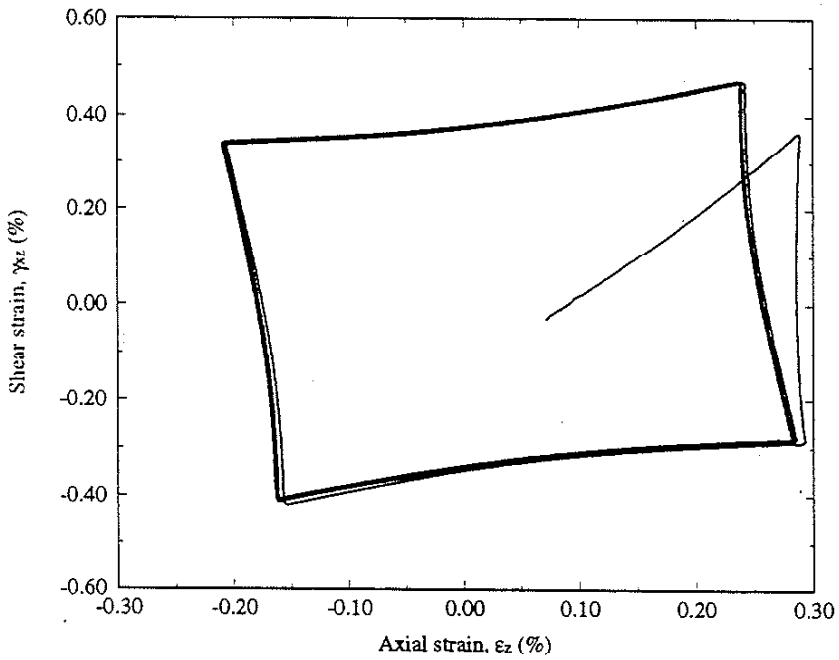

(b)

Figure 6.27. (a) Nominal stress path and (b) measured strain response for maximum nominal stresses of S_z=296 MPa, and S_{xz}=193 MPa.

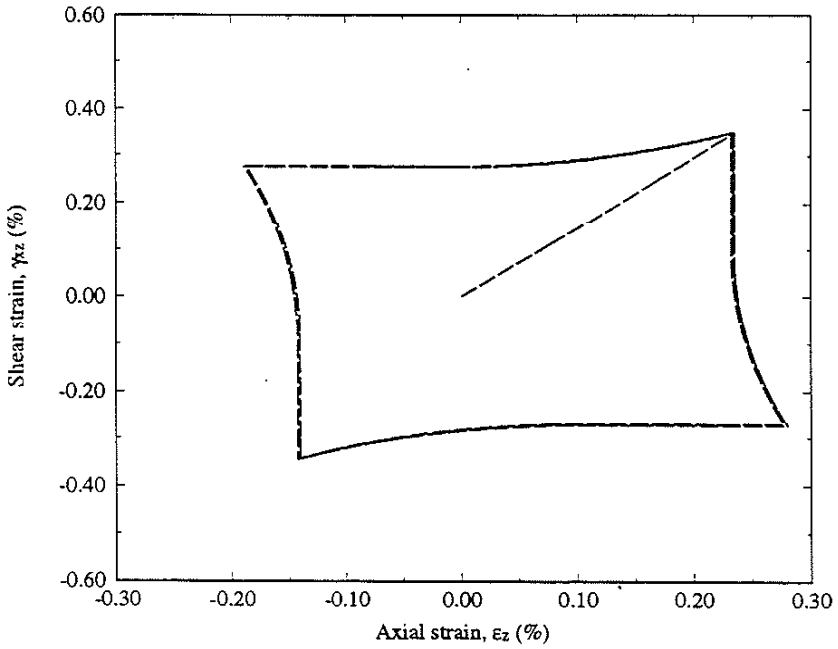

(c)

Figure 6.27 (continued). (c) Calculation using the simplified method for maximum nominal stresses of S_z=296 MPa, and S_{xz}=193 MPa.

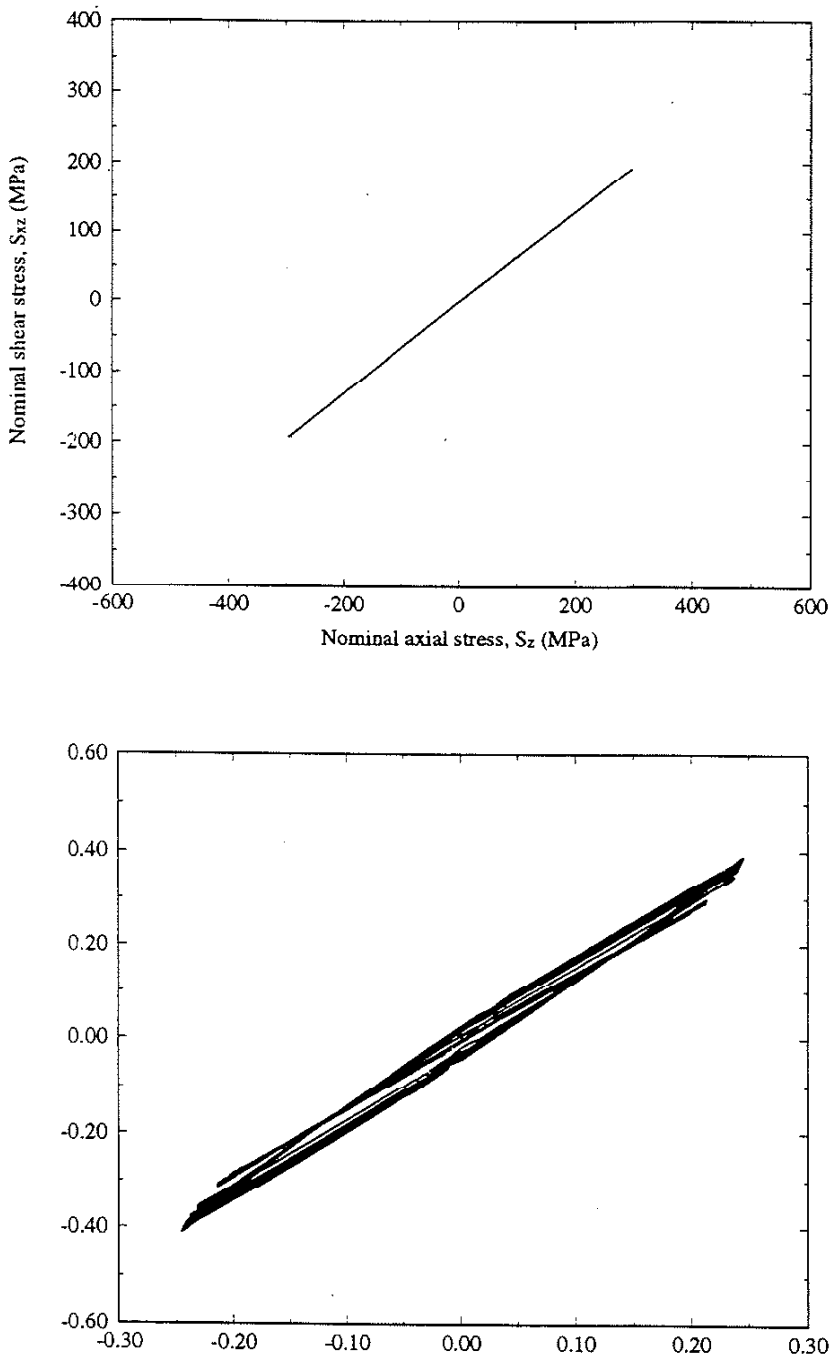

Figure 6.28. (a) Nominal stress path and (b) measured strain response for maximum nominal stresses of S_z=296 MPa, and S_{xz}=193 MPa.

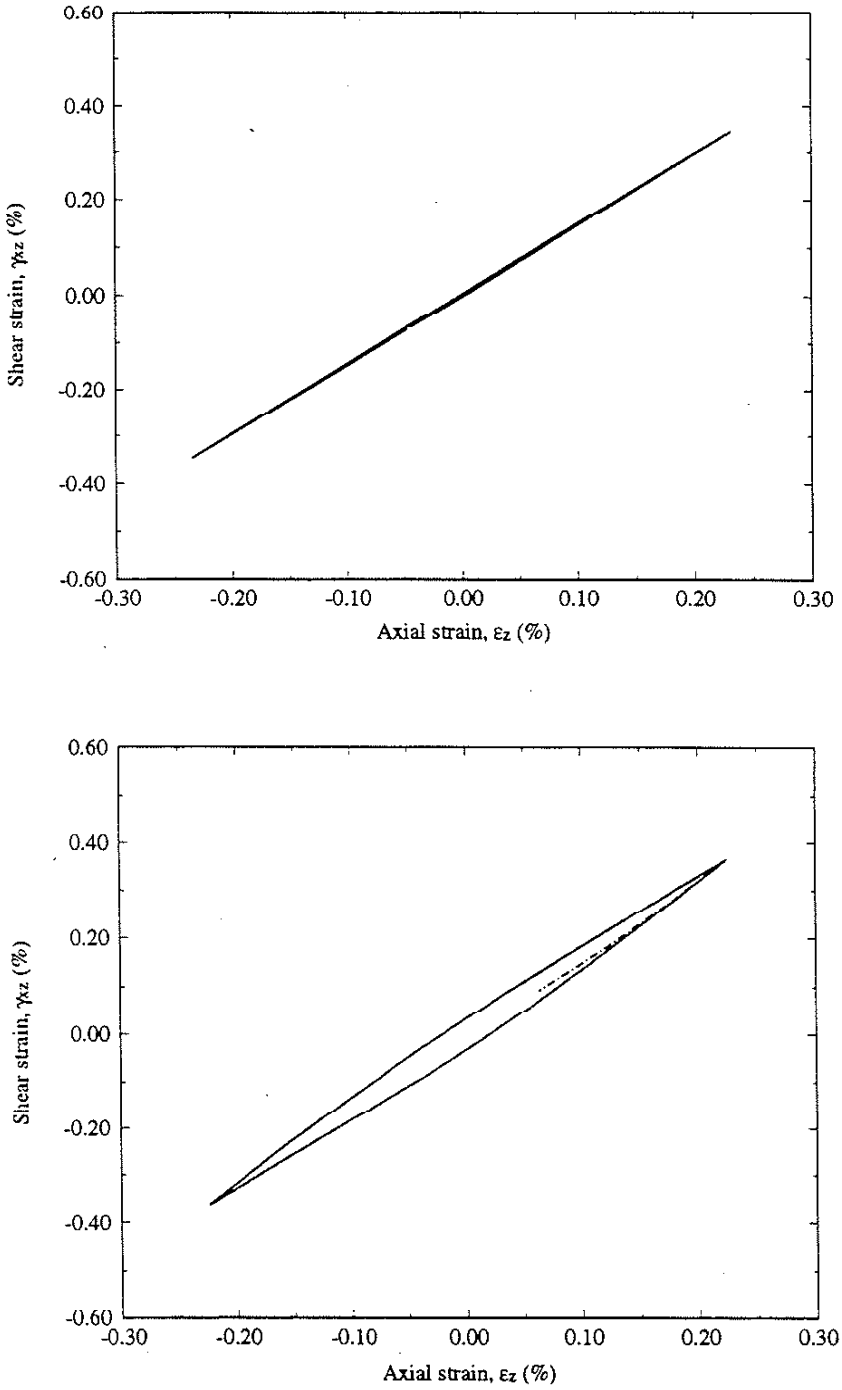

Figure 6.28 (continued). (c) Calculation using the simplified method and (d) calculation using the finite element method for maximum nominal stresses of S_z=296 MPa, and S_{xz}=193 MPa.

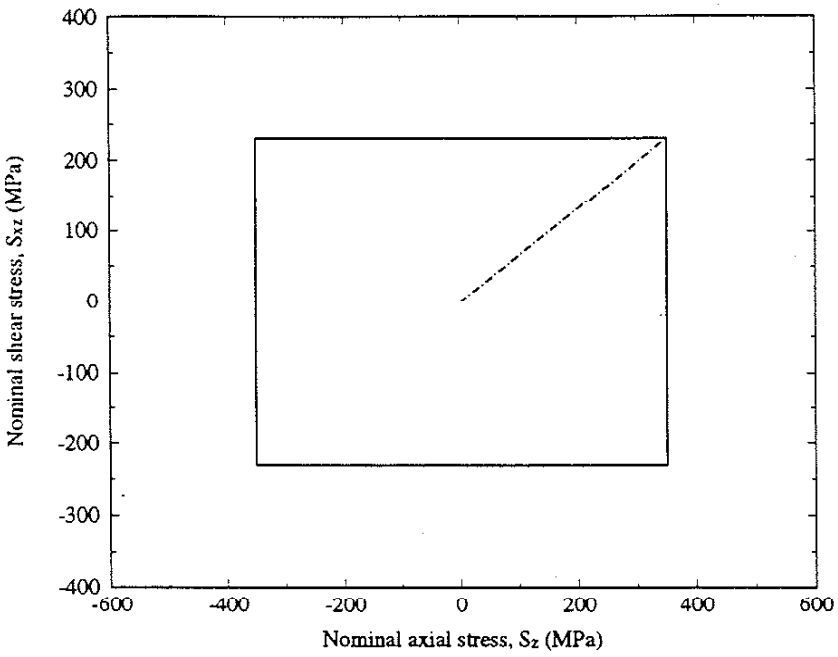

(a)

Figure 6.29. (a) Nominal stress path.

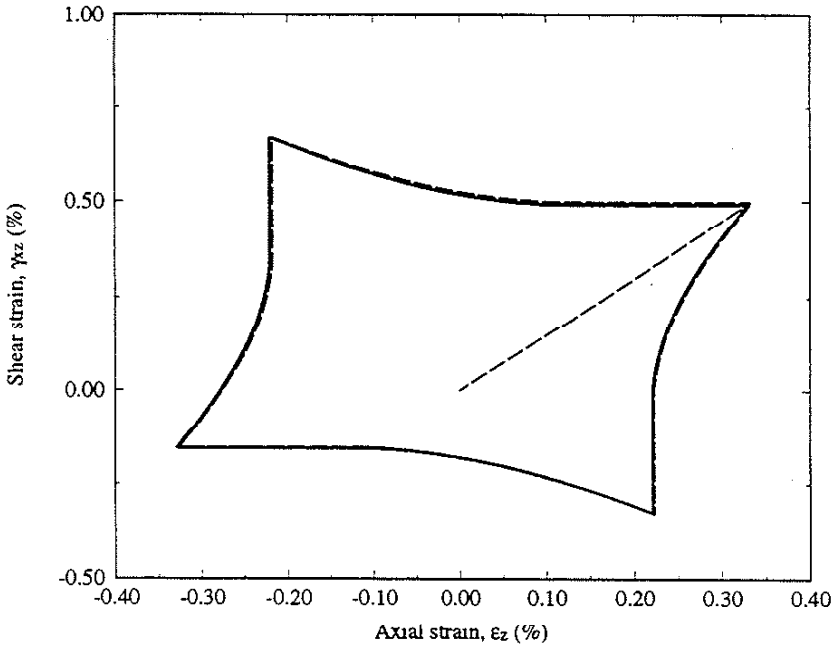

(b)

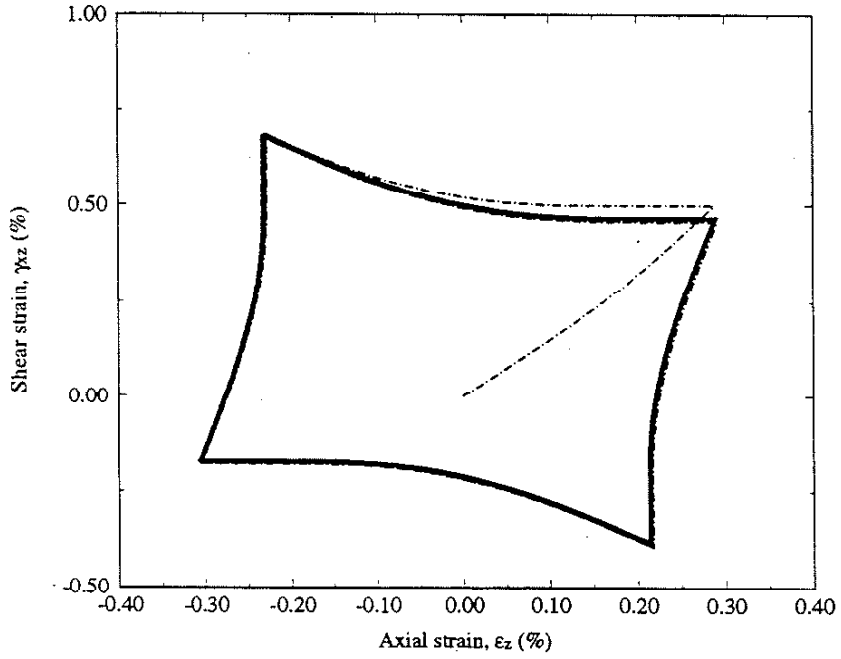

(c)

Figure 6.29 (continued). (b) Calculation using the simplified method and (c) calculation using the finite element method.

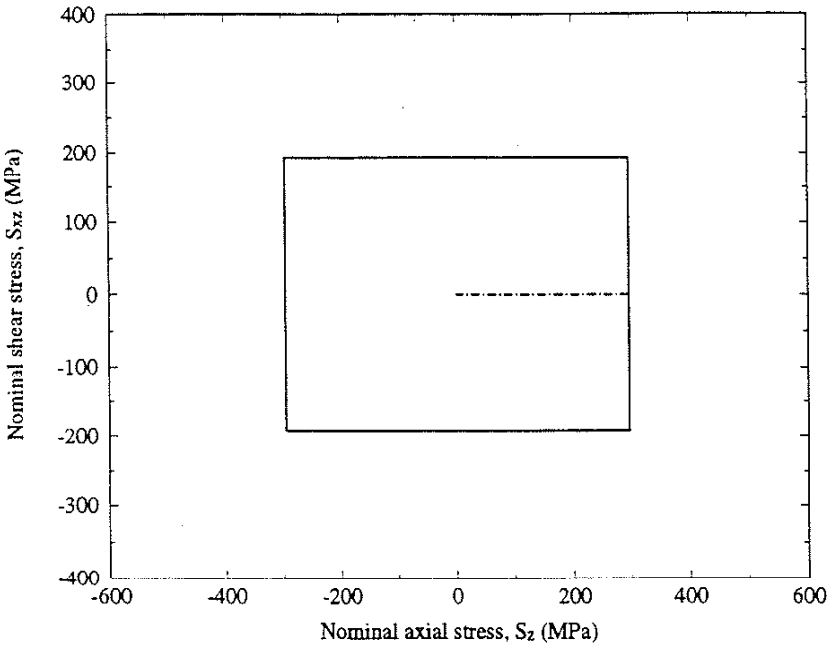

(a)

Figure 6.30. (a) Nominal stress path.

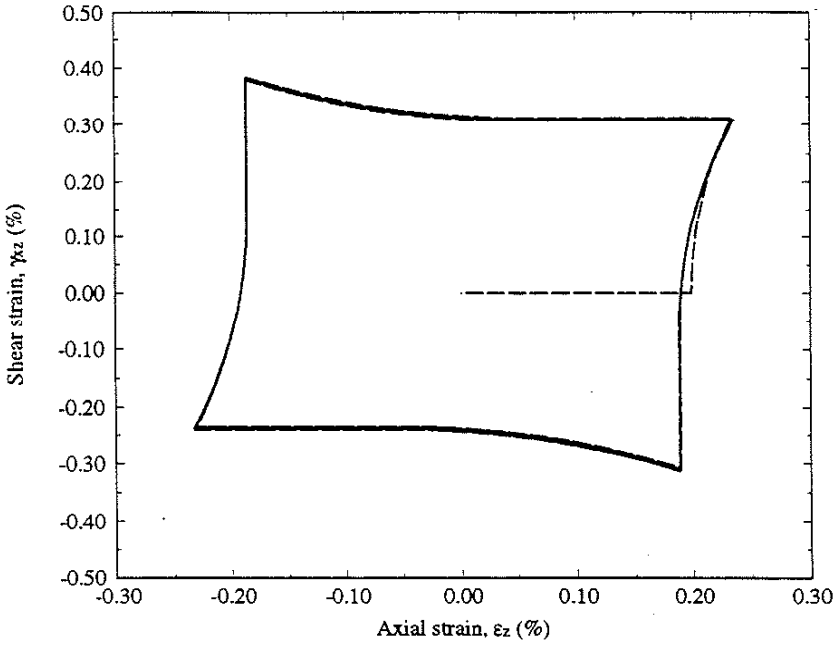

(b)

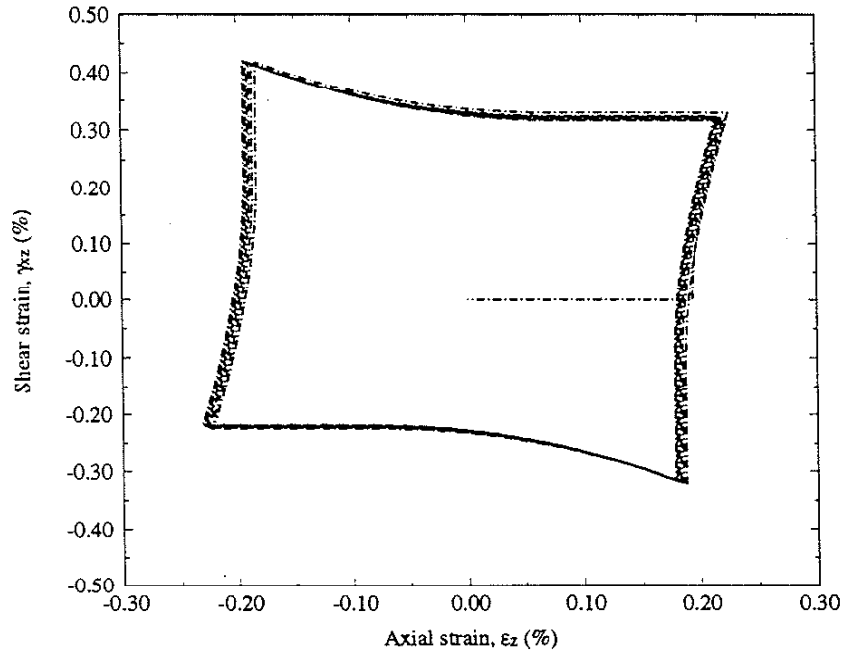

(c)

Figure 6.30 (continued). (b) Calculation using the simplified method and (c) calculation using the finite element method.

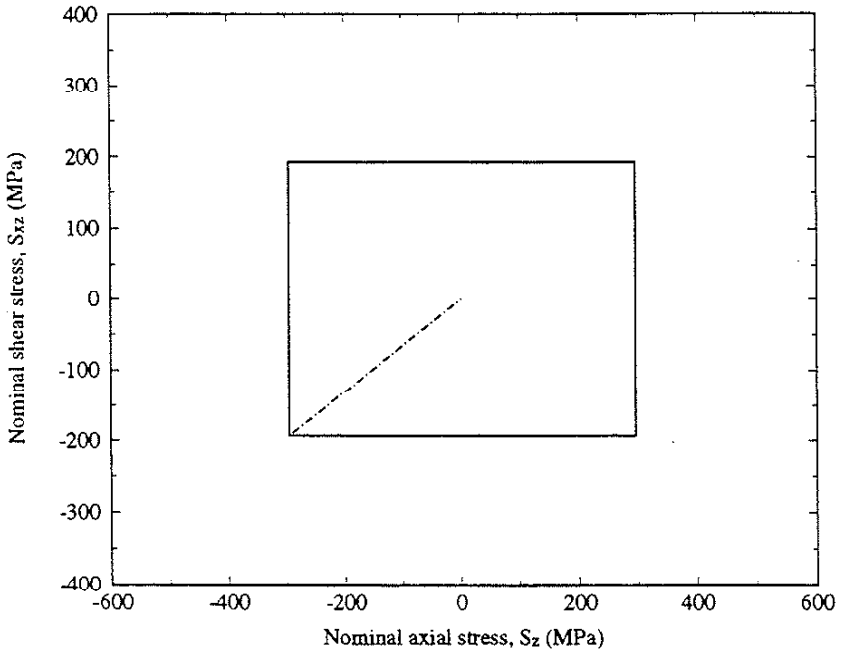

(a)

Figure 6.31. (a) Nominal stress path.

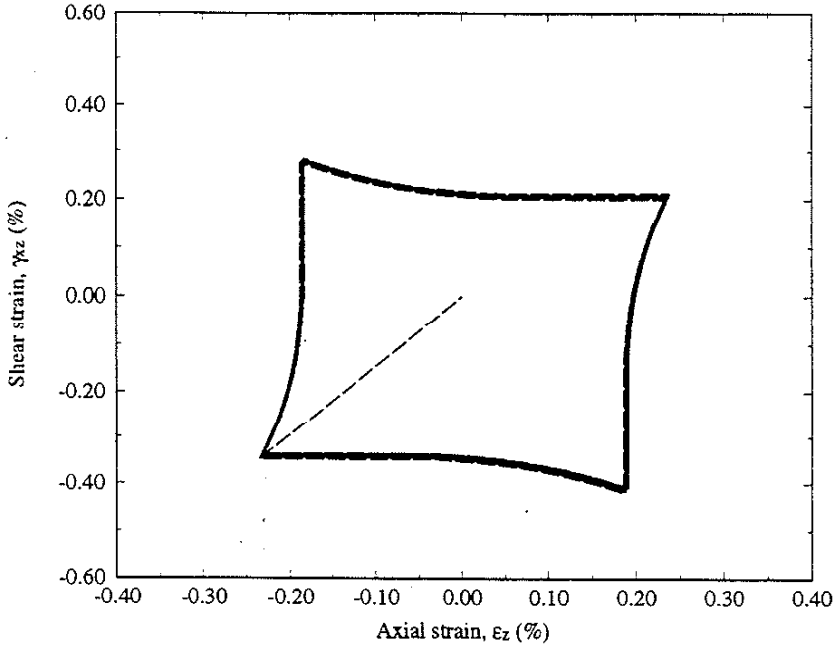

(b)

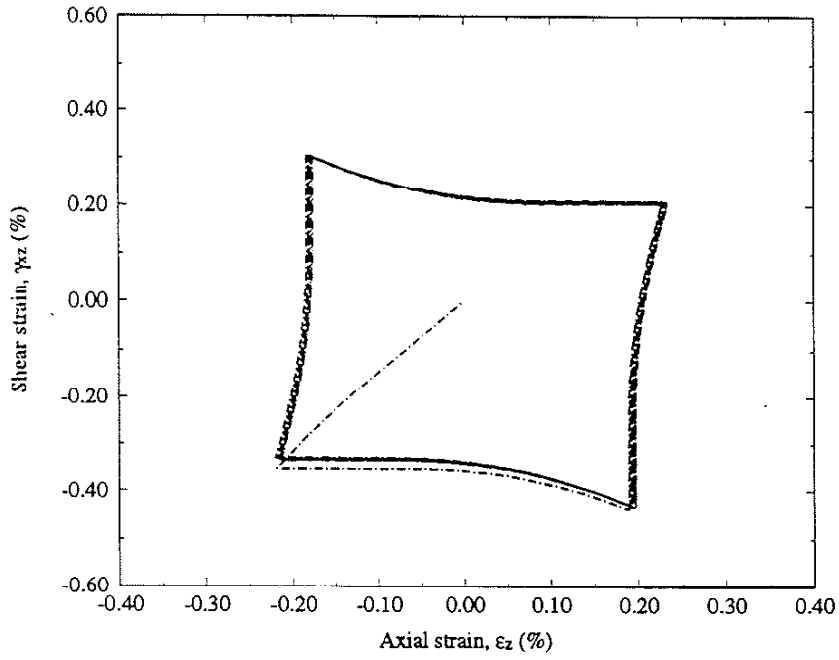

(c)

Figure 6.31 (continued). (b) Calculation using the simplified method and (c) calculation using the finite element method.

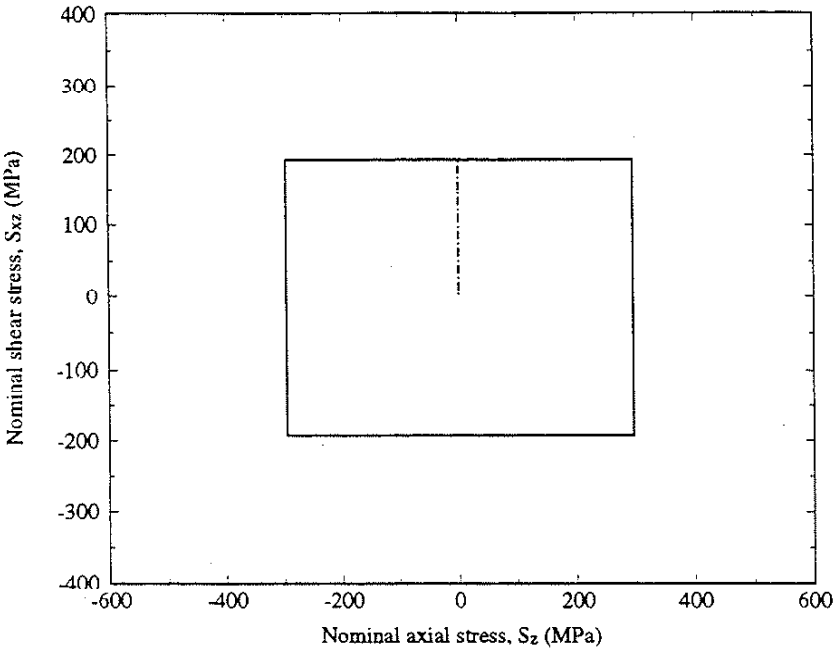

(a)

Figure 6.32. (a) Nominal stress path.

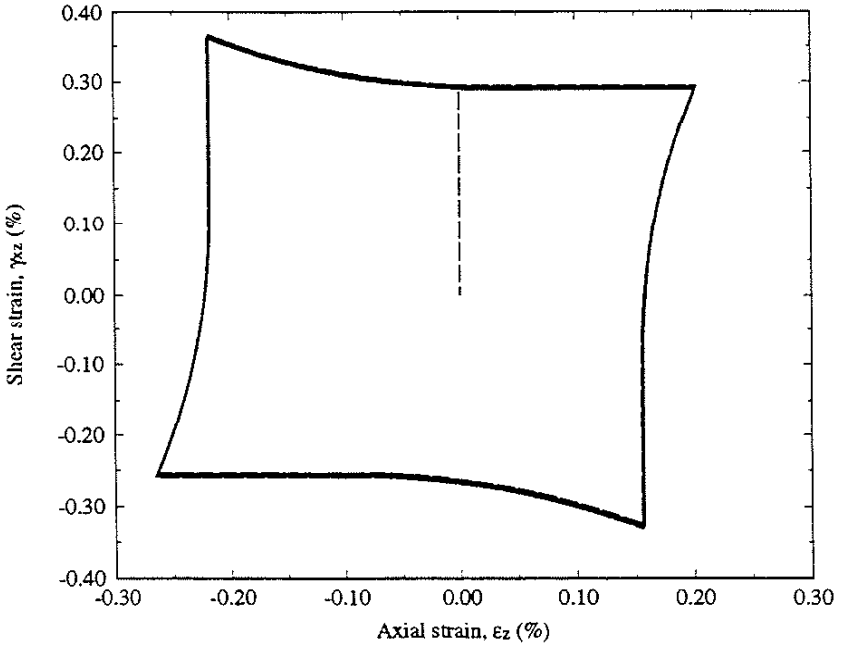

(b)

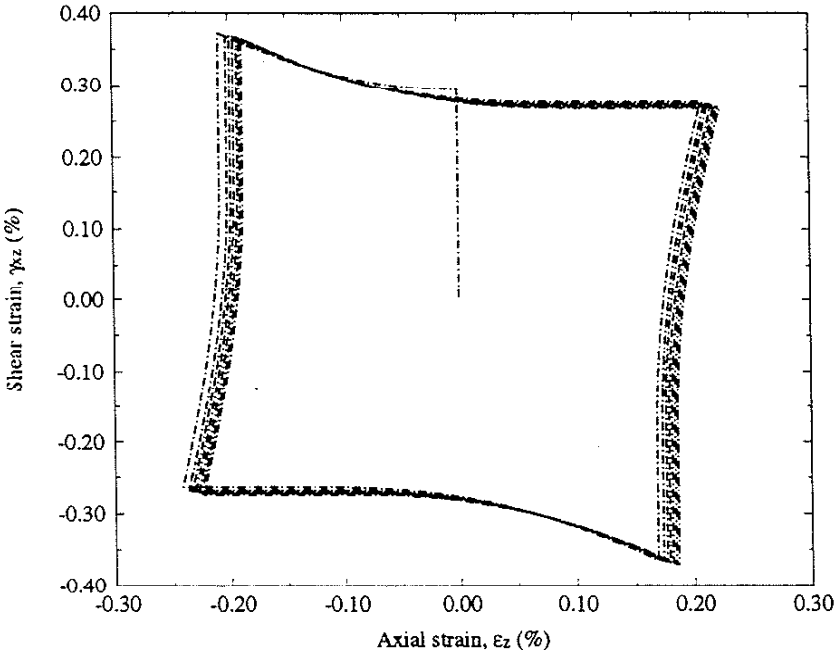

(c)

Figure 6.32 (continued). (b) Calculation using the simplified method and (c) calculation using the finite element method.

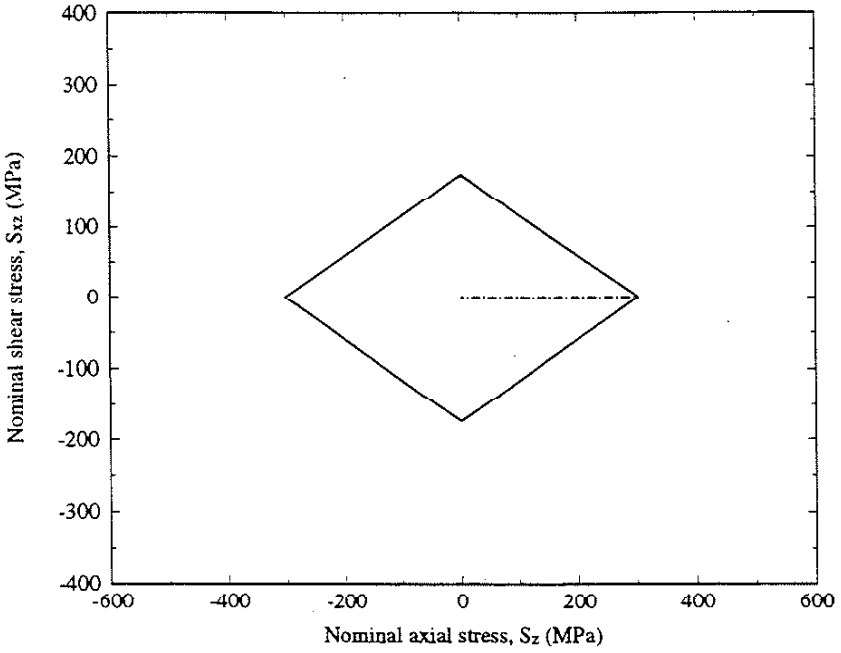

(a)

Figure 6.33. (a) Nominal stress path.

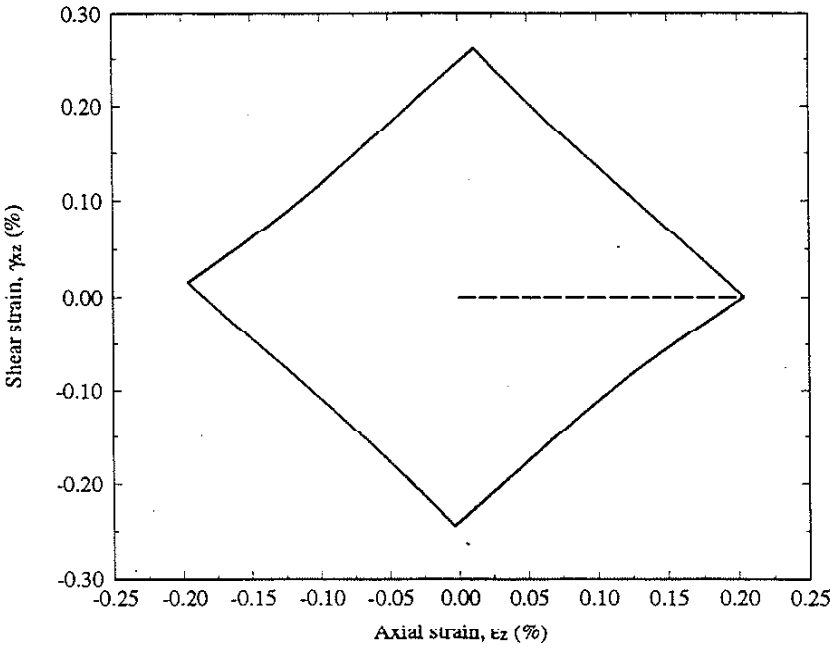

(b)

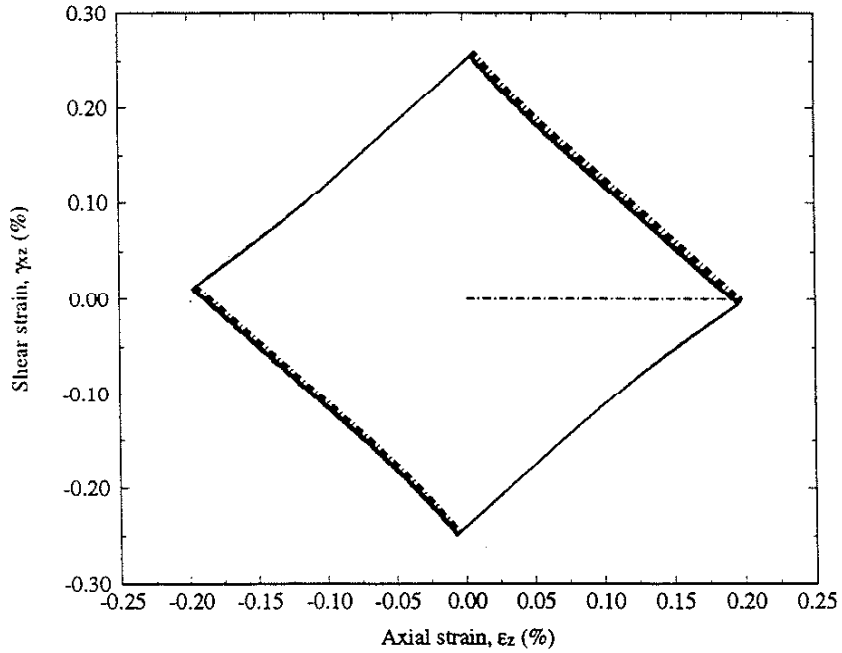

(c)

Figure 6.33 (continued). (b) Calculation using the simplified method and (c) calculation using the finite element method.

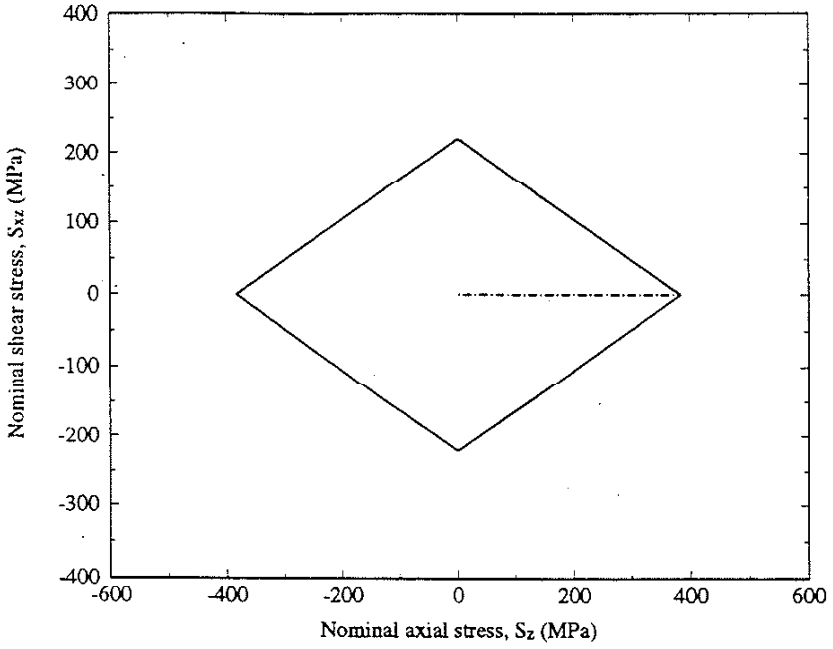

(a)

Figure 6.34. (a) Nominal stress path.

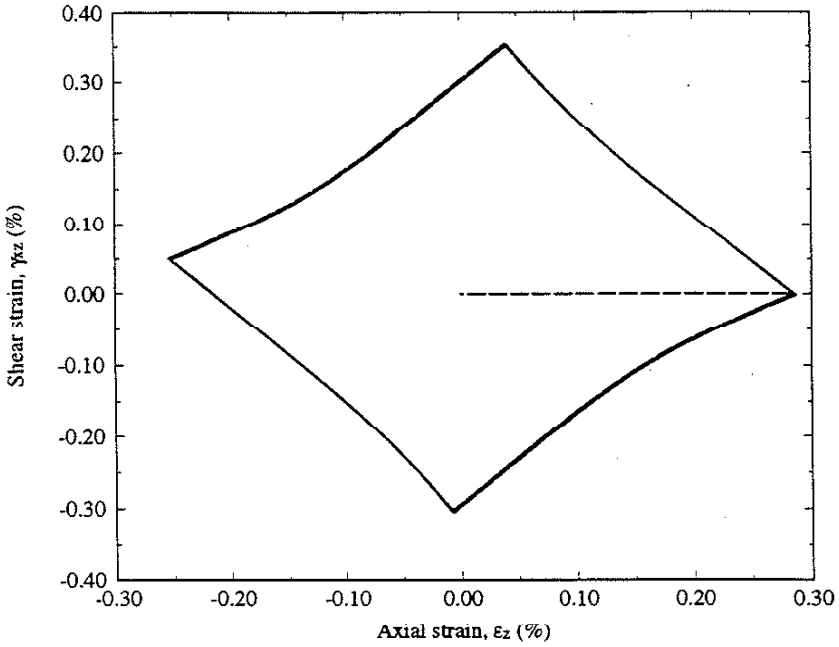

(b)

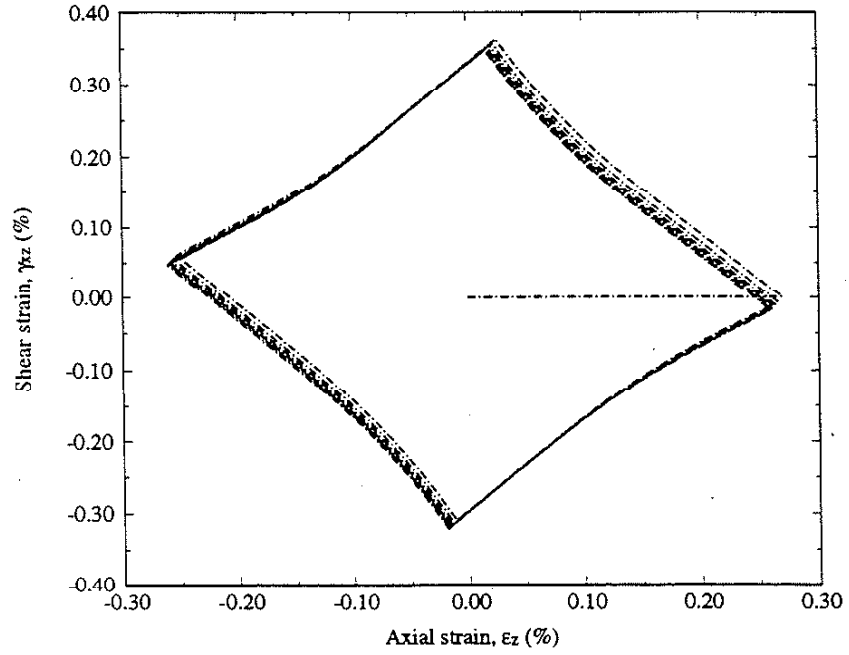

(c)

Figure 6.34 (continued). (b) Calculation using the simplified method and (c) calculation using the finite element method.

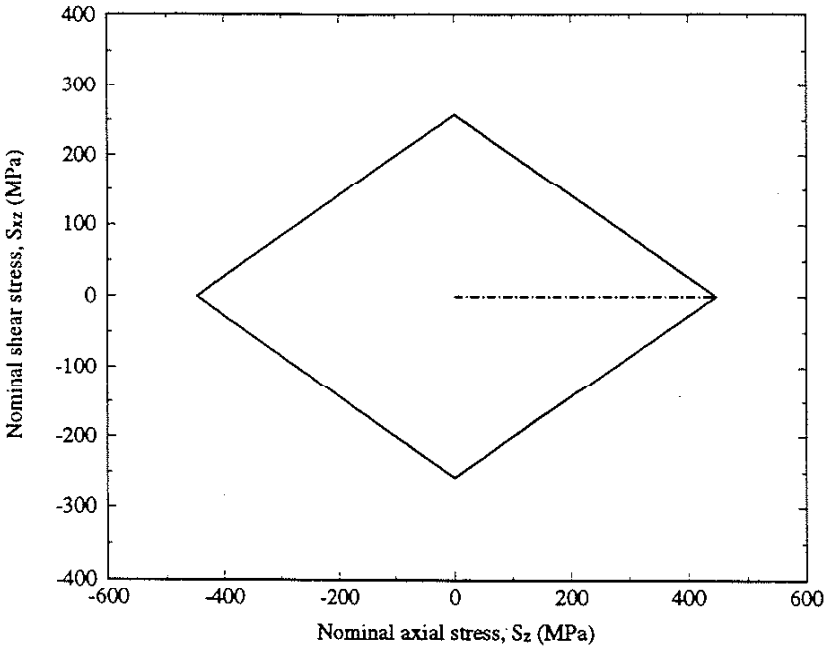

(a)

Figure 6.35. (a) Nominal stress path.

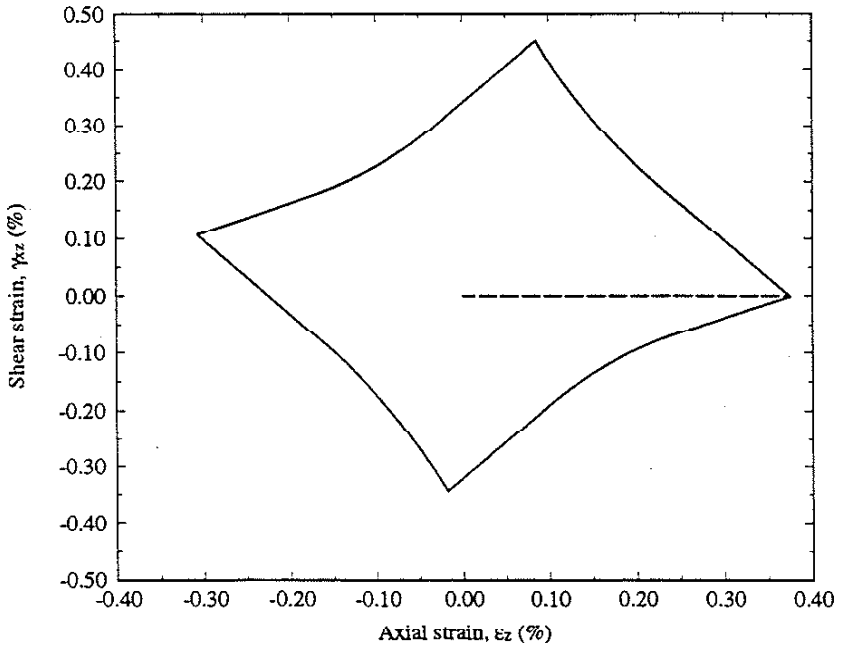

(b)

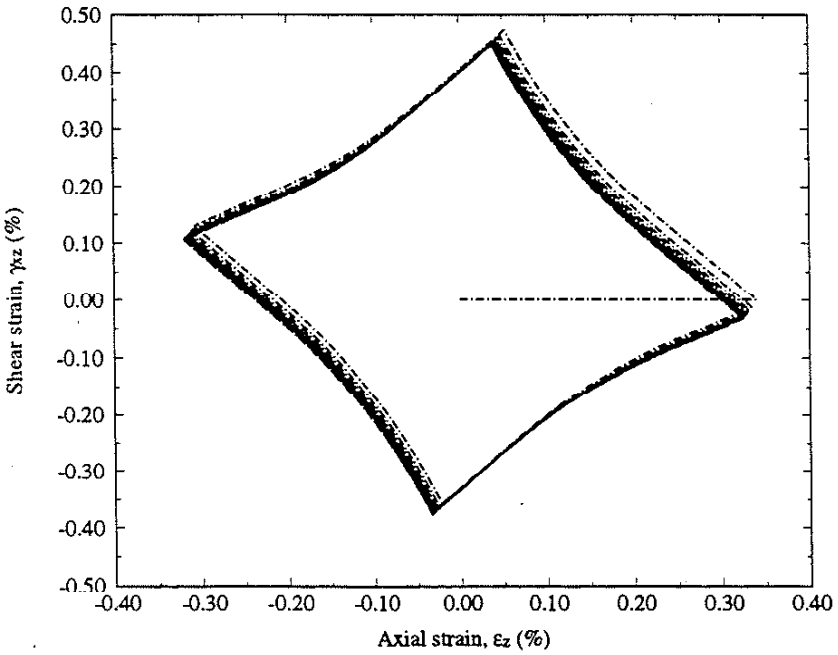

(c)

Figure 6.35 (continued). (b) Calculation using the simplified method and (c) calculation using the finite element method.

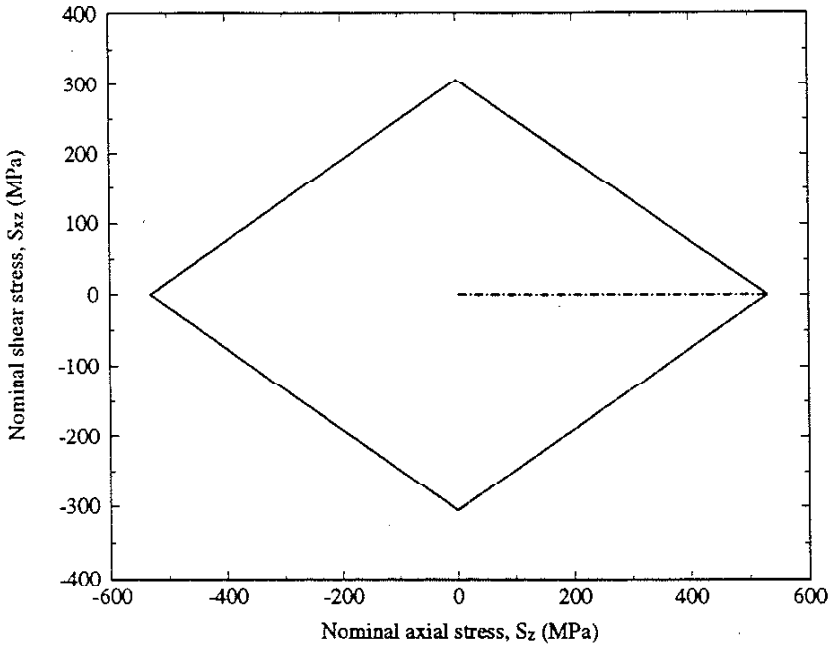

(a)

Figure 6.36. (a) Nominal stress path.

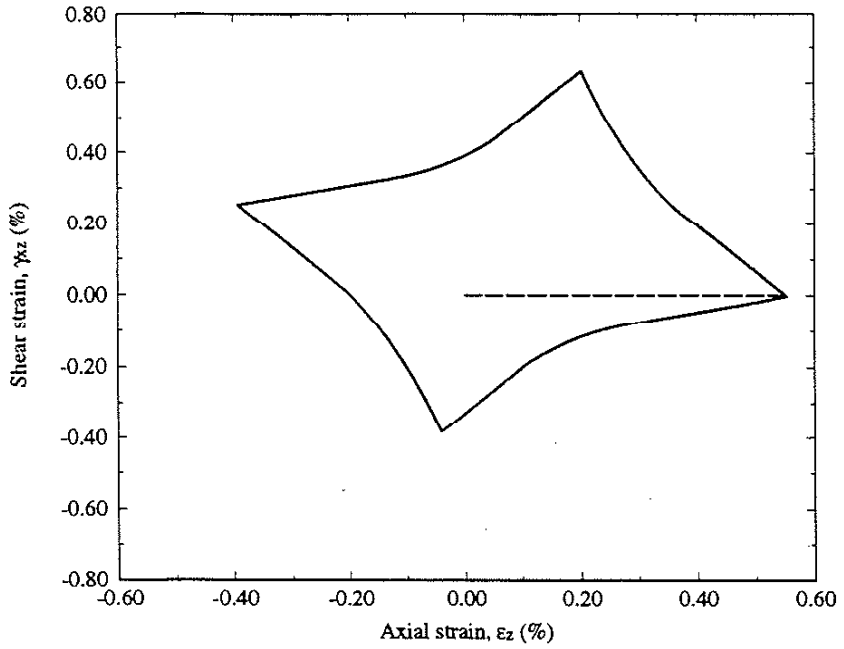

(b)

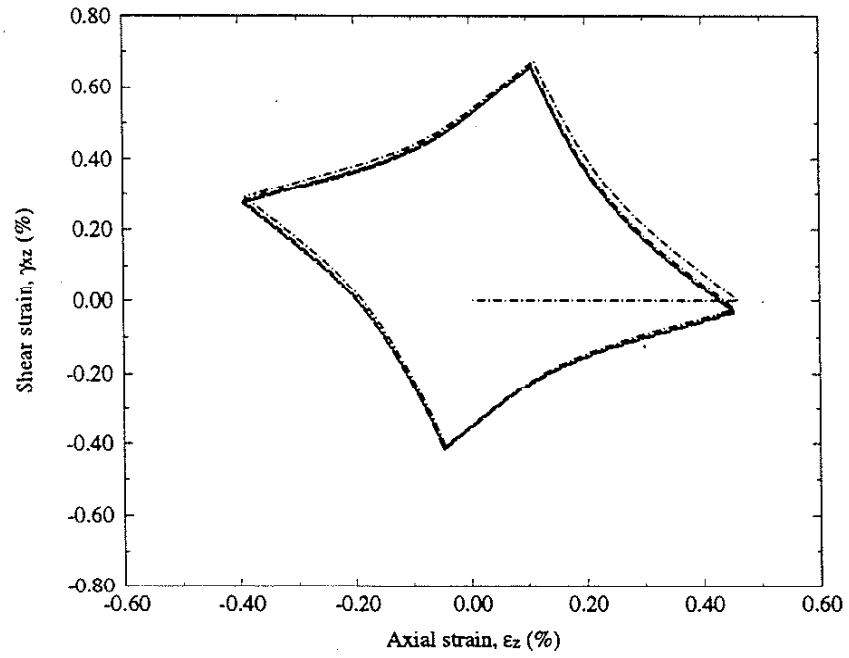

(c)

Figure 6.36 (continued). (b) Calculation using the simplified method and (c) calculation using the finite element method.

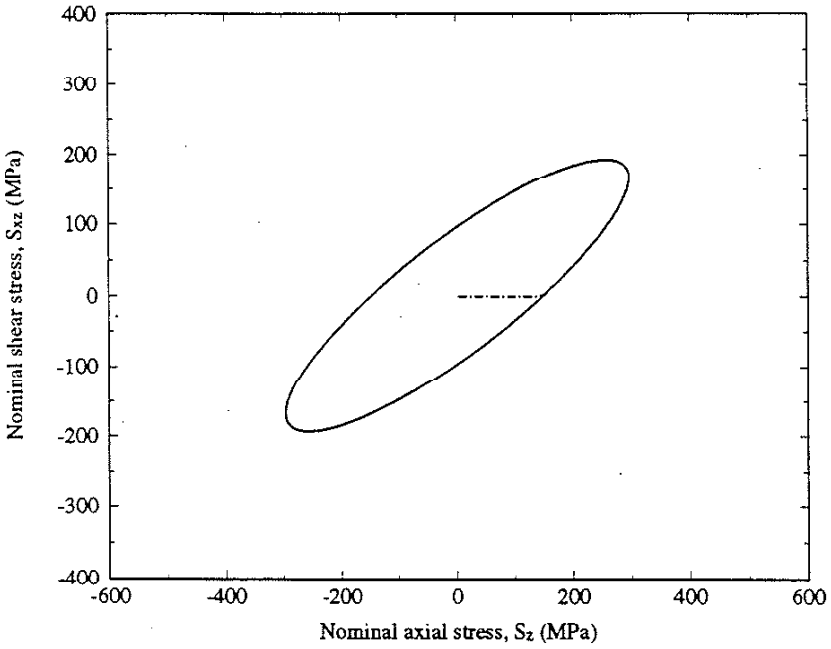

(a)

Figure 6.37. (a) Nominal stress path.

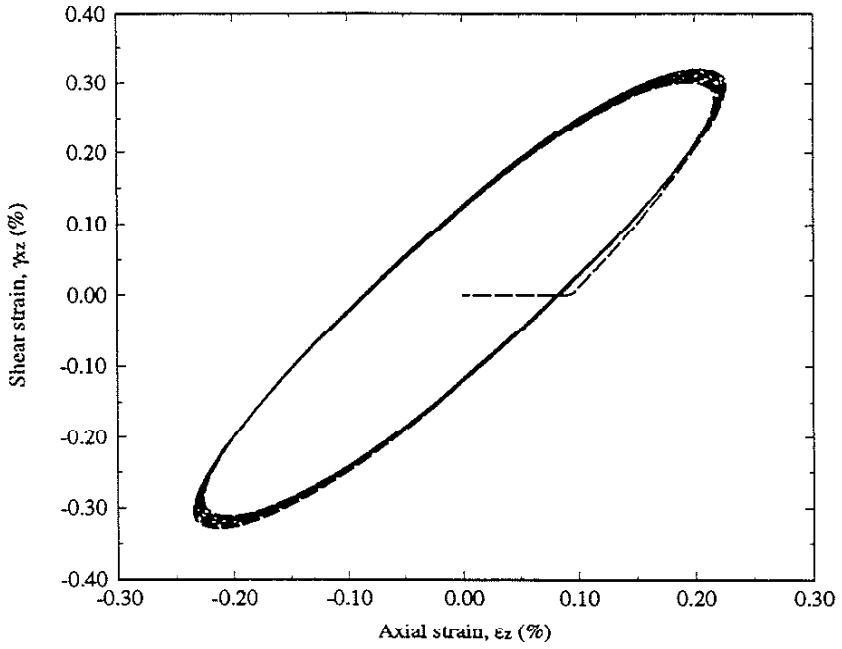

(b)

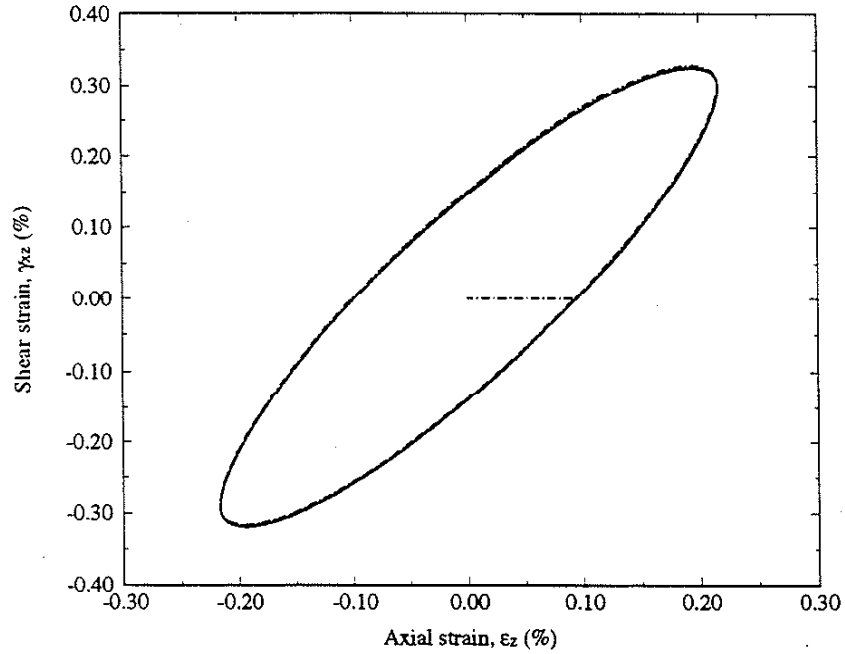

(c)

Figure 6.37 (continued). (b) Calculation using the simplified method and (c) calculation using the finite element method.

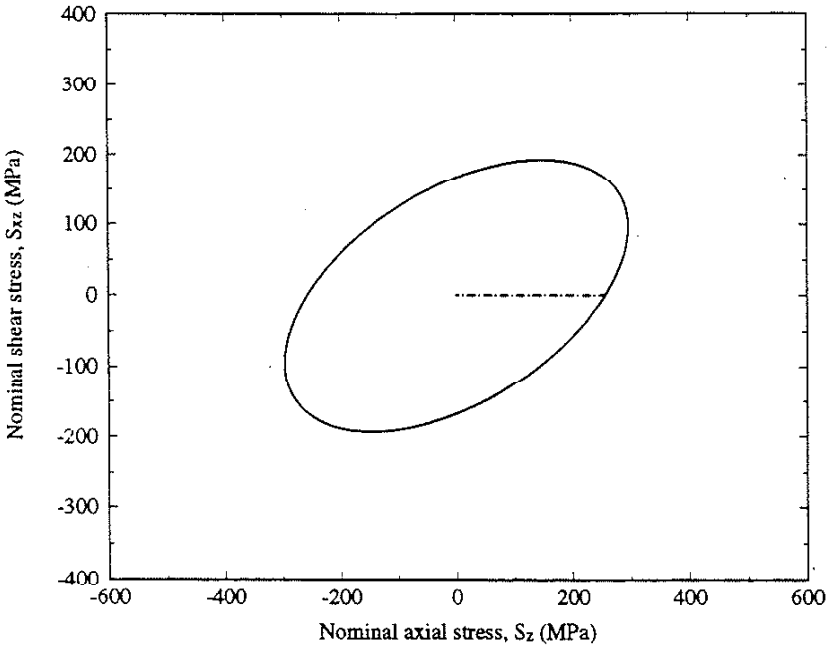

(a)

Figure 6.38. (a) Nominal stress path.

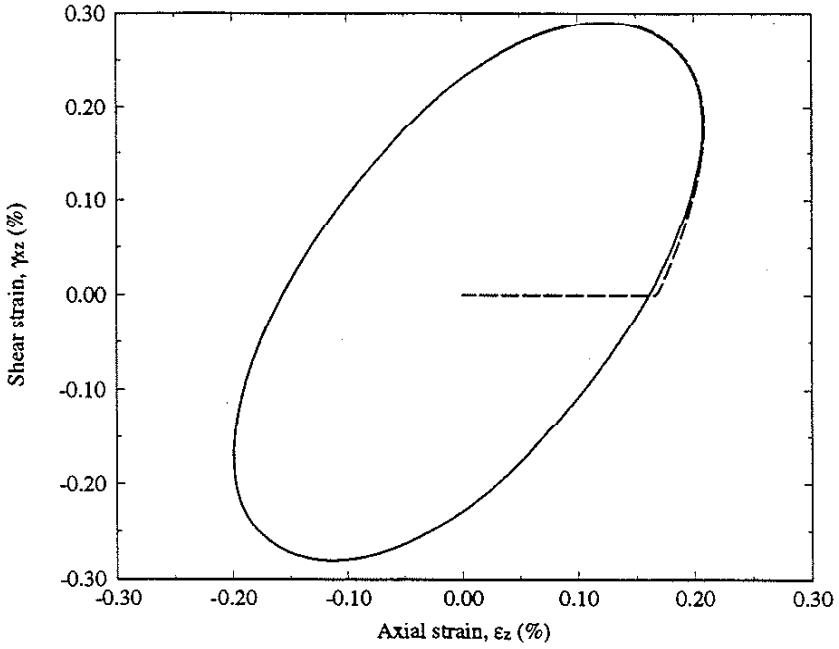

(b)

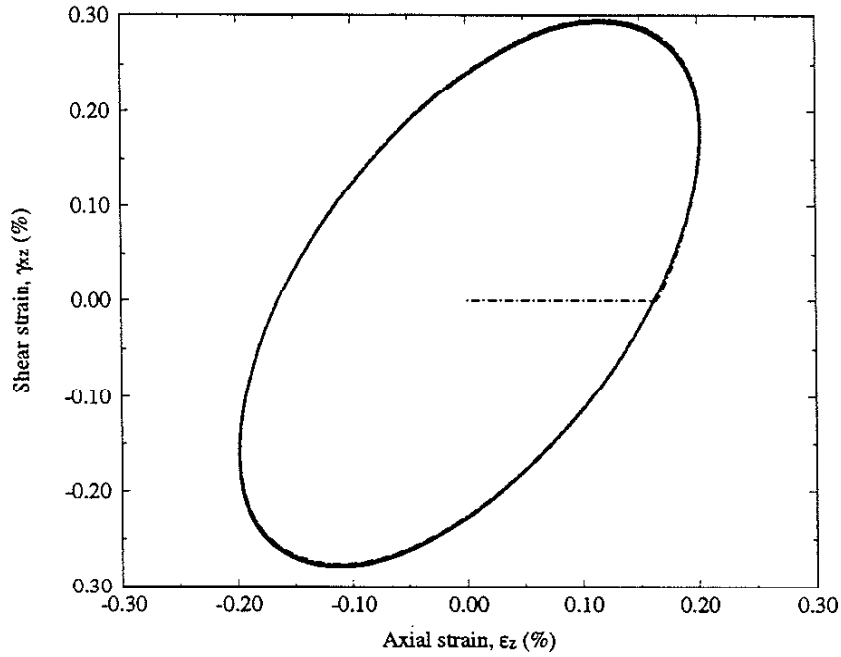

(c)

Figure 6.38 (continued). (b) Calculation using the simplified method and (c) calculation using the finite element method.

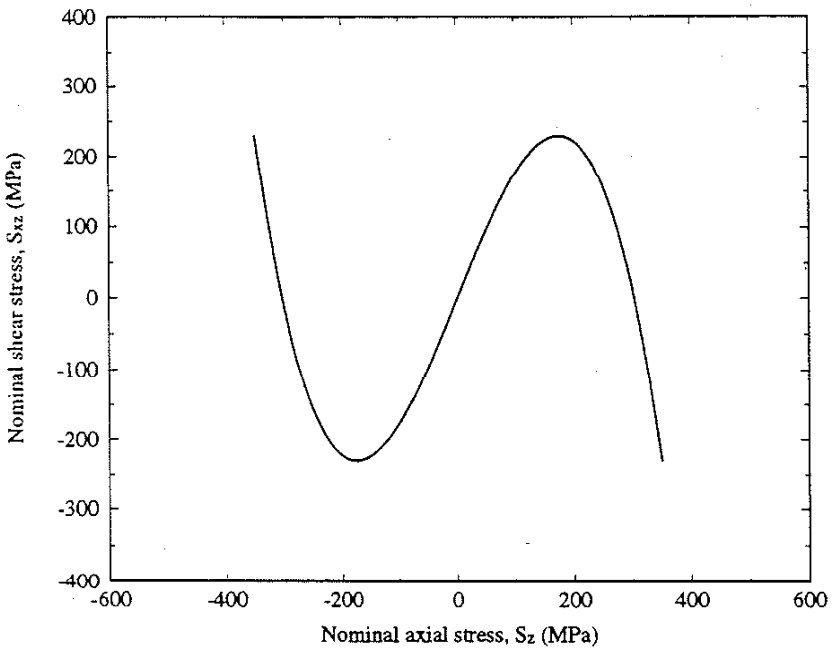

(a)

Figure 6.39. (a) Nominal stress path.

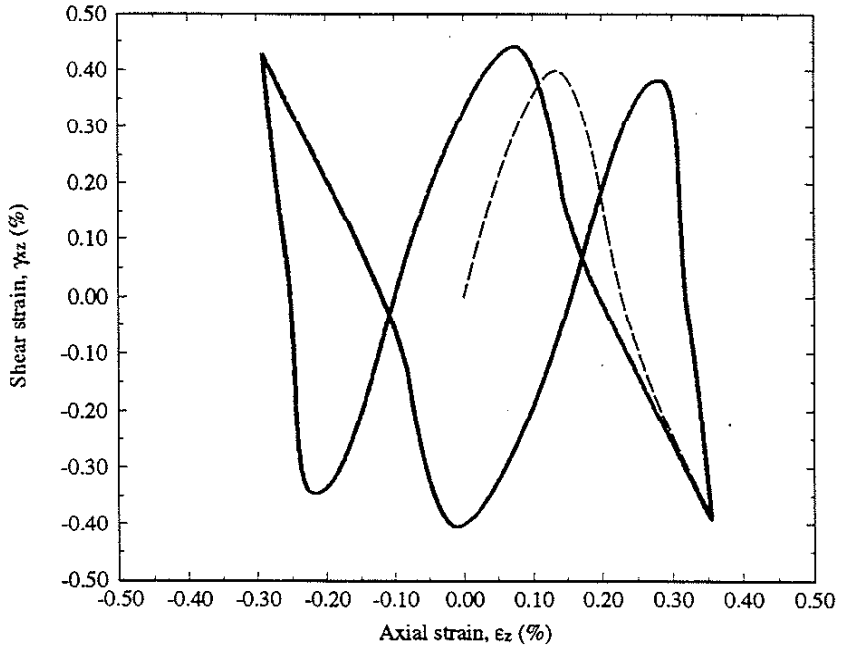

(b)

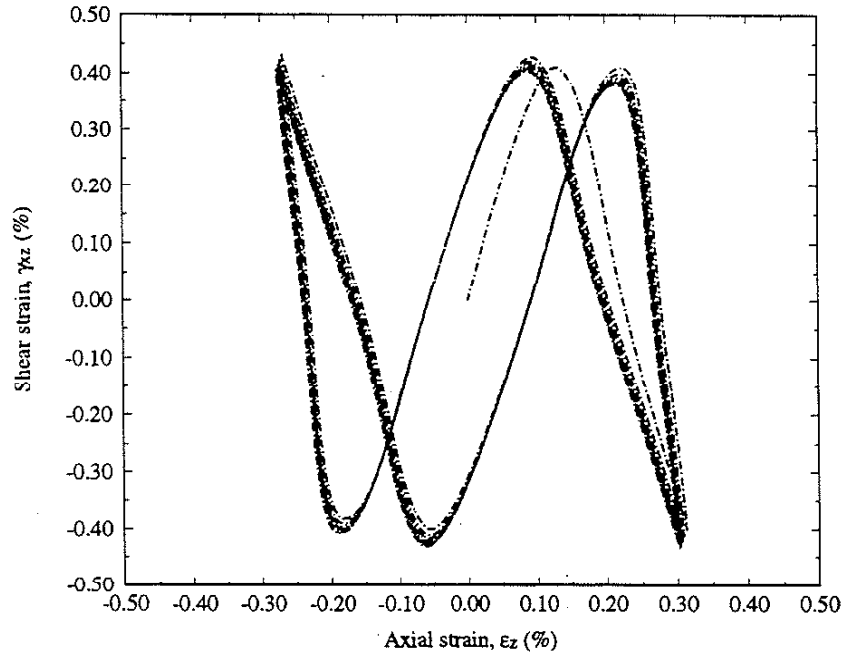

(c)

Figure 6.39 (continued). (b) Calculation using the simplified method and (c) calculation using the finite element method.

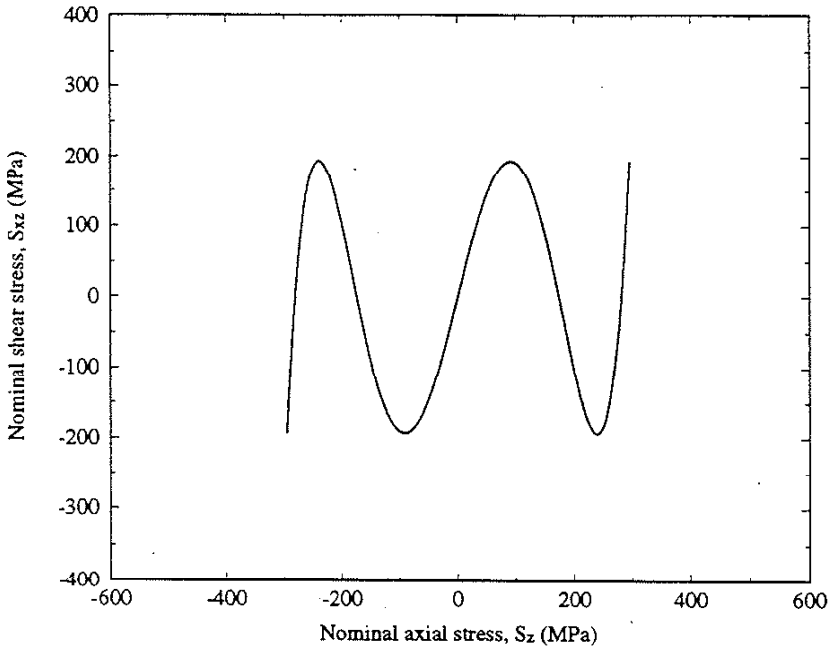

(a)

Figure 6.40. (a) Nominal stress path.

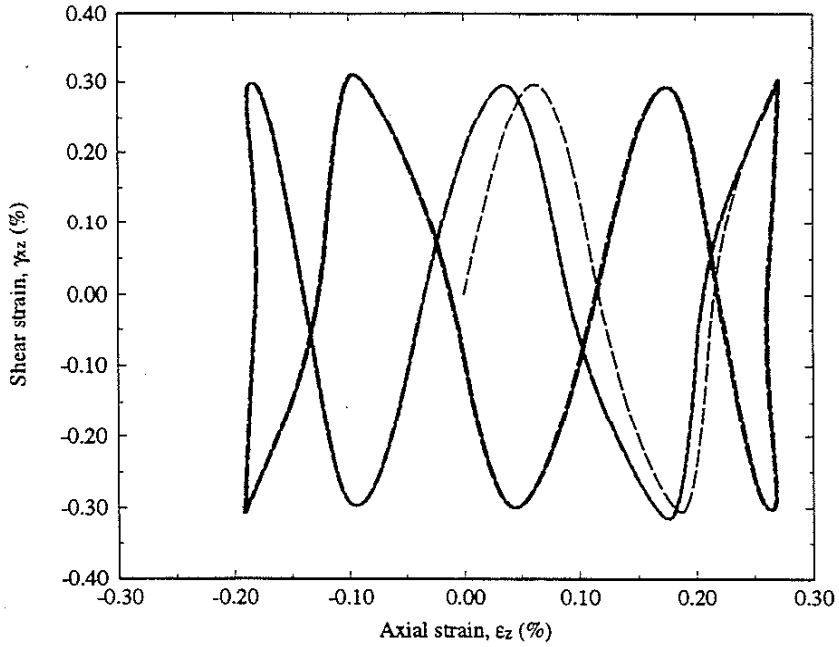

(b)

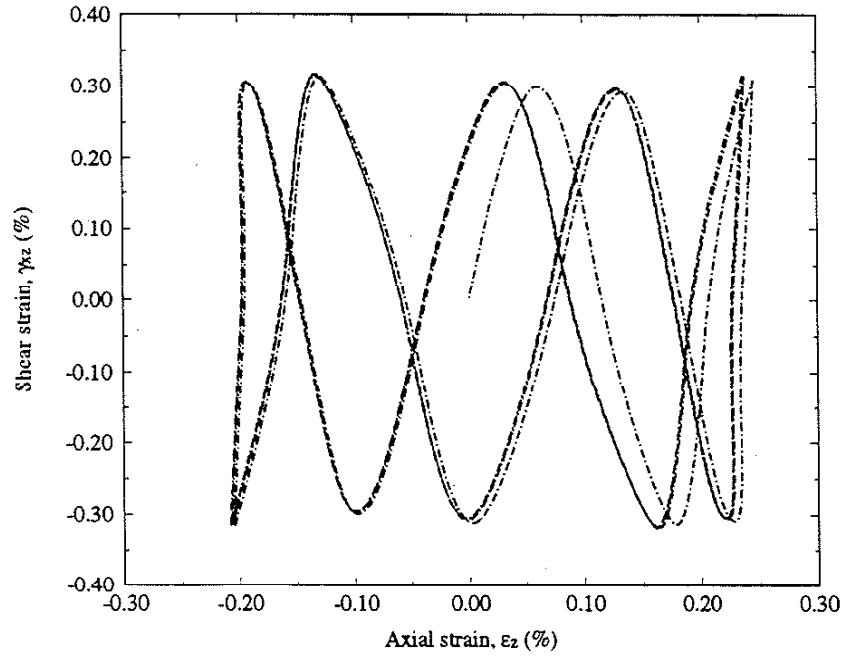

(c)

Figure 6.40 (continued). (b) Calculation using the simplified method and (c) calculation using the finite element method.

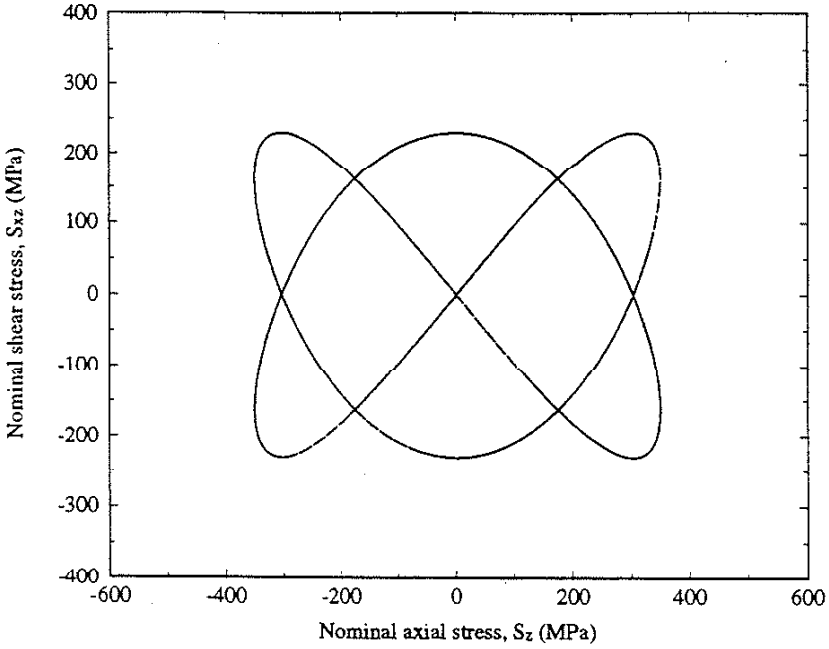

(a)

Figure 6.41. (a) Nominal stress path.

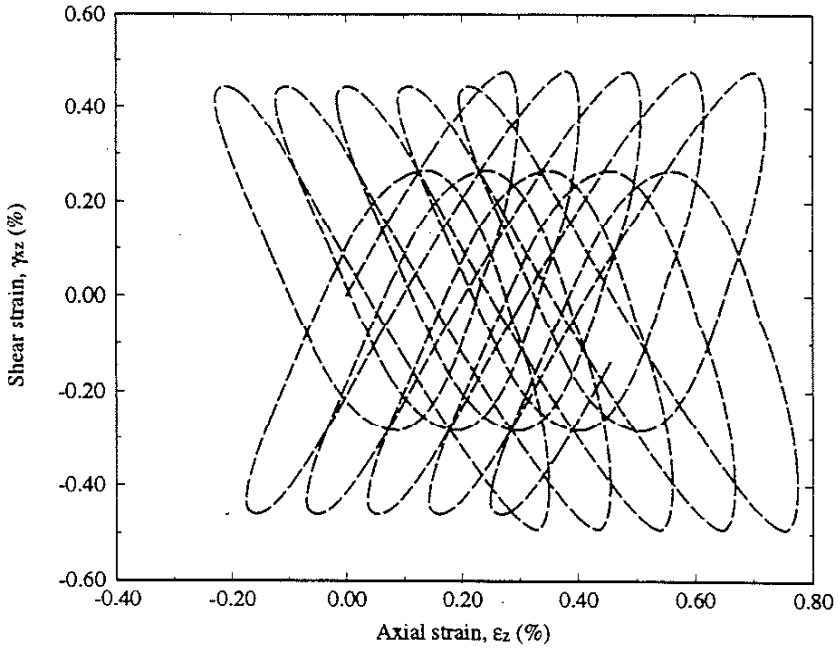

(b)

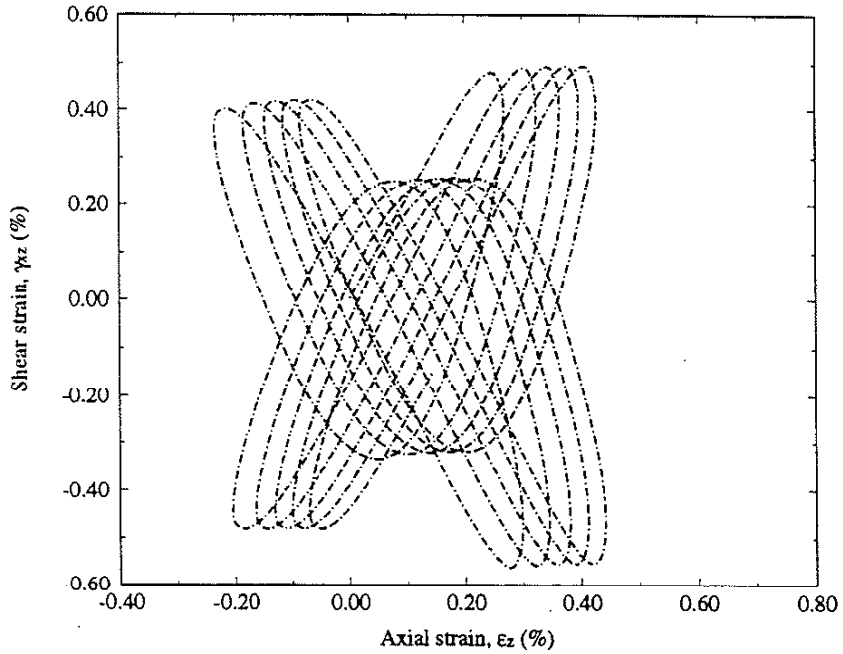

(c)

Figure 6.41 (continued). (b) Calculation using the simplified method and (c) calculation using the finite element method.

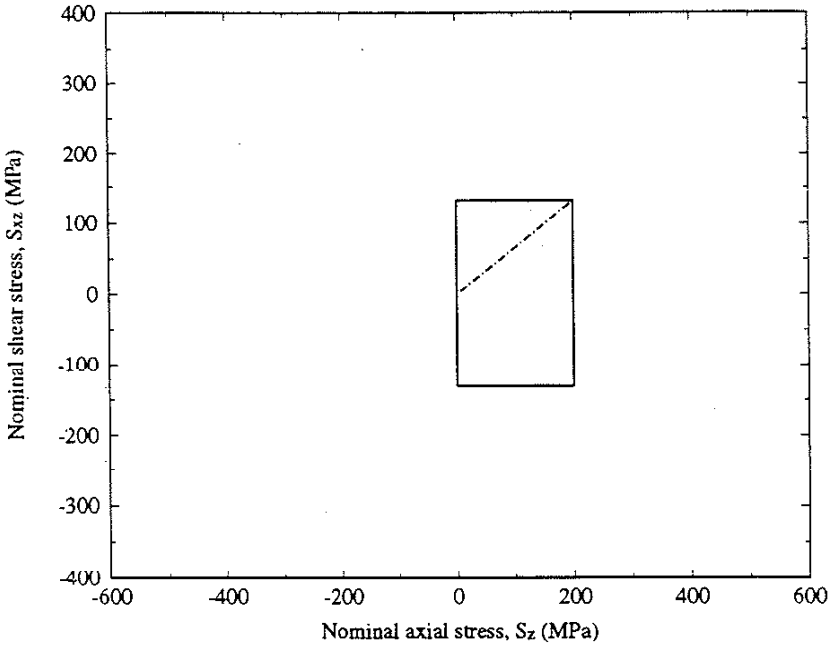

(a)

Figure 6.42. (a) Nominal stress path.

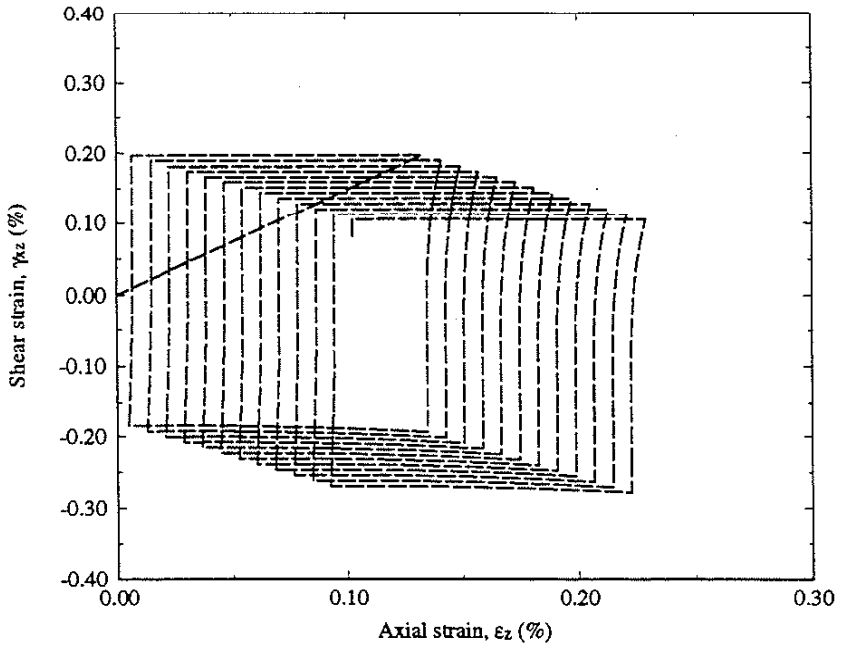

(b)

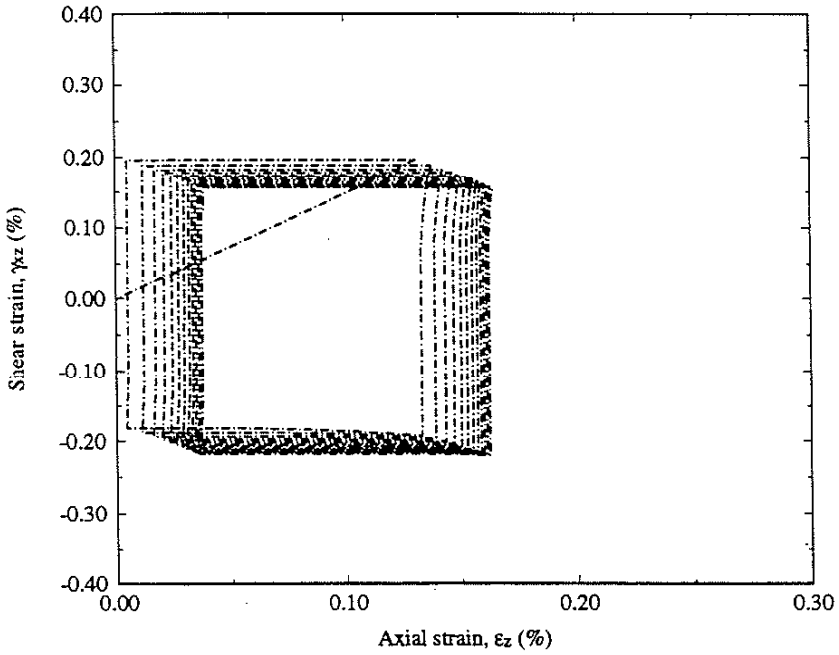

(c)

Figure 6.42 (continued). (b) Calculation using the simplified method and (c) calculation using the finite element method.

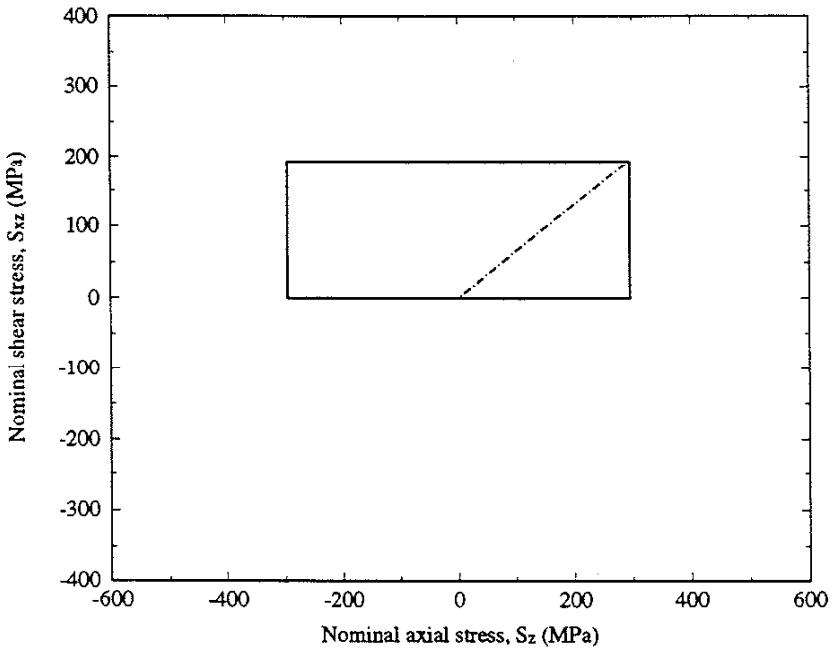

(a)

Figure 6.43. (a) Nominal stress path.

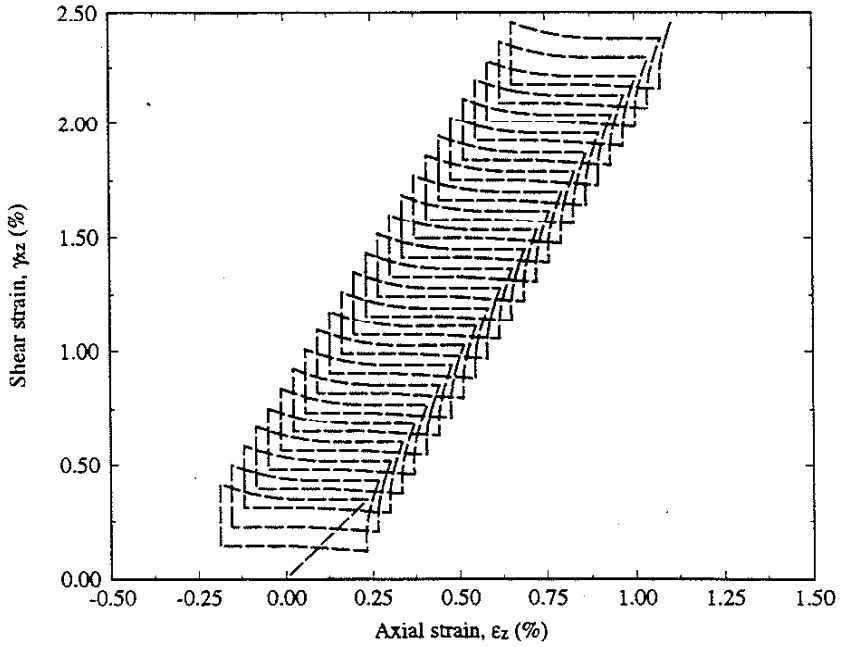

(b)

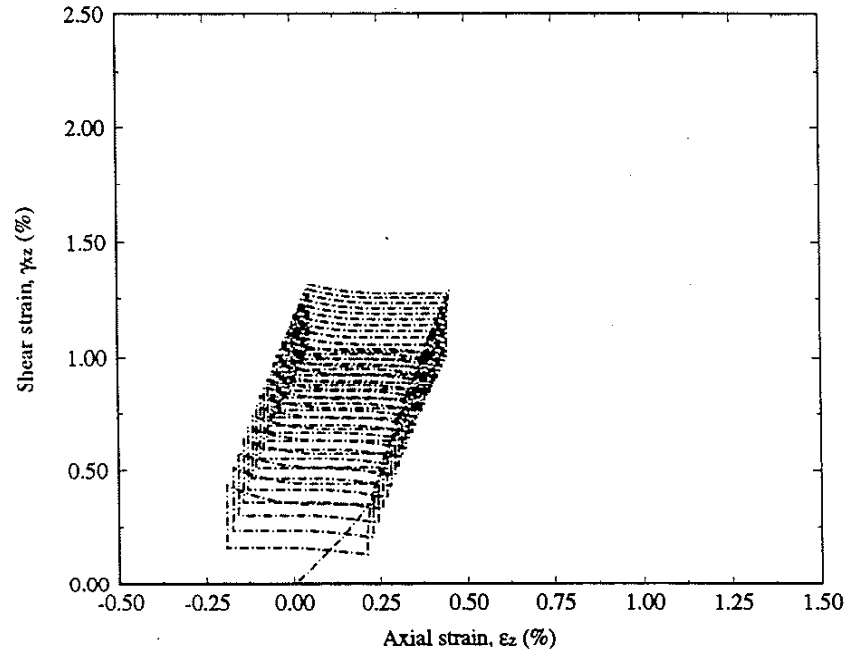

(c)

Figure 6.43 (continued). (b) Calculation using the simplified method and (c) calculation using the finite element method.

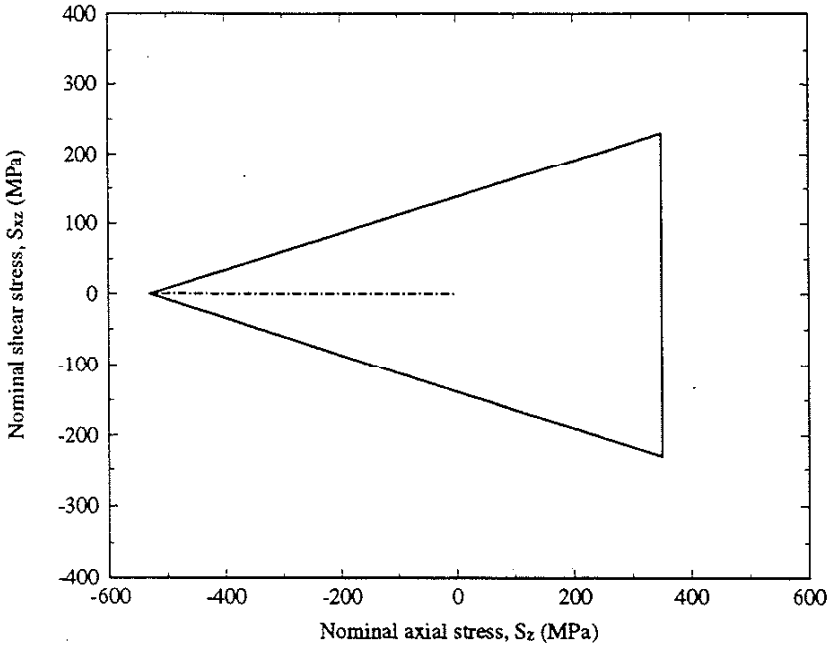

(a)

Figure 6.44. (a) Nominal stress path.

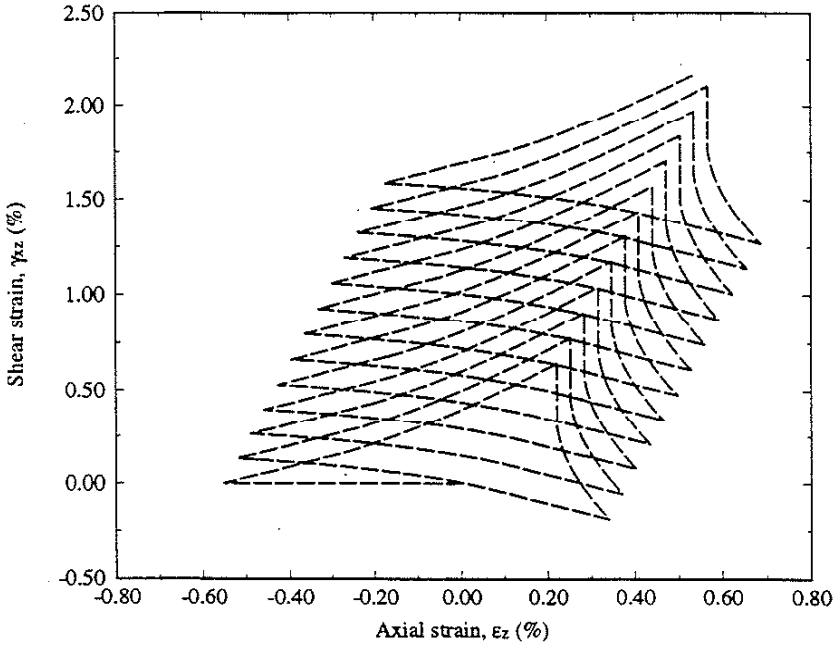

(b)

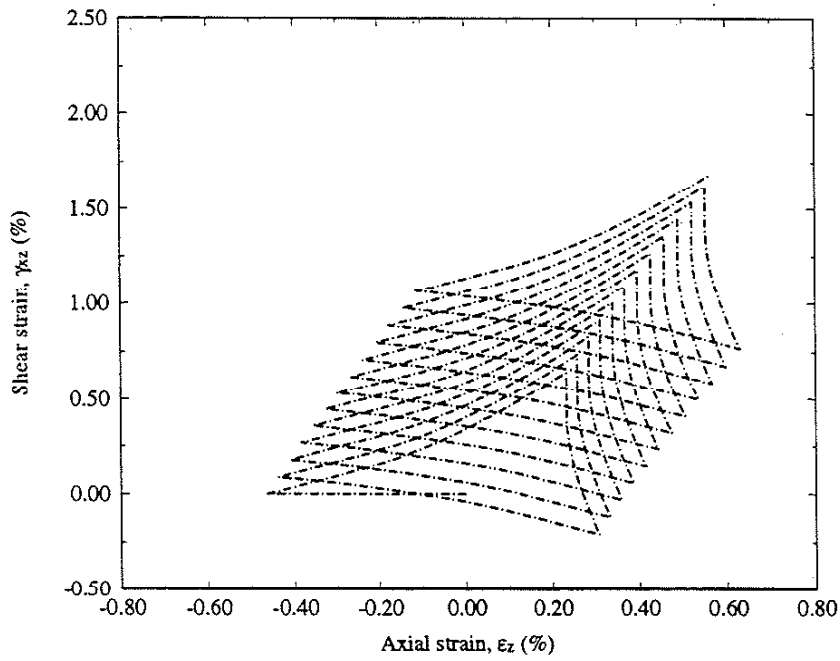

(c)

Figure 6.44 (continued). (b) Calculation using the simplified method and (c) calculation using the finite element method.

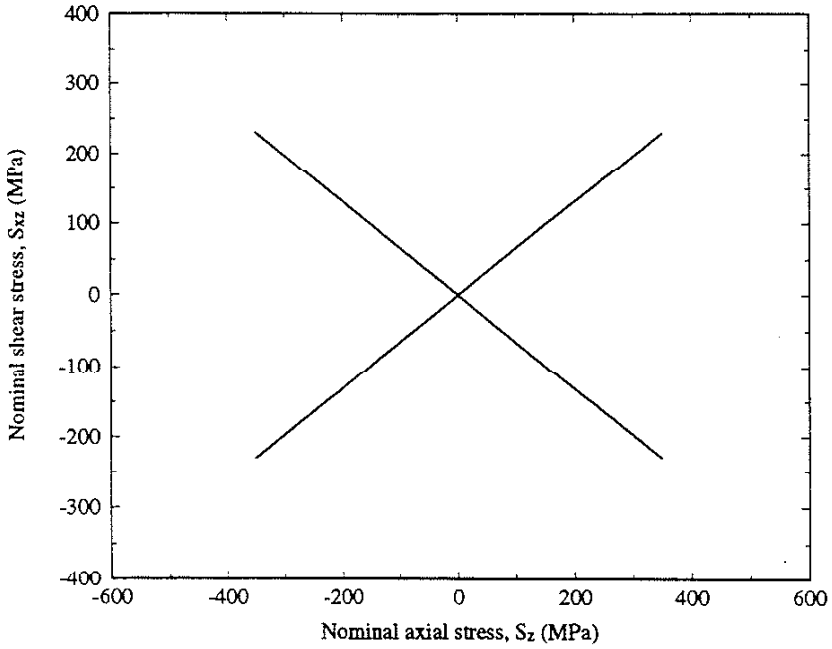

(a)

Figure 6.45. (a) Nominal stress path.

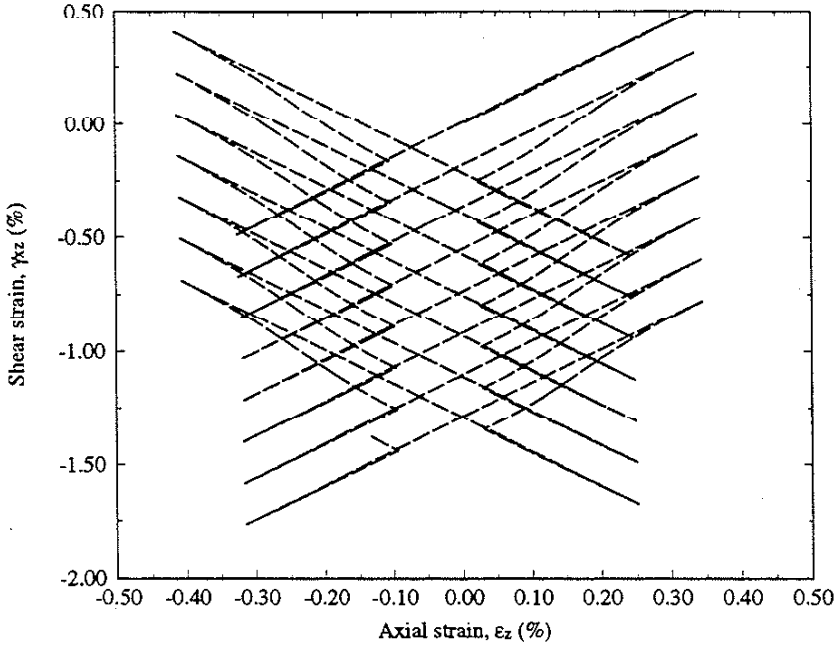

(b)

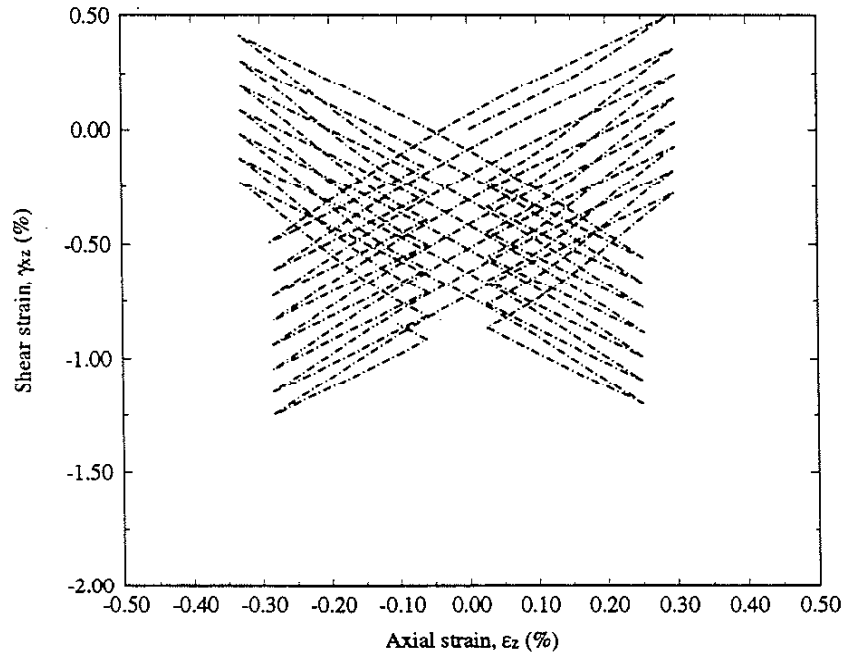

(c)

Figure 6.45 (continued). (b) Calculation using the simplified method and (c) calculation using the finite element method.

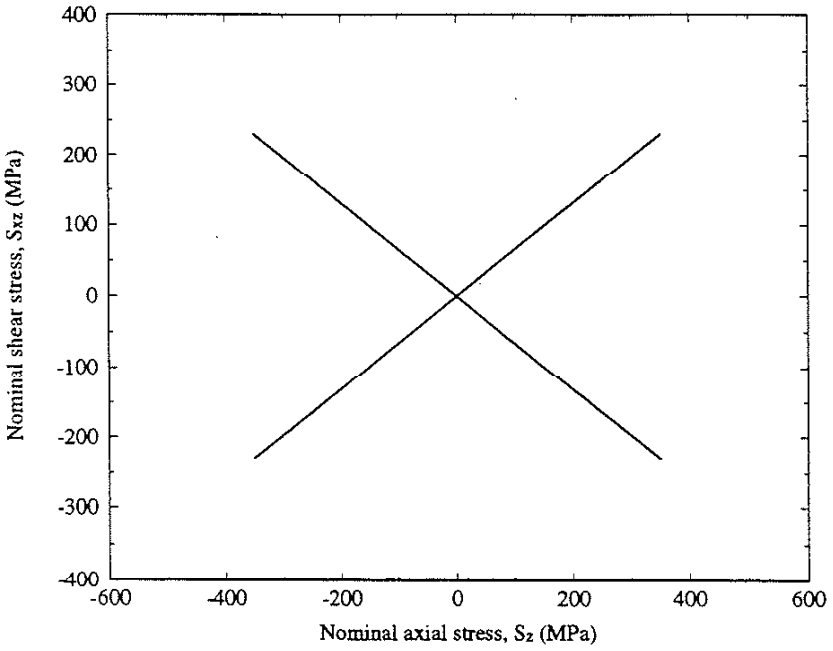

(a)

Figure 6.46. (a) Nominal stress path.

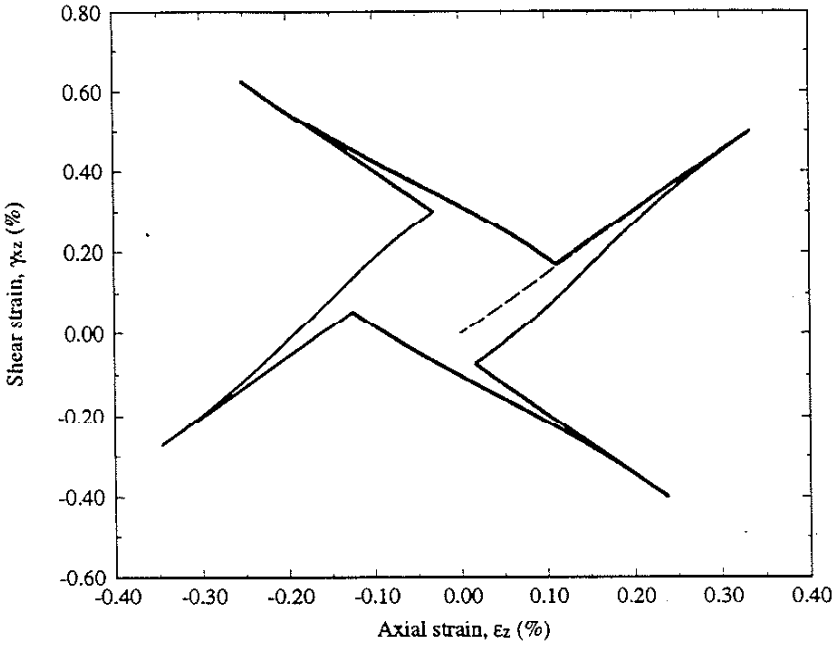

(b)

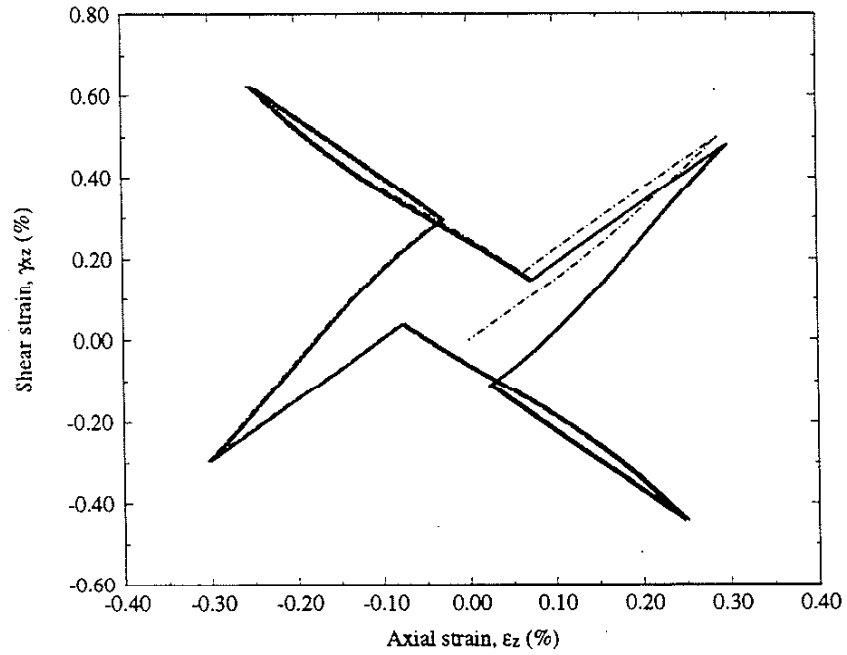

(c)

Figure 6.46 (continued). (b) Calculation using the simplified method and (c) calculation using the finite element method.

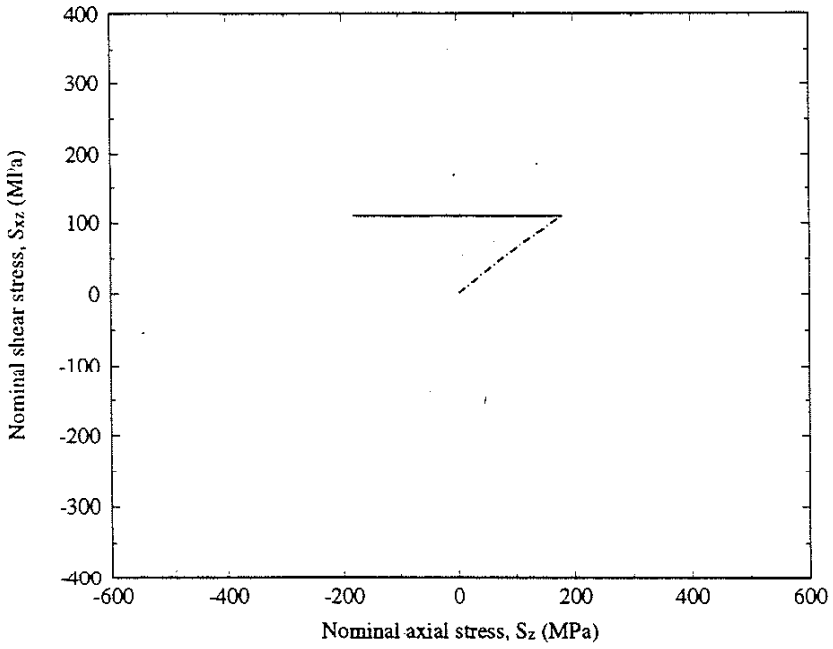

(a)

Figure 6.47. (a) Nominal stress path.

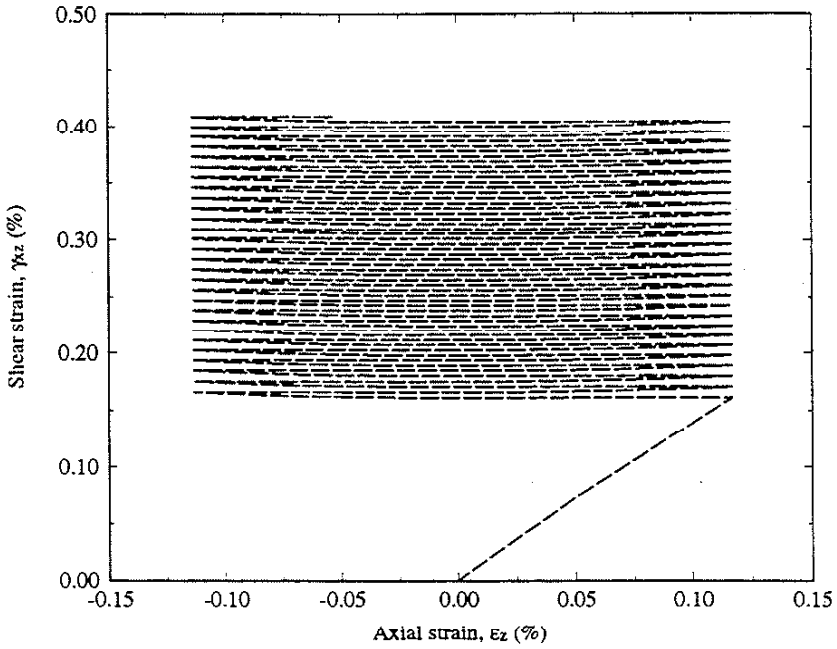

(b)

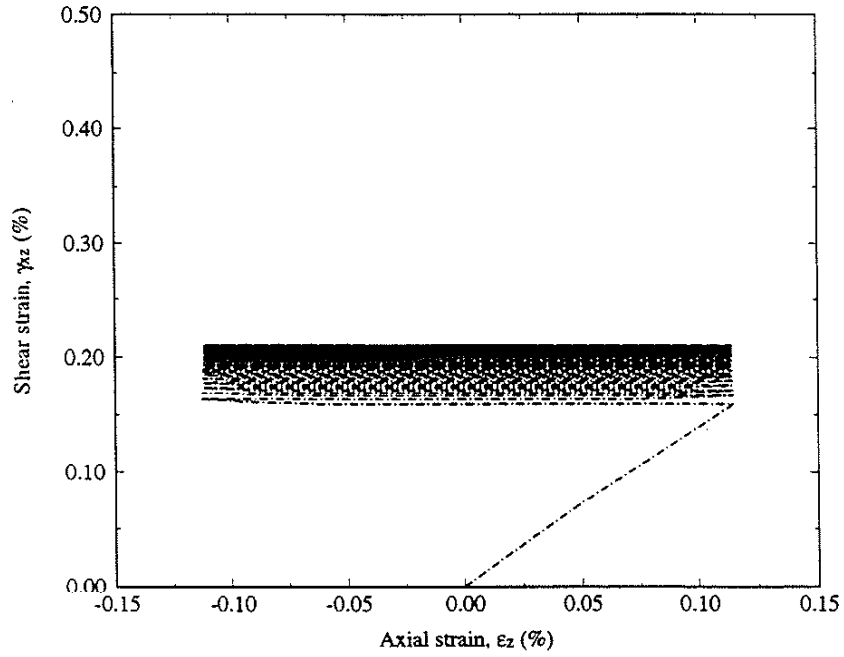

(c)

Figure 6.47 (continued). (b) Calculation using the simplified method and (c) calculation using the finite element method.

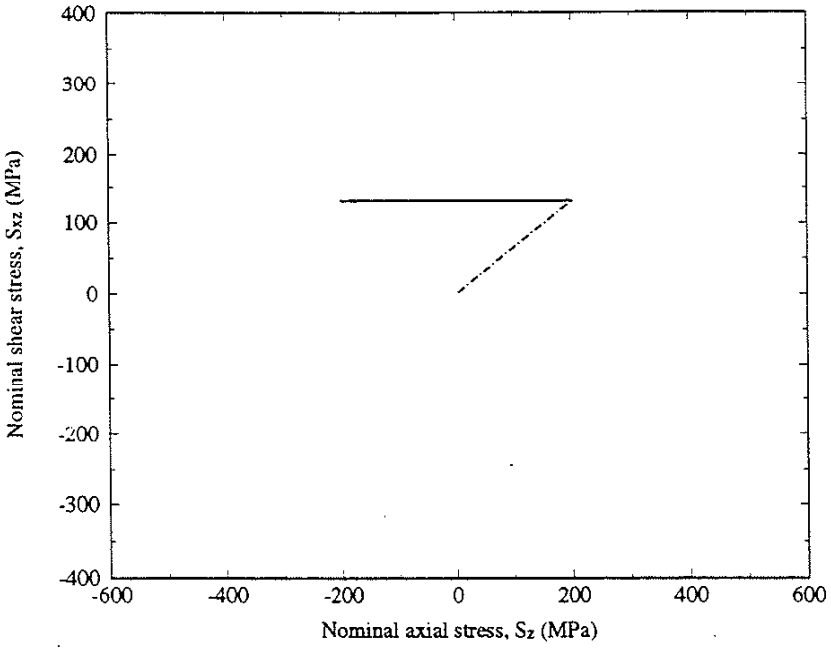

(a)

Figure 6.48. (a) Nominal stress path.

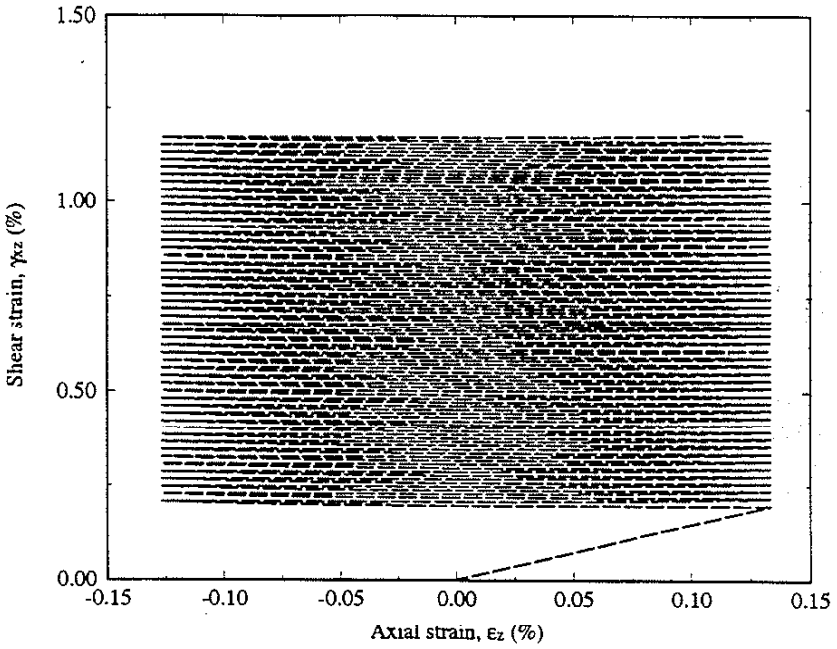

(b)

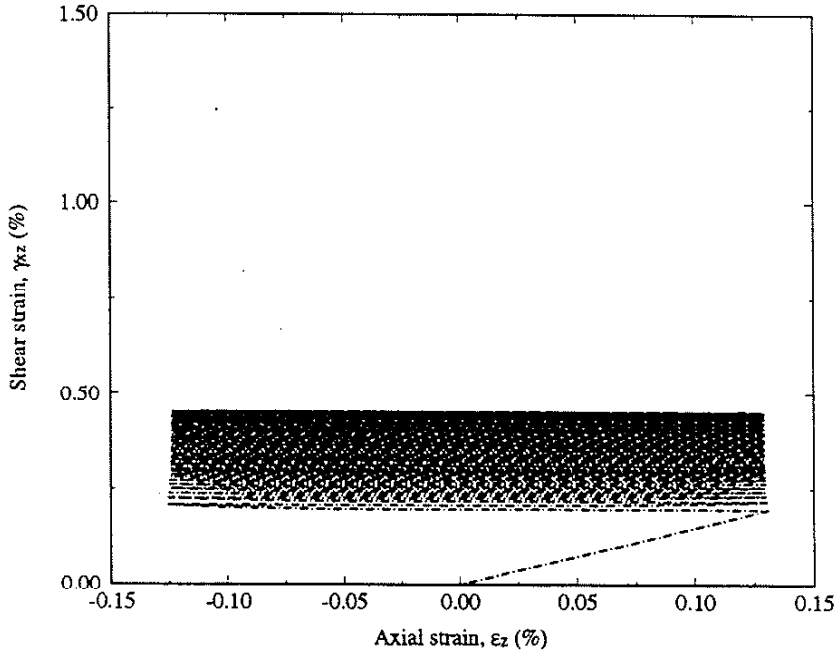

(c)

Figure 6.48 (continued). (b) Calculation using the simplified method and (c) calculation using the finite element method.

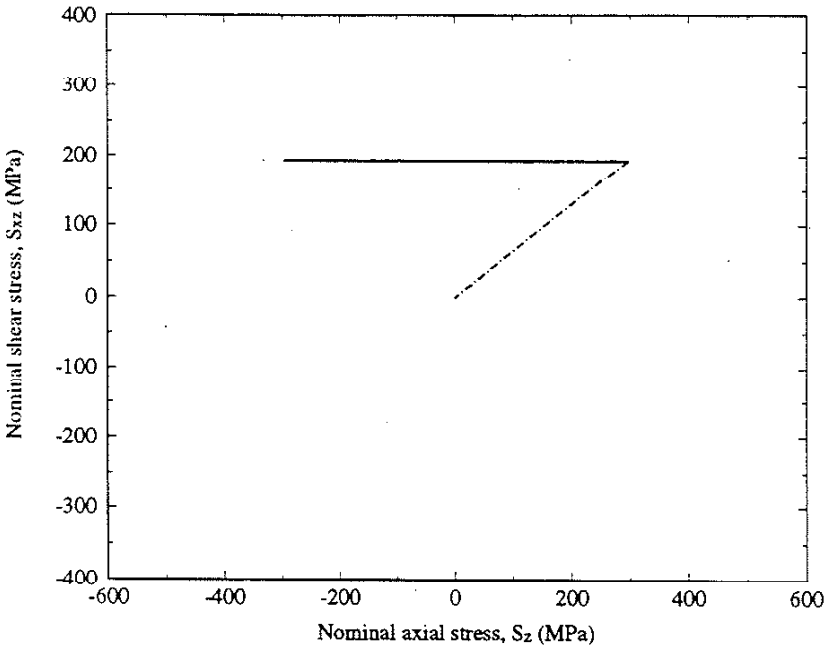

(a)

Figure 6.49. (a) Nominal stress path.

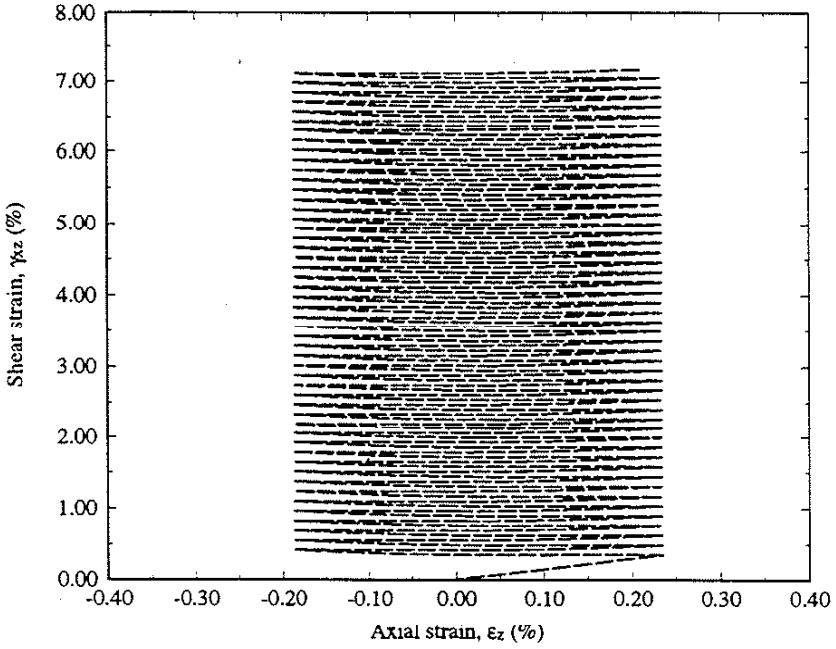

(b)

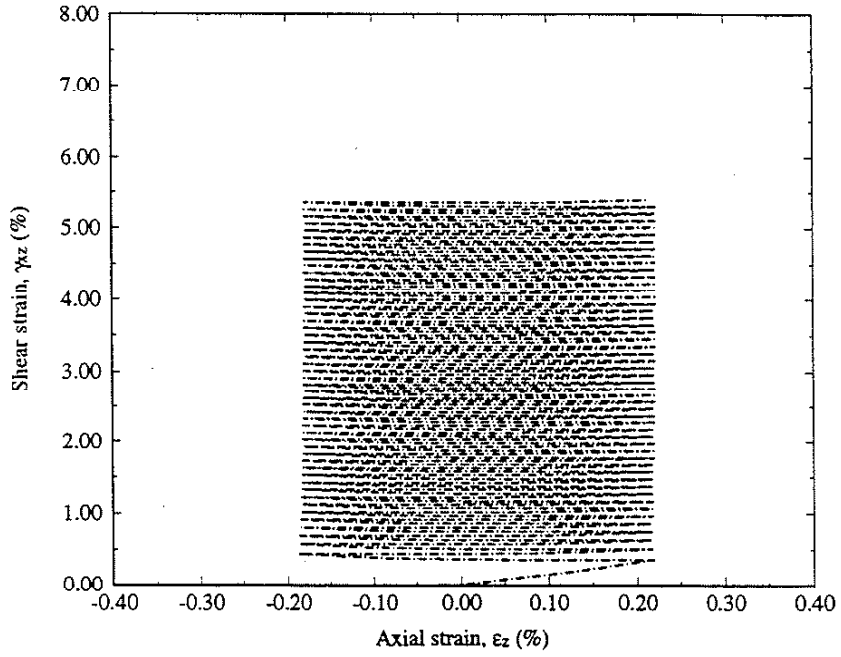

(c)

Figure 6.49 (continued). (b) Calculation using the simplified method and (c) calculation using the finite element method.

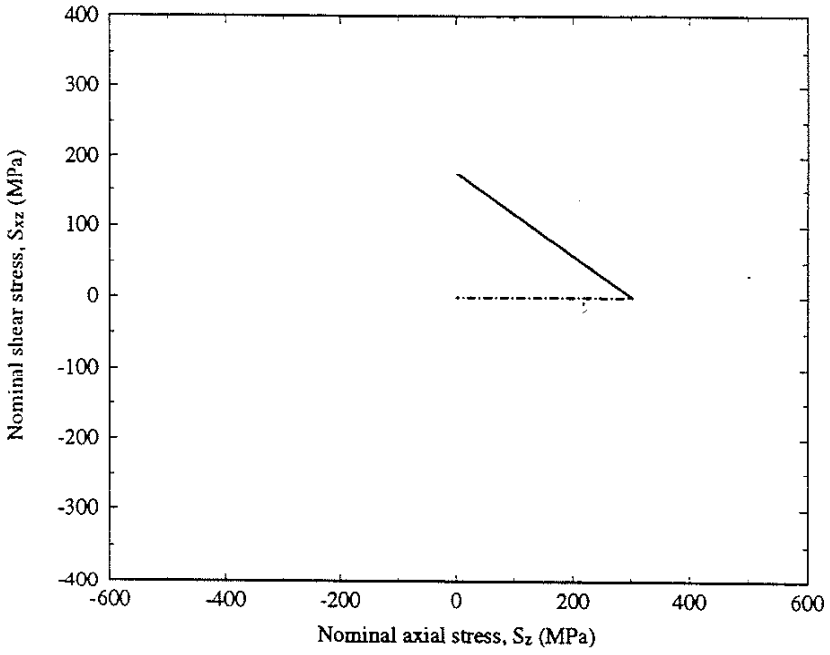

(a)

Figure 6.50. (a) Nominal stress path.

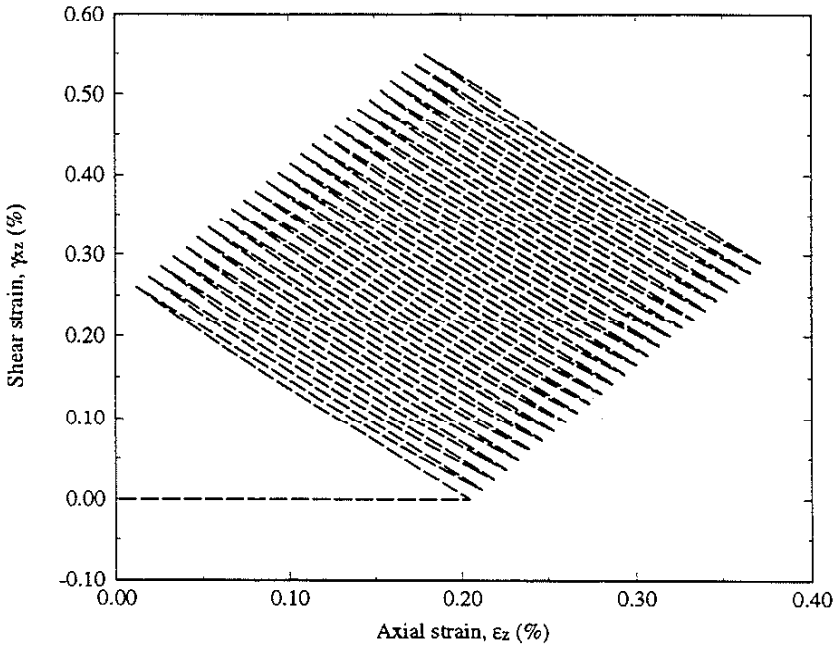

(b)

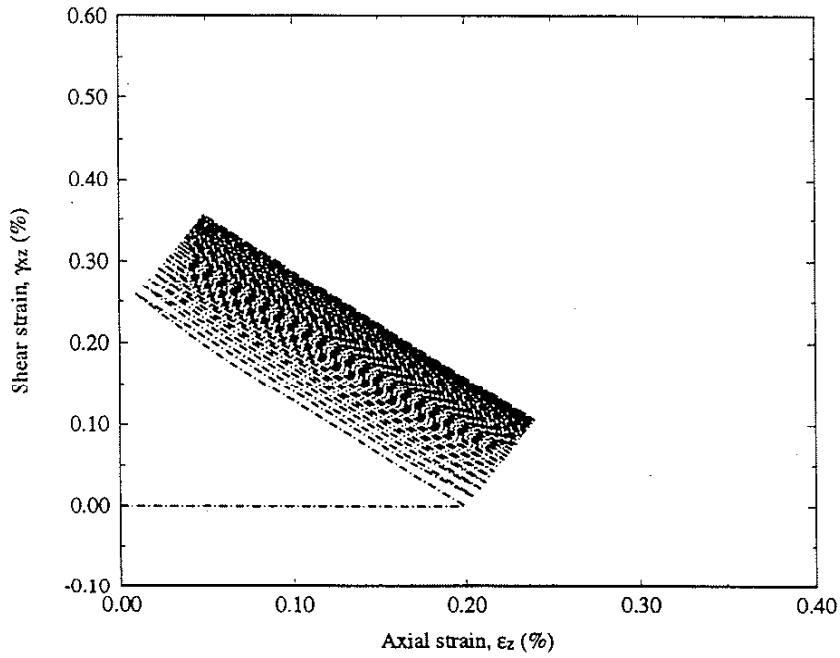

(c)

Figure 6.50 (continued). (b) Calculation using the simplified method and (c) calculation using the finite element method.

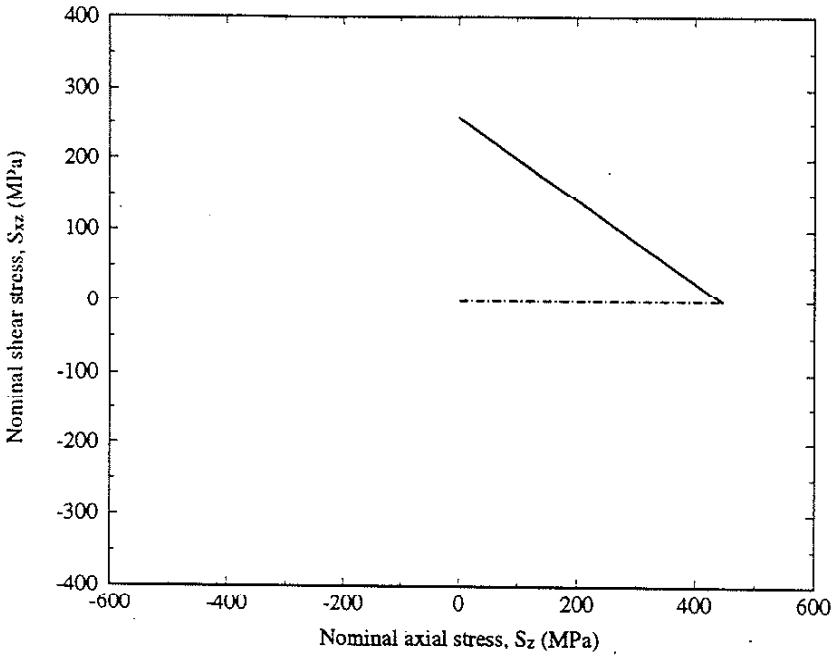

(a)

Figure 6.51. (a) Nominal stress path.

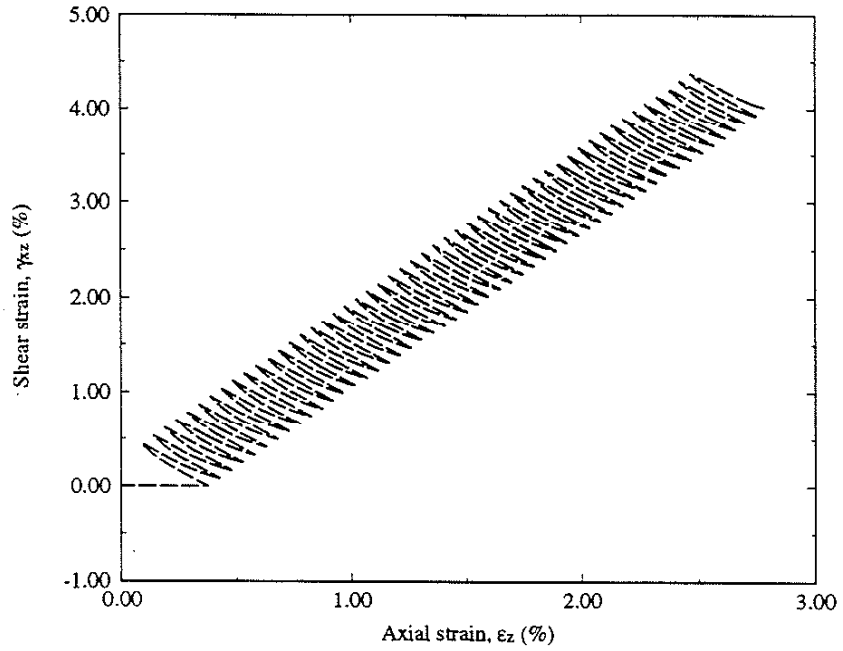

(b)

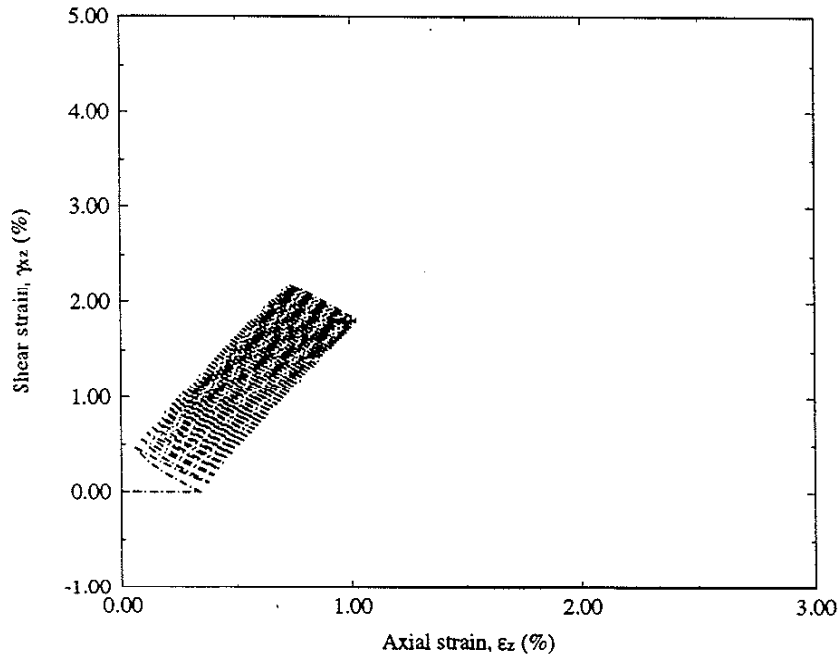

(c)

Figure 6.51 (continued). (b) Calculation using the simplified method and (c) calculation using the finite element method.

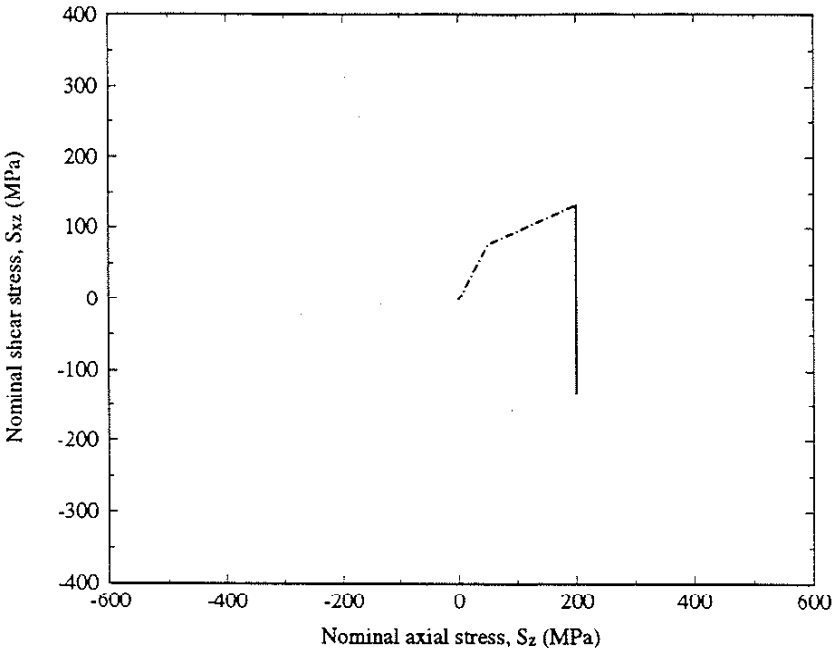

(a)

Figure 6.52. (a) Nominal stress path.

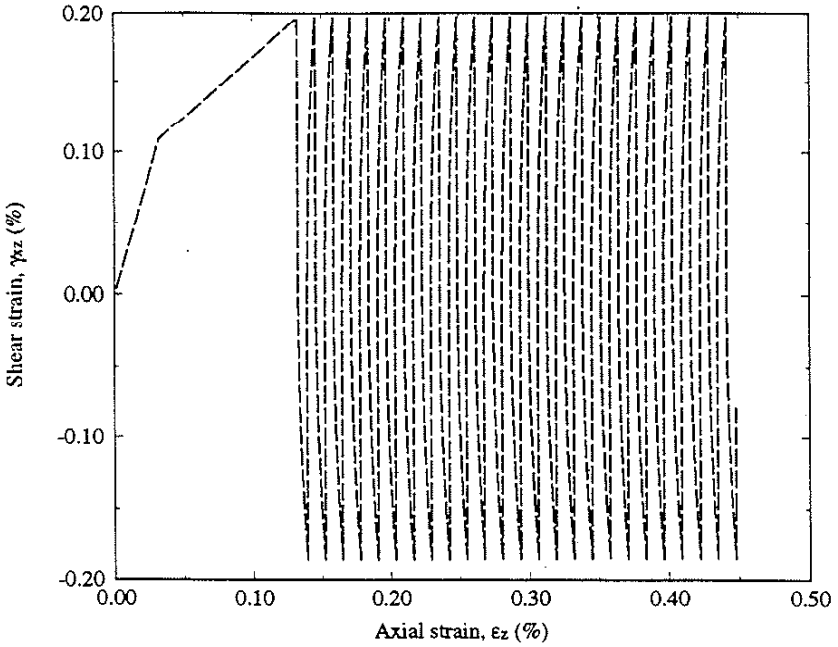

(b)

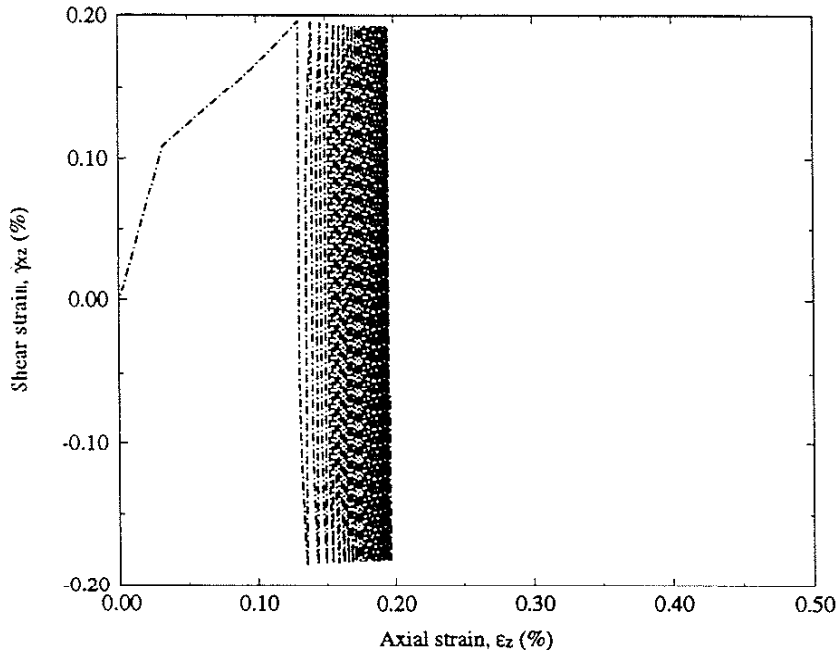

(c)

Figure 6.52 (continued). (b) Calculation using the simplified method and (c) calculation using the finite element method.

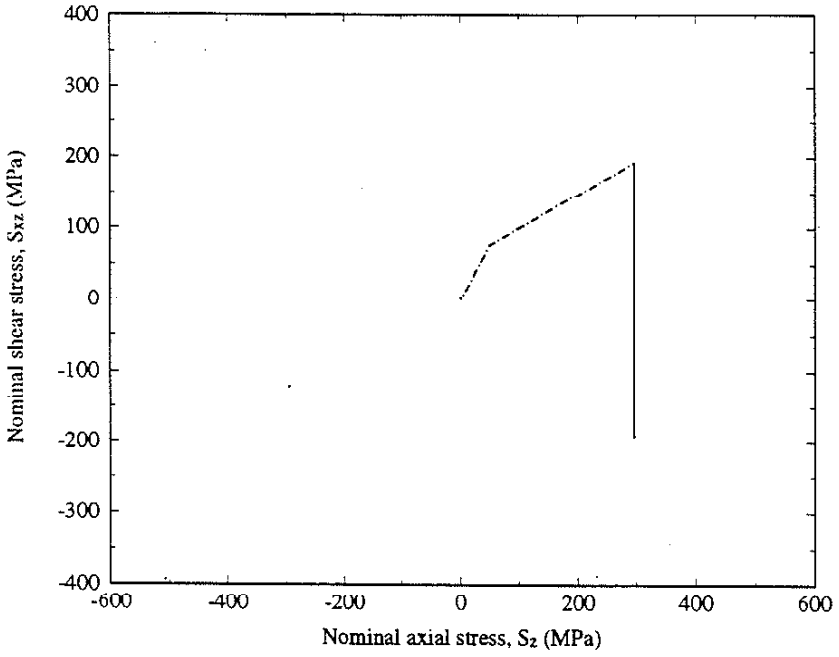

(a)

Figure 6.53. (a) Nominal stress path.

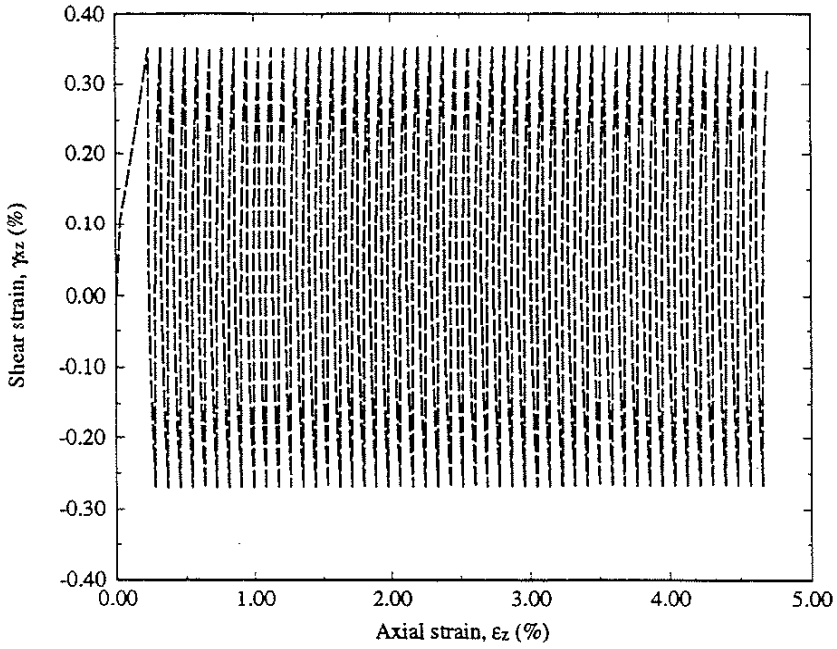

(b)

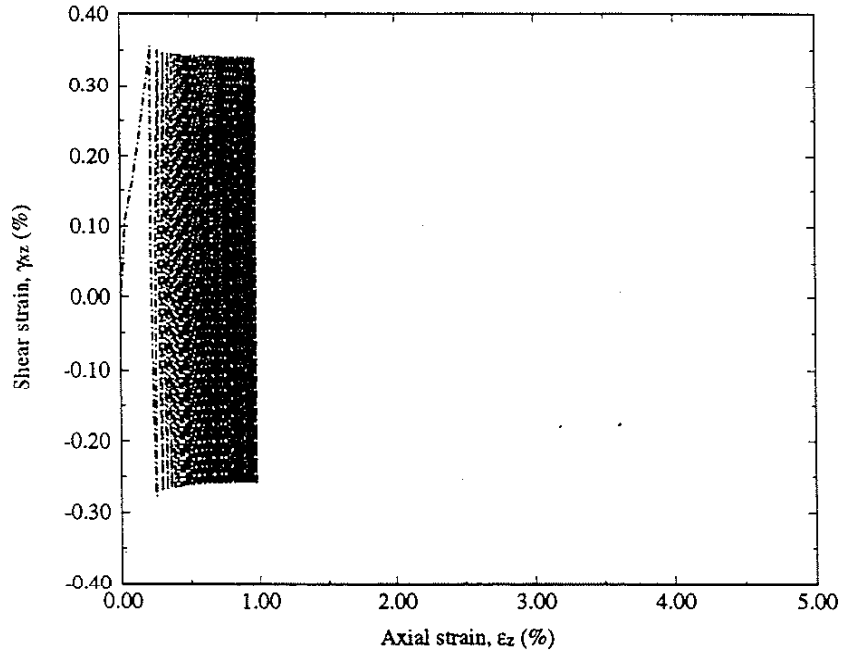

(c)

Figure 6.53 (continued). (b) Calculation using the simplified method and (c) calculation using the finite element method.

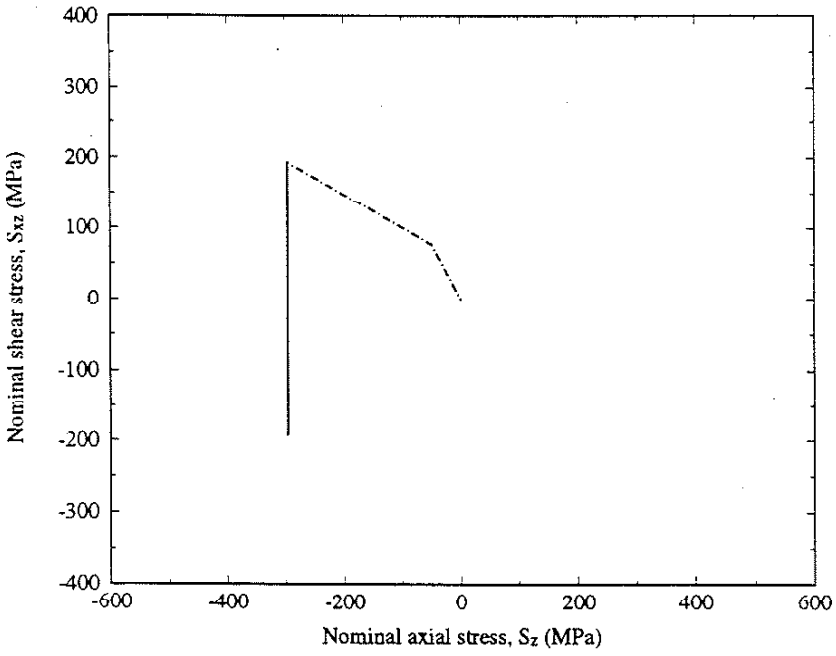

(a)

Figure 6.54. (a) Nominal stress path.

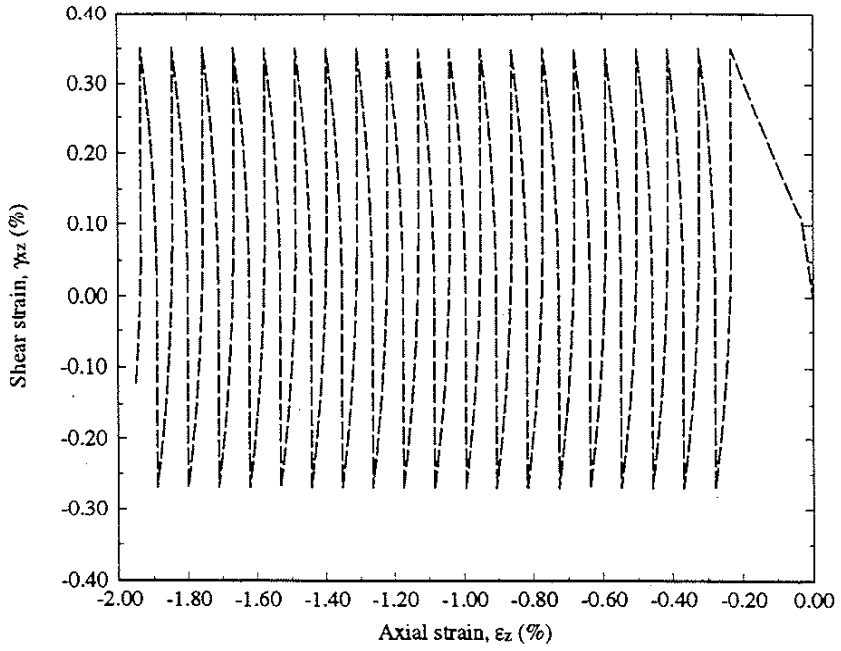

(b)

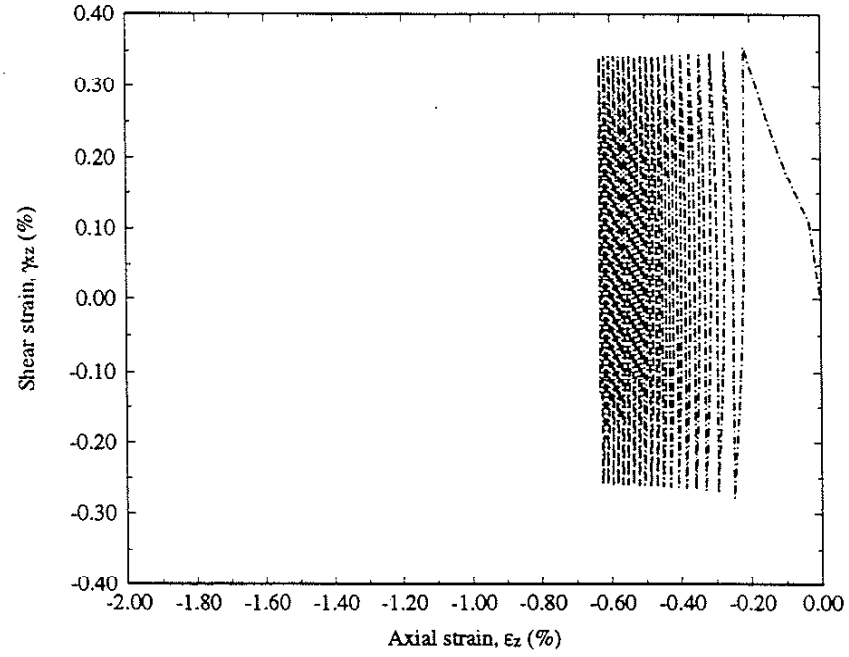

(c)

Figure 6.54 (continued). (b) Calculation using the simplified method and (c) calculation using the finite element method.

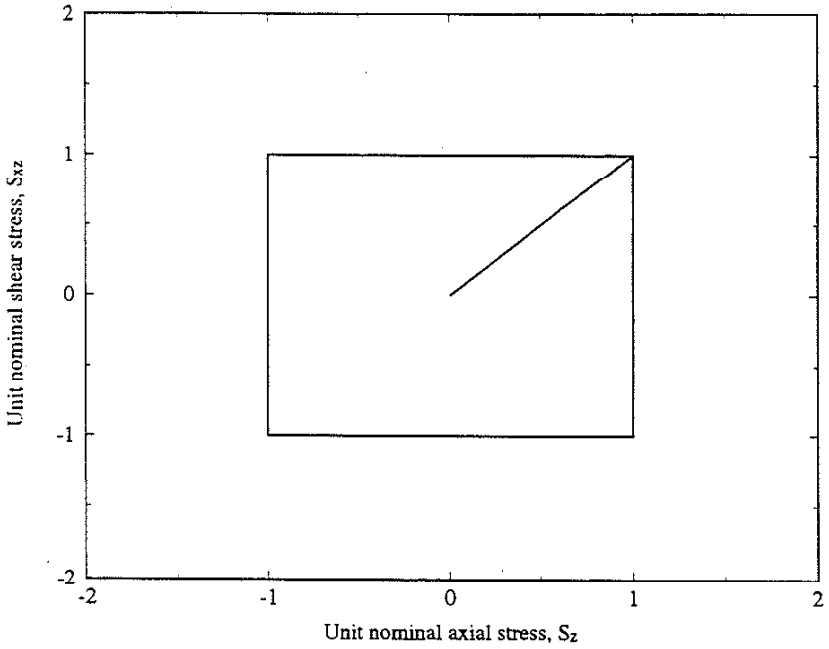

Figure 6.55. Nominal stress box-path.

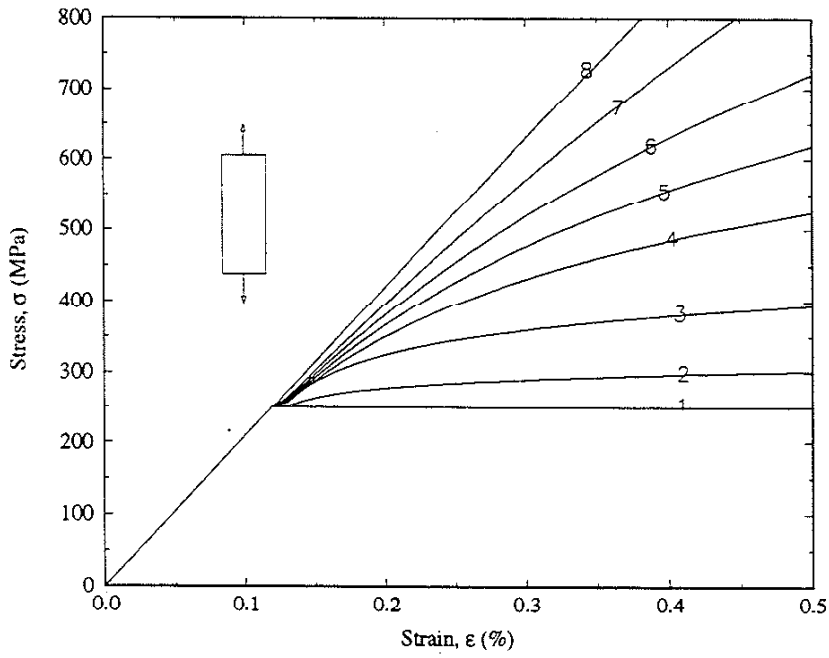

Figure 6.56. Uniaxial smooth bar stress strain curves.

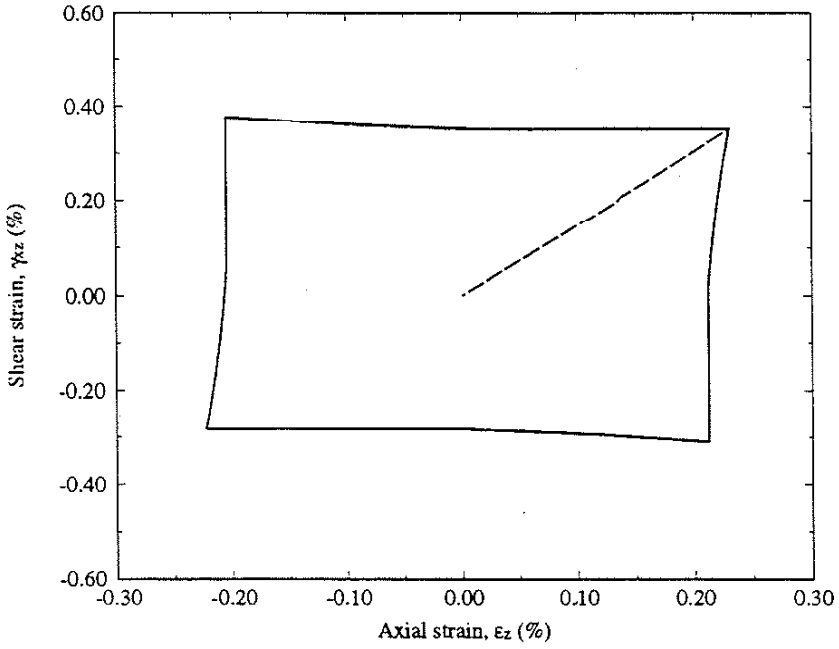

(a)

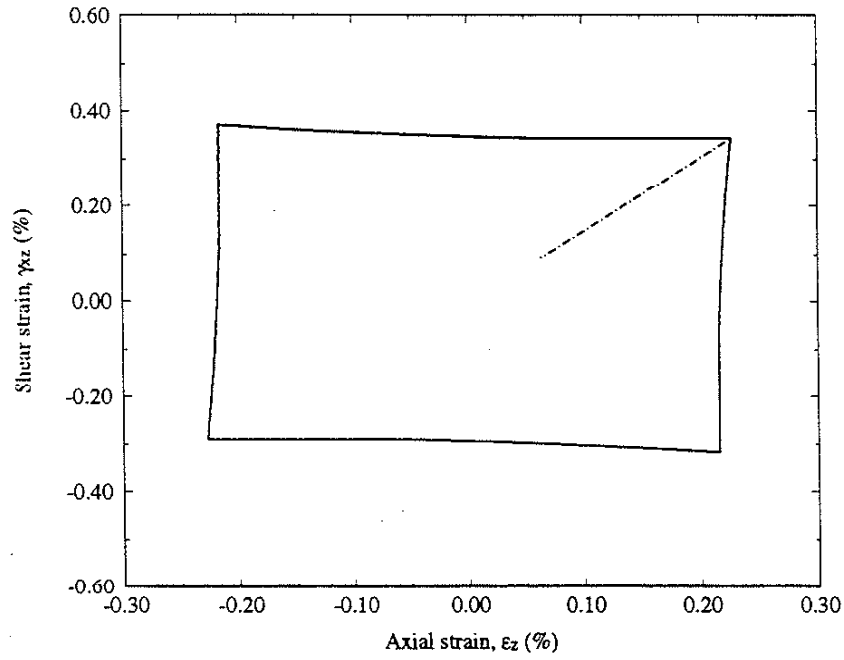

(b)

Figure 6.57. (a) Calculation for material 7 using the simplified method and (b) calculation for material 7 using the finite element method with maximum nominal stresses of S_z = 340 MPa, and S_{xz} = 222 MPa.

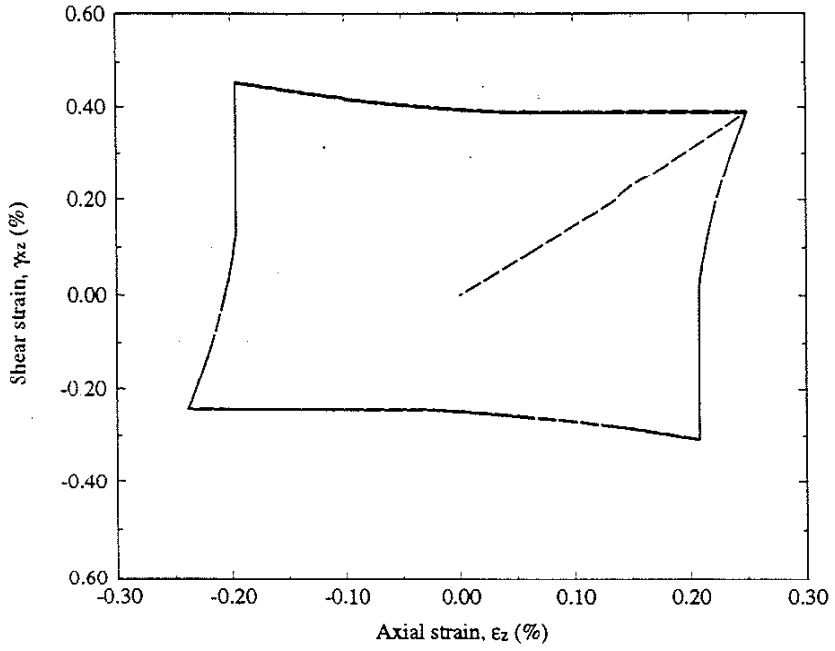

(a)

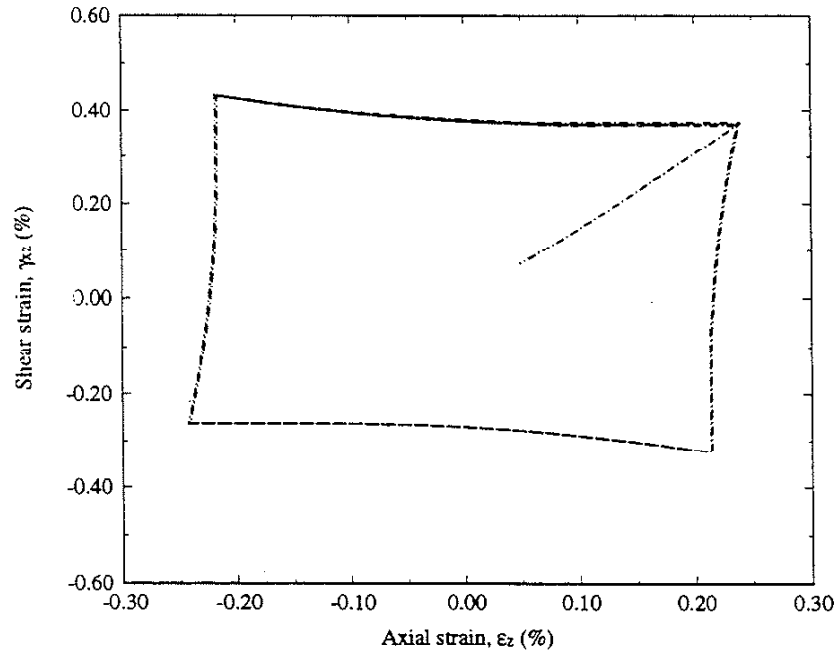

(b)

Figure 6.58. (a) Calculation for material 6 using the simplified method and (b) calculation for material 6 using the finite element method with maximum nominal stresses of S_z = 340 MPa, and S_{xz} = 222 MPa.

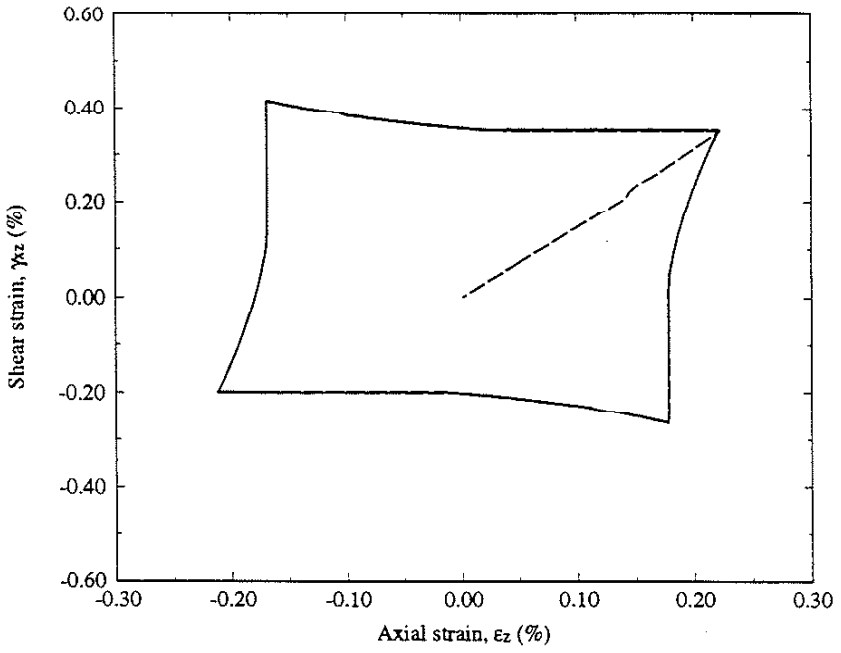

(a)

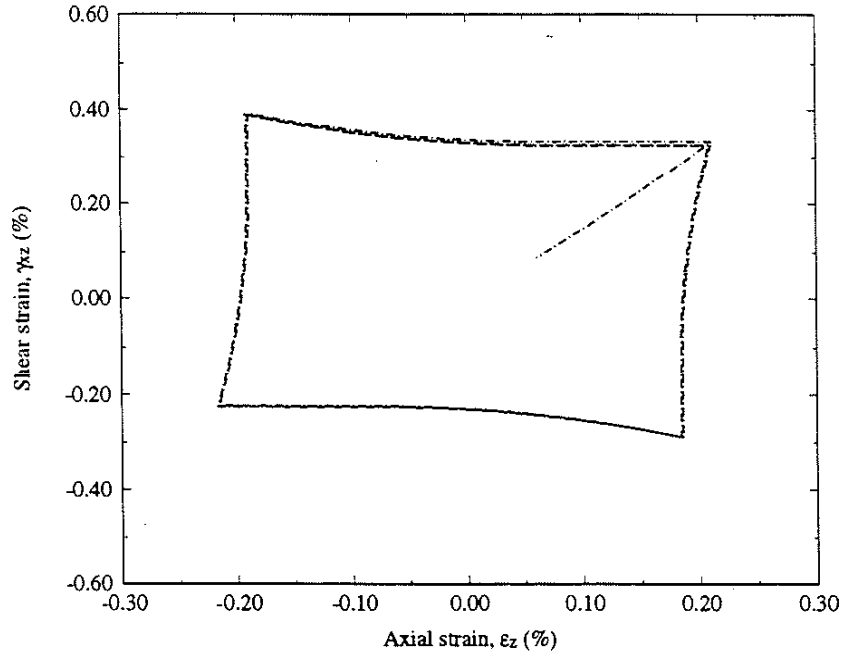

(b)

Figure 6.59. (a) Calculation for material 5 using the simplified method and (b) calculation for material 5 using the finite element method with maximum nominal stresses of S_z = 296 MPa, and S_{xz} = 193 MPa.

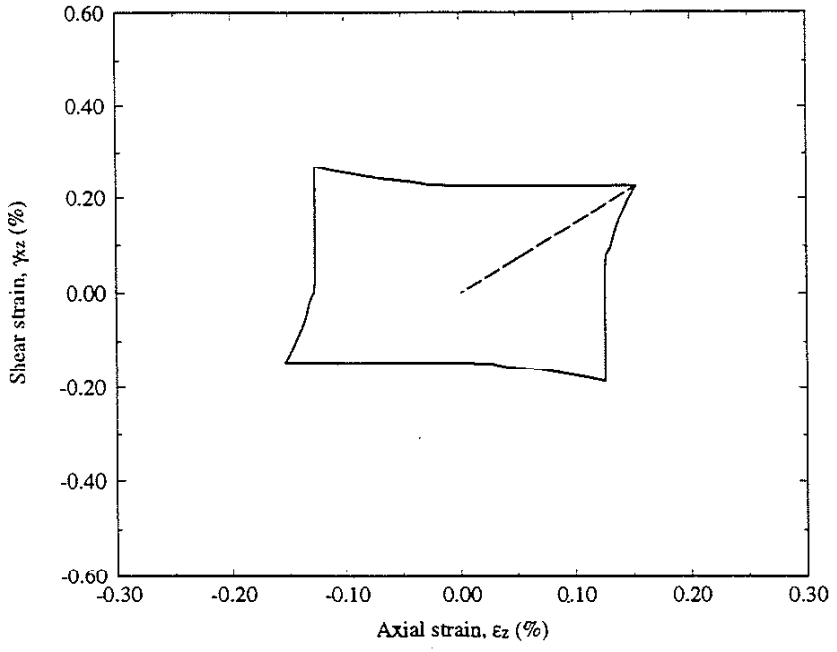

(a)

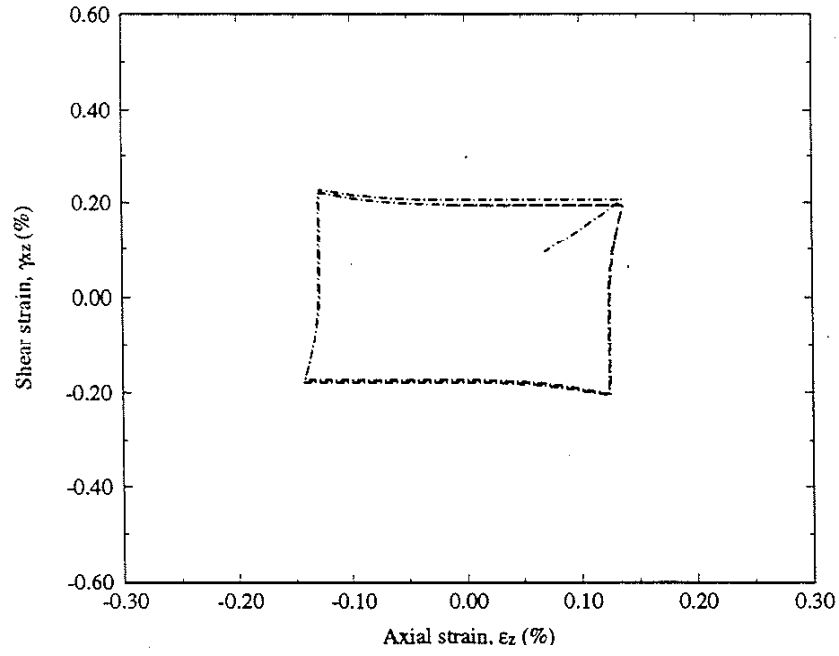

(b)

Figure 6.60. (a) Calculation for material 3 using the simplified method and (b) calculation for material 3 using the finite element method with maximum nominal stresses of S_z = 200 MPa, and S_{xz} = 131 MPa.

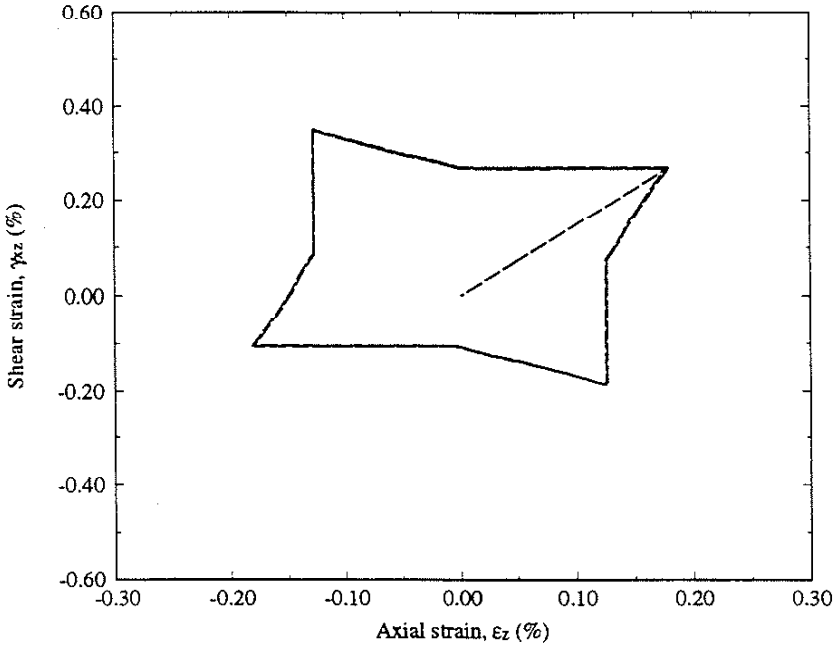

(a)

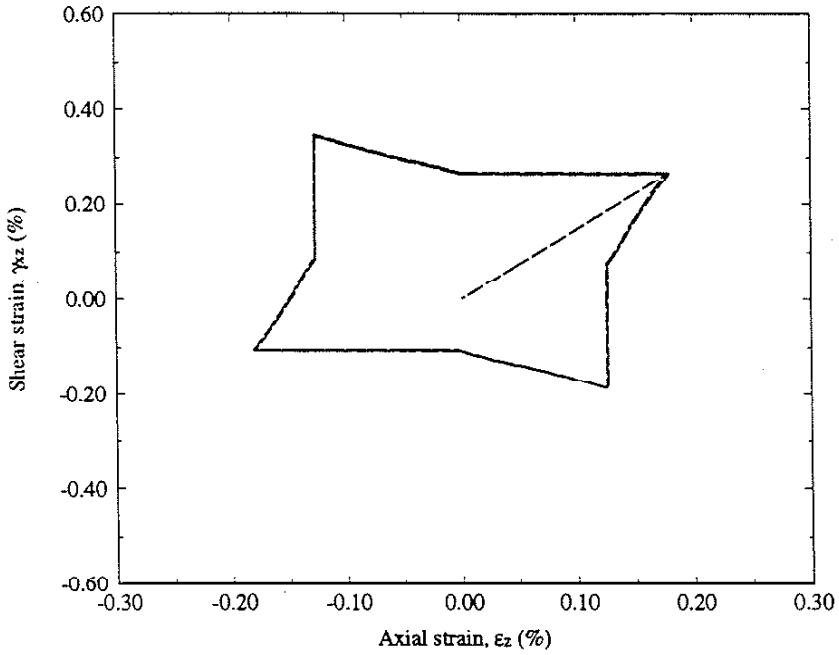

(b)

Figure 6.61. (a) Calculation for material 2 using the simplified method and (b) calculation for material 2 using the finite element method with maximum nominal stresses of S_z = 200 MPa, and S_{xz} = 131 MPa.

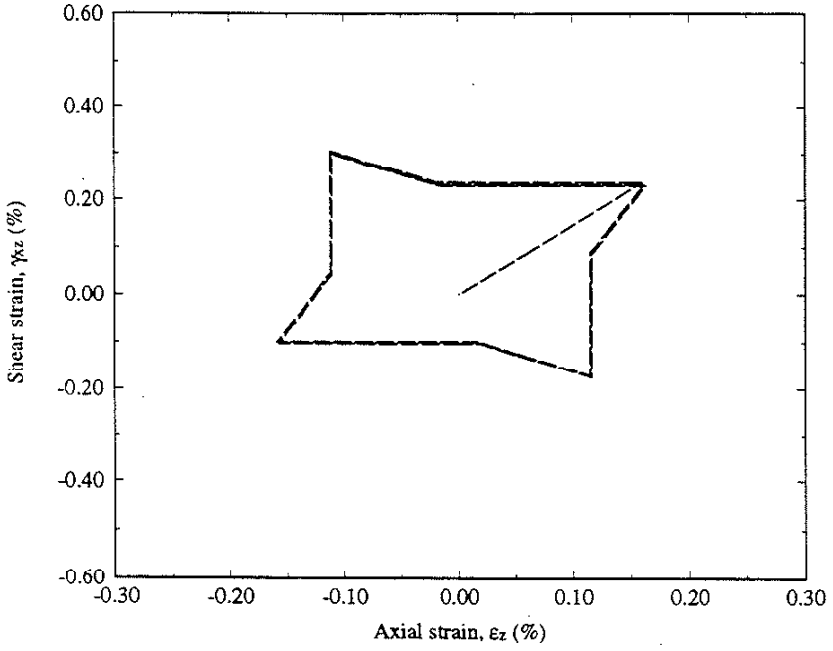

(a)

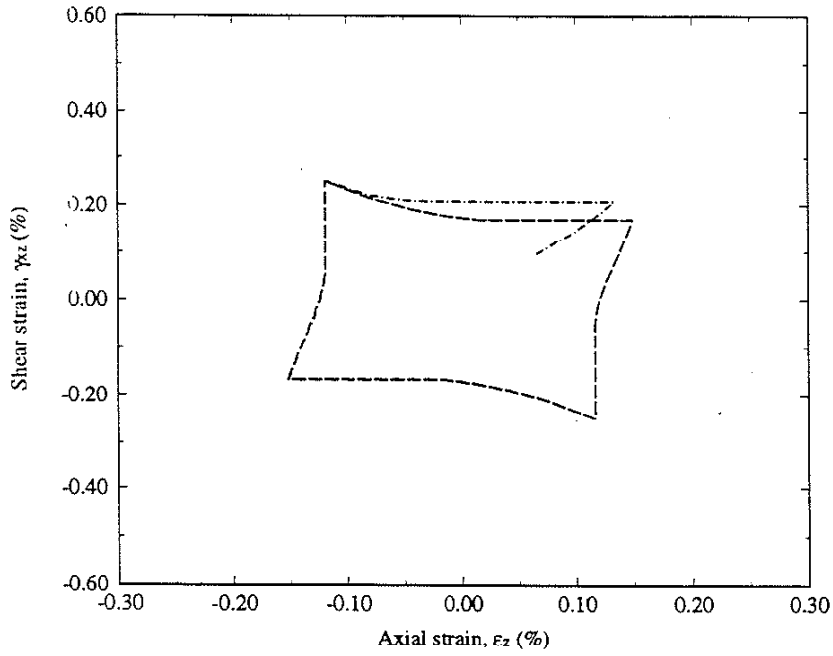

(b)

Figure 6.62. (a) Calculation for material 1 (elastic-perfectly plastic) using the simplified method and (b) calculation for material 1 (elastic-perfectly plastic) using the finite element method with maximum nominal stresses of S_z = 179 MPa, and S_{xz} = 117 MPa.

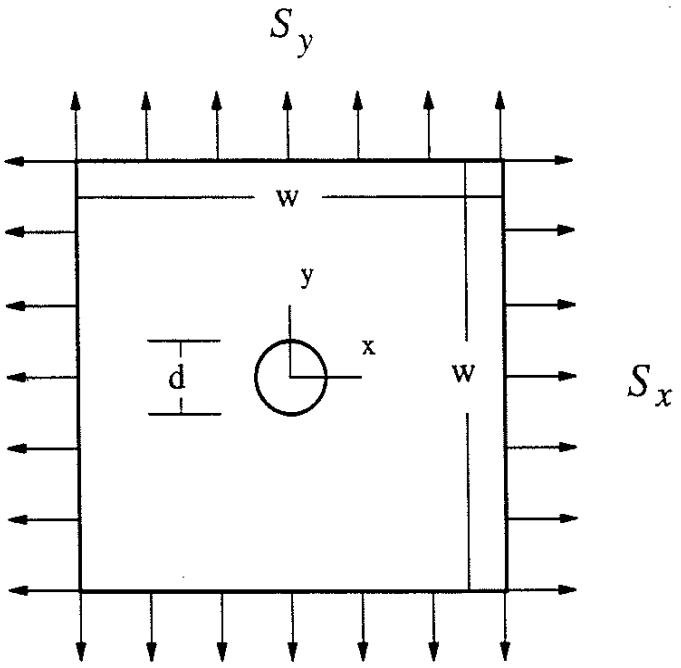

Figure 7.1. Plate geometry.

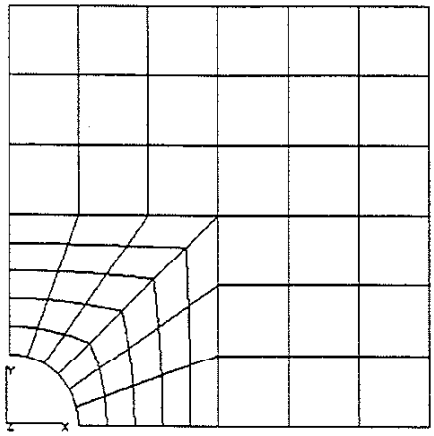

Figure 7.2. Finite element mesh of plate.

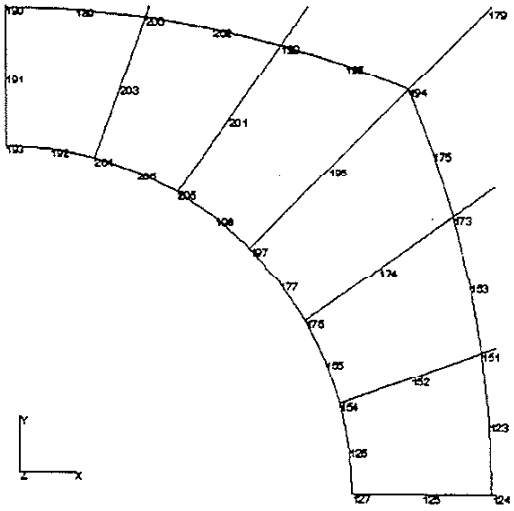

Figure 7.3. Detailed view of finite element mesh.

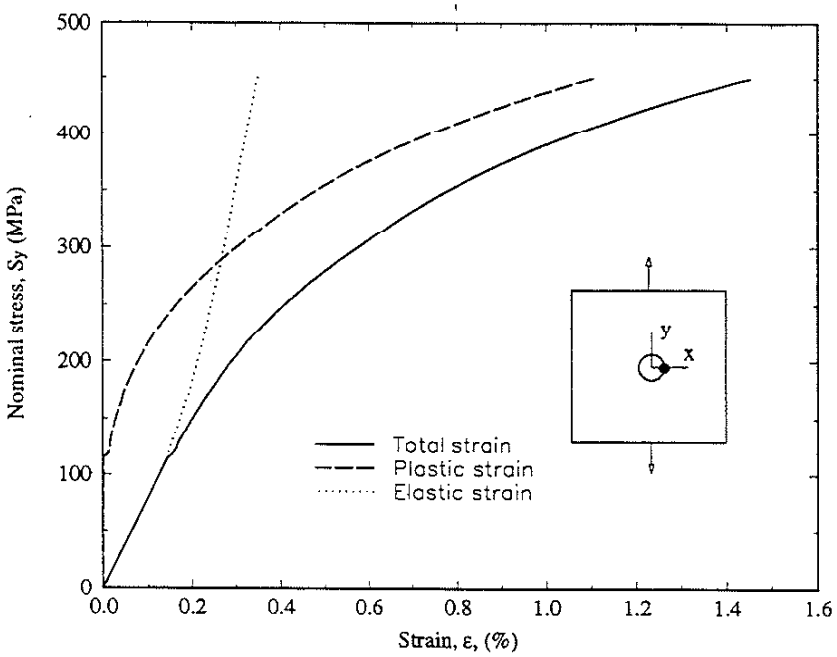

Figure 7.4. Nominal stress-notch strain response of plate.

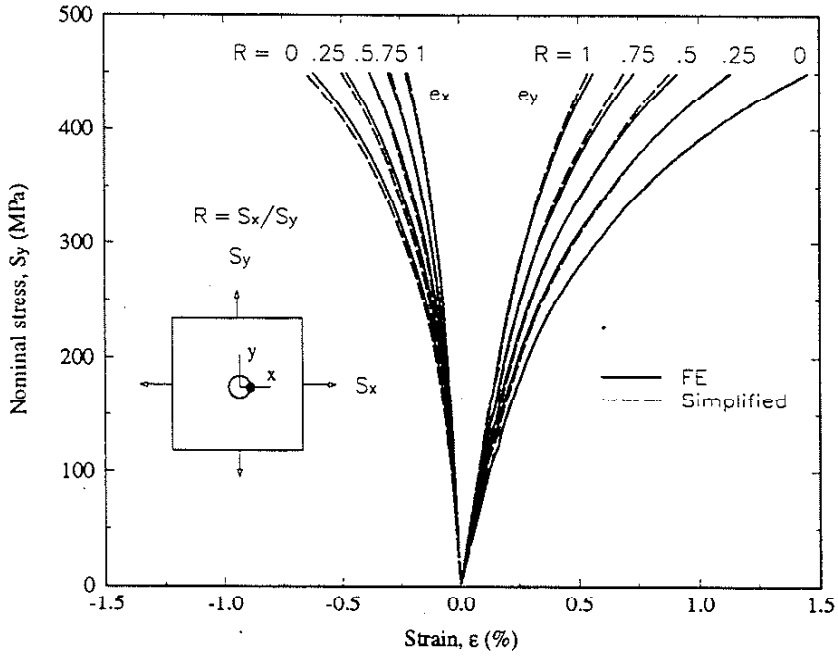

Figure 7.5. Monotonic analyses at various ratios of applied nominal loads.

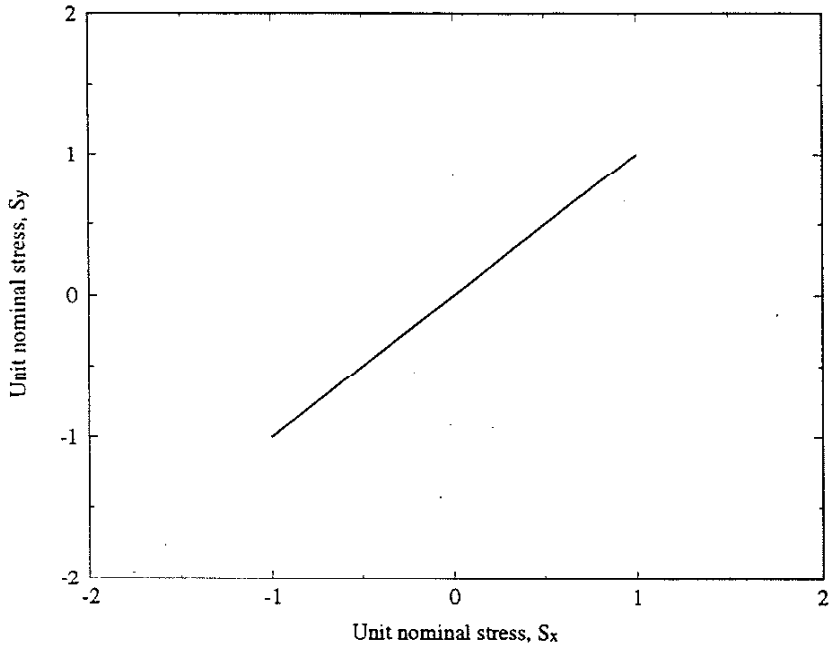

Figure 7.6a. Nominal stress path for balanced biaxial cyclic nominal loading.

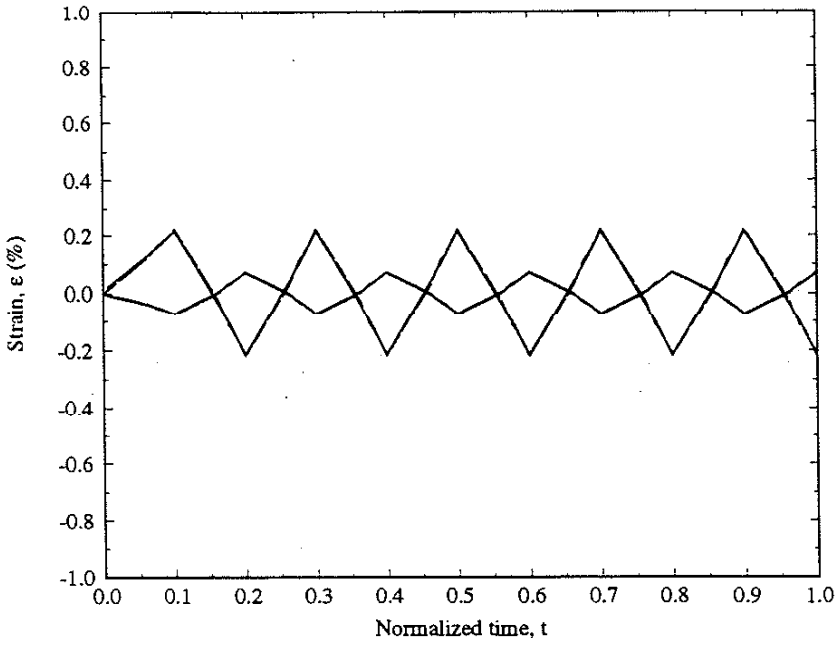

Figure 7.6b. Strain response for S_{max} = 250 MPa.

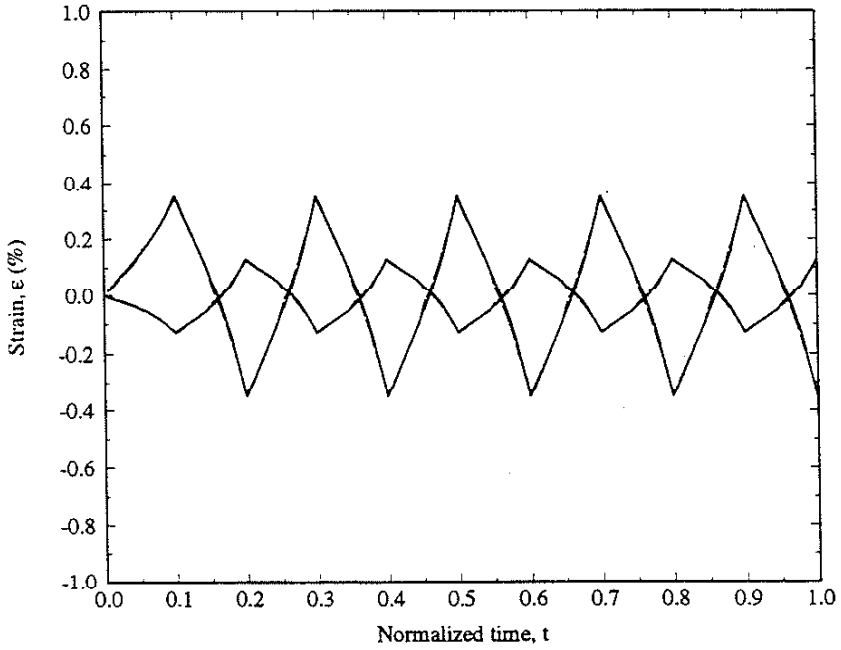

Figure 7.6c. Strain response for S_{max} = 350 MPa.

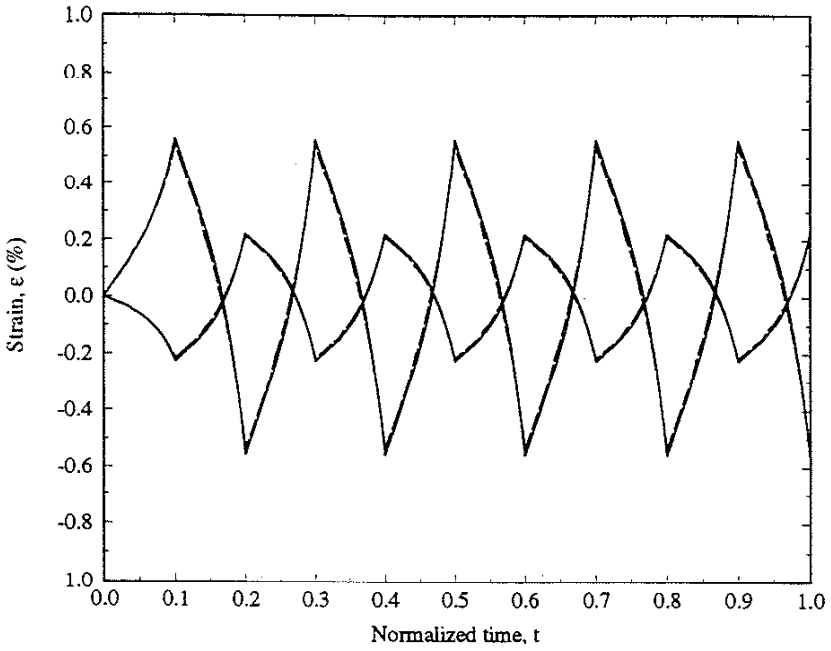

Figure 7.6d. Strain response for S_{max} = 450 MPa.

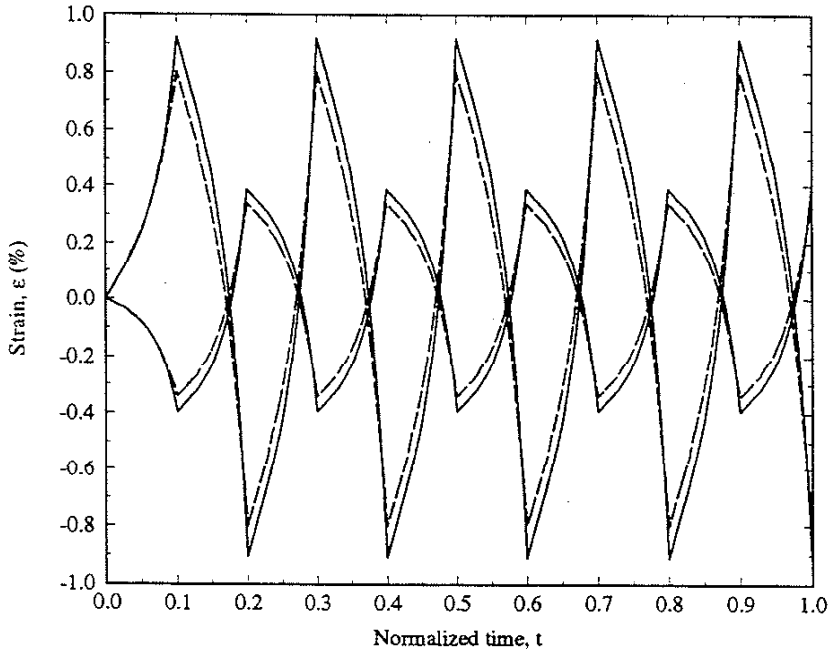

Figure 7.6e. Strain response for S_{max} = 550 MPa.

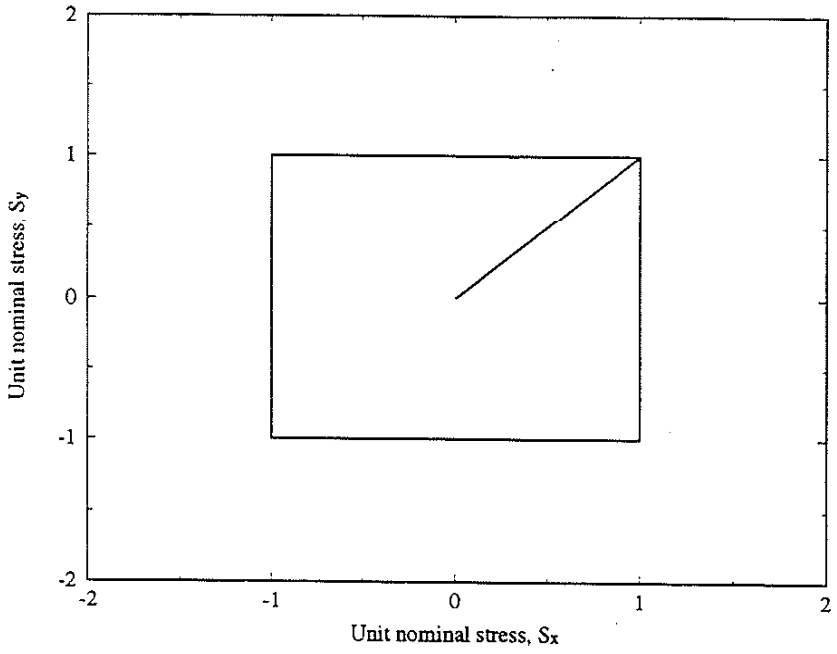

Figure 7.7a. Nominal stress path for box path biaxial cyclic nominal loading.

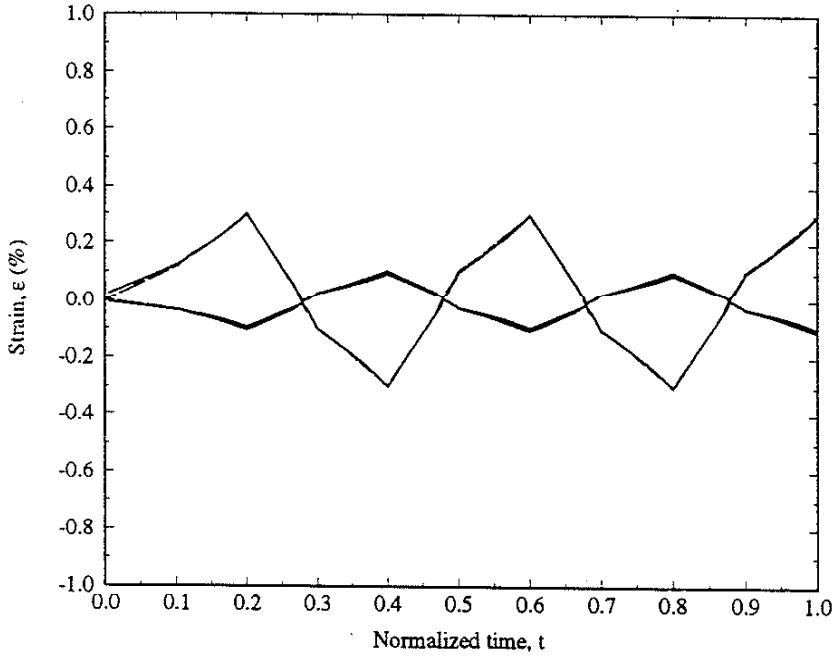

Figure 7.7b. Strain response for S_{max} = 150 MPa.

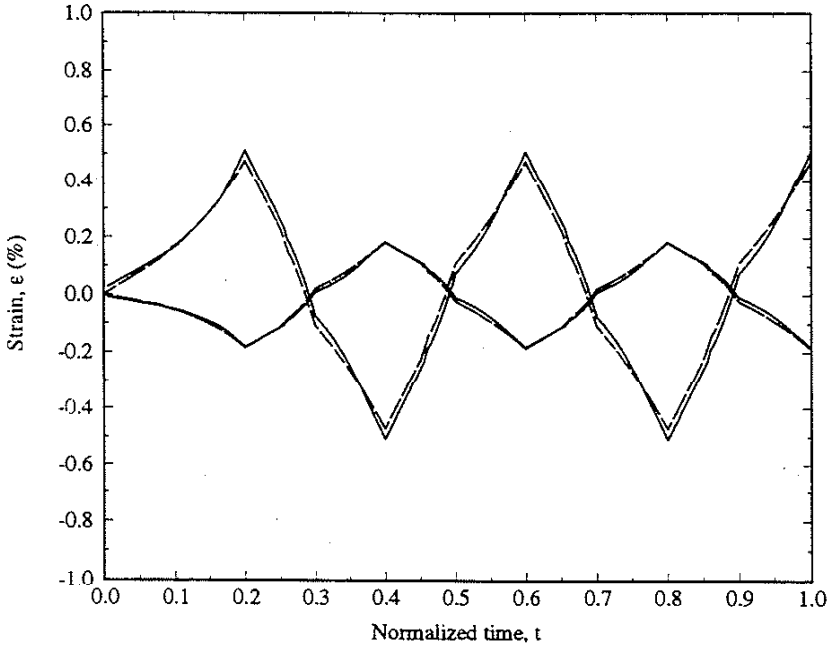

Figure 7.7c. Strain response for S_{max} = 200 MPa.

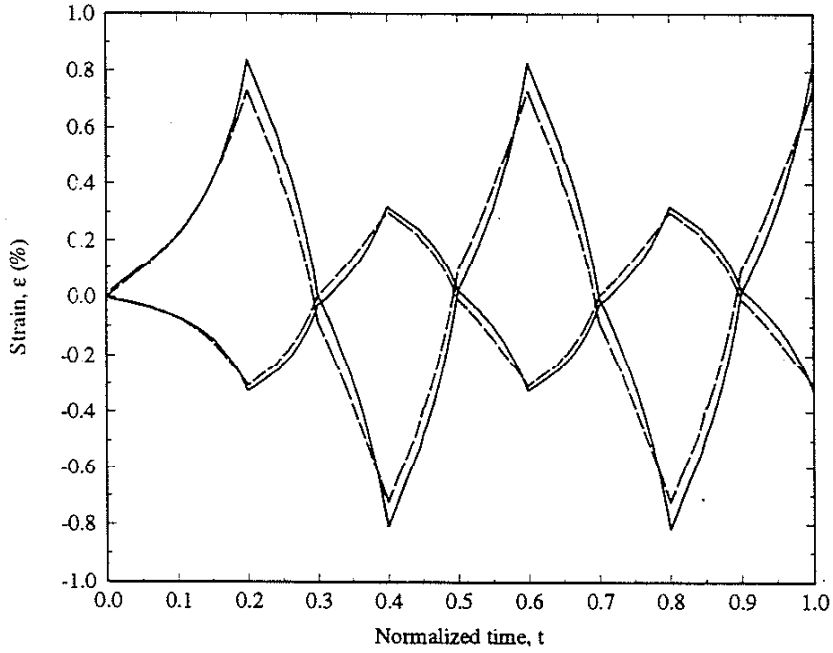

Figure 7.7d. Strain response for S_{max} = 250 MPa.

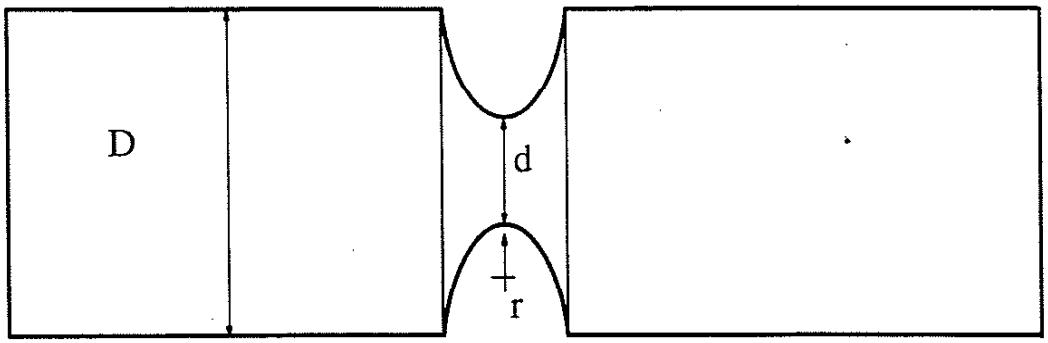

D = 144 mm d = 120 mm

r = 3 mm

Figure 8.1. Geometry of sharply notched shaft.

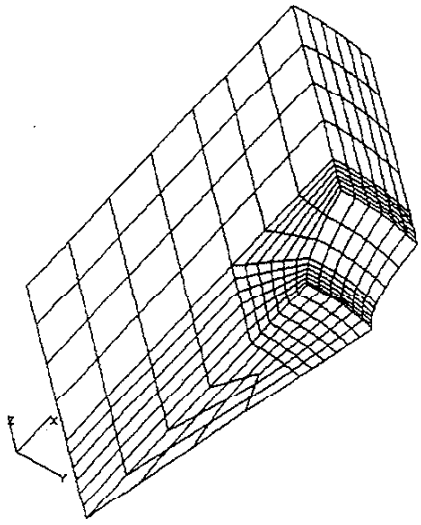

Figure 8.2a. Finite element mesh of sharply notched shaft.

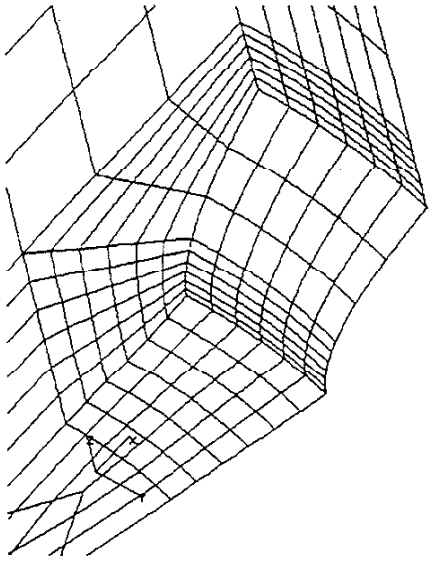

Figure 8.2b. Detailed view of notch root.

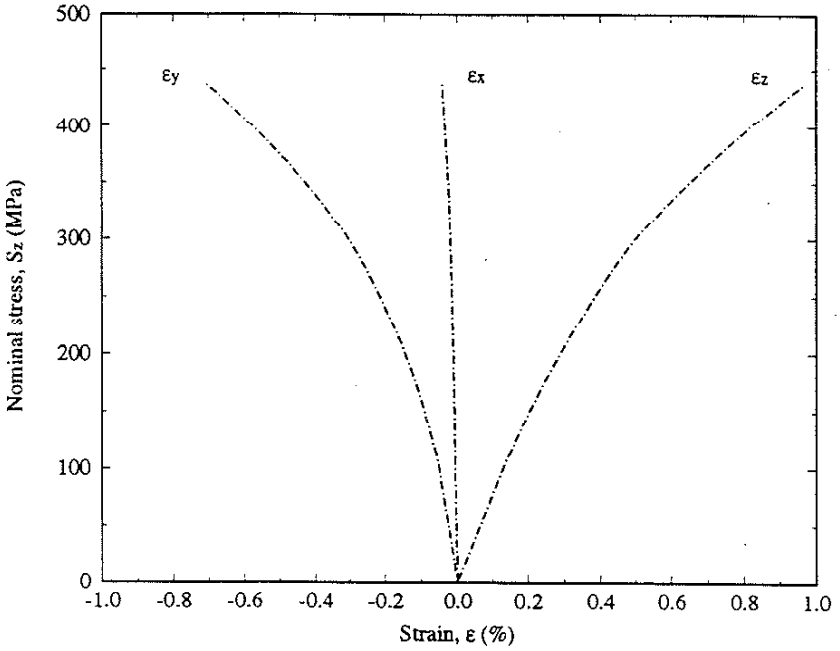

Figure 8.3. Notch root response for uniaxial load calculated by the finite element method.

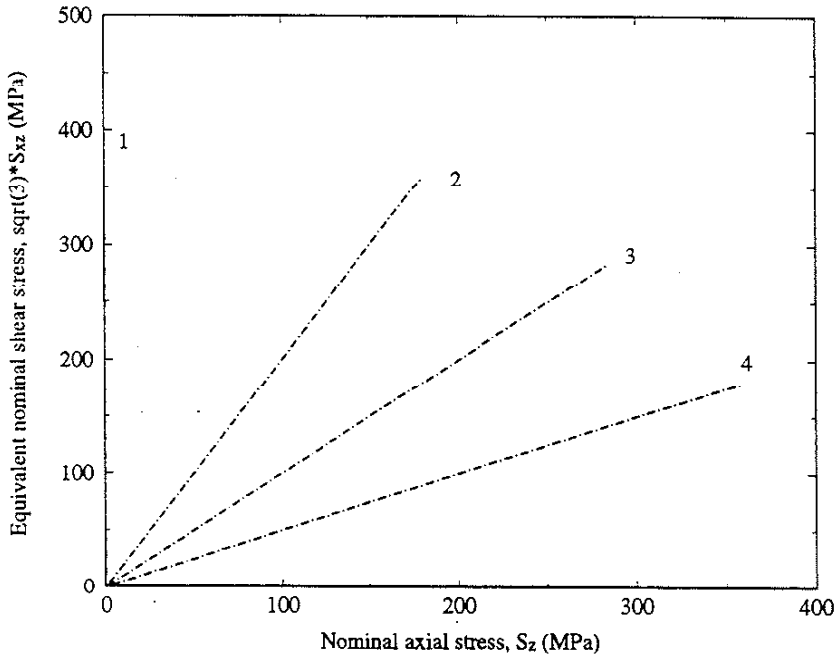

Figure 8.4. Proportional loading paths.

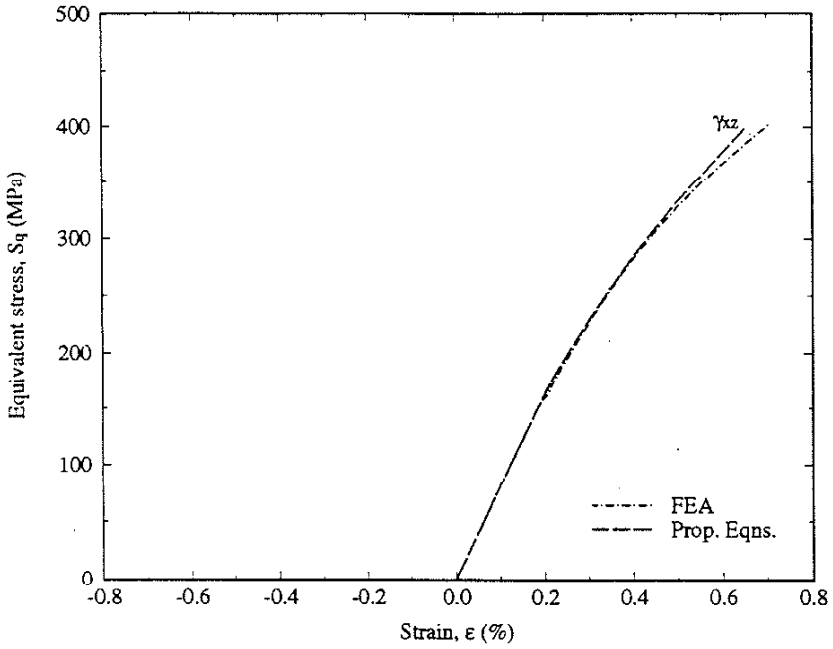

Figure 8.5a. Calculated strain response for pure torsional loading (path 1).

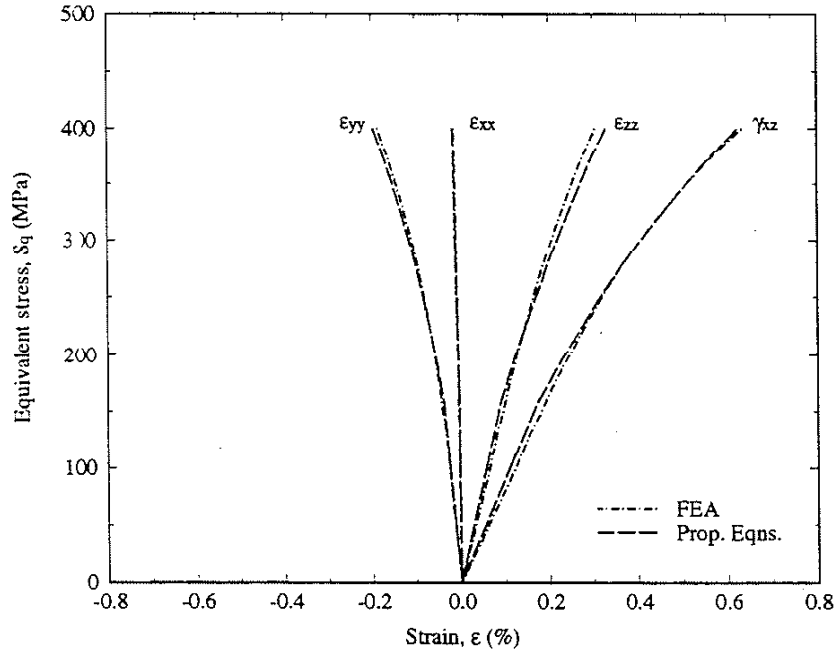

Figure 8.5b. Calculated strain response for proportional loading path 2.

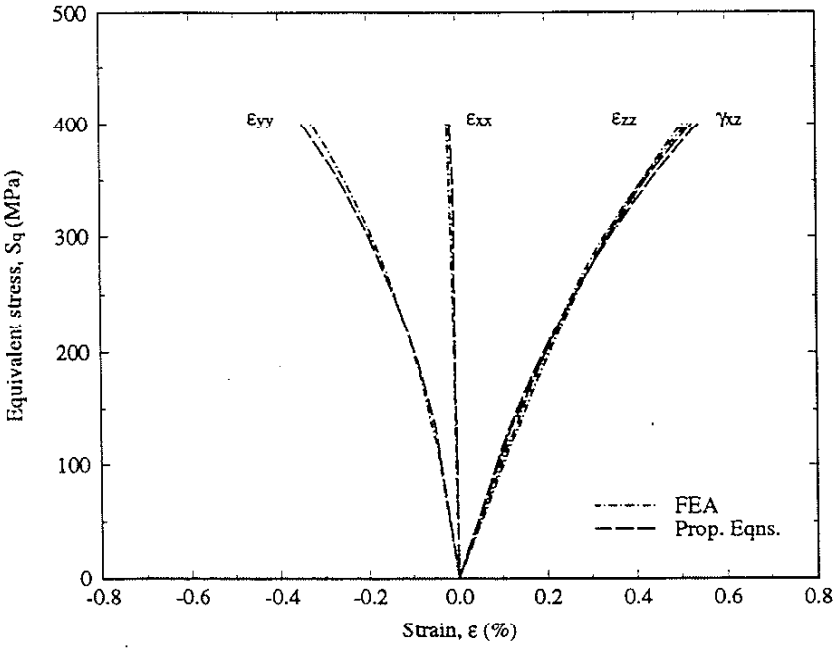

Figure 8.5c. Calculated strain response for proportional loading path 3.

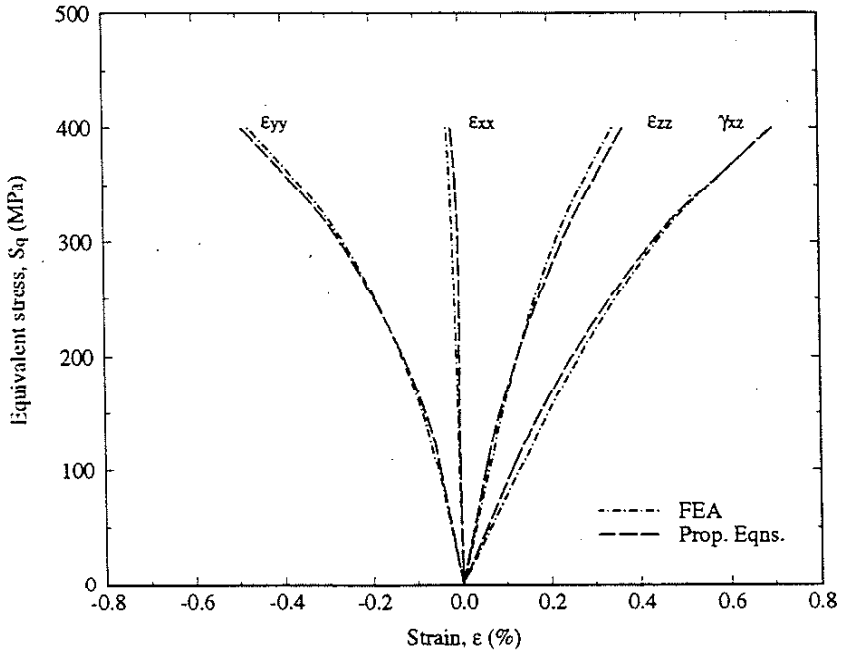

Figure 8.5d. Calculated strain response for proportional loading path 4.

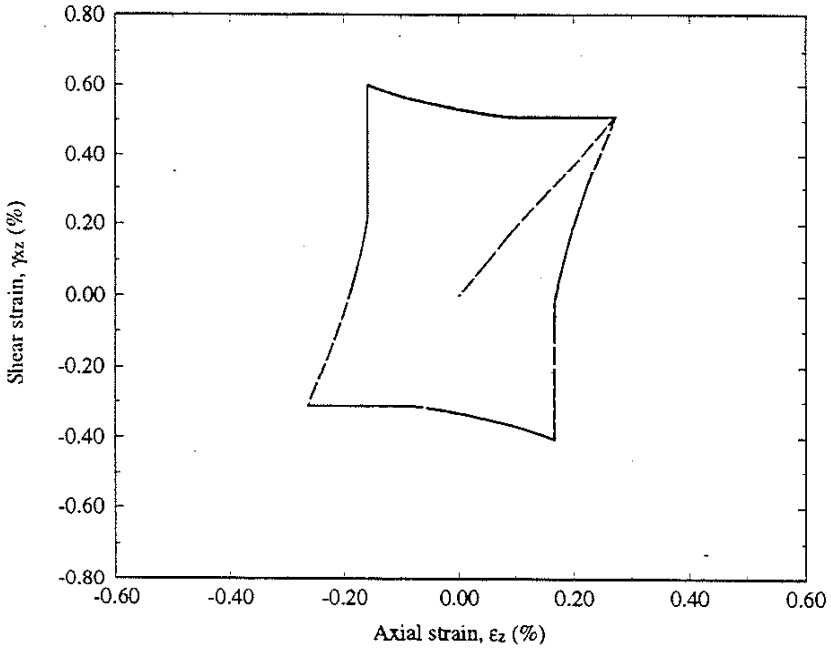

(a)

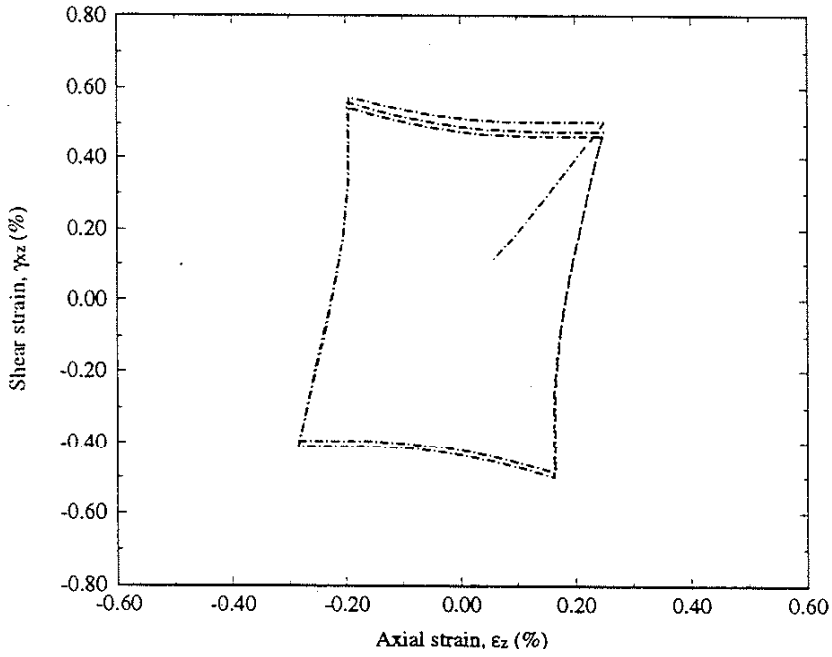

(b)

Figure 8.6. (a) Calculation using the simplified method and (b) calculation using the finite element method for box-shaped loading path corresponding to proportional path 2.

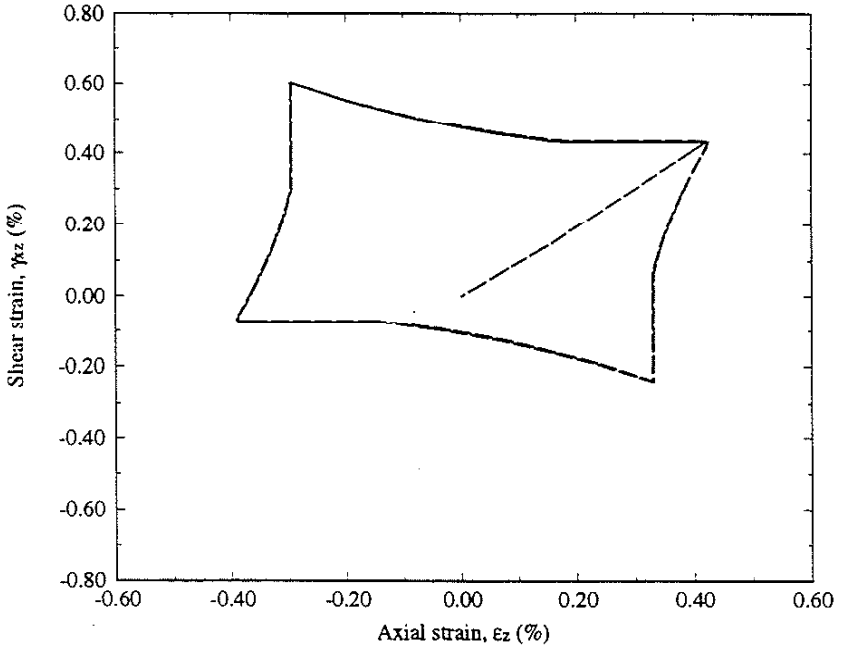

(a)

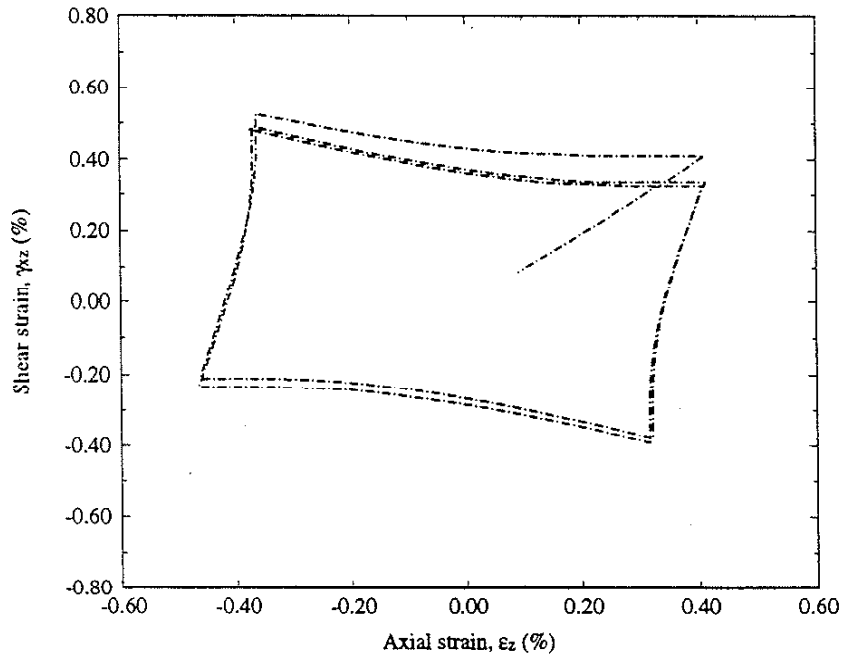

(b)

Figure 8.7. (a) Calculation using the simplified method and (b) calculation using the finite element method for box-shaped loading path corresponding to proportional path 3.

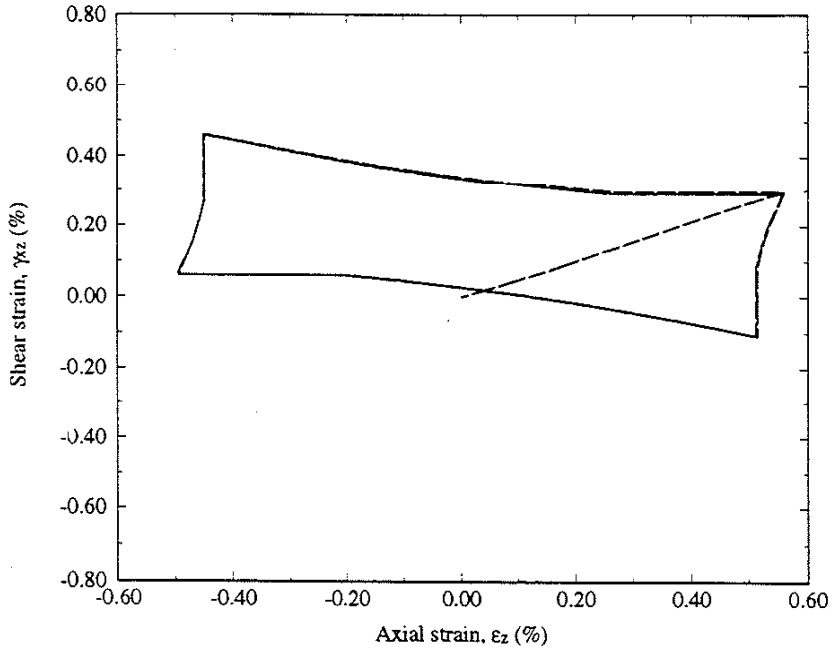

(a)

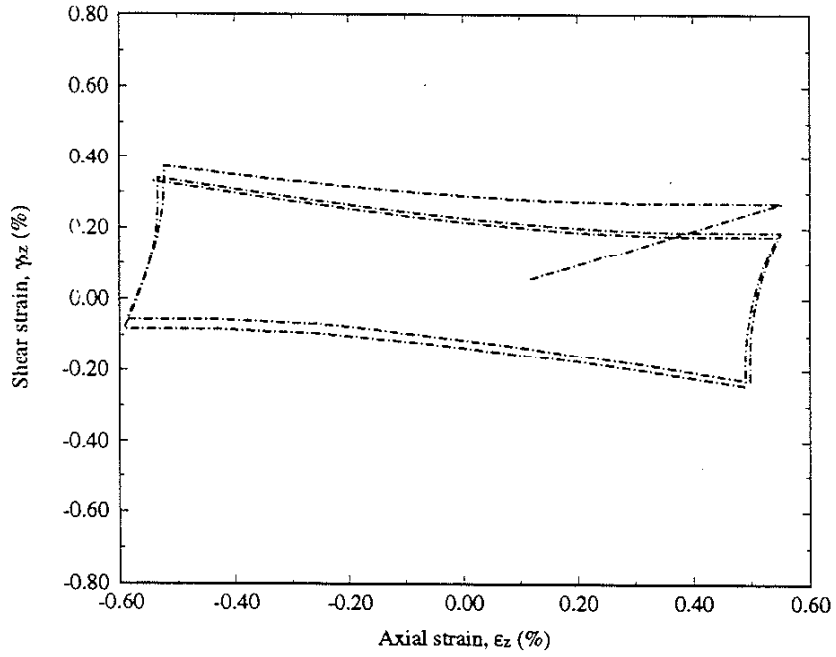

(b)

Figure 8.8. (a) Calculation using the simplified method and (b) calculation using the finite element method for box-shaped loading path corresponding to proportional path 4.

APPENDIX

The following note (Köttgen and Seeger 1993a) describes the discretization of the Ramberg-Osgood material curve used in the finite element analysis of the 1070 steel.

> "The Ramberg-Osgood equation describes a cyclic stress-strain curve without a yield stress, i.e. which is elastoplastic from the start. This approach cannot be mapped one-to-one to a discrete Mroz model, because there the yield surface separating elastic from elastoplastic behavior must be of finite size. The cyclic stress-strain curve is defined in the Mroz model in terms of work-hardening moduli $H'(k)$, which are constant between yield surfaces k and $k+1$. If values for $H'(k)$ used by the Mroz model are determined only by the local slope of the stress-strain curve, the plasticity associated with the part of the curve below the chosen yield stress in the original Ramberg-Osgood formulation will be lost when numerically integrating the deformation model during the finite element analysis. However, if the first $H'(1)$ value on input to the Mroz model is chosen to be the secant modulus of the Ramberg-Osgood σ-ε^p curve between $\varepsilon^p = 0$ and the plastic strain corresponding to the *second* yield surface, the numerical integration will account for the plasticity below the chosen yield stress whenever the stress moves between the first and second yield surface. Because $H'(1) > H'(2)$ numerical anomalies should not occur.
>
> When defining the input for the finite element analyses the approach defined above was mistakingly not used. Instead $H'(1)$ was defined as the local slope of the stress-plastic strain curve between the yield stress $\sigma_0(1) = 242$ MPa and the second yield surface $\sigma_0(2) = 245$ Mpa. Thus, the equivalent plastic strain below $\sigma_0(1) = 242$ MPa ($\varepsilon^p = 5.01809^{-5}$) was not accounted for in the analyses. The actual error caused by this is below 3% in the worst case."

LIST OF REFERENCES

Amstutz, H., M. Hoffmann, and T. Seeger. Kerbbeanspruchungen II. 1988. Mehrachsige Kerbbeanspruchungen im nichtlinearen Bereich bei proportional und nichtproportional wechselnder Belastung. Abschlußbericht zum FKM-Vorhaben Nr. 97. Forschungshefte Forschungskuratorium Maschinenbau e.v. Heft 139 (in German).

Bannantine, J.A. 1989. A variable amplitude multiaxial fatigue life prediction method. Ph.D. thesis, Department of Mechanical and Industrial Engineering, University of Illinois at Urbana-Champaign, Urbana, Illinois.

Barkey, M.E., D.F. Socie, and K.J. Hsia. 1993. A yield surface approach to the estimation of notch strains for proportional and nonproportional cyclic loading. Theoretical and Applied Mechanics report number 709, University of Illinois at Urbana, Urbana, Illinois. (To appear in the *Journal of Engineering Materials and Technology*.)

Box, W.A. 1951. The effect of plastic strains on stress concentrators. *Proceedings of the Society for Experimental Stress Analysis* 8:99-110.

Brose, W.R. 1977. Fatigue life predictions for a notched plate with analysis of mean stress and overstrain effects. *Fatigue Under Complex Loading: Analyses and Experiments*, Advances in Engineering volume 6, edited by R.M. Wetzel. Society of Automotive Engineers, Warrendale, Pennsylvania 119-135.

Chen, W.R., and L.M. Keer. 1991. An application of incremental plasticity theory to fatigue life prediction of steels. *Journal of Applied Mechanics* 113:404-410.

Chu, C.C. 1987. The analysis of multiaxial cyclic problems with an anisotropic hardening model. *International Journal of Solids and Structures* 23(5):569-579.

Chu, C.C. 1991. Multiaxial stress-strain modeling and fatigue life predictions for the SAE axle shaft. SAE Fatigue, Design, and Evaluation Committee meeting, October 2, 1991 at Urbana, Illinois.

Chu, C.C. 1992. Programming of a multiaxial stress-strain model for fatigue analysis. SAE 920662.

Conle, A., and H. Nowack. 1977. Verification of a Neuber-based notch analysis by the companion-specimen method. *Experimental Mechanics* 17:57-63.

Dowling, N.E., W.R. Brose, and W.K. Wilson. 1977. Notched member fatigue life predictions by the local strain approach. *Fatigue Under Complex Loading: Analyses and Experiments*, Advances in Engineering volume 6, edited by R.M. Wetzel. Society of Automotive Engineers, Warrendale, Pennsylvania 55-84.

Downing, S.D., and D.R. Galliart. 1985. A fatigue test system for a notched shaft in combined bending and torsion. *Multiaxial Fatigue, ASTM STP 853,* K.J. Miller and M.W. Brown, Eds., American Society for Testing and Materials, Philadelphia, 24-32.

Durelli, A.J., and C.A. Sciammarella. 1963. Elastoplastic stress and strain distribution in a finite plate with a circular hole subjected to unidimensional load. ASME *Journal of Applied Mechanics* 30:115-121.

Ellyin, F., and D. Kujawski. 1989. Generalization of notch analysis and its extension to cyclic loading. *Engineering Fracture Mechanics* 32(5):819-826.

Fash, J.W. 1985. An evaluation of damage development during multiaxial fatigue of smooth and notched specimens. Ph.D. Thesis, Department of Mechanical and Industrial Engineering, University of Illinois at Urbana-Champaign, Urbana, Illinois.

Garud, Y.S. 1981. Multiaxial fatigue: A survey of the state of the art. *Journal of Testing and Evaluation* 9(3):165-178.

Glinka, G. 1985a. Energy density approach to calculation of inelastic strain-stress near notches and cracks. *Engineering Fracture Mechanics* 22(3):485-508.

Glinka, G. 1985b. Calculation of inelastic notch-tip strain-stress histories under cyclic loading. *Engineering Fracture Mechanics* 22(5):839-854.

Glinka, G., W. Ott, and H. Nowack. 1988. Elastoplastic plane strain analysis of stresses and strains at the notch root. *Journal of Engineering Materials and Technology* 110:195-204.

Griffith, G.E. 1948. Experimental investigation of the effects of plastic flow in a tension panel with a circular hole. National Advisory Committee for Aeronautics Technical Note 1705.

Guillot, M.W., and W.N. Sharpe, Jr. 1983. A technique for cyclic-plastic notch-strain measurement. *Experimental Mechanics* 23:352-360.

Hardrath, H.F., and L. Ohman. 1951. A study of elastic and plastic stress concentration factors due to notches and fillets in flat plates. National Advisory Committee for Aeronautics Technical Note 2566.

Hill, R. 1948. A theory of the yielding and plastic flow of anisotropic metals. *Proceedings of the Royal Society of London*, Series A, 193:281-297.

Hill, R., 1956. *The Mathematical Theory of Plasticity*. Clarendon Press, Oxford, Chapter XII "Plastic Anisotropy."

Hoffmann, M., and T. Seeger. 1985a. Kerbbeanspruchungen I. Ermittlung und Beschreibung mehrachsiger Kerbbeanspruchungen im nichtlinearen Bereich. Abschlußbericht zum FKM-Vorhaben Nr. 71. Forschungshefte Forschungskuratorium Maschinenbau e.v. Heft 115 (in German).

Hoffmann, M., and T. Seeger. 1985b. A generalized method for estimating multiaxial elastic-plastic notch stresses and strains, Part 1: Theory. *Journal of Engineering Materials and Technology* 107:250-254.

Hoffmann, M., and T. Seeger. 1985c. A generalized method for estimating multiaxial elastic-plastic notch stresses and strains, Part 2: Applications. *Journal of Engineering Materials and Technology* 107:255-260.

Hoffmann, M., and T. Seeger. 1989a. Estimating multiaxial elastic-plastic notch stresses and strains in combined loading. *Biaxial and Multiaxial Fatigue,* EGF3 (Edited by M.W. Brown and K.J. Miller), Mechanical Engineering Publications, London, 3-24.

Hoffmann, M., and T. Seeger. 1989b. Stress-strain analysis and life predictions of a notched shaft under multiaxial loading. *Multiaxial Fatigue: Analysis and Experiments,* Advances in Engineering volume 14, edited by D. F. Socie *et al.* Society of Automotive Engineers, Warrendale, Pennsylvania 81-99.

Hoffmann, M., H Amstutz, and T. Seeger. 1991. Local strain approach in non-proportional loading. *Fatigue under Biaxial and Multiaxial Loading* ESIS10 (Edited by K. Kussmaul, D. McDiarmid, and D. Socie), Mechanical Engineering Publications, London 357-376.

Jiang, Y.R., and H. Sehitoglu. 1992. Fatigue and stress analyses of rolling contact: A collection of resports prepared for thc Association of American Railroads. Materials Engineering-Mechnical Behavior Report Number 413, University of Illinois, Urbana, Illinois.

Klann, D.A., S.M. Tipton, and T.S. Cordes. 1993. Notch stress and strain estimation considering multiaxial constraint. Society of Automotive Engineers technical paper number 930401.

Köttgen, V. B., R.J. Anthes, and T. Seeger. 1991a. Implementation des Werkstoffmodells von Mróz in das Finite Element Programm ABAQUS - Teil 1: Grundlagen. Bericht FW-8/1991. Fachgebiet Werkstoffmechanik, Technische Hochschule Darmstadt.

Köttgen, V. B., R.J. Anthes, and T. Seeger. 1991b. Implementation des Werkstoffmodells von Mróz in das Finite Element Programm ABAQUS - Teil 2: Quelltext und Beispiele. Bericht FW-8/1991. Fachgebiet Werkstoffmechanik, Technische Hochschule Darmstadt.

Köttgen, V. B. 1992. Private communications. 1992-1993.

Köttgen, V. B. and T. Seeger. 1993a. Finite element analyses of a notched bar under multiaxial nonproportional loading using the Mróz model. Bericht FF-7/1993. Fachgebiet Werkstoffmechanik, Technische Hochschule Darmstadt.

Köttgen, V. B. and T. Seeger. 1993b. A Masing type integration of the Mróz model for some nonproportional stress-controlled paths. Fachgebiet Werkstoffmechanik, Technische Hochschule Darmstadt.

Krieg, R.D. 1975. A practical two surface plasticity theory. *Journal of Applied Mechanics* 42:641-646.

Lamba, H.S., and O.M. Sidebottom. 1978. Cyclic plasticity for nonproportional paths: Part 1--Cyclic hardening, erasure of memory and subsequent strain hardening experiments, and Part 2--Comparison with predictions of three incremental plasticity models. *Journal of Engineering Materials and Technology* 100:96-111.

Landgraf, R.W., F.D. Richards, and N.R. LaPointe. 1977. Fatigue life predictions for a notched member under complex load histories. *Fatigue Under Complex Loading: Analyses and Experiments*, Advances in Engineering volume 6, edited by R.M. Wetzel. Society of Automotive Engineers, Warrendale, Pennsylvania 95-106.

Leis, B.N., C.V.B. Gowda, and T.H. Topper. 1973. Some studies of the influence of localized and gross plasticity on the monotonic and cyclic concentration factors. *Journal of Testing and Evaluation* 1(4):341-348.

Leis, B.N., and N.D. Frey. 1982. Cyclic-inelastic deformation and fatigue resistance of notched-thin aluminum plates. *Experimental Mechanics* 39:287-295.

Lubliner, J. 1990. *Plasticity theory*. Macmillan Publishing Company, New York.

McDowell, D.L. 1985a. A two surface model for transient nonproportional cyclic plasticity: Part 1: Development of appropriate equations, and Part 2: Comparison of theory with experiments. *Journal of Applied Mechanics* 52:298-308.

McDowell, D.L. 1985b. An experimental study of the structure of constitutive equations for nonproportional cyclic plasticity. *Journal of Engineering Materials and Technology* 107:307-315.

McDowell, D.L. 1987. An evaluation of recent developments in hardening and flow rules for rate-independent, nonproportional cyclic plasticity. *Journal of Applied Mechanics* paper number 87-APM-37.

Mendelson, A. 1968. *Plasticity: Theory and Application.* Robert E. Kreiger Publishing Company, incorporated, Malabar, Florida.

Mises, R. 1928. Mechanik der plastischen Formänderung von Kristallen. *Zeitschrift für angewandte Mathematik und Mechanik* 8(3):161-185.

Moftakhar, A., and G. Glinka. 1992. Elastic-plastic stress-strain analysis methods for notched bodies. (Submitted to the *Journal of Engineering Materials and Technology.*)

Molski, K., and G. Glinka. 1981. A method of elastic-plastic stress and strain calculation at a notch root. *Materials Science and Engineering* 50:93-100.

Moosbrugger, J.C., and D.L. McDowell. 1990. A rate-dependent bounding surface model with a generalized image point for cyclic nonproportional viscoplasticty. *Journal of Mechanics and Physics of Solids* 38(5):627-656.

Morrow, JoDean. 1965. Cyclic plastic strain energy and fatigue of metals. ASTM STP 378, 45-87.

Mróz, Z. 1967. On the description of anisotropic work-hardening. *Journal of the Mechanics and Physics of Solids* 15:163-175.

Neuber, H. 1946. *Theory of Notch Stresses.* J.W. Edwards Co., Ann Arbor, Michigan.

Neuber, H. 1961. Theory of stress concentration for shear-strained prismatical bodies with arbitrary nonlinear stress-strain law. ASME *Journal of Applied Mechanics* 28(4):544-550.

Papirno, R. 1971. Plastic stress-strain history at notch roots in tensile strips under monotonic loading. *Experimental Mechanics* 11:446-452.

Peterson, R.E. 1966. *Stress Concentration Design Factors*. John Wiley and Sons, New York. Fifth printing.

Ramberg, W., and W.R. Osgood. 1943. Description of stress-strain curves by three parameters. National Advisory Committee for Aeronautics Technical Note 902.

Seeger, T., A. Beste, and H. Amstutz. 1977. Elastic-plastic stress-strain behaviour of monotonic and cyclic loaded notched plates. Proceedings from the Fourth International Conference on Fracture at the University of Waterloo, entitled: *Advances in the Research on the Strength and Fracture of Materials*, volume 2B: Fatigue, edited by D.M.R. Taplin.

Seeger, T., and P. Heuler. 1980. Generalized application of Neuber's rule. *Journal of Testing and Evaluation* 8(4):199-204.

Sharpe, W.N., Jr., C.H. Yang, and R.L. Tregoning. 1992. An evaluation of the Neuber and Glinka relations for monotonic loading. ASME *Journal of Applied Mechanics* 59:S50-S56.

Sharpe, W.N., Jr. 1991. Measurement of monotonic biaxial elastoplastic stresses at notch roots. ASME *Journal of Applied Mechanics* 58:916-922.

Sharpe, W.N., Jr. and K.C. Wang. 1991. Evaluation of a modified monotonic Neuber relation. *Journal of Engineering Materials and Technology* 113:1-8.

Socie, D.F., N.E. Dowling, and P. Kurath. 1984. Fatigue life estimation of notched members. *Fracture Mechanics: Fifteenth Symposium, ASTM STP 833*, R.J. Sanford, Ed., American Society for Testing and Materials, Philadelphia. 284-299.

Socie, D.F. 1987. Multiaxial fatigue damage models. *Journal of Engineering Materials and Technology* 109:293-298.

Stowell, E.Z. 1950. Stress and strain concentration at a circular hole in an infinite plate. National Advisory Committee for Aeronautics Technical Note 2073.

Tipton, S.M. 1985. Fatigue behavior under multiaxial loading in the presence of a notch: Methodologies for the prediction of life to crack initiation and life spent in crack propagation. Ph.D. thesis, Stanford University.

Tipton, S.M. 1991. A review of the development and use of Neuber's rule for fatigue analysis. Society of Automotive Engineers technical paper number 910165.

Topper, T.H., R.M. Wetzel, and J. Morrow. 1969. Neuber's rule applied to fatigue of notched specimens. *Journal of Materials* 4(1):200-209.

Walker, E.K. 1977. Multiaxial stress-strain approximations for notch fatigue behaviors. *Journal of Testing and Evaluation* 5(2):106-113.

Wang, K.C., and W.N. Sharpe, Jr. 1991. Evaluation of a modified cyclic Neuber relation. ASME *Journal of Engineering Materials and Technology* 113:350-353.

Wetzel, R.M. 1968. Smooth specimen simulation of fatigue behavior of notches. *Journal of Materials* 3(3):646-657.

Wilson, W.K. 1974. Elastic-plastic analysis of blunt notched CT specimens and applications. *Journal of Pressure Vessel Technology* 96:293-298.

VITA

Mark Edward Barkey was born near St. Louis, Missouri, on August 14, 1967. In August 1985, he entered the University of Missouri at Rolla and graduated *summa cum laude* in May 1989, with a Bachelor of Science degree in Engineering Mechanics and a minor in Applied Mathematics. In August 1989, he entered the University of Illinois at Urbana-Champaign, and received the Master of Science degree in Theoretical and Applied Mechanics in January 1991. He continued his education in the doctoral program in Theoretical and Applied Mechanics and worked as a research and teaching assistant. During the summers of 1989, 1990, and 1991, he worked in the Current Product Engineering division of General Motors Corporation in the areas of finite element analysis, metal fatigue, and plasticity. He has made presentations regarding notch behavior and stain gage rosette analysis techniques before the Society of Automotive Engineers, and has coauthored a paper regarding notch strain calculation, to appear in the *Journal of Engineering Materials and Technology*.

Mr. Barkey is a member of Phi Kappa Phi and Tau Beta Pi scholastic honor societies, and has received a University of Illinois Fellowship during the first year of his graduate study.